

January 2015

Drug Delivery to Solid Tumors via Polymeric Nanoparticles

Sara Ahmed
Purdue University

Follow this and additional works at: https://docs.lib.purdue.edu/open_access_dissertations

Recommended Citation

Ahmed, Sara, "Drug Delivery to Solid Tumors via Polymeric Nanoparticles" (2015). *Open Access Dissertations*. 1080.
https://docs.lib.purdue.edu/open_access_dissertations/1080

This document has been made available through Purdue e-Pubs, a service of the Purdue University Libraries.
Please contact epubs@purdue.edu for additional information.

**PURDUE UNIVERSITY
GRADUATE SCHOOL
Thesis/Dissertation Acceptance**

This is to certify that the thesis/dissertation prepared

By Sara Ahmed

Entitled

Drug Delivery to Solid Tumors via Polymeric Nanoparticles

For the degree of Doctor of Philosophy

Is approved by the final examining committee:

Yoon Yeo

Chair

Mohamed Seleem

Kinam Park

Elizabeth Topp

David Thompson

To the best of my knowledge and as understood by the student in the Thesis/Dissertation Agreement, Publication Delay, and Certification Disclaimer (Graduate School Form 32), this thesis/dissertation adheres to the provisions of Purdue University's "Policy of Integrity in Research" and the use of copyright material.

Approved by Major Professor(s): Yoon Yeo

Approved by: Lynne Taylor

Head of the Departmental Graduate Program

11/19/2015

Date

DRUG DELIVERY TO SOLID TUMORS VIA POLYMERIC
NANOPARTICLES

A Dissertation

Submitted to the Faculty

of

Purdue University

by

Sara Ahmed

In Partial Fulfillment of the

Requirements for the Degree

of

Doctor of Philosophy

December 2015

Purdue University

West Lafayette, Indiana

To my parents, Afaf Aglan and Ahmed AbouElmagd, my role models, first teachers and ever-enthusiastic supporters.

ACKNOWLEDGEMENTS

First, I would like to sincerely thank my adviser and mentor, Dr. Yoon Yeo, for her generous support in every step of my PhD study. In addition to all the academic guidance, as an adviser, she has taught me plenty just by being dedicated, honest and fair. As I start my academic career, I am immensely grateful for enjoying her as a role model.

Also, I would like to thank my committee members, Dr. Kinam Park, Dr. Elizabeth Topp, Dr. David Thompson and Dr. Mohamed Seleem for accepting to be on my advising committee in the first place, and for their insightful guidance and eye-opening critique.

I thank all the previous and current members of the Yeo lab for their help, support and knowledge. I could not have asked for a better lab mates or a more supportive atmosphere. You have been generous with your knowledge, experience and kindness. I have always felt at home and I know that I have made friendships that would last a life time. Specifically, I would like to thank Youn Jin Ku, my undergraduate student for helping me with research throughout a year and half, and for making our time in the lab even more enjoyable!

I would also like to thank Dr. Kinam Park, Dr. Dor Ben-Amotz, Dr. Gregory Knipp, Dr. Lynne Taylor, Dr. Peter Dunn, Dr. Aaron Taylor and Dr. Mary Wirth for being such inspiring teachers, and for all the knowledge you have given in your classes.

Also, I would like to thank the Egyptian Government and the tax payers in Egypt for funding me for this fellowship, enabling me to learn and grow on different levels in Purdue.

Finally, I would thank my family and friends for their support and love. My parents, my husband Omar Amen, and daughter Salma Amen.

TABLE OF CONTENTS

	Page
LIST OF TABLES	ix
LIST OF FIGURES	x
LIST OF ABBREVIATIONS.....	xvi
ABSTRACT.....	xviii
CHAPTER 1. INTRODUCTION ON DELIVERY OF NANOPARTICLES TO TUMORS.....	1
1.1 Nanoparticles in Chemotherapy.....	1
1.2 Factors Affecting the Effectiveness of NP Drug Delivery Systems	3
1.2.1 Biocompatibility	4
1.2.2 Particle Size	4
1.2.3 Particle Surface Charge	5
1.2.4 Circulation Half-life.....	5
1.2.5 Tumor Retention and Cellular Uptake.....	6
1.2.6 Drug Release.....	7
1.3 Remaining Challenges in NP Development.....	9
1.3.1 Tumor Physiology	9
1.3.2 Formulation Challenges.....	12
1.3.2.1 ‘PEG Dilemma’	12
1.3.2.2 Maintaining Particle Size	13

	Page
1.3.2.3 Controlling Drug Release.....	14
1.3.2.4 Clinical Translation of Developed NP systems.....	18
1.4 Extracellularly Activatable NPs for Tumor Drug Delivery	19
1.4.1 Extracellular Stimuli Adapted for NP Activation.....	19
1.4.2 Nanocarriers Responsive to Tumor Extracellular pH.....	20
1.4.2.1 Drug Release:	20
1.4.2.2 Cell Interaction.....	22
1.5 Conclusions.....	24
1.6 References.....	25
CHAPTER 2. PREPARATION AND EVALUATION OF LOW MOLECULAR WEIGHT CHITOSAN COATED NPS MEDIATED VIA DOPAMINE POLYMERIZATION.....	40
2.1 Introduction.....	40
2.2 Materials and Methods.....	43
2.2.1 Materials	43
2.2.2 Preparation of PLGA Cores.....	43
2.2.3 Preparation and Characterization of LMWC.....	44
2.2.4 Preparation of Coated Particles	44
2.2.5 Particle Characterization.....	46
2.2.6 PTX Release from PLGA Matrices	46
2.2.6.1 <i>In Vitro</i> Release Study.....	46
2.2.6.2 Cell Culture	47
2.2.6.3 Cytotoxicity of PLGA NPs.....	47
2.2.7 Protein Adsorption to NP surface	47

	Page
2.2.8 NP-Cell Interaction Studies	48
2.2.8.1 Cell Culture	48
2.2.8.2 Quantitative Analysis of Cell-Particle Interactions.....	48
2.2.8.3 Visualization of Cell-Particle Interactions	49
2.2.9 pH Selective PTX Delivery to Cancer Cells by NPs	50
2.3 Results.....	51
2.3.1 Preparation and Characterization of PLGA Cores.....	51
2.3.2 Preparation and Characterization of Coated NPs.....	53
2.3.3 <i>In Vitro</i> PTX Release of Coated PLGA NPs	56
2.3.4 Protein Adsorption to NP Surface.....	57
2.3.5 NP-Cell Interaction Studies	59
2.4 Discussion	65
2.5 Conclusions	68
2.6 References	69
CHAPTER 3. <i>IN VIVO</i> evaluation OF LMWC-COATED NPS IN TUMOR BEARING MICE.....	73
3.1 Introduction	73
3.2 Materials and Methods	74
3.2.1 Materials.....	74
3.2.2 Preparation of NPs	75
3.2.2.1 Preparation of NP Cores.....	75
3.2.2.2 <i>In Vitro</i> Release of ICG from NP Cores.....	75
3.2.2.3 Coating of NP Cores.....	76
3.2.3 Development of Xenograft Tumor Model	77

	Page
3.2.3.1 Cell Culture.....	77
3.2.3.2 Tumor Inoculation	77
3.2.3.3 Tumor Measurement.....	77
3.2.4 Antitumor Effect of PTX-Loaded NPs on LS174T Tumor-Bearing Mice	78
3.2.5 Antitumor Effect of PTX-Loaded NPs on MCF-7 Tumor-Bearing Mice	79
3.2.6 Tracking of ICG-Labeled NPs in MCF-7 Tumor-Bearing Mice	79
3.3 Results.....	81
3.3.1 NP preparation and Characterization	81
3.3.2 Antitumor Effect of PTX-Loaded NPs on LS174T and MCF-7 Tumor-Bearing Mice.....	81
3.3.3 Tracking of ICG-Loaded NPs in MCF-7 Tumor-Bearing Mice	86
3.4 Discussion	90
3.5 Conclusions	92
3.6 References	93
CHAPTER 4. EXPERIMENTAL DESIGN of RELEASE STUDIES for NANOPARTICLE FORMULATIONS	95
4.1 Introduction	95
4.2 Materials and Methods	98
4.2.1 Materials.....	98
4.2.2 PTX Solubility Studies.....	98
4.2.3 PLGA NP Preparation and Characterization	99
4.2.4 <i>In Vitro</i> Release of PTX from PLGA NPs.....	99
4.3 Results.....	100
4.3.1 PTX Solubility in Different Media	100

	Page
4.3.2 In vitro Release of PTX from PLGA NPs.....	102
4.4 Discussion	105
4.5 Conclusions	107
4.6 References	108
CHAPTER 5. APPLICATION OF TANNIC ACID FOR SURFACE FUNCTIONALIZATION OF NANOPARTICLES.....	111
5.1 Introduction	111
5.2 Materials and Methods.....	115
5.2.1 Materials.....	115
5.2.2 Preparation and Characterization of NPs.....	115
5.2.3 NP Characterization	116
5.2.4 <i>In Vitro</i> Cytotoxicity of TA coated NPs	117
5.3 Results.....	118
5.3.1 NPs Preparation and Characterization	118
5.3.2 Quantification of TA Coating	121
5.3.3 Functionalization of PLGA-TA NPs.....	121
5.3.4 Cytotoxicity of PLGA-TA NPs.....	124
5.4 Discussion	125
5.5 Conclusion.....	127
5.6 References	129
APPENDIX	131
VITA.....	132
PUBLICATIONS.....	133

LIST OF TABLES

Table	Page
Table 1: Some nanomedicinal formulations approved or undergoing clinical trials.	9
Table 2: Particle size, zeta potential and loading efficiency of PTX loaded NPs	51
Table 3: Reported PTX solubility in different media (Abouelmagd et al., 2015).	97

LIST OF FIGURES

Figure	Page
Figure 1: Biodistribution of intravenously injected NPs and their transport pathway to solid tumors.	2
Figure 2: A typical design of NPs as drug carriers for systemic delivery of chemotherapeutics.....	2
Figure 3: Schematic diagram of PLGA-pD-LMWC NP preparation and following cellular interactions.....	42
Figure 4: <i>In vitro</i> release profiles of PTX from NPs of different polymer matrices in PBS (0.2% Tween 80, pH 7.4).....	52
Figure 5: Viability of SKOV-3 cells exposed to free PTX and PTX loaded NPs for 24 (a) or 72 hour (b), and blank PLGA NPs for 24 (c) or 72 hour (d).....	53
Figure 6: (a) Analysis of LMWC via MALDI-TOF/TOF using sinapinic acid as a matrix (1:1), (b) pH-dependent change in transmittance for LMWC (n=2) and undegraded chitosan (0.5 mg/mL in water) measured at 500 nm.	54
Figure 7: Particle size and surface charge analysis of different NPs: (a) Average diameter (Z_{avg}) and polydispersity index, (b) Zeta potential at pH 7.4 and 6.2.	55
Figure 8: Transmission electron microscopy (TEM) images of NPs negatively stained with 2% uranyl acetate. Scale bar: 50 nm (top panel), 100 nm (bottom panel).....	56
Figure 9: <i>In vitro</i> release of PTX from different NPs in PBS (0.2% Tween 80) at 37°C. At 7th hour, release % is significantly different among three types of NPs ($p < 0.05$, two-tailed T-test, n=3).....	57

Figure	Page
Figure 10: Analysis of NPs hard corona composition post incubation in 50% FBS. Proteins were stripped off NPs and resolved via SDS-PAGE. Protein extracts of different NPs post incubation for 1 or 24 hours were run on 12% gels and compared to standards ‘ladder’ (left) and FBS (right of gel). A representative Coomassie blue-stained gel of resolved corona proteins is shown in (a), where arrows point to bands of interest. Relative band intensity of most prominent proteins pointed with arrows in (a) was analyzed via ImageJ 1.48v software. Average of four different gels is shown in (b).	58
Figure 11: Zeta potential of protein coated PLGA-pD-LMWC and PLGA-pD-PEG NPs. NPs were incubated in PBS or 50% FBS in PBS. (n=3).	59
Figure 12: Analysis of different fluorescent particles: Average diameter (Z_{avg}) of fluorescent NPs (a), and Zeta potential at pH 7.4 and 6.2 of fluorescent NPs (b) and MPs (c).	60
Figure 13: pH dependent cellular interaction of different fluorescently labeled NPs (*PLGA) with SKOV-3 cells as quantified by (a) Flow-cytometry (Geometric mean at pH 6.2 was significantly different for *PLGA-LMWC and *PLGA-pD-LMWC from that of *PLGA, *PLGA-pD and *PLGA-pD-PEG, two tailed t-test, $P < 0.05$) or visualized via confocal microscopy (b) after three hours of incubation (Green= NPs labeled by FITC, Blue= nuclei stained by Hoechst).	60
Figure 14: Cellular uptake of *PLGA-pD-LMWC NPs by SKOV-3 cells after three hours of incubation at pH 7.4 or 6.2, imaged via confocal microscopy as thin sections (a) or z-stack (b, right panel). A cross section showing XY, XZ and YZ planes demonstrates NPs intracellular localization (b, left panel) (Green= NPs labeled by FITC, Red= cell membrane labeled by CellMask deep red).	61
Figure 15: Intracellular trafficking of *PLGA-pD-LMWC NPs in SKOV-3 cells imaged by confocal microscopy after three hours of incubation at pH 7.4 or 6.2 (a). Time lapse imaging of *PLGA-pD-LMWC NPs incubated with SKOV-3 cells at pH 6.2 over 270 minutes (b) (Green= NPs labeled by FITC, Red= LysoTracker Red DND-99).	62

Figure	Page
Figure 16: Time lapse imaging of *PLGA-pD-LMWC NPs after incubation with SKOV-3 cells over 270 minutes at pH 6.2 (Green= NPs labeled by FITC).	63
Figure 17: J774A.1 macrophage uptake of fluorescently labeled MPs at pH 7.4 after three hours analyzed via flow cytometry (a) or visualized with Cytation 3 fluorescence imaging system (b). All geometric means were significantly different from each other (One-way Anova test, $P < 0.05$). ** $p = 0.0034$ and *** $p = 0.0004$ (two-tailed t-test). (Green= MPs labeled by FITC).....	64
Figure 18: pH dependent PTX retention post incubation of SKOV-3 cells with PTX loaded NPs or free PTX at pH 7.4 or 6. NPs were incubated with the cells for two and half hours at either pH after which cells were harvested, separated from NPs and analyzed for PTX content (* $p = 0.03$, two-tailed T-test, $n = 4-8$).....	65
Figure 19: Outline of <i>in vivo</i> studies carried out using LS174T and MCF-7 subcutaneous tumor models.	78
Figure 20: Dosing schedule of glucose and MIBG for the acidity-enhanced tumor model. Glucose and MIBG were injected IP once daily for three days, while *NPs were delivered via the retro-orbital injection on the first day.	80
Figure 21: Characterization of freeze-dried PTX loaded NPs after redispersion: a) Particle size and polydispersity index, b) Zeta potential at pH 7.4 and 6.2 ($n = 4$).....	81
Figure 22: Subcutaneous xenografts of MCF-7 and LS174T tumors post extraction.	82
Figure 23: Growth profile of LS174T tumors receiving different treatments over time (a) average fold increase in tumor volume (average \pm SD), (b) growth profiles of individual tumors. Arrows indicate the days treatments were administered.	83
Figure 24: Growth profile of MCF-7 tumors receiving different treatments over time (a) average fold increase in tumor volume (average \pm SD), (b) growth profiles of individual tumors. Arrows indicate the days treatments were administered.	84

Figure	Page
Figure 25: Average fold change in body weight of (a) LS174T and (b) MCF-7 tumor xenograft model after intravenous administration of different formulations (average \pm SD).	85
Figure 26: ICG loaded PLGA NPs (*PLGA) and pD coated *PLGA (*PLGA-pD).	86
Figure 27: Characterization of freeze-dried ICG loaded NPs after redispersion: (a) Particle size and polydispersity index, (b) Zeta potential at pH 7.4 and 6.2 (average \pm SD, n=3-4).	86
Figure 28: <i>In vitro</i> release of ICG from PLGA cores (*PLGA) dispersed in serum containing medium at 37°C at different time points (average \pm SD, n=3).	87
Figure 29: Tracking of ICG loaded NPs in MCF-7 xenograft model (n=5), (a) Representative image of whole body imaging performed, using IVIS Lumina system, on mice after injection of ICG loaded NPs, *PLGA-pD-LMWC and *PLGA-pD-PEG. Fluorescence signal was quantified throughout the 48 hour of the study (tumor tissue outlined), (b) Corresponding fluorescence signal (total radiance efficiency) of tumors after subtraction of background signal (signal prior to NP injection) and normalization to tumor weight (average \pm SD).	88
Figure 30: Fluorescence imaging and quantification of ICG content of extracted MCF-7 tumors and livers, (a) <i>Ex-vivo</i> fluorescence imaging of extracted organs at the end of the study, (b) Weight-normalized fluorescence signal of tumors and livers for LMWC and PEG coated NPs post ICG extraction, (c) Weight-normalized tumor/liver ratio of ICG fluorescence for LMWC and PEG coated NPs (average \pm SD , n=5, *p<0.05, **p<0.005, Two-tailed T-test).	89
Figure 31: Tracking of ICG loaded NPs in acidity-enhanced MCF-7 tumor models versus normal model, (a) Fluorescence signal (total radiance efficiency) of tumors after subtraction of background signal (signal prior to NP injection) and normalization to tumor weight, (b) Weight-normalized <i>ex-vivo</i> fluorescence signal of tumors and livers for LMWC and PEG coated NPs in both tumor models (averages \pm SD, n=3).	90

Figure	Page
Figure 32: PTX solubility in 0.2% Tween 80/PBS (a) and 50% FBS in PBS (b) was determined by incubating excess PTX in 1 mL of the medium at 37 °C for 7 and/or 24 h with agitation.	101
Figure 33: PTX solubility in 0.2% Tween 80/PBS (24 hr) (a) and 50% FBS in PBS (7 and 24 hr) (b) was determined by an alternative method. PTX was added to each medium in the amount indicated in the x-axis from a 10 mg/mL stock in DMSO. Samples were incubated for different times at 37 °C with agitation.....	101
Figure 34: Release kinetics of PTX/NPs in media containing PBS, FBS, or Tween 80. PTX/NPs equivalent to (a) 4.4 µg or (b) 27 µg of PTX were suspended in 1 mL of release medium and incubated at 37°C with constant agitation.	104
Figure 35: Mass balance after release kinetic studies of PTX/NPs in media containing PBS, FBS or Tween 80.	104
Figure 36: Plant derived phenolic and polyphenolic compounds investigated for formation of colorless multifunctional coatings (adapted from Sileika et al, 2013).	113
Figure 37: Particle size and surface charge of different NPs: (a) Particle size and polydispersity index, (b) Zeta potential of NPs in pH 7.4 phosphate buffer (average ±SD, n=4-5, Anova test, **p<0.005).	119
Figure 38: Suspension of PLGA NPs post coating with pD or TA (conventional method) showing the different colors of the coated NPs.	119
Figure 39: PLGA and PLGA-TA NPs (conventional method) post incubation in AgNO ₃ aqueous solution (17 mg/mL) overnight. TA presence is indicated by the darkening of NP suspension due to reduction of AgNO ₃ and deposition of metallic Ag (a). When visualized using TEM (1% PTA negative stain) (b), electron dense Ag can be seen depositing on PLGA-TA NP surface, but not on PLGA NPs.	120
Figure 40: Quantification of TA using BCA assay. (a) Calibration curve of TA in bicine buffer (pH 7.4, 0.1 M), (b) Consumption of TA in solution by PLGA coating. Decrease in absorbance post incubation of PLGA NPs for 3 hours in comparison to control (100% TA incubated for 3 hours in absence of NPs) was used to indirectly quantify amount of TA in	

Figure	Page
PLGA-TA NPs, (c) TA weight% per NP as determined by both direct and indirect methods (average \pm SD, Two-tailed T-test, * $p < 0.05$).....	121
Figure 41: FA was conjugated to PLGA-pD and PLGA-TA NPs. FA is a small molecule with a free amine group (a) (Adapted from Durate et al, 2015). Amount of FA conjugated to the surface in PLGA-pD-FA and PLGA-TA-FA NPs after NPs incubation in 15 μ g/mL solution of FA (b) (average \pm SD).	122
Figure 42: The functionalization of PLGA-TA NPs with human serum albumin: (a) The 3D structure of human serum albumin (Adapted from Abou-Zeid et al, 2013), (b) The particle size and polydispersity of PLGA-TA and PLGA-TA-Al NPs, (c) Zeta potential of the same NPs measured in phosphate buffer (pH 7.4) (average \pm SD, n=3-6, Two-tailed T-test, * $p < 0.05$).	123
Figure 43: Albumin content of PLGA-Al and PLGA-TA-Al represented as Albumin per NP w%. PLGA-TA-Al (average \pm SD, n=5-8, Two-tailed T-test, * $p < 0.05$).....	123
Figure 44: Transmission electron microscopy (TEM) images of PLGA-TA-Al NPs negatively stained with 2% uranyl acetate at low and high magnification levels (left and right images, respectively).....	124
Figure 45: Viability of NIH/3T3 fibroblasts after incubation with different concentrations (mg/mL) of PTX-free PLGA-TA or PLGA NPs for 72 hours as determined with MTT assay.....	125
Figure 46: Comparison of chemical and physical properties of different precursors (dopamine and TA), and the polymerized coatings they form. Circles in top panel point to catechol and trihydroxyphenyl groups of dopamine and TA. References: ¹ = (Park et al, 2014), ² = (Barette et al, 2014).....	127

LIST OF ABBREVIATIONS

ABC	Accelerated blood clearance
AUC	Analytical Ultracentrifugation
BCA	Bicinchoninic acid
CMC	Carboxymethylcellulose
DCM	Dichloromethane
DMSO	Dimethylsulfoxide
DOX	Doxorubicin
DPPC	Dipalmitoyl phosphatidylcholine
ECM	Extracellular matrix
EDC	1-Ethyl-3-(3-dimethylaminopropyl) carbodiimide
EPR	Enhanced Permeability and Retention
FA	Fluoresceinamine
FBS	Fetal bovine serum
FITC	Fluorescein isothiocyanate
HOBT	Hydroxybenzotriazole
HSA	Human Serum Albumin
ICG	Indocyanine green
IFP	Interstitial Fluid Pressure
IP	Intraperitoneal
LA:GA	Lactic acid: Glycolic acid
LbL	Layer-by-Layer
LE	Loading efficiency
LMWC	Low molecular weight chitosan

MIBG	<i>Meta</i> -iodo-benzylguanidine hemisulfate salt
MMP	Matrix metalloproteinase
MPs	Microparticles
MTT	(3-(4,5-Dimethylthiazol-2-yl)-2,5-diphenyltetrazolium bromide)
MTX	Methotrexate
NPs	Nanoparticles
PAMAM	Polyamidoamine
pD	Polydopamine
PDGF	Platelet-derived growth factor
PEG	Polyethylene glycol
pHLIP	pH low insertion peptide
PLGA	Poly(lactic-co-glycolic) acid
PTX	Paclitaxel
PVA	Polyvinyl alcohol
QD	Quantum dot
RES	Reticuloendothelial system
ROS	Reactive oxygen species
SDS	Sodium dodecylsulfate
TA	Tannic acid
TEMED	Tetramethylethylenediamine
VEGF	Vascular endothelial growth factor
XPS	X-ray photoelectron spectroscopy

ABSTRACT

Ahmed, Sara. Ph.D., Purdue University, December 2015. Drug Delivery to Solid Tumors via Polymeric Nanoparticles. Major Professor: Yoon Yeo.

A main challenge in chemotherapy is to deliver an anti-cancer drug selectively to tumor and avoid off-target exposure to other body tissues and organs. Nanoparticles (NPs) have been considered a promising approach for tumor drug delivery, with popularity attributable to the famous “Enhanced Permeability and Retention effect”, where small particles enter tumor tissues through leaky vasculature and be retained there. Currently, the phagocytic clearance of NPs is avoided by coating NP surface with Polyethylene glycol (PEG). Although successful in prolonging NPs circulation, PEG prevents proper interaction of NPs with the target cells, known as “PEG dilemma”. Low molecular weight chitosan (LMWC) can function as a hydrophilic pH-sensitive alternative stealth coating for NPs. The LMWC-coated NPs were previously made with a conjugate of poly(lactide-co-glycolic) acid (PLGA) and LMWC (PLGA-LMWC) and showed pH-sensitive surface charge. However, this preparation method has disadvantages such as production complexity and difficulty in drug encapsulation. We used an alternative surface modification method based on dopamine polymerization, which formed a layer of polydopamine (pD) on NP surface allowing for conjugation of LMWC to the preformed NP cores. When compared to PLGA-LMWC NPs, PLGA-pD-LMWC NPs had superior control over drug release. Additionally, obtained PLGA-pD-LMWC NPs had similar cellular interactions to that of PLGA-LMWC NPs, achieving cellular uptake in cancer cells under mildly acidic conditions, which was not achieved with PEG coated NPs. However, when tested *in vivo*, there was no significant difference between LMWC and PEG-coated NPs in terms of tumor growth suppression and tumor accumulation. While the exact reason

Additionally, the use of tannic acid (TA) as an alternative functionalizing coating material for polymeric NPs was investigated. In a preliminary study, TA helped functionalize PLGA NPs with small ligands (FA) or macromolecules (albumin). Considering the strong interactions of TA with different macromolecules (e.g. proteins and nucleic acids), TA is hypothesized to be an ideal coating material to functionalize NPs for drug delivery applications. However, the stability of the coating in physiological conditions is yet to be investigated.

CHAPTER 1. INTRODUCTION ON DELIVERY OF NANOPARTICLES TO TUMORS

1.1 Nanoparticles in Chemotherapy

Most chemotherapeutic agents are low molecular weight compounds with large volumes of distribution (Bharali et al., 2009). These molecules are typically administered as intravenous (IV) injection and spread in the whole body; therefore, the dose administered to achieve effective concentrations in tumors also affects healthy tissues and organs, resulting in adverse side effects (Banerjee & Sengupta, 2011; Bharali et al., 2009). For example, taxanes (paclitaxel and docetaxel) are associated with bone marrow suppression, alopecia and hypersensitivity (Markman, 2003), and anthracyclines like doxorubicin and epirubicin are known to cause severe cardiotoxicity (Raschi et al., 2010). Cisplatin, a potent metal-based anticancer drug, is also implicated with nephrotoxicity and neurotoxicity (Cerri et al., 2011). In addition, many anticancer drugs have poor water solubility, necessitating the use of toxic solubilizers. For example, paclitaxel is formulated in a vehicle composed of ethanol and ethoxylated castor oil (Cremophor EL) (Hawkins et al., 2008), where the latter causes severe side effects such as hypersensitivity and neuropathy (Gelderblom et al., 2001; Kwon, 2003; ten Tije et al., 2003). Similarly, docetaxel is formulated with Polysorbate 80 as a solubilizer, which has comparable side effects (Hawkins et al., 2008). The toxicity of active and inactive ingredients has significant impact on the clinical outcomes, including poor patient quality of life, limited therapeutic options, and early dropouts from treatment in extreme cases (Stam & Challis, 1989).

In order to maximize therapeutic outcomes of chemotherapy, it is critical to deliver anticancer agents using formulations with minimal toxicity and concentrate the effect of drugs to tumors without harming healthy tissues. To achieve this goal, nanoparticles (NPs) with a diameter in the range of 10-100 nm have long been pursued as a drug carrier. In 1995, the U.S. Food and Drug Administration (US FDA) approved *Doxil*[®], doxorubicin sulfate loaded in long-circulating liposomes, for treatment of AIDS-associated Kaposi sarcoma and later for metastatic ovarian cancer and breast cancer (Barenholz, 2012). The liposomal formulation contributed to reducing cardiotoxicity of doxorubicin (Barenholz, 2012) and has been used for the delivery of other drugs, such as vincristine (*Marqibo*[®]), cytarabine (*DepoCyte*[®]) and daunorubicin (*DaunoXome*[®]) (Venditto & Szoka, 2013). In 2005, albumin-bound paclitaxel (*nab*-paclitaxel or *Abraxane*[®]), a solvent-free NP formulation with an average diameter of 130 nm, was approved by the US FDA, eliminating the previously mentioned side effects caused by Cremophor EL (M. R. Green et al., 2006; Hawkins et al., 2008).

An important role of NP drug delivery systems is to modulate pharmacokinetics and biodistribution of a drug (Blanco et al., 2011). **Figure 1** describes biodistribution of IV injected NPs and their transport pathway to tumors. Compared to low molecular weight drugs, NPs have relatively selective opportunity to access solid tumors due to the unique features of tumor vasculature. Due to the increasing nutritional demands, proliferating tumors rapidly recruit new blood vessels (angiogenesis) (Kerbel, 2000). The formed vessels are structurally and functionally abnormal, with excessive branching and hyperpermeable epithelial lining (Baish & Jain, 2000; Peter Vaupel Md, 2009). The leakiness of blood vessels in tumors allows for extravasation of blood-borne macromolecules including NPs, which would not readily leave capillaries in normal tissues (Matsumura & Maeda, 1986b). In addition, lymphatic drainage near tumors is not fully functional and, thus, allows for longer retention of the extravasated NPs in the interstitial space of tumors. This phenomenon, collectively called the Enhanced Permeability and Retention (EPR) effect (Maeda et al., 2001; Matsumura & Maeda, 1986a; V. Torchilin, 2011), has been the most pronounced principle in tumor-targeted drug delivery using NPs. To take advantage of the EPR effect, particle size and surface chemistry are modified to

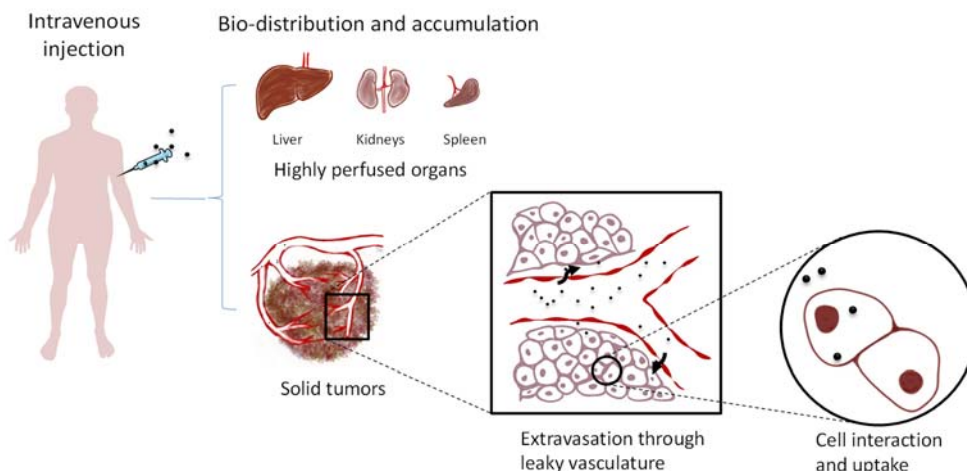


Figure 1: Biodistribution of intravenously injected NPs and their transport pathway to solid tumors.

ensure long-term circulation in the blood. To further enhance drug delivery to tumor cells and intracellular targets, NPs can be modified with surface ligands that interact with membrane proteins with a high degree of specificity. Several other variables also influence the fate and drug delivery efficiency of NPs in the body.

1.2 Factors Affecting the Effectiveness of NP Drug Delivery Systems

An ideal NP system should incorporate specific functions to combat biological challenges during circulation and provide target-specific drug release. **Figure 2** summarizes several features to be considered in designing NP drug carriers for systemic applications. This section discusses how each property of NPs influences its effectiveness as a drug carrier.

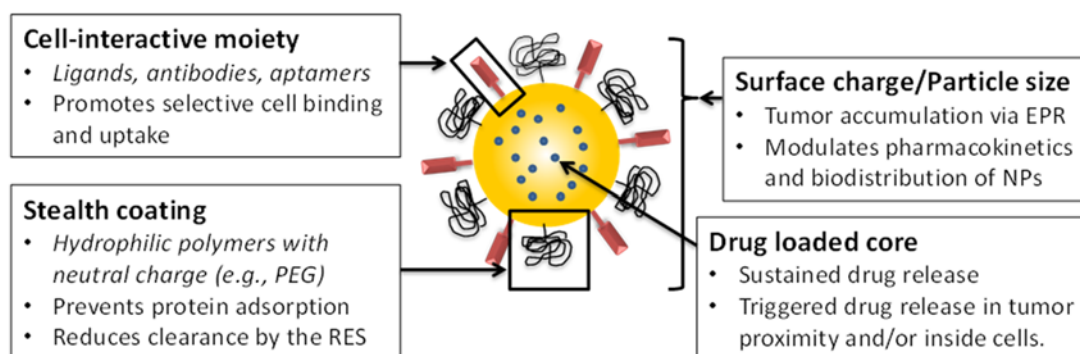


Figure 2: A typical design of NPs as drug carriers for systemic delivery of chemotherapeutics.

1.2.1 Biocompatibility

An inactive ingredient of a NP (the material that constitutes the NP structure) and its degradation products are expected to have no biological effects that will influence therapy. NPs are built with biocompatible biomaterials of natural and synthetic origin (Amoozgar et al., 2012; M. Green et al., 2006; Ramishetti & Huang, 2012; Vivek et al., 2013). Natural materials include lipids (Barenholz, 2012), polysaccharides (Amoozgar et al., 2012), and proteins (S. Jain et al., 2011). Lipid-based NPs include liposomes (vesicles composed of bilayers of phospholipids) and solid lipid NPs (solid lipid matrices containing different glycerides) (Puri et al., 2009). Polysaccharides such as chitosan, alginate, and hyaluronic acid are also used in preparation of NPs (Doh & Yeo, 2012; Jee et al., 2012; Z. H. Liu et al., 2008). NPs of synthetic origin include polymeric solid NPs, polymeric micelles and dendrimers (Cho et al., 2008). Poly(lactic-co-glycolic acid) (PLGA) and polylactic acid (PLA) have commonly been used due to the biodegradability and excellent track records in FDA-approved products (R. A. Jain, 2000). Polymeric dendrimers are also pursued as a drug carrier due to the functionalization potential. Amine-terminated dendrimers are found to have a hemolytic effect (Domanski et al., 2004); however, the terminal groups can be altered with anionic functional groups to lower the toxicity (Malik et al., 2000).

1.2.2 Particle Size

Ideally, NPs should be larger than 10 nm to avoid renal filtration during circulation (Venturoli & Rippe, 2005) but smaller than the cutoff size of the pores in tumor vessels, which ranges from 100 to 600 nm, to extravasate and reach tumors (Yuan et al., 1995). It is generally believed that particles larger than 10 nm and smaller than 100 nm will be optimal for avoiding renal clearance and extravasation at tumors, respectively, although NPs of this size range will still enter the liver through the sinusoid (Davis et al., 2008). Particle size is also an important determinant of NP penetration into the tumor interstitium. Reports show that smaller particles (20-60 nm) can penetrate deeper into the tumor matrix than larger particles (100-200 nm), which tend to stay close to blood vessels (Goodman et al., 2008; H. Lee et al., 2010; Perrault et al., 2009).

1.2.3 Particle Surface Charge

Colloidal stability of NPs is largely dependent on their surface charge. Highly charged NPs repel each other in solution, lowering the possibility of flocculation and aggregation during storage (Heurtault et al., 2003). The cell-NP interaction is also influenced by the NP surface charge (Nel et al., 2009). Positively charged NPs bind via electrostatic interactions to the cell membrane, which is negatively charged due to lipid components. In addition, NP surface charge influences the degree of protein adsorption and the type of the adsorbed proteins (Hirsch et al., 2013; Lundqvist et al., 2008; S. Patil et al., 2007).

One study reports that the extent of quaternary ammonium groups on the surface of silica NPs dictates their cellular internalization mechanisms. For example, mesoporous silica NPs with low or no quaternary ammonium groups (0-0.98 mmol/g) were taken up by human mesenchymal stem cells via clathrin- and actin-dependent endocytosis (T. H. Chung et al., 2007). On the other hand, silica NPs with higher quaternary ammonium content (1.7 mmol/g) were taken up efficiently, not influenced by the inhibitors of cellular uptake mechanisms (T. H. Chung et al., 2007). Highly charged micelles, irrespective of the charge, showed high liver uptake, due to phagocytosis by Kupffer cells (Xiao et al., 2011). In contrast, less charged micelles of the same particle size showed relatively low liver uptake due to the reduced protein binding (Xiao et al., 2011). Similar findings were reported with polymeric NPs (C. B. He et al., 2010).

1.2.4 Circulation Half-life

The body immune system reacts to foreign particles introduced into the blood stream. As NPs enter the circulation, plasma proteins rapidly adsorb to the surface, a process called 'opsonization', followed by macrophage uptake. Therefore, NPs that are readily opsonized in blood end up in the reticuloendothelial system (RES) such as the liver and spleen before they reach the target tissues (Jokerst et al., 2011b; Walkey & Chan, 2012). For NPs to avoid premature clearance, they must hide surface properties prone to opsonization, such as high charge density and hydrophobicity. For this purpose, NP surface is modified with hydrophilic and electrically neutral polymers such as polyethylene glycol

(PEG). Surface modification with PEG stabilizes the NPs sterically and reduces adsorption of plasma proteins, thereby extending the circulation half-life of the NPs (Senior et al., 1991; V. P. Torchilin et al., 1994). In addition to PEG, other hydrophilic materials such as polysaccharides and synthetic polymers are used for similar purposes (Amoozgar et al., 2012; Doh & Yeo, 2012; Tan et al., 1993).

For optimization of the stealth effect, molecular weight, grafting density, and conformation of the surface polymers need to be carefully chosen (Gref et al., 2000). It was shown with polymeric NPs (Gref et al., 1994), liposomes (Mori et al., 1991), and quantum dots (Daou et al., 2009) that their circulation times increased with the molecular weight of PEG when all other factors are comparable. On the other hand, silica NPs showed the least protein adsorption and phagocytosis when coated with 10 kD PEG as compared to 4, 6 or 20 kDa PEG (Q. J. He et al., 2010). In Doxil[®] liposomes, ~5 mol% PEG was found optimal for the stealth effect (S. D. Li & Huang, 2010). Depending on the surface density, PEG can acquire two conformations, a *mushroom-like* or a denser *brush* conformation (Jokerst et al., 2011a). The brush conformation, obtained at >8 mol%, is believed to coat the surface of the NPs completely, providing the best protection and enhancement of circulation time (Jokerst et al., 2011b; S. D. Li & Huang, 2010; Perry et al., 2012), while the mushroom-like conformation provides a PEG layer that does not extend far from the NPs surface (Perry et al., 2012). However, excessive PEG content is not always helpful at least for liposomes, as the integrity of membrane can be compromised by the detergent effect of PEG-lipid conjugates (S. D. Li & Huang, 2010) or the lateral repulsion of PEG chains (Tirosh et al., 1998). At comparable surface density of PEG, the stealth effect is influenced by the size of particles covered with PEG. Chen et al compared serum protein adsorption to gold NPs with a diameter in 15-90 nm range varying the PEG surface density and found that at an equal PEG density, 15 nm NPs showed the greatest protein adsorption, due to the relatively large curvature that gave a greater steric freedom to each PEG molecule (Walkey et al., 2012).

1.2.5 Tumor Retention and Cellular Uptake

Once NPs arrive at tumors after long-term circulation and extravasation via the leaky vasculature, their interactions with target cells play an important role in exerting

therapeutic effect on the cells. PEGylation interferes with NP-cell interactions (Hatakeyama et al., 2011b); thus, it is often necessary to functionalize NP surfaces to improve their tumor localization and retention. As a result of the small particle size, NPs have a relatively high surface area per volume, which serves as a substrate for conjugating different ligands. Monoclonal antibodies can be used as a ligand to decorate NPs, which reacts with specific antigens located on tumor cells (Kohler & Milstein, 1975). Many other receptors over-expressed on tumor cells compared to normal ones, such as transferrin (Hatakeyama et al., 2004), folate (R. J. Lee & Low, 1994), and biotin (Na et al., 2003) receptors, have been exploited to enhance NP-cell interactions and retention in tumors.

1.2.6 Drug Release

Ideal NPs should release the drug in a controlled manner at tumor tissues rather than in blood. However, due to the large surface area per volume, the loaded drug tends to leach out by diffusion, leading to premature drug release during circulation (Chen et al., 2008; de Smet et al., 2011). Given that it typically takes 24-48 hours for circulating NPs to achieve tumor accumulation via the EPR effect (Iyer et al., 2006), it is critical to minimize drug release from NPs in blood during this period. On the other hand, if the drug is retained in NPs too well, its therapeutic effect is also diminished. For example, daunorubicin entrapped in polymeric NPs had the IC_{50} value of 2.05 $\mu\text{g/mL}$ as opposed to 0.37 $\mu\text{g/mL}$ of free drug in HL-60 cells after 24 hours incubation (J. Liu et al., 2010). Therefore, an ideal NP should have a built-in mechanism to trigger drug release in a timely manner at the intended targets, whether they are extracellular matrix or intracellular organelles.

Another consequence of the increased nutritional demands is the formation of new blood vessels. This is mediated by the release of different angiogenic factors from tumor cells such as vascular endothelial growth factor (VEGF) and platelet-derived growth factor (PDGF) (Folkman, 1974; Gasparini et al., 2005; Harper & Moses, 2006; Malonne et al., 1999; Pietras et al., 2002). The formed blood vessels are hyperpermeable to circulating macromolecules, which results in increase of osmotic pressure and influx of interstitial fluid, and, thus, interstitial fluid pressure (IFP) (Boucher et al., 1996; Heldin et al., 2004). High IFP represents a physical barrier to mass transport into the tumors, resulting in poor and heterogeneous distribution of drugs and radiation (Curti, 1993; Hompland et al., 2012; R. K. Jain, 1998; Milosevic et al., 1998; Roh et al., 1991; Rutz, 1999) as well as intratumoral delivery of NPs (Holback & Yeo, 2011).

The difficulty in cancer therapy is aggravated by the heterogeneity of tumors. *Inter-tumoral* heterogeneity refers to antigenic, immunogenic and metabolic properties of different tumors, which account for differences in drug resistance, growth rate, and metastatic capabilities. Such variability also exists at the level of a single tumor mass, causing *intra-tumoral* heterogeneity in cell morphology, phenotype, and metabolism (I. Fidler, 1978; I. J. Fidler & Hart, 1982; Gerlinger et al., 2012; A. Marusyk & K. Polyak, 2010; Shibata, 2012). Tumor heterogeneity is a significant challenge to chemotherapy as it can lead to selection of drug-resistant cell types and relapse of drug-resistant tumors (Andriy Marusyk & Kornelia Polyak, 2010). The diversity and genetic instability of tumors also account for, at least partly, the difficulty in advancing NPs with a single type of ligand to clinical practice.

Consequently, many have hypothesized that drug delivery to tumors can be improved by alleviating these physiological barrier properties of tumors. Auxiliary agents have been used to increase tumoral blood flow (e.g. Angiotensin), normalize blood vessels (e.g. anti-VEGF antibodies), or reduce stromal barriers (e.g., paclitaxel, hyaluronidase), thereby enhancing drug or NP penetration into tumors (Eikenes et al., 2005; Holback & Yeo, 2011; Marcucci & Corti, 2012). Radiation is also used to improve intratumoral drug delivery. In addition to its standard use as a standalone cancer therapy, radiation can help increase NPs tumor accumulation by decreasing IFP and increasing vascular permeability

(Giustini et al., 2012). A single dose of 15-Gy radiation decreased IFP by ~40% over a period of 5 days and vascular permeability by 60% (Giustini et al., 2012). When PEGylated iron oxide NPs were injected 3 days post irradiation, their accumulation increased by 2.5 folds

1.3 Remaining Challenges in NP Development

After decades of research on nanomedicines for chemotherapy, several nanomedicines have been approved by various regulatory bodies, and dozens of clinical trials are currently ongoing (**Table 1**) (R. B. Wang et al., 2013). However, NPs have limitations in overcoming biological challenges imposed by the complexity of tumor physiology. Several challenges also remain in formulation development.

1.3.1 Tumor Physiology

A growing tumor goes through a dormant primary phase where it directly obtains essential nutrients and oxygen from the environment, followed by a characteristic rapid growth phase in both size and demand for nutrition and oxygen. One consequence of rapid tumor growth is hypoxia, which leads to upregulation of hypoxia-induced factor 1 (HIF-1), responsible for alteration of metabolism and extracellular microenvironment of tumors (Tannock & Rotin, 1989; Tian & Bae, 2012a; Vaupel et al., 1981; Wike-Hooley et al., 1984). The microenvironmental changes influence different biochemical processes in cells, making them resistant to chemo- and radiation therapy (Tannock & Rotin, 1989; Vaupel et al., 1981; Wike-Hooley et al., 1984). For example, the increasing acidity of tumor interstitium can change cell membrane fluidity and reduce active drug uptake (Wike-Hooley et al., 1984). Another consequence of the increased nutritional demands is the formation of new blood vessels. This is mediated by the release of different angiogenic factors from tumor cells such as vascular endothelial growth factor (VEGF) and platelet-derived growth factor (PDGF) (Folkman, 1974; Gasparini et al., 2005; Harper & Moses, 2006; Malonne et al., 1999; Pietras et al., 2002).

Table 1: Some nanomedicinal formulations approved or undergoing clinical trials.

Commercial name	Manufacturer	NP type	Drug	Status	Ref.
Abraxane	Celgene	Albumin NPs (<i>nab</i> technology)	Paclitaxel	Approved	(M. R. Green et al., 2006)
Doxil/Caelyx	Ortho Biotech Schering-Plough	PEGylated liposomes	Doxorubicin	Approved	(Barenholz, 2012)
DepoCyte	Skye Pharma	Liposomes	Cytarabine	Approved	(Slingerland et al., 2012)
Marqibo	Talon Therapeutics, Inc.	Liposomes	Vincristine	Approved	(Silverman & Deitcher, 2013)
DaunoXome	Galen Ltd.	Liposomes	Daunorubicin	Approved	(Forssen, 1997)
Myocet	Cephalon	Liposomes	Doxorubicin	Approved	(R. B. Wang et al., 2013)
ThermoDox	Celsion	Heat activated liposomes	Doxorubicin	Phase III	(Landon et al., 2011)
Lipoplatin	Regulon Inc.	PEGylated Liposomes	Cisplatin	Phase III	(Stathopoulos et al., 2011)
OSI-211	OSI Pharmaceuticals	Liposomes	Lurtotecan	Phase II	(Duffaud et al., 2004)
Lipo-Dox	TTY Biopharm Co. Ltd.	PEGylated liposomes	Doxorubicin	Phase II	(Chou et al., 2006)
NK-105	Nippon Kayaku Co. Ltd	Polymeric NPs	Paclitaxel	Phase II	(K. Kato et al., 2012; R. B. Wang et al., 2013)
CRLX101	Cerulean Pharma	Cyclodextrin polymeric NPs	Camptothecin	Phase II	(Ng et al., 2013; R. B. Wang et al., 2013)
BIND-014	BIND Bioscience	Polymeric NPs	Docetaxel	Phase I	(Hrkach et al., 2012)
MBP-426	Mebiopharm	Liposomes	Oxaliplatin	Phase I	(Sankhala et al., 2009)
CPX-1	Celator Pharmaceuticals	Liposomes	Irinotecan and floxuridine	Phase I	(Batist et al., 2009)

The formed blood vessels are hyperpermeable to circulating macromolecules, which results in increase of osmotic pressure and influx of interstitial fluid, and, thus, interstitial fluid pressure (IFP) (Boucher et al., 1996; Heldin et al., 2004). High IFP

represents a physical barrier to mass transport into the tumors, resulting in poor and heterogeneous distribution of drugs and radiation (Curti, 1993; Hompland et al., 2012; R. K. Jain, 1998; Milosevic et al., 1998; Roh et al., 1991; Rutz, 1999) as well as intratumoral delivery of NPs (Holback & Yeo, 2011).

The difficulty in cancer therapy is aggravated by the heterogeneity of tumors. *Inter-tumoral* heterogeneity refers to antigenic, immunogenic and metabolic properties of different tumors, which account for differences in drug resistance, growth rate, and metastatic capabilities. Such variability also exists at the level of a single tumor mass, causing *intra-tumoral* heterogeneity in cell morphology, phenotype, and metabolism (I. Fidler, 1978; I. J. Fidler & Hart, 1982; Gerlinger et al., 2012; A. Marusyk & K. Polyak, 2010; Shibata, 2012). Tumor heterogeneity is a significant challenge to chemotherapy as it can lead to selection of drug-resistant cell types and relapse of drug-resistant tumors (Andriy Marusyk & Kornelia Polyak, 2010). The diversity and genetic instability of tumors also account for, at least partly, the difficulty in advancing NPs with a single type of ligand to clinical practice. Consequently, many have hypothesized that drug delivery to tumors can be improved by alleviating these physiological barrier properties of tumors. Auxiliary agents have been used to increase tumoral blood flow (e.g. Angiotensin), normalize blood vessels (e.g. anti-VEGF antibodies), or reduce stromal barriers (e.g., paclitaxel, hyaluronidase), thereby enhancing drug or NP penetration into tumors (Eikenes et al., 2005; Holback & Yeo, 2011; Marcucci & Corti, 2012). Radiation is also used to improve intratumoral drug delivery. In addition to its standard use as a standalone cancer therapy, radiation can help increase NPs tumor accumulation by decreasing IFP and increasing vascular permeability (Giustini et al., 2012; Znati et al., 1996). A single dose of 15-Gy radiation decreased IFP by ~40% over a period of 5 days and vascular permeability by 60% (Giustini et al., 2012). When PEGylated iron oxide NPs were injected 3 days post irradiation, their accumulation increased by 2.5 folds (Giustini et al., 2012).

1.3.2 Formulation Challenges

1.3.2.1 'PEG Dilemma'

As mentioned previously, surface PEGylation contributes to increasing blood circulation time of NPs by helping NPs avoid non-specific interactions with immune cells during circulation. However, upon arrival of NPs at tumors, the same effect interferes with NP interaction with target cells and subsequent cellular internalization. Moreover, PEG interferes with the endosomal escape of NPs, leading to lysosomal degradation of the therapeutic payload (Amoozgar & Yeo, 2012; Du et al., 1997; Hatakeyama et al., 2011a). This phenomenon, known as 'PEG dilemma', has prompted many researchers to revisit the routine use of PEG as the stealth polymer of choice and pursue alternative options (Amoozgar & Yeo, 2012; Doh & Yeo, 2012). Immune responses to PEG are also reported. PEGylated liposomes showed a decrease in circulation half-life upon subsequent administrations (Dams et al., 2000). This was explained by the formation of anti-PEG-IgM at the first introduction of PEGylated liposomes, followed by activation of the complement system, ending in accelerated blood clearance (ABC) of the subsequent doses (Immordino et al., 2006; X. Y. Wang et al., 2007). Anti-PEG antibodies were detected in 22-25% of human blood donors without known prior PEG exposure, which means that PEGylated drug carriers are less likely to be effective in these individuals (Armstrong, 2009; Garay et al., 2012).

Several approaches have been pursued to overcome the limitations of PEG as stealth coating. To achieve the stealth effect of PEGylation without compromising proper interaction between target cells and NPs, removable PEG coatings have been proposed. In this approach, PEG chains are conjugated to the NP surface via stimuli-sensitive linkers that can be cleaved by chemical or enzymatic conditions specific to the tumor ECM or the intracellular environment (Amoozgar & Yeo, 2012). For example, acid-labile linkers, such as hydrazone, diorthoester and vinyl ether bonds (Romberg et al., 2008; Sawant et al., 2006), were used to take advantage of slightly acidic pH of tumor stroma (Tannock & Rotin, 1989) or lysosomes (R. Cheng et al., 2013). Difference in redox potential between the extracellular and intracellular matrices is another stimulus employed

to remove the PEG layer in an environment-specific manner. Molecules with sulfhydryl group are concentrated inside the cell (Arner & Holmgren, 2000). In particular, glutathione is present in mM range in the cytosol, while its extracellular concentration is as low as ~10 μM (Arner & Holmgren, 2000; Saito et al., 2003). Therefore, reduction-sensitive disulfide bond can remain stable in blood and be reduced at cell surface and in the cells (Romberg et al., 2008; Sun et al., 2009). Another reduction-sensitive linker is dithiobenzyl carbamate, which is sensitive to milder thiolytic conditions (Zalipsky et al., 1999). This linker was used to conjugate PEG to distearoylphosphatidylethanolamine (DSPE), forming reduction-sensitive liposomes (Zalipsky et al., 1999). The NPs with removable PEG are additionally modified with cell-interactive ligands such as TAT peptide (Gullotti et al., 2013a) and galactose (Zhong et al., 2013) so that NPs can be readily taken up by cells after the removal of stealth polymer.

In addition, several hydrophilic polymers, including polysaccharides (Amoozgar et al., 2012; Doh & Yeo, 2012), poly(amino acids) (Romberg et al., 2007), and polyoxazolines (Zalipsky et al., 1996), have been pursued as alternative stealth coating materials. Polysaccharides, such as chitosan (Amoozgar et al., 2012), heparin, and dextran (Passirani et al., 1998), are biodegradable and biocompatible. Poly(amino acids) are degraded by lysosomal proteases (Romberg et al., 2007). Examples are poly(hydroxyethyl L-asparagine) and poly(hydroxyethyl L-glutamine) (Metselaar et al., 2003). Poly(amino acid)-coated liposomes showed a long circulation time comparable to that of PEG (Romberg et al., 2007). Mucin is another stealth coating inspired by cell surface glycoproteins, which can avoid the RES uptake but maintain specific cellular recognition (Thasneem et al., 2013).

1.3.2.2 Maintaining Particle Size

Nanometric particle size is one of the most fundamental properties that determine the biodistribution and pharmacokinetics of NPs. However, NPs do not necessarily maintain the particle size as the 'factory setting' during circulation. Abraxane[®], albumin-bound paclitaxel NPs with an average diameter of 130 nm, improves water solubility of paclitaxel, eliminates the surfactant-related hypersensitivity and the need for pretreatment

with antihistamines and steroids, and enables dose administration in a much shorter infusion time (M. R. Green et al., 2006; Hawkins et al., 2008). However, Abraxane breaks down to paclitaxel-albumin molecules during circulation (Desai, 2008), which do not fully leverage the benefits of the EPR effect (Ernsting et al., 2012).

Conversely, liposomal systems are thermodynamically unstable and prone to aggregation and/or fusion (Evans & Metcalfe, 1984), especially in plasma (Yoshioka, 1991). Therefore, designing liposomes for systemic drug delivery requires a formulation strategy to stabilize the membrane. Liposomal stability can be improved by inclusion of cholesterol and phospholipids with high phase transition temperature, which increase rigidity of the bilayer (Demel & De Kruffy, 1976; A Gabizon & Papahadjopoulos, 1988; A. Gabizon et al., 2003; Semple et al., 1996). Additionally, liposomes can be stabilized with hydrophilic polymers. PEG is most widely used (Yoshioka, 1991), but other polymers are also reported. For example, dipalmitoyl phosphatidylcholine (DPPC) liposomes coated with chitosan showed greater resistance to detergent treatment (Mady et al., 2009). Liposomes stabilized with alkylated polyvinyl alcohol (PVA) were resistant to serum-induced aggregation and/or fusion, as compared to uncoated liposomes, which showed 10-fold particle size increase after incubation in calf serum (Takeuchi et al., 1998). Recent studies propose decoration of liposomal surfaces with small, charged NPs to stabilize the lipid bilayer (Michel et al., 2013; Zhang & Granick, 2006). Liposomes based on DPPC, ~100 nm in diameter, were coated with negatively charged ~8 nm silica NPs (Michel et al., 2013). The silica NPs provided a concentration-dependent stabilizing effect and helped inhibit liposomal aggregation in water for more than 800 hours (Michel et al., 2013). In the absence of silica NPs, the liposomes's size increases dramatically over 400 hours. A potential advantage of this method, as compared to traditional polymer coatings, is that the stabilizing component occupies relatively little NP surface area, leaving a substantial portion of surface available for functionalization (Zhang & Granick, 2006).

1.3.2.3 Controlling Drug Release

Spatiotemporal control of drug release is another fundamental feature of NPs as a drug carrier. A number of NP designs are predicated on the assumption that a NP

will retain a drug during circulation until it reaches the target cells. Otherwise, the therapeutic effect of NPs may not be different from that of the free drug (Gullotti & Yeo, 2012). However, initial burst release occurs in almost all types of delivery systems, especially in NPs with relatively large surface areas per volume ratios (Bae & Yin, 2008; Dai et al., 2011; Hasan et al., 2007; Yeo & Park, 2004). Therefore, various efforts are made to ensure stable drug retention in NPs in blood. At the same time, stimuli-responsive systems are pursued in parallel to make the carried drugs available at target locations in a timely manner.

Incorporating a diffusion barrier on NP surface. To prevent the initial burst release and provide sustained drug release, a self-assembled layer of water-insoluble material is added as a diffusion barrier. For example, a lecithin layer was used to coat a PLGA core encapsulating docetaxel, resulting in a hybrid polymer-lipid NP with an attenuated docetaxel release as compared to bare NPs (Zhang et al., 2008). Similarly, the release of doxorubicin entrapped in PLGA core was suppressed with an external layer of diethylenetriaminepentaacetic acid (DTPA)-gadolinium lipid, which also served as a paramagnetic image contrast agent (Liao et al., 2011).

Crosslinking. Parts of a NP can be crosslinked to improve the stability of self-assembled NP structures. Polymeric micelles are prone to disassembly and dissociation upon introduction into the blood stream due to interactions with amphiphilic blood components and dilution below their critical micelle concentrations (Deng et al., 2012). Burt et al studied biodistribution of polymeric micelles based on a block co-polymer of D,L-lactic acid and methoxypolyethylene glycol (PDLLA-MePEG) encapsulating paclitaxel (Burt et al., 1999). They reported that the drug and polymer showed distinct biodistribution profiles, indicating premature drug release and micelle dissociation (Burt et al., 1999). The stability of polymeric micelles can be improved by crosslinking of the core, shell or the interface (Deng et al., 2012). One approach is to crosslink the micelle core made of anionic polymethacrylate via metal cations such as Ca^{2+} (Bronich et al., 2005). In another example, the PLA core of a polymeric micelle was stabilized by introducing methacrylol end groups at the terminus of the PLA block, which could be covalently crosslinked after micelle formation (Iijima et al., 1999). These micelles had high stability even in presence of

surfactants (Iijima et al., 1999). Instead of NP core, the interface between hydrophilic shell and hydrophobic core was stabilized via crosslinking mediated by UV irradiation (Yang et al., 2011). For this purpose, photocrosslinkable polymer, poly(acryloyl carbonate), was introduced as the center block of a block co-polymer. Thus formed PEG-poly(acryloyl carbonate)-polycaprolactone (PEG-PAC-PCL) formed more stable micelles in both size and drug retention as compared to those made with non-crosslinkable counterpart (PEG-PCL) (Yang et al., 2011). Due to the improved stability, paclitaxel loaded in the photocrosslinked PEG-PAC-PCL micelles showed greater *in vivo* tumor inhibition activity than paclitaxel in PEG-PCL micelles (Yang et al., 2011).

Stimuli-responsive systems. To confine drug release specifically to target tissues or organelles, stimuli-responsive NPs are developed. NPs are designed to change their physicochemical properties in response to intrinsic conditions of target locations (more details in section 1.4) or external stimuli focused on the targets (R. Cheng et al., 2013). For example, a drug was encapsulated in mesoporous silica NPs, capped with large molecules, such as cadmium sulfide (CdS) nanocrystals (Lai et al., 2003) or PAMAM dendrimers (Gruenhagen et al., 2005) via disulfide bond. These capping materials prevented drug release but were removed in a reductive environment inside the cell. In another example, reduction-sensitive NPs encapsulating doxorubicin were prepared with dextran-lipoic acid derivative crosslinked via disulfide bonds (Y. L. Li et al., 2009). This system showed minimal drug release under extracellular condition and fast release in reductive environments, verified with *in vitro* release experiments (Y. L. Li et al., 2009). Similarly, cathepsin B, a lysosomal cysteine proteinase, was used to trigger drug release from NPs in the lysosomes (Meng et al., 2012). Cathepsin B is also overexpressed in some tumor cells, present in the extracellular environment and on the cell surface of tumors (Campo et al., 1994; Sloane, 1990). Therefore, a peptide linker specifically degraded by cathepsin B was incorporated in a PEG NP system via photocrosslinkable diacrylate for tumor selective drug release (Glangchai et al., 2008b). Matrix metalloproteinases (MMPs), another type of enzymes over-expressed in tumor microenvironment, are also used for controlling drug release (Danhier et al., 2010). Doxorubicin was loaded in mesoporous silica NPs, coated with conjugates of PEG diacrylate and MMP-degradable peptides with different

sensitivities (Singh et al., 2011). Drug release and cytotoxicity of doxorubicin-loaded NPs were proportional to degradability of the peptide linker, and the MMP-sensitive NPs resulted in greater cell death in MMP-overexpressing tumors as compared to MMP-insensitive PEG-coated NPs (Singh et al., 2011). Acidic pH of endo/lysosomes is frequently used to achieve intracellular drug release. Mesoporous silica NPs were capped with calcium phosphate, soluble in pH 4-5 but insoluble in pH 7.4. To limit the calcium phosphate deposition on the surface, the silica NPs were conjugated with urease, which hydrolyzed urea and created a high pH zone around the NPs forming a layer of calcium phosphate (Rim et al., 2011). The coated NPs significantly attenuated drug release at pH 7.4 but released drug intracellularly, indicated by sustained nuclear localization of doxorubicin (Rim et al., 2011).

Multiple-stimuli responsive systems. To increase the selective reactivity of the NPs, two or more mechanisms are utilized either simultaneously or sequentially. NPs are engineered to respond to dual stimuli, such as pH and temperature, pH and reductive potential, or temperature and enzyme (R. Cheng et al., 2013; Dai et al., 2011; Sankaranarayanan et al., 2010). For example, polymeric NPs with a dual pH-sensitivity were formulated using a random co-polymer that degraded via both bulk dissolution and surface degradation at weakly acidic pH (Sankaranarayanan et al., 2010). The advantage of this system is the good stability at physiological pH and quick onset of degradation, which are often conflicting with each other (Sankaranarayanan et al., 2010). In another study, polymeric micelles dual-responsive to acidic endosomal pH and intracellular reductive potential were prepared using a tri-block copolymer made of a pH-sensitive hydrophobic block, disulfide-crosslinkable middle block, and PEG (Dai et al., 2011). This micelle system showed minimal drug release at pH 7.4 and increasing drug release in response to dithiothreitol (10 mM) and/or pH 5 (Dai et al., 2011). Taking this approach a step further, triple-stimuli responsive micellar system was developed using a block copolymer with a pH-sensitive hydrophobic block and a temperature-sensitive hydrophilic block connected via a reduction-sensitive disulfide linker (Klaikherd et al., 2009). The block-copolymer lost amphiphilic properties in response to temperature increase, acidic pH, or high reductive potential, allowing for tunable control of drug release with single stimulus or simultaneous

multiple stimuli. Notably, individual stimulus caused slow or incomplete dye release, but combined stimuli resulted in a significantly faster and greater drug release (Klaikherd et al., 2009).

Covalent conjugation of a drug to carrier. For stable drug encapsulation, a drug may be conjugated to a NP matrix via a linker, which may be hydrolyzed or cleaved in a stimuli-responsive manner. pH-activatable NPs was made with paclitaxel conjugated to PEG-poly(acrylic acid) via an acid-labile acetal linker (Gu et al., 2013). The NPs showed >80% drug release in pH 5 in 2 days, while they released only 29% of the total drug at pH 7.4 (Gu et al., 2013). In another study, drug-poly(lactide) conjugates were synthesized using a drug (paclitaxel, docetaxel, and camptothecin) as an initiator of polymerization (Tong & Cheng, 2008). The conjugates formed NPs with high drug contents (5-36 wt%), which showed minimal initial burst release followed by gradual drug release over a week *in vitro* (Tong & Cheng, 2008). Similarly, docetaxel was conjugated to PEGylated carboxymethylcellulose (CMC) to assemble into 120 nm NPs releasing the drug in a controlled release manner (Ernsting et al., 2011). Notably, the CMC-based NPs had an anti-stromal effect, increasing tumoral perfusion and lowering the IFP, with a greater anti-metastatic effect than Abraxane (Murakami et al., 2013). In another study, camptothecin was conjugated to a β -sheet-forming peptide to make drug amphiphiles, which assembled into supramolecular structures (nanotubes) with definite structure (Cheetham et al., 2013). Serving as a part of the carrier building block, the drug molecules constituted up to 38% of the nanotubes (Cheetham et al., 2013). An important consideration in design of drug-polymer conjugates is that cleavage of the conjugate should restore a pharmacologically active drug (Stella & Nti-Addae, 2007). Although it is an efficient way of controlling drug release, worth mentioning is that drug-polymer conjugate is considered a new chemical entity, which needs a new FDA approval for clinical use (Kim et al., 2009).

1.3.2.4 Clinical Translation of Developed NP systems

Taking into consideration the enormous interest in nanomedicine development, it is critical to consider the challenges of clinical translation of such systems from early development phase. The rate of clinical translation of publications and patents does not

meet the expectations. This can be attributed to many reasons, some related to NP design and others related to screening and *in vivo* evaluation (J. M. Lim & Karnik, 2014; Valencia et al., 2012). Among the NP-related reasons is the complexity of the developed systems from the commercial and industrial standpoint, which often makes the scale up extremely challenging (Z. L. Cheng et al., 2012; Goldberg et al., 2013). Long complicated synthetic chemistry is often used to produce polymeric NP systems of certain core and surface properties, tailored for the delivery of a certain therapeutic agent. Such chemical reactions are frequently carried out in presence of toxic organic solvents and under harsh conditions (J. Cheng et al., 2007; Y. I. Chung et al., 2010; Y. B. Patil et al., 2009). Even the simpler and safer “click chemistry” procedures require prior chemical modification of the substrate, the presence of catalysts and/or long purification steps (Joralemon et al., 2005; Kamphuis et al., 2010; Kolb et al., 2001; Lallana et al., 2012; von Maltzahn et al., 2008)

1.4 Extracellularly Activatable NPs for Tumor Drug Delivery

Despite the fact that tumor tissues are heterogenous, with various types of tumors having significantly different pathophysiologies (Denison & Bae, 2012), they can still be distinguished from normal tissues by many features (Gerweck & Seetharaman, 1996; Vaupel & Mayer, 2007) and eventually, selectivity of the nanocarrier action would depend on both distribution of a stimulus within different body tissues and sensitivity of the nanocarrier to different stimulus levels (Abouelmagd et al., 2014).

1.4.1 Extracellular Stimuli Adapted for NP Activation

Mildly acidic pH of the tumor microenvironment (6.8-7.2) (Gerweck & Seetharaman, 1996) is one of the most widely used features for the extracellular activation of nanocarriers (Tian & Bae, 2012b). The acidity of a solid tumor is attributable to metabolic abnormalities in tumor cells, including the high rate of aerobic and anaerobic glycolysis, which leads to accumulation of lactic acid (Cairns et al., 2006; Y. Kato et al., 2013), and the increased proton-pump activities in the plasma membrane, which promote the secretion of acidic metabolites to extracellular milieu (Y. Kato et al., 2013). Moreover, the acidified tissues do not readily return to neutral pH due to the reduced blood flow in

tumors (Tian & Bae, 2012b). In designing stimuli-sensitive drug carriers, the acidic pH is used to change the ionization status of the carrier molecules (Amoozgar et al., 2012; Guan et al., 2013; Hu et al., 2013; K. C. Liu & Yeo, 2013) or induce cleavage of acid-labile linkers, thereby modulating the ability of carriers to interact with cells (Gullotti et al., 2013b; Tian & Bae, 2012b). A challenge in exploiting acidic pH of tumors is the narrow pH range useful for extracellular activation of nanocarriers, which require high sensitivity of the carrier molecules to pH change (Tian & Bae, 2012b).

Hypoxia is another hallmark of cancer, as a direct result of fast unorganized tumor growth and poor oxygenation and nutrition in some tumor areas (Denison & Bae, 2012; Vaupel & Mayer, 2007). Hypoxic tissue is usually located in center of tumor (Denison & Bae, 2012), where 50–60% of locally advanced solid tumors have heterogeneously distributed regions of significant hypoxia (Vaupel & Mayer, 2007) and is one of the causes chemotherapy and radiation failure (Wilson & Hay, 2011). A different class of stimuli is enzymes present overexpressed in tumor, like MMPs, present extracellularly. Usually, their expression is tightly regulated throughout the body, but abundant in many cancers, due to involvement in degradation of extracellular matrix and tumor progression (Danhier et al., 2010; Egeblad & Werb, 2002; Lehner et al., 2012; Niidome et al., 2010). They also can be present in some cardiovascular conditions (Elegbede et al., 2008; Fingleton, 2007). Peptides sensitive to MMP-2 and MMP-9 have been used in designing responsive nanocarriers (Elegbede et al., 2008; Gullotti et al., 2013a). Similarly, cathepsin B, which is a lysosomal proteinase generally existing intracellularly in lysosomes, can be found overexpressed extracellularly in some tumor types as well (Campo et al., 1994; Glangchai et al., 2008a; Sloane, 1990).

1.4.2 Nanocarriers Responsive to Tumor Extracellular pH

NP systems were engineered to respond to tumor mildly acidic pH, resulting in enhanced cellular interactions or triggered drug release through different mechanisms.

1.4.2.1 Drug Release:

For pH-triggered drug release, acid-labile linkers such as hydrazone, acetal, or ester bonds are frequently used, although the triggering pHs for these linkers are somewhat low for extracellular drug release. For example, Lee *et al.* conjugated doxorubicin (DOX) to mesoporous silica nanoparticles (MSNs) with a hydrazone linker, which hydrolyzed in acidic pH (J. E. Lee et al., 2011). DOX release in neutral pH was minimal (4%) but significantly increased as the pH dropped to 4 (78% in 56 hours) (J. E. Lee et al., 2011).

Polyhistidine (pHis) is another chemical moiety widely used for pH-sensitive drug carriers. The pH sensitivity of pHis comes from the imidazole group, which protonates in acidic pH with a pKa value of ~6 (Eun Seong Lee, Shin, et al., 2003). Polymeric micelles prepared with a block-copolymer of pHis and PEG showed higher drug release at acidic pH as pHis block turned hydrophilic with protonation (Eun Seong Lee, Na, et al., 2003; Eun Seong Lee, Shin, et al., 2003). More recently, a pHis-based AB₂-miktoarm polymer (mPEG-b-pHis₂) was designed to form polymersomes, thin-walled polymer vesicles similar to liposomes (Yin et al., 2012). Below pH 7.4, the polymersomes underwent conformation changes to cylindrical micelles, spherical micelles, and finally to unimers showing increasing drug release (Yin et al., 2012).

Alternatively, chitosan and its derivatives are used as a component of NPs for pH-triggered drug release. Magnetic nanocrystals and DOX were encapsulated in micelles made of amphiphilic chitosan derivative, N-naphthyl-O-dimethylmaleoyl chitosan (N-nap-O-MalCS) with an average size of 158.8 nm at pH 7.4. Exposure to acidic medium (pH 5.5) induced hydrolysis of maleoyl group, which caused the loss of amphiphilicity and destabilization of micelle structure (E. K. Lim et al., 2013). The pH-induced change caused abrupt DOX release (90% release in 24 hours) as compared to 20% at pH 7.4 (E. K. Lim et al., 2013). In another study, chitosan NPs were used as a pH-sensitive carrier of methotrexate (MTX). MTX-loaded chitosan NPs (MTX-CS-NPs) were prepared by ionic gelation of chitosan via tripolyphosphate and an anionic surfactant (77KL), which has a membrane-lytic activity (Nogueira et al., 2013). MTX release from the NPs increased with pH decrease, due to the protonation of 77KL and MTX, leading to decreased electrostatic

interactions with chitosan and destabilization of the NPs. Consequently, MTX-CS-NPs showed enhanced cytotoxic effect on MCF-7 cells at pH 6.6 as compared to at pH 7.4, while free MTX did not show such a pH sensitivity (Nogueira et al., 2013).

1.4.2.2 Cell Interaction

Most nanocarriers are protected by non-ionic hydrophilic polymers to avoid non-specific interactions with immune cells and normal tissues during circulation. Triggered removal or transformation of such a protective surface results in exposure of cationic charges or cell-interactive ligands, thereby allowing for electrostatic or ligand-mediated interactions with the cell membrane.

To increase cellular uptake at acidic tumoral pH, a polymeric micelle system was developed using a blend of polyhistidine (polyHis)-based amphiphilic polymers (E. S. Lee et al., 2008). The micelle was made of a blend of polyHis_{5kD}-*b*-PEG and PLA-*b*-PEG-*b*-polyHis_{2kD}-TAT, where polyHis_{5kD} and PLA blocks from each polymer formed a hydrophobic core and PEG the shell. At pH 7.4, PEG from the latter polymer formed a loop as polyHis_{2kD} block remained unionized and associated with the hydrophobic core, keeping the cell-interactive TAT away from the surface. Below pH 7.2, polyHis_{2kD} started to ionize, exposing the TAT on the surface to facilitate cellular uptake of the polymeric micelles (E. S. Lee et al., 2008). Due to the enhanced cellular uptake, the micelles carrying DOX showed a greater cytotoxic effect on drug-resistant NCI/ADR-RES cells upon the acid-triggered activation (E. S. Lee et al., 2008). A consistent result was observed in a mouse model of a drug-resistant ovarian cancer xenograft (E. S. Lee et al., 2008).

In another study, a layer-by-layer (LbL) approach was used to make multilayered ~80 nm NPs with a fluorescent core and PEG-coated surface (Poon et al., 2011). The core particle was a carboxyl-functionalized quantum dot (QD), of which negative charge allowed building of polymer films. The core was first coated with poly-L-lysine (PLL)-iminobiotin conjugate and neutravidin, which was then coated with mPEG-biotin conjugate. Under acidic pH (4-6), the iminobiotin-neutravidin linker was decomposed due to the reduced affinity of the protonated iminobiotin for neutravidin, causing the external PEG layer to be shed and exposing a cationic PLL layer, which facilitated QD uptake. NPs

showed higher uptake by five different cancer cell lines after incubation in a pH 5.5 medium but minimal uptake at pH 7.4 (Poon et al., 2011). As a consequence of pH-sensitive tumoral uptake, the NPs modified with iminobiotin showed longer retention in tumors than control NPs with biotin (Poon et al., 2011).

pH-sensitive polymers have been used to form a surface layer that becomes more cell-interactive in tumoral pH. For example, low molecular weight chitosan (LMWC) was used as a pH-sensitive surface coating. Chitosan is a polysaccharide with primary amines, which impart a unique pKa of 6.5, matching the weakly acidic pH of tumor tissues (Amoozgar et al., 2012). Due to the reduced molecular weight (<6500 Da), LMWC remains neutral yet hydrophilic at pH 7.4, thus qualifying for a stealth polymer. LMWC was conjugated to PLGA, yielding a polymeric NP with a PLGA core and a LMWC surface (Amoozgar et al., 2012). The PLGA-LMWC NPs showed a slightly negative charge at pH 7.4 but acquired a positive charge in acidic pH. Consequently, PLGA-LMWC NPs showed greater interactions with SKOV-3 cells at pH 6.2 than at pH 7.4, whereas the unmodified PLGA NPs showed limited cellular uptake irrespective of the pH (Amoozgar et al., 2012).

Another example involves a cationic polyamidoamine (PAMAM) dendrimer coated with a zwitterionic chitosan derivative (ZWC) (K. C. Liu & Yeo, 2013). Amine-terminated PAMAM dendrimer is an attractive carrier of drug and gene therapeutics due to the well-defined structure and functionalization potential; however, the utility is limited because of undesirable cytotoxic effects (Domanski et al., 2004). Created by partial amidation of chitosan, ZWC showed a negative charge in a relatively basic condition and positive charge in an acidic condition, where the transition pH is readily tunable according to the extent of amidation (Xu et al., 2010). The PAMAM dendrimer was electrostatically coated with ZWC, which was anionic in neutral pH, reducing toxicity associated with the cationic charge of the dendrimer. On the other hand, in mildly acidic pH, where ZWC charge switched from negative to positive, the PAMAM dendrimer was no longer protected and allowed to interact with the cell membrane and enter the cells (K. C. Liu & Yeo, 2013).

Peptides are another class of pH-sensitive material that can be used to promote pH-sensitive cell interactions (Yao et al., 2013). A pH low insertion peptide (pHLIP) is a pH-

sensitive peptide made of 38 amino acids with moderate water solubility (Yao et al., 2013). As pH drops from 7.4 to 6.5, it becomes more hydrophobic with protonation of Asp and Glu residues and inserts its tail into the cell membrane lipid bilayer, helping NPs modified with the peptide to enter cells (Yao et al., 2013; Zhao et al., 2013). pHLIP was conjugated with MSN, an inorganic drug carrier, via a disulfide bond (Zhao et al., 2013). When placed in mildly acidic pH, the pHLIP-conjugated MSNs were readily taken up by cells, in which the disulfide linker was reduced and the loaded DOX released. Due to the pH-induced cellular uptake, this system showed greater cytotoxic effects in both drug sensitive (MCF-7) and resistant (MCF-7/ADR) cell lines at pH 6.5 relative to those at pH 7.4 (Zhao et al., 2013). A similar approach was used to enhance tumor uptake of gold NPs (Yao et al., 2013).

1.5 Conclusions

NP drug carriers have overcome several challenges in administration of anti-cancer drugs, such as poor water-solubility and side effects associated with toxic solubilizers. They also hold a great promise to potentiate the effectiveness of chemotherapy by modulating biodistribution of drugs and concentrating their effects on tumor tissues. Designing smart systems that can respond to special nature of the tumor tissue can greatly enhance their efficiency and specificity. To translate the idealized concepts into clinical practice, it is important to design NPs to satisfy multiple (often conflicting) requirements, such as stable drug retention during circulation and site-specific drug release, and evasion of the immune surveillance and preferential interaction with target cells. Moreover, the NP design must consider physiological challenges of tumors such as heterogeneity, genetic instability, and increasing resistance to drug transport on tissue and cellular levels, which can counteract chemical and structural features of the NPs. Decades of research effort has brought substantial technological advancement in individual aspect. The remaining task is to integrate these technologies in a simple and scalable manner, which will justify capital investment in the translation of bench-top inventions to clinical product.

1.6 References

- Abouelmagd, S. A., Hyun, H., & Yeo, Y. (2014). "Extracellularly activatable nanocarriers for drug delivery to tumors." Expert Opin Drug Deliv 11(10): 1601-1618.
- Amoozgar, Z., Park, J. Y., Lin, Q. N., & Yeo, Y. (2012). "Low Molecular-Weight Chitosan as a pH-Sensitive Stealth Coating for Tumor-Specific Drug Delivery." Mol Pharm 9(5): 1262-1270.
- Amoozgar, Z., & Yeo, Y. (2012). "Recent advances in stealth coating of nanoparticle drug delivery systems." Wiley Interdiscip Rev Nanomed Nanobiotechnol 4(2): 219-233.
- Armstrong, J. K. (2009). "The occurrence, induction, specificity and potential effect of antibodies against poly(ethylene glycol)." Pegylated Protein Drugs: Basic Science and Clinical Applications: 147-168.
- Arner, E. S. J., & Holmgren, A. (2000). "Physiological functions of thioredoxin and thioredoxin reductase." European Journal of Biochemistry 267(20): 6102-6109.
- Bae, Y. H., & Yin, H. (2008). "Stability issues of polymeric micelles." J Control Release 131(1): 2-4.
- Baish, J. W., & Jain, R. K. (2000). "Fractals and cancer." Cancer Res 60(14): 3683-3688.
- Banerjee, D., & Sengupta, S. (2011). "Nanoparticles in cancer chemotherapy." Prog Mol Biol Transl Sci 104: 489-507.
- Barenholz, Y. (2012). "Doxil (R) - The first FDA-approved nano-drug: Lessons learned." Journal of Controlled Release 160(2): 117-134.
- Batist, G., Gelmon, K. A., Chi, K. N., Miller, W. H., Chia, S. K. L., Mayer, L. D., Swenson, C. E., Janoff, A. S., & Louie, A. C. (2009). "Safety, Pharmacokinetics, and Efficacy of CPX-1 Liposome Injection in Patients with Advanced Solid Tumors." Clinical Cancer Research 15(2): 692-700.
- Bharali, D. J., Khalil, M., Gurbuz, M., Simone, T. M., & Mousa, S. A. (2009). "Nanoparticles and cancer therapy: a concise review with emphasis on dendrimers." Int J Nanomedicine 4: 1-7.
- Blanco, E., Hsiao, A., Mann, A. P., Landry, M. G., Meric-Bernstam, F., & Ferrari, M. (2011). "Nanomedicine in cancer therapy: Innovative trends and prospects." Cancer Science 102(7): 1247-1252.
- Boucher, Y., Leunig, M., & Jain, R. K. (1996). "Tumor angiogenesis and interstitial hypertension." Cancer Res 56(18): 4264-4266.
- Bronich, T. K., Keifer, P. A., Shlyakhtenko, L. S., & Kabanov, A. V. (2005). "Polymer micelle with cross-linked ionic core." J Am Chem Soc 127(23): 8236-8237.
- Burt, H. M., Zhang, X., Toleikis, P., Embree, L., & Hunter, W. L. (1999). "Development of copolymers of poly(D,L-lactide) and methoxypolyethylene glycol as micellar carriers of paclitaxel." Colloids and Surfaces B: Biointerfaces 16(1-4): 161-171.
- Cairns, R., Papandreou, I., & Denko, N. (2006). "Overcoming physiologic barriers to cancer treatment by molecularly targeting the tumor microenvironment." Molecular Cancer Research 4(2): 61-70.
- Campo, E., Munoz, J., Miquel, R., Palacin, A., Cardesa, A., Sloane, B. F., & Emmert-Buck, M. R. (1994). "Cathepsin B expression in colorectal carcinomas correlates with tumor progression and shortened patient survival." Am J Pathol 145(2): 301-309.

- Cerri, S., Piccolini, V. M., Santin, G., Bottone, M. G., De Pascali, S. A., Migoni, D., Iadarola, P., Fanizzi, F. P., & Bernocchi, G. (2011). "The developmental neurotoxicity study of platinum compounds. Effects of cisplatin versus a novel Pt(II) complex on rat cerebellum." Neurotoxicology and Teratology 33(2): 273-281.
- Cheetham, A. G., Zhang, P., Lin, Y. A., Lock, L. L., & Cui, H. (2013). "Supramolecular nanostructures formed by anticancer drug assembly." J Am Chem Soc 135(8): 2907-2910.
- Chen, H., Kim, S., He, W., Wang, H., Low, P. S., Park, K., & Cheng, J.-X. (2008). "Fast Release of Lipophilic Agents from Circulating PEG-PDLLA Micelles Revealed by in Vivo Förster Resonance Energy Transfer Imaging." Langmuir 24(10): 5213-5217.
- Cheng, J., Teply, B. A., Sherifi, I., Sung, J., Luther, G., Gu, F. X., Levy-Nissenbaum, E., Radovic-Moreno, A. F., Langer, R., & Farokhzad, O. C. (2007). "Formulation of functionalized PLGA-PEG nanoparticles for in vivo targeted drug delivery." Biomaterials 28(5): 869-876.
- Cheng, R., Meng, F. H., Deng, C., Klok, H. A., & Zhong, Z. Y. (2013). "Dual and multi-stimuli responsive polymeric nanoparticles for programmed site-specific drug delivery." Biomaterials 34(14): 3647-3657.
- Cheng, Z. L., Al Zaki, A., Hui, J. Z., Muzykantov, V. R., & Tsourkas, A. (2012). "Multifunctional Nanoparticles: Cost Versus Benefit of Adding Targeting and Imaging Capabilities." Science 338(6109): 903-910.
- Cho, K. J., Wang, X., Nie, S. M., Chen, Z., & Shin, D. M. (2008). "Therapeutic nanoparticles for drug delivery in cancer." Clinical Cancer Research 14(5): 1310-1316.
- Chou, H. H., Wang, K. L., Chen, C. A., Wei, L. H., Lai, C. H., Hsieh, C. Y., Yang, Y. C., Twu, N. F., Chang, T. C., & Yen, M. S. (2006). "Pegylated liposomal doxorubicin (Lipo-Dox (R)) for platinum-resistant or refractory epithelial ovarian carcinoma: A Taiwanese gynecologic oncology group study with long-term follow-up." Gynecologic Oncology 101(3): 423-428.
- Chung, T. H., Wu, S. H., Yao, M., Lu, C. W., Lin, Y. S., Hung, Y., Mou, C. Y., Chen, Y. C., & Huang, D. M. (2007). "The effect of surface charge on the uptake and biological function of mesoporous silica nanoparticles 3T3-L1 cells and human mesenchymal stem cells." Biomaterials 28(19): 2959-2966.
- Chung, Y. I., Kim, J. C., Kim, Y. H., Tae, G., Lee, S. Y., Kim, K., & Kwon, I. C. (2010). "The effect of surface functionalization of PLGA nanoparticles by heparin- or chitosan-conjugated Pluronic on tumor targeting." Journal of Controlled Release 143(3): 374-382.
- Curti, B. D. (1993). "Physical barriers to drug delivery in tumors." Crit Rev Oncol Hematol 14(1): 29-39.
- Dai, J., Lin, S. D., Cheng, D., Zou, S. Y., & Shuai, X. T. (2011). "Interlayer-Crosslinked Micelle with Partially Hydrated Core Showing Reduction and pH Dual Sensitivity for Pinpointed Intracellular Drug Release." Angewandte Chemie-International Edition 50(40): 9404-9408.

- Dams, E. T. M., Laverman, P., Oyen, W. J. G., Storm, G., Scherphof, G. L., Vander Meer, J. W. M., Corstens, F. H. M., & Boerman, O. C. (2000). "Accelerated blood clearance and altered biodistribution of repeated injections of sterically stabilized liposomes." Journal of Pharmacology and Experimental Therapeutics 292(3): 1071-1079.
- Danhier, F., Feron, O., & Preat, V. (2010). "To exploit the tumor microenvironment: Passive and active tumor targeting of nanocarriers for anti-cancer drug delivery." Journal of Controlled Release 148(2): 135-146.
- Daou, T. J., Li, L., Reiss, P., Jossierand, V., & Texier, I. (2009). "Effect of Poly(ethylene glycol) Length on the in Vivo Behavior of Coated Quantum Dots." Langmuir 25(5): 3040-3044.
- Davis, M. E., Chen, Z., & Shin, D. M. (2008). "Nanoparticle therapeutics: an emerging treatment modality for cancer." Nat Rev Drug Discov 7(9): 771-782.
- de Smet, M., Heijman, E., Langereis, S., Hijnen, N. M., & Grull, H. (2011). "Magnetic resonance imaging of high intensity focused ultrasound mediated drug delivery from temperature-sensitive liposomes: An in vivo proof-of-concept study." Journal of Controlled Release 150(1): 102-110.
- Demel, R. A., & De Kruyff, B. (1976). "The function of sterols in membranes." Biochim Biophys Acta 457(2): 109-132.
- Deng, C., Jiang, Y. J., Cheng, R., Meng, F. H., & Zhong, Z. Y. (2012). "Biodegradable polymeric micelles for targeted and controlled anticancer drug delivery: Promises, progress and prospects." Nano Today 7(5): 467-480.
- Denison, T. A., & Bae, Y. H. (2012). "Tumor heterogeneity and its implication for drug delivery." Journal of Controlled Release 164(2): 187-191.
- Desai, N. (2008). "Nab Technology: A Drug Delivery Platform Utilising Endothelial gp60 Receptor-based Transport and Tumour-derived SPARC for Targeting " Drug Delivery Report Winter 2007/2008: 37-41.
- Doh, K. O., & Yeo, Y. (2012). "Application of polysaccharides for surface modification of nanomedicines." Ther Deliv 3(12): 1447-1456.
- Domanski, D. M., Klajnert, B., & Bryszewska, M. (2004). "Influence of PAMAM dendrimers on human red blood cells." Bioelectrochemistry 63(1-2): 189-191.
- Du, H., Chandaroy, P., & Hui, S. W. (1997). "Grafted poly-(ethylene glycol) on lipid surfaces inhibits protein adsorption and cell adhesion." Biochim Biophys Acta 1326(2): 236-248.
- Duffaud, F., Borner, M., Chollet, P., Vermorcken, J. B., Bloch, J., Degardin, M., Rolland, F., Dittrich, C., Baron, B., Lacombe, D., Fumoleau, P., & Grp, E.-N. D. D. (2004). "Phase II study of OSI-211 (liposomal lurtotecan) in patients with metastatic or loco-regional recurrent squamous cell carcinoma of the head and neck - An EORTC New Drug Development Group Study." European Journal of Cancer 40(18): 2748-2752.
- Egeblad, M., & Werb, Z. (2002). "New functions for the matrix metalloproteinases in cancer progression." Nature Reviews Cancer 2(3): 161-174.
- Eikenes, L., Tari, M., Tufto, I., Bruland, O. S., & Davies, C. D. (2005). "Hyaluronidase induces a transcapillary pressure gradient and improves the distribution and uptake of liposomal doxorubicin (Caelyx (TM)) in human osteosarcoma xenografts." British Journal of Cancer 93(1): 81-88.

- Elegbede, A. I., Banerjee, J., Hanson, A. J., Tobwala, S., Ganguli, B., Wang, R. Y., Lu, X. N., Srivastava, D. K., & Mallik, S. (2008). "Mechanistic studies of the triggered release of liposomal contents by matrix metalloproteinase-9." Journal of the American Chemical Society 130(32): 10633-10642.
- Ernsting, M. J., Murakami, M., Undzys, E., Aman, A., Press, B., & Li, S. D. (2012). "A docetaxel-carboxymethylcellulose nanoparticle outperforms the approved taxane nanoformulation, Abraxane, in mouse tumor models with significant control of metastases." J Control Release 162(3): 575-581.
- Ernsting, M. J., Tang, W. L., MacCallum, N., & Li, S. D. (2011). "Synthetic Modification of Carboxymethylcellulose and Use Thereof to Prepare a Nanoparticle Forming Conjugate of Docetaxel for Enhanced Cytotoxicity against Cancer Cells." Bioconjugate Chemistry 22(12): 2474-2486.
- Evans, E., & Metcalfe, M. (1984). "Free energy potential for aggregation of giant, neutral lipid bilayer vesicles by Van der Waals attraction." Biophysical Journal 46(3): 423-426.
- Fidler, I. (1978). "Tumor heterogeneity and the biology of cancer invasion and metastasis." Cancer research 38(9): 2651-2660.
- Fidler, I. J., & Hart, I. R. (1982). "Biological diversity in metastatic neoplasms: origins and implications." Science 217(4564): 998-1003.
- Fingleton, B. (2007). "Matrix metalloproteinases as valid clinical targets." Current Pharmaceutical Design 13(3): 333-346.
- Folkman, J. (1974). "Proceedings: Tumor angiogenesis factor." Cancer Res 34(8): 2109-2113.
- Forsen, E. A. (1997). "The design and development of DaunoXome(R) for solid tumor targeting in vivo." Advanced Drug Delivery Reviews 24(2-3): 133-150.
- Gabizon, A., & Papahadjopoulos, D. (1988). "Liposome formulations with prolonged circulation time in blood and enhanced uptake by tumors." Proceedings of the National Academy of Sciences 85(18): 6949-6953.
- Gabizon, A., Shmeeda, H., & Barenholz, Y. (2003). "Pharmacokinetics of pegylated liposomal doxorubicin - Review of animal and human studies." Clinical Pharmacokinetics 42(5): 419-436.
- Garay, R. P., El-Gewely, R., Armstrong, J. K., Garratty, G., & Richette, P. (2012). "Antibodies against polyethylene glycol in healthy subjects and in patients treated with PEG-conjugated agents." Expert Opin Drug Deliv 9(11): 1319-1323.
- Gasparini, G., Longo, R., Fanelli, M., & Teicher, B. A. (2005). "Combination of antiangiogenic therapy with other anticancer therapies: results, challenges, and open questions." J Clin Oncol 23(6): 1295-1311.
- Gelderblom, H., Verweij, J., Nooter, K., & Sparreboom, A. (2001). "Cremophor EL: the drawbacks and advantages of vehicle selection for drug formulation." Eur J Cancer 37(13): 1590-1598.
- Gerlinger, M., Rowan, A., Horswell, S., Larkin, J., Endesfelder, D., Gronroos, E., Martinez, P., Matthews, N., Stewart, A., Tarpey, P., Varela, I., Phillimore, B., Begum, S., McDonald, N., Butler, A., Jones, D., M., Szallasi, Z., Downward, J., Futreal, P., & Swanton, C. (2012). "Intratumor heterogeneity and branched evolution revealed by multiregion sequencing." The New England journal of medicine 366(10): 883-892.

- Gerweck, L. E., & Seetharaman, K. (1996). "Cellular pH gradient in tumor versus normal tissue: Potential exploitation for the treatment of cancer." Cancer Research 56(6): 1194-1198.
- Giustini, A. J., Petryk, A. A., & Hoopes, P. J. (2012). "Ionizing radiation increases systemic nanoparticle tumor accumulation." Nanomedicine-Nanotechnology Biology and Medicine 8(6): 818-821.
- Glangchai, L. C., Caldorera-Moore, M., Shi, L., & Roy, K. (2008a). "Nanoimprint lithography based fabrication of shape-specific, enzymatically-triggered smart nanoparticles." Journal of Controlled Release 125(3): 263-272.
- Glangchai, L. C., Caldorera-Moore, M., Shi, L., & Roy, K. (2008b). "Nanoimprint lithography based fabrication of shape-specific, enzymatically-triggered smart nanoparticles." Journal of Controlled Release 125(3): 263-272.
- Goldberg, M. S., Hook, S. S., Wang, A. Z., Bulte, J. W. M., Patri, A. K., Uckun, F. M., Cryns, V. L., Hanes, J., Akin, D., Hall, J. B., Gharkholo, N., & Mumper, R. J. (2013). "Biotargeted nanomedicines for cancer: six tenets before you begin." Nanomedicine 8(2): 299-308.
- Goodman, T. T., Chen, J. Y., Matveev, K., & Pun, S. H. (2008). "Spatio-temporal modeling of nanoparticle delivery to multicellular tumor spheroids." Biotechnol Bioeng 101(2): 388-399.
- Green, M., Manikhas, G., Orlov, S., Afanasyev, B., Makhson, A., Bhar, P., & Hawkins, M. (2006). "Abraxane, a novel Cremophor-free, albumin-bound particle form of paclitaxel for the treatment of advanced non-small-cell lung cancer." Annals of oncology : official journal of the European Society for Medical Oncology / ESMO 17(8): 1263-1268.
- Green, M. R., Manikhas, G. M., Orlov, S., Afanasyev, B., Makhson, A. M., Bhar, P., & Hawkins, M. J. (2006). "Abraxane((R)), a novel Cremophor((R))-free, albumin-bound particle form of paclitaxel for the treatment of advanced non-small-cell lung cancer." Annals of Oncology 17(8): 1263-1268.
- Gref, R., Luck, M., Quellec, P., Marchand, M., Dellacherie, E., Harnisch, S., Blunk, T., & Muller, R. H. (2000). "'Stealth' corona-core nanoparticles surface modified by polyethylene glycol (PEG): influences of the corona (PEG chain length and surface density) and of the core composition on phagocytic uptake and plasma protein adsorption." Colloids and Surfaces B-Biointerfaces 18(3-4): 301-313.
- Gref, R., Minamitake, Y., Peracchia, M. T., Trubetskoy, V., Torchilin, V., & Langer, R. (1994). "Biodegradable long-circulating polymeric nanospheres." Science 263(5153): 1600-1603.
- Gruenhagen, J. A., Lai, C. Y., Radu, D. R., Lin, V. S., & Yeung, E. S. (2005). "Real-time imaging of tunable adenosine 5-triphosphate release from an MCM-41-type mesoporous silica nanosphere-based delivery system." Appl Spectrosc 59(4): 424-431.
- Gu, Y. D., Zhong, Y. N., Meng, F. H., Cheng, R., Deng, C., & Zhong, Z. Y. (2013). "Acetal-Linked Paclitaxel Prodrug Micellar Nanoparticles as a Versatile and Potent Platform for Cancer Therapy." Biomacromolecules 14(8): 2772-2780.

- Guan, X. W., Li, Y. H., Jiao, Z. X., Chen, J., Guo, Z. P., Tian, H. Y., & Chen, X. S. (2013). "A pH-sensitive charge-conversion system for doxorubicin delivery." Acta Biomater 9(8): 7672-7678.
- Gullotti, E., Park, J., & Yeo, Y. (2013a). "Polydopamine-Based Surface Modification for the Development of Peritumorally Activatable Nanoparticles." Pharmaceutical Research 30(8): 1956-1967.
- Gullotti, E., Park, J., & Yeo, Y. (2013b). "Polydopamine-based surface modification for the development of peritumorally activatable nanoparticles." Pharm Res 30(8): 1956-1967.
- Gullotti, E., & Yeo, Y. (2012). "Beyond the imaging: limitations of cellular uptake study in the evaluation of nanoparticles." Journal of Controlled Release 164(2): 170-176.
- Harper, J., & Moses, M. (2006). "Molecular regulation of tumor angiogenesis: mechanisms and therapeutic implications." Cancer: Cell Structures.
- Hasan, A. S., Socha, M., Lamprecht, A., El Ghazouani, F., Sapin, A., Hoffman, A., Maincent, P., & Ubrich, N. (2007). "Effect of the microencapsulation of nanoparticles on the reduction of burst release." International Journal of Pharmaceutics 344(1-2): 53-61.
- Hatakeyama, H., Akita, H., & Harashima, H. (2011a). "A multifunctional envelope type nano device (MEND) for gene delivery to tumours based on the EPR effect: a strategy for overcoming the PEG dilemma." Adv Drug Deliv Rev 63(3): 152-160.
- Hatakeyama, H., Akita, H., & Harashima, H. (2011b). "A multifunctional envelope type nano device (MEND) for gene delivery to tumours based on the EPR effect: A strategy for overcoming the PEG dilemma." Advanced Drug Delivery Reviews 63(3): 152-160.
- Hatakeyama, H., Akita, H., Maruyama, K., Suhara, T., & Harashima, H. (2004). "Factors governing the in vivo tissue uptake of transferrin-coupled polyethylene glycol liposomes in vivo." International Journal of Pharmaceutics 281(1-2): 25-33.
- Hawkins, M. J., Soon-Shiong, P., & Desai, N. (2008). "Protein nanoparticles as drug carriers in clinical medicine." Advanced Drug Delivery Reviews 60(8): 876-885.
- He, C. B., Hu, Y. P., Yin, L. C., Tang, C., & Yin, C. H. (2010). "Effects of particle size and surface charge on cellular uptake and biodistribution of polymeric nanoparticles." Biomaterials 31(13): 3657-3666.
- He, Q. J., Zhang, J. M., Shi, J. L., Zhu, Z. Y., Zhang, L. X., Bu, W. B., Guo, L. M., & Chen, Y. (2010). "The effect of PEGylation of mesoporous silica nanoparticles on nonspecific binding of serum proteins and cellular responses." Biomaterials 31(6): 1085-1092.
- Heldin, C.-H., Rubin, K., Pietras, K., & Ostman, A. (2004). "High interstitial fluid pressure - an obstacle in cancer therapy." Nature reviews. Cancer 4(10): 806-813.
- Heurtault, B., Saulnier, P., Pech, B., Proust, J. E., & Benoit, J. P. (2003). "Physico-chemical stability of colloidal lipid particles." Biomaterials 24(23): 4283-4300.
- Hirsch, V., Kinnear, C., Moniatte, M., Rothen-Rutishauser, B., Clift, M. J. D., & Fink, A. (2013). "Surface charge of polymer coated SPIONs influences the serum protein adsorption, colloidal stability and subsequent cell interaction in vitro." Nanoscale 5(9): 3723-3732.

- Holback, H., & Yeo, Y. (2011). "Intratumoral Drug Delivery with Nanoparticulate Carriers." Pharm Res 28(8): 1819-1830.
- Hompland, T., Ellingsen, C., Ovrebo, K. M., & Rofstad, E. K. (2012). "Interstitial fluid pressure and associated lymph node metastasis revealed in tumors by dynamic contrast-enhanced MRI." Cancer Res 72(19): 4899-4908.
- Hrkach, J., Von Hoff, D., Ali, M. M., Andrianova, E., Auer, J., Campbell, T., De Witt, D., Figa, M., Figueiredo, M., Horhota, A., Low, S., McDonnell, K., Peeke, E., Retnarajan, B., Sabnis, LoRusso, P., Kantoff, P. W., Bander, N. H., Sweeney, C., Farokhzad, O. C., Langer, R., & Zale, S. (2012). "Preclinical Development and Clinical Translation of a PSMA-Targeted Docetaxel Nanoparticle with a Differentiated Pharmacological Profile." Science Translational Medicine 4(128).
- Hu, J., Miura, S., Na, K., & Bae, Y. H. (2013). "pH-responsive and charge shielded cationic micelle of poly(L-histidine)-block-short branched PEI for acidic cancer treatment." Journal of Controlled Release 172(1): 69-76.
- Iijima, M., Nagasaki, Y., Okada, T., Kato, M., & Kataoka, K. (1999). "Core-polymerized reactive micelles from heterotelechelic amphiphilic block copolymers." Macromolecules 32(4): 1140-1146.
- Immordino, M. L., Dosio, F., & Cattel, L. (2006). "Stealth liposomes: review of the basic science, rationale, and clinical applications, existing and potential." Int J Nanomedicine 1(3): 297-315.
- Iyer, A. K., Khaled, G., Fang, J., & Maeda, H. (2006). "Exploiting the enhanced permeability and retention effect for tumor targeting." Drug Discovery Today 11(17-18): 812-818.
- Jain, R. A. (2000). "The manufacturing techniques of various drug loaded biodegradable poly(lactide-co-glycolide) (PLGA) devices." Biomaterials 21(23): 2475-2490.
- Jain, R. K. (1998). "The next frontier of molecular medicine: Delivery of therapeutics." Nat Med 4(6): 655-657.
- Jain, S., Mathur, R., Das, M., Swarnakar, N., & Mishra, A. (2011). "Synthesis, pharmacoscintigraphic evaluation and antitumor efficacy of methotrexate-loaded, folate-conjugated, stealth albumin nanoparticles." Nanomedicine (London, England) 6(10): 1733-1754.
- Jee, J. P., Na, J. H., Lee, S., Kim, S. H., Choi, K., Yeo, Y., & Kwon, I. C. (2012). "Cancer targeting strategies in nanomedicine: Design and application of chitosan nanoparticles." Current Opinion in Solid State & Materials Science 16(6): 333-342.
- Jokerst, J. V., Lobovkina, T., Zare, R. N., & Gambhir, S. S. (2011a). "Nanoparticle PEGylation for imaging and therapy." Nanomedicine 6(4): 715-728.
- Jokerst, J. V., Lobovkina, T., Zare, R. N., & Gambhir, S. S. (2011b). "Nanoparticle PEGylation for imaging and therapy." Nanomedicine (Lond) 6(4): 715-728.
- Joralemon, M. J., O'Reilly, R. K., Hawker, C. J., & Wooley, K. L. (2005). "Shell click-crosslinked (SCC) nanoparticles: a new methodology for synthesis and orthogonal functionalization." J Am Chem Soc 127(48): 16892-16899.
- Kamphuis, M. M. J., Johnston, A. P. R., Such, G. K., Dam, H. H., Evans, R. A., Scott, A. M., Nice, E. C., Heath, J. K., & Caruso, F. (2010). "Targeting of Cancer Cells Using Click-Functionalized Polymer Capsules." Journal of the American Chemical Society 132(45): 15881-15883.

- Kato, K., Chin, K., Yoshikawa, T., Yamaguchi, K., Tsuji, Y., Esaki, T., Sakai, K., Kimura, M., Hamaguchi, T., Shimada, Y., Matsumura, Y., & Ikeda, R. (2012). "Phase II study of NK105, a paclitaxel-incorporating micellar nanoparticle, for previously treated advanced or recurrent gastric cancer." Investigational New Drugs 30(4): 1621-1627.
- Kato, Y., Ozawa, S., Miyamoto, C., Maehata, Y., Suzuki, A., Maeda, T., & Baba, Y. (2013). "Acidic extracellular microenvironment and cancer." Cancer Cell Int 13(1): 89.
- Kerbel, R. (2000). "Tumor angiogenesis: past, present and the near future." Carcinogenesis 21(3): 505-515.
- Kim, S., Kim, J. H., Jeon, O., Kwon, I. C., & Park, K. (2009). "Engineered polymers for advanced drug delivery." European Journal of Pharmaceutics and Biopharmaceutics 71(3): 420-430.
- Klaikherd, A., Nagamani, C., & Thayumanavan, S. (2009). "Multi-Stimuli Sensitive Amphiphilic Block Copolymer Assemblies." J Am Chem Soc 131(13): 4830-4838.
- Kohler, G., & Milstein, C. (1975). "Continuous cultures of fused cells secreting antibody of predefined specificity." Nature 256(5517): 495-497.
- Kolb, H. C., Finn, M. G., & Sharpless, K. B. (2001). "Click chemistry: Diverse chemical function from a few good reactions." Angewandte Chemie-International Edition 40(11): 2004-+.
- Kwon, G. S. (2003). "Polymeric micelles for delivery of poorly water-soluble compounds." Crit Rev Ther Drug Carrier Syst 20(5): 357-403.
- Lai, C. Y., Trewyn, B. G., Jeftinija, D. M., Jeftinija, K., Xu, S., Jeftinija, S., & Lin, V. S. Y. (2003). "A mesoporous silica nanosphere-based carrier system with chemically removable CdS nanoparticle caps for stimuli-responsive controlled release of neurotransmitters and drug molecules." J Am Chem Soc 125(15): 4451-4459.
- Lallana, E., Sousa-Herves, A., Fernandez-Trillo, F., Riguera, R., & Fernandez-Megia, E. (2012). "Click chemistry for drug delivery nanosystems." Pharm Res 29(1): 1-34.
- Landon, C. D., Park, J. Y., Needham, D., & Dewhirst, M. W. (2011). "Nanoscale Drug Delivery and Hyperthermia: The Materials Design and Preclinical and Clinical Testing of Low Temperature-Sensitive Liposomes Used in Combination with Mild Hyperthermia in the Treatment of Local Cancer." Open Nanomed J 3: 38-64.
- Lee, E. S., Gao, Z., Kim, D., Park, K., Kwon, I. C., & Bae, Y. H. (2008). "Super pH-sensitive multifunctional polymeric micelle for tumor pH(e) specific TAT exposure and multidrug resistance." Journal of Controlled Release 129(3): 228-236.
- Lee, E. S., Na, K., & Bae, Y. H. (2003). "Polymeric micelle for tumor pH and folate-mediated targeting." J. Control. Release 91(1-2): 103-113.
- Lee, E. S., Shin, H. J., Na, K., & Bae, Y. H. (2003). "Poly(-histidine)-PEG block copolymer micelles and pH-induced destabilization." Journal of Controlled Release 90(3): 363-374.
- Lee, H., Fonge, H., Hoang, B., Reilly, R. M., & Allen, C. (2010). "The effects of particle size and molecular targeting on the intratumoral and subcellular distribution of polymeric nanoparticles." Mol Pharm 7(4): 1195-1208.

- Lee, J. E., Lee, D. J., Lee, N., Kim, B. H., Choi, S. H., & Hyeon, T. (2011). "Multifunctional mesoporous silica nanocomposite nanoparticles for pH controlled drug release and dual modal imaging." Journal of Materials Chemistry 21(42): 16869-16872.
- Lee, R. J., & Low, P. S. (1994). "Delivery of Liposomes into Cultured Kb Cells Via Folate Receptor-Mediated Endocytosis." Journal of Biological Chemistry 269(5): 3198-3204.
- Lehner, R., Wang, X., Wolf, M., & Hunziker, P. (2012). "Designing switchable nanosystems for medical application." Journal of Controlled Release 161(2): 307-316.
- Li, S. D., & Huang, L. (2010). "Stealth nanoparticles: High density but sheddable PEG is a key for tumor targeting." Journal of Controlled Release 145(3): 178-181.
- Li, Y. L., Zhu, L., Liu, Z. Z., Cheng, R., Meng, F. H., Cui, J. H., Ji, S. J., & Zhong, Z. Y. (2009). "Reversibly Stabilized Multifunctional Dextran Nanoparticles Efficiently Deliver Doxorubicin into the Nuclei of Cancer Cells." Angewandte Chemie-International Edition 48(52): 9914-9918.
- Liao, Z. Y., Wang, H. J., Wang, X. D., Zhao, P. Q., Wang, S., Su, W. Y., & Chang, J. (2011). "Multifunctional Nanoparticles Composed of A Poly(DL-lactide-co-glycolide) Core and A Paramagnetic Liposome Shell for Simultaneous Magnetic Resonance Imaging and Targeted Therapeutics." Advanced Functional Materials 21(6): 1179-1186.
- Lim, E. K., Sajomsang, W., Choi, Y., Jang, E., Lee, H., Kang, B., Kim, E., Haam, S., Suh, J. S., Chung, S. J., & Huh, Y. M. (2013). "Chitosan-based intelligent theragnosis nanocomposites enable pH-sensitive drug release with MR-guided imaging for cancer therapy." Nanoscale Res Lett 8(1): 467.
- Lim, J. M., & Karnik, R. (2014). "Optimizing the discovery and clinical translation of nanoparticles: could microfluidics hold the key?" Nanomedicine (Lond) 9(8): 1113-1116.
- Liu, J., Qiu, Z. Y., Wang, S. Q., Zhou, L., & Zhang, S. M. (2010). "A modified double-emulsion method for the preparation of daunorubicin-loaded polymeric nanoparticle with enhanced in vitro anti-tumor activity." Biomedical Materials 5(6).
- Liu, K. C., & Yeo, Y. (2013). "Zwitterionic chitosan-polyamidoamine dendrimer complex nanoparticles as a pH-sensitive drug carrier." Mol Pharm 10(5): 1695-1704.
- Liu, Z. H., Jiao, Y. P., Wang, Y. F., Zhou, C. R., & Zhang, Z. Y. (2008). "Polysaccharides-based nanoparticles as drug delivery systems." Advanced Drug Delivery Reviews 60(15): 1650-1662.
- Lundqvist, M., Stigler, J., Elia, G., Lynch, I., Cedervall, T., & Dawson, K. A. (2008). "Nanoparticle size and surface properties determine the protein corona with possible implications for biological impacts." Proc Natl Acad Sci U S A 105(38): 14265-14270.
- Mady, M. M., Darwish, M. M., Khalil, S., & Khalil, W. M. (2009). "Biophysical studies on chitosan-coated liposomes." European Biophysics Journal with Biophysics Letters 38(8): 1127-1133.

- Maeda, H., Sawa, T., & Konno, T. (2001). "Mechanism of tumor-targeted delivery of macromolecular drugs, including the EPR effect in solid tumor and clinical overview of the prototype polymeric drug SMANCS." J Control Release 74(1-3): 47-61.
- Malik, N., Wiwattanapatapee, R., Klopsch, R., Lorenz, K., Frey, H., Weener, J. W., Meijer, E. W., Paulus, W., & Duncan, R. (2000). "Dendrimers: Relationship between structure and biocompatibility in vitro, and preliminary studies on the biodistribution of I-125-labelled polyamidoamine dendrimers in vivo (vol 65, pg 133, 2000)." Journal of Controlled Release 68(2): 299-302.
- Malonne, H., Langer, I., Kiss, R., & Atassi, G. (1999). "Mechanisms of tumor angiogenesis and therapeutic implications: angiogenesis inhibitors." Clin Exp Metastasis 17(1): 1-14.
- Marcucci, F., & Corti, A. (2012). "Improving drug penetration to curb tumor drug resistance." Drug Discovery Today 17(19-20): 1139-1146.
- Markman, M. (2003). "Managing taxane toxicities." Supportive Care in Cancer 11(3): 144-147.
- Marusyk, A., & Polyak, K. (2010). "Tumor heterogeneity: causes and consequences." Biochimica et biophysica acta 1805(1): 105-117.
- Matsumura, Y., & Maeda, H. (1986a). "A new concept for macromolecular therapeutics in cancer chemotherapy: mechanism of tumoritropic accumulation of proteins and the antitumor agent smancs." Cancer Res 46(12 Pt 1): 6387-6392.
- Matsumura, Y., & Maeda, H. (1986b). "A new concept for macromolecular therapeutics in cancer chemotherapy: mechanism of tumoritropic accumulation of proteins and the antitumor agent smancs." Cancer research 46(12 Pt 1): 6387-6392.
- Meng, F. H., Cheng, R., Deng, C., & Zhong, Z. Y. (2012). "Intracellular drug release nanosystems." Materials Today 15(10): 436-442.
- Metselaar, J. M., Bruin, P., de Boer, L. W., de Vringer, T., Snel, C., Oussoren, C., Wauben, M. H., Crommelin, D. J., Storm, G., & Hennink, W. E. (2003). "A novel family of L-amino acid-based biodegradable polymer-lipid conjugates for the development of long-circulating liposomes with effective drug-targeting capacity." Bioconjug Chem 14(6): 1156-1164.
- Michel, R., Plostica, T., Abezgauz, L., Danino, D., & Gradzielski, M. (2013). "Control of the stability and structure of liposomes by means of nanoparticles." Soft Matter 9(16): 4167-4177.
- Milosevic, M. F., Fyles, A. W., Wong, R., Pintilie, M., Kavanagh, M. C., Levin, W., Manchul, L. A., Keane, T. J., & Hill, R. P. (1998). "Interstitial fluid pressure in cervical carcinoma - Within tumor heterogeneity, and relation to oxygen tension." Cancer 82(12): 2418-2426.
- Mori, A., Klibanov, A. L., Torchilin, V. P., & Huang, L. (1991). "Influence of the Steric Barrier Activity of Amphipathic Poly(Ethyleneglycol) and Ganglioside Gm1 on the Circulation Time of Liposomes and on the Target Binding of Immunoliposomes In vivo." Febs Letters 284(2): 263-266.
- Murakami, M., Ernsting, M. J., Undzys, E., Holwell, N., Foltz, W. D., & Li, S. D. (2013). "Docetaxel Conjugate Nanoparticles That Target alpha-Smooth Muscle Actin-Expressing Stromal Cells Suppress Breast Cancer Metastasis." Cancer research 73(15): 4862-4871.

- Na, K., Bum Lee, T., Park, K. H., Shin, E. K., Lee, Y. B., & Choi, H. K. (2003). "Self-assembled nanoparticles of hydrophobically-modified polysaccharide bearing vitamin H as a targeted anti-cancer drug delivery system." *Eur J Pharm Sci* 18(2): 165-173.
- Nel, A. E., Madler, L., Velegol, D., Xia, T., Hoek, E. M. V., Somasundaran, P., Klaessig, F., Castranova, V., & Thompson, M. (2009). "Understanding biophysicochemical interactions at the nano-bio interface." *Nature Materials* 8(7): 543-557.
- Ng, T. S. C., Wert, D., Sohi, H., Procissi, D., Colcher, D., Raubitschek, A. A., & Jacobs, R. E. (2013). "Serial Diffusion MRI to Monitor and Model Treatment Response of the Targeted Nanotherapy CRLX101." *Clinical Cancer Research* 19(9): 2518-2527.
- Niidome, T., Ohga, A., Akiyama, Y., Watanabe, K., Niidome, Y., Mori, T., & Katayama, Y. (2010). "Controlled release of PEG chain from gold nanorods: Targeted delivery to tumor." *Bioorganic & Medicinal Chemistry* 18(12): 4453-4458.
- Nogueira, D. R., Tavano, L., Mitjans, M., Perez, L., Infante, M. R., & Vinardell, M. P. (2013). "In vitro antitumor activity of methotrexate via pH-sensitive chitosan nanoparticles." *Biomaterials* 34(11): 2758-2772.
- Passirani, C., Barratt, G., Devissaguet, J. P., & Labarre, D. (1998). "Long-circulating nanoparticles bearing heparin or dextran covalently bound to poly(methyl methacrylate)." *Pharmaceutical Research* 15(7): 1046-1050.
- Patil, S., Sandberg, A., Heckert, E., Self, W., & Seal, S. (2007). "Protein adsorption and cellular uptake of cerium oxide nanoparticles as a function of zeta potential." *Biomaterials* 28(31): 4600-4607.
- Patil, Y. B., Toti, U. S., Khair, A., Ma, L., & Panyam, J. (2009). "Single-step surface functionalization of polymeric nanoparticles for targeted drug delivery." *Biomaterials* 30(5): 859-866.
- Perrault, S. D., Walkey, C., Jennings, T., Fischer, H. C., & Chan, W. C. W. (2009). "Mediating Tumor Targeting Efficiency of Nanoparticles Through Design." *Nano Letters* 9(5): 1909-1915.
- Perry, J. L., Reuter, K. G., Kai, M. P., Herlihy, K. P., Jones, S. W., Luft, J. C., Napier, M., Bear, J. E., & DeSimone, J. M. (2012). "PEGylated PRINT nanoparticles: the impact of PEG density on protein binding, macrophage association, biodistribution, and pharmacokinetics." *Nano Letters* 12(10): 5304-5310.
- Peter Vaupel Md, M. (2009). "Pathophysiology of solid tumors." *Springer*: 51-92.
- Pietras, K., Rubin, K., Sjoblom, T., Buchdunger, E., Sjoquist, M., Heldin, C. H., & Ostman, A. (2002). "Inhibition of PDGF receptor signaling in tumor stroma enhances antitumor effect of chemotherapy." *Cancer Res* 62(19): 5476-5484.
- Poon, Z., Chang, D., Zhao, X., & Hammond, P. T. (2011). "Layer-by-layer nanoparticles with a pH-sheddable layer for in vivo targeting of tumor hypoxia." *ACS Nano* 5(6): 4284-4292.
- Puri, A., Loomis, K., Smith, B., Lee, J. H., Yavlovich, A., Heldman, E., & Blumenthal, R. (2009). "Lipid-Based Nanoparticles as Pharmaceutical Drug Carriers: From Concepts to Clinic." *Crit Rev Ther Drug Carrier Syst* 26(6): 523-580.

- Ramishetti, S., & Huang, L. (2012). "Intelligent design of multifunctional lipid-coated nanoparticle platforms for cancer therapy." *Therapeutic delivery* 3(12): 1429-1445.
- Raschi, E., Vasina, V., Ursino, M. G., Boriani, G., Martoni, A., & De Ponti, F. (2010). "Anticancer drugs and cardiotoxicity: Insights and perspectives in the era of targeted therapy." *Pharmacology & Therapeutics* 125(2): 196-218.
- Rim, H. P., Min, K. H., Lee, H. J., Jeong, S. Y., & Lee, S. C. (2011). "pH-Tunable calcium phosphate covered mesoporous silica nanocontainers for intracellular controlled release of guest drugs." *Angew Chem Int Ed Engl* 50(38): 8853-8857.
- Roh, H. D., Boucher, Y., Kalnicki, S., Buchsbaum, R., Bloomer, W. D., & Jain, R. K. (1991). "Interstitial Hypertension in Carcinoma of Uterine Cervix in Patients - Possible Correlation with Tumor Oxygenation and Radiation Response." *Cancer research* 51(24): 6695-6698.
- Romberg, B., Hennink, W. E., & Storm, G. (2008). "Sheddable coatings for long-circulating nanoparticles." *Pharmaceutical Research* 25(1): 55-71.
- Romberg, B., Metselaar, J. M., Baranyi, L., Snel, C. J., Bungler, R., Hennink, W. E., Szebeni, J., & Storm, G. (2007). "Poly(amino acid)s: promising enzymatically degradable stealth coatings for liposomes." *International Journal of Pharmaceutics* 331(2): 186-189.
- Rutz, H. P. (1999). "A biophysical basis of enhanced interstitial fluid pressure in tumors." *Med Hypotheses* 53(6): 526-529.
- Saito, G., Swanson, J. A., & Lee, K. D. (2003). "Drug delivery strategy utilizing conjugation via reversible disulfide linkages: role and site of cellular reducing activities." *Advanced Drug Delivery Reviews* 55(2): 199-215.
- Sankaranarayanan, J., Mahmoud, E. A., Kim, G., Morachis, J. M., & Almutairi, A. (2010). "Multiresponse strategies to modulate burst degradation and release from nanoparticles." *ACS Nano* 4(10): 5930-5936.
- Sankhala, K. K., Mita, A. C., Adinin, R., Wood, L., Beeram, M., Bullock, S., Yamagata, N., Matsuno, K., Fujisawa, T., & Phan, A. (2009). "A phase I pharmacokinetic (PK) study of MBP-426, a novel liposome encapsulated oxaliplatin." *Journal of Clinical Oncology* 27(15).
- Sawant, R. M., Hurley, J. P., Salmaso, S., Kale, A., Tolcheva, E., Levchenko, T. S., & Torchilin, V. P. (2006). ""SMART" drug delivery systems: Double-targeted pH-responsive pharmaceutical nanocarriers." *Bioconjugate Chemistry* 17(4): 943-949.
- Semple, S. C., Chonn, A., & Cullis, P. R. (1996). "Influence of cholesterol on the association of plasma proteins with liposomes." *Biochemistry* 35(8): 2521-2525.
- Senior, J., Delgado, C., Fisher, D., Tilcock, C., & Gregoriadis, G. (1991). "Influence of Surface Hydrophilicity of Liposomes on Their Interaction with Plasma-Protein and Clearance from the Circulation - Studies with Poly(Ethylene Glycol)-Coated Vesicles." *Biochimica et biophysica acta* 1062(1): 77-82.
- Shibata, D. (2012). "Cancer. Heterogeneity and tumor history." *Science (New York, N.Y.)* 336(6079): 304-305.
- Silverman, J. A., & Deitcher, S. R. (2013). "Marqibo (R) (vincristine sulfate liposome injection) improves the pharmacokinetics and pharmacodynamics of vincristine." *Cancer Chemother Pharmacol* 71(3): 555-564.

- Singh, N., Karambelkar, A., Gu, L., Lin, K., Miller, J. S., Chen, C. S., Sailor, M. J., & Bhatia, S. N. (2011). "Bioresponsive mesoporous silica nanoparticles for triggered drug release." J Am Chem Soc 133(49): 19582-19585.
- Slingerland, M., Guchelaar, H. J., & Gelderblom, H. (2012). "Liposomal drug formulations in cancer therapy: 15 years along the road." Drug Discovery Today 17(3-4): 160-166.
- Sloane, B. F. (1990). "Cathepsin B and cystatins: evidence for a role in cancer progression." Semin Cancer Biol 1(2): 137-152.
- Stam, H. J., & Challis, G. B. (1989). "Ratings of cancer chemotherapy toxicity by oncologists, nurses, and pharmacists." J Pain Symptom Manage 4(1): 7-13.
- Stathopoulos, G. P., Antoniou, D., Dimitroulis, J., Stathopoulos, J., Marosis, K., & Michalopoulou, P. (2011). "Comparison of liposomal cisplatin versus cisplatin in non-squamous cell non-small-cell lung cancer." Cancer Chemother Pharmacol 68(4): 945-950.
- Stella, V. J., & Nti-Addae, K. W. (2007). "Prodrug strategies to overcome poor water solubility." Advanced Drug Delivery Reviews 59(7): 677-694.
- Sun, H. L., Guo, B. N., Cheng, R., Meng, F. H., Liu, H. Y., & Zhong, Z. Y. (2009). "Biodegradable micelles with sheddable poly(ethylene glycol) shells for triggered intracellular release of doxorubicin." Biomaterials 30(31): 6358-6366.
- Takeuchi, H., Yamamoto, H., Toyoda, T., Toyoboku, H., Hino, T., & Kawashima, Y. (1998). "Physical stability of size controlled small unilamellar liposomes coated with a modified polyvinyl alcohol." International Journal of Pharmaceutics 164(1-2): 103-111.
- Tan, J. S., Butterfield, D. E., Voycheck, C. L., Caldwell, K. D., & Li, J. T. (1993). "Surface Modification of Nanoparticles by PEO-PPO Block-Copolymers to Minimize Interactions with Blood Components and Prolong Blood-Circulation in Rats." Biomaterials 14(11): 823-833.
- Tannock, I., & Rotin, D. (1989). "Acid pH in tumors and its potential for therapeutic exploitation." Cancer research 49(16): 4373-4384.
- ten Tije, A. J., Verweij, J., Loos, W. J., & Sparreboom, A. (2003). "Pharmacological effects of formulation vehicles - Implications for cancer chemotherapy." Clinical Pharmacokinetics 42(7): 665-685.
- Thasneem, Y. M., Rekha, M. R., Sajeesh, S., & Sharma, C. P. (2013). "Biomimetic mucin modified PLGA nanoparticles for enhanced blood compatibility." J Colloid Interface Sci 409: 237-244.
- Tian, L., & Bae, Y. H. (2012a). "Cancer nanomedicines targeting tumor extracellular pH." Colloids Surf B Biointerfaces 99: 116-126.
- Tian, L., & Bae, Y. H. (2012b). "Cancer nanomedicines targeting tumor extracellular pH." Colloids and Surfaces B-Biointerfaces 99: 116-126.
- Tirosh, O., Barenholz, Y., Katzhendler, J., & Prie, A. (1998). "Hydration of polyethylene glycol-grafted liposomes." Biophysical Journal 74(3): 1371-1379.
- Tong, R., & Cheng, J. (2008). "Paclitaxel-initiated, controlled polymerization of lactide for the formulation of polymeric nanoparticulate delivery vehicles." Angew Chem Int Ed Engl 47(26): 4830-4834.

- Torchilin, V. (2011). "Tumor delivery of macromolecular drugs based on the EPR effect." Advanced Drug Delivery Reviews 63(3): 131-135.
- Torchilin, V. P., Omelyanenko, V. G., Papisov, M. I., Bogdanov, A. A., Trubetskoy, V. S., Herron, J. N., & Gentry, C. A. (1994). "Poly(Ethylene Glycol) on the Liposome Surface - on the Mechanism of Polymer-Coated Liposome Longevity." Biochimica Et Biophysica Acta-Biomembranes 1195(1): 11-20.
- Valencia, P. M., Farokhzad, O. C., Karnik, R., & Langer, R. (2012). "Microfluidic technologies for accelerating the clinical translation of nanoparticles." Nat Nanotechnol 7(10): 623-629.
- Vaupel, P., Frinak, S., & Bicher, H. (1981). "Heterogeneous oxygen partial pressure and pH distribution in C3H mouse mammary adenocarcinoma." Cancer research 41(5): 2008-2013.
- Vaupel, P., & Mayer, A. (2007). "Hypoxia in cancer: significance and impact on clinical outcome." Cancer and Metastasis Reviews 26(2): 225-239.
- Venditto, V. J., & Szoka, F. C. (2013). "Cancer nanomedicines: So many papers and so few drugs!" Advanced Drug Delivery Reviews 65(1): 80-88.
- Venturoli, D., & Rippe, B. (2005). "Ficoll and dextran vs. globular proteins as probes for testing glomerular permselectivity: effects of molecular size, shape, charge, and deformability." American Journal of Physiology-Renal Physiology 288(4): F605-F613.
- Vivek, R., Nipun Babu, V., Thangam, R., Subramanian, K., & Kannan, S. (2013). "pH-responsive drug delivery of chitosan nanoparticles as Tamoxifen carriers for effective anti-tumor activity in breast cancer cells." Colloids and surfaces. B, Biointerfaces 111C: 117-123.
- von Maltzahn, G., Ren, Y., Park, J. H., Min, D. H., Kotamraju, V. R., Jayakumar, J., Fogal, V., Sailor, M. J., Ruoslahti, E., & Bhatia, S. N. (2008). "In vivo tumor cell targeting with "click" nanoparticles." Bioconjug Chem 19(8): 1570-1578.
- Walkey, C. D., & Chan, W. C. (2012). "Understanding and controlling the interaction of nanomaterials with proteins in a physiological environment." Chem Soc Rev 41(7): 2780-2799.
- Walkey, C. D., Olsen, J. B., Guo, H., Emili, A., & Chan, W. C. (2012). "Nanoparticle size and surface chemistry determine serum protein adsorption and macrophage uptake." J Am Chem Soc 134(4): 2139-2147.
- Wang, R. B., Billone, P. S., & Mullett, W. M. (2013). "Nanomedicine in Action: An Overview of Cancer Nanomedicine on the Market and in Clinical Trials." Journal of Nanomaterials.
- Wang, X. Y., Ishida, T., & Kiwada, H. (2007). "Anti-PEG IgM elicited by injection of liposomes is involved in the enhanced blood clearance of a subsequent dose of PEGylated liposomes." Journal of Controlled Release 119(2): 236-244.
- Wike-Hooley, J., Haveman, J., & Reinhold, H. (1984). "The relevance of tumour pH to the treatment of malignant disease." Radiotherapy and oncology : journal of the European Society for Therapeutic Radiology and Oncology 2(4): 343-366.
- Wilson, W. R., & Hay, M. P. (2011). "Targeting hypoxia in cancer therapy." Nature Reviews Cancer 11(6): 393-410.

- Xiao, K., Li, Y. P., Luo, J. T., Lee, J. S., Xiao, W. W., Gonik, A. M., Agarwal, R. G., & Lam, K. S. (2011). "The effect of surface charge on in vivo biodistribution of PEG-oligocholeic acid based micellar nanoparticles." *Biomaterials* 32(13): 3435-3446.
- Xu, P., Bajaj, G., Shugg, T., Van Alstine, W. G., & Yeo, Y. (2010). "Zwitterionic Chitosan Derivatives for pH-Sensitive Stealth Coating." *Biomacromolecules* 11(9): 2352-2358.
- Yang, R., Meng, F. H., Ma, S. B., Huang, F. S., Liu, H. Y., & Zhong, Z. Y. (2011). "Galactose-Decorated Cross-Linked Biodegradable Poly(ethylene glycol)-b-poly(epsilon-caprolactone) Block Copolymer Micelles for Enhanced Hepatoma-Targeting Delivery of Paclitaxel." *Biomacromolecules* 12(8): 3047-3055.
- Yao, L., Daniels, J., Moshnikova, A., Kuznetsov, S., Ahmed, A., Engelman, D. M., Reshetnyak, Y. K., & Andreev, O. A. (2013). "pHLIP peptide targets nanogold particles to tumors." *Proc Natl Acad Sci U S A* 110(2): 465-470.
- Yeo, Y., & Park, K. N. (2004). "Control of encapsulation efficiency and initial burst in polymeric microparticle systems." *Archives of Pharmacal Research* 27(1): 1-12.
- Yin, H., Kang, H. C., Huh, K. M., & Bae, Y. H. (2012). "Biocompatible, pH-sensitive AB(2) Miktoarm Polymer-Based Polymersomes: Preparation, Characterization, and Acidic pH-Activated Nanostructural Transformation." *Journal of Materials Chemistry* 22(36): 91968-91978.
- Yoshioka, H. (1991). "Surface modification of haemoglobin-containing liposomes with polyethylene glycol prevents liposome aggregation in blood plasma." *Biomaterials* 12(9): 861-864.
- Yuan, F., Dellian, M., Fukumura, D., Leunig, M., Berk, D. A., Torchilin, V. P., & Jain, R. K. (1995). "Vascular-Permeability in a Human Tumor Xenograft - Molecular-Size Dependence and Cutoff Size." *Cancer research* 55(17): 3752-3756.
- Zalipsky, S., Hansen, C. B., Oaks, J. M., & Allen, T. M. (1996). "Evaluation of blood clearance rates and biodistribution of poly(2-oxazoline)-grafted liposomes." *J Pharm Sci* 85(2): 133-137.
- Zalipsky, S., Qazen, M., Walker, J. A., 2nd, Mullah, N., Quinn, Y. P., & Huang, S. K. (1999). "New detachable poly(ethylene glycol) conjugates: cysteine-cleavable lipopolymers regenerating natural phospholipid, diacyl phosphatidylethanolamine." *Bioconjug Chem* 10(5): 703-707.
- Zhang, L. F., Chan, J. M., Gu, F. X., Rhee, J. W., Wang, A. Z., Radovic-Moreno, A. F., Alexis, F., Langer, R., & Farokhzad, O. C. (2008). "Self-assembled lipid-polymer hybrid nanoparticles: A robust drug delivery platform." *ACS Nano* 2(8): 1696-1702.
- Zhang, L. F., & Granick, S. (2006). "How to stabilize phospholipid liposomes (using nanoparticles)." *Nano Letters* 6(4): 694-698.
- Zhao, Z., Meng, H., Wang, N., Donovan, M. J., Fu, T., You, M., Chen, Z., Zhang, X., & Tan, W. (2013). "A controlled-release nanocarrier with extracellular pH value driven tumor targeting and translocation for drug delivery." *Angew Chem Int Ed Engl* 52(29): 7487-7491.
- Zhong, Y., Yang, W., Sun, H., Cheng, R., Meng, F., Deng, C., & Zhong, Z. (2013). "Ligand-Directed Reduction-Sensitive Shell-Sheddable Biodegradable Micelles Actively Deliver Doxorubicin into the Nuclei of Target Cancer Cells." *Biomacromolecules*.

CHAPTER 2. PREPARATION AND EVALUATION OF LOW MOLECULAR WEIGHT CHITOSAN COATED NPS MEDIATED VIA DOPAMINE POLYMERIZATION

2.1 Introduction

To take advantage of the EPR effect, NPs should be able to circulate avoiding immune surveillance, until they reach tumors. Upon arrival at target tumors, NPs should be stably retained in the tissues and/or taken up by cancer cells to release the loaded drug. Traditionally, NPs are coated with hydrophilic neutral polymers such as PEG, which sterically stabilizes the NPs and delays adsorption of plasma proteins to the surface (Senior et al., 1991; Torchilin et al., 1994), to achieve long-term circulation. However, the PEG surface can also limit cellular interactions with target cells and cellular internalization, creating a ‘PEG dilemma’ (H. Du et al., 1997; Hatakeyama et al., 2011). As a way of overcoming the dilemma, we previously proposed a low molecular weight chitosan (LMWC) as an alternative surface layer (Amoozgar et al., 2012a). Chitosan is a linear polyaminosaccharide with a pKa value close to 6.5, which helps establish electrostatic interactions with negatively charged cell membrane in weakly acidic microenvironment of tumors (pH 6.8-7.2) (Gerweck & Seetharaman, 1996). At neutral pH, chitosan coated on polymeric NPs protects them from phagocytic uptake (Parveen & Sahoo, 2011) and prolongs their circulation time (Ishak et al., 2013). By reducing the MW to <6.5 kDa, we intended to increase hydrophilicity of the polymer and reduce pH-independent interactions with cells mediated by polymer chain entanglement, further improving its protective effect at neutral pH (Amoozgar et al., 2012a). We obtained the proof of concept in the previous study, using NPs produced with PLGA covalently conjugated to LMWC via an amide bond (PLGA-LMWC) (Amoozgar et al., 2012a)

The PLGA-LMWC NPs, consisting of PLGA core and LMWC surface, showed a pH-sensitive surface charge profile, which translated to NP-cell interactions at weakly acidic pH with reduced phagocytic uptake and little non-specific NP-cell interactions at neutral pH (Amoozgar et al., 2012a). However, the covalent conjugation of LMWC to PLGA had several drawbacks. First, the chemical conjugation procedure is lengthy and inefficient and requires reactive reagents and catalysts that need to be completely removed after the reaction. Moreover, the conjugation process reduces the potential of NPs as a drug carrier. LMWC conjugation requires a sufficient number of carboxyl termini, which necessitates the use of a low molecular weight PLGA (4 kDa, PLGA₄). This polymer is relatively hydrophilic and, thus, has an inherent limitation in encapsulating hydrophobic drugs. Covalent conjugation of LMWC makes the product even more hydrophilic, further compromising the ability of the formed NPs to load and retain a drug. Prolonged reaction in basic pH also accelerates degradation of the polymer and aggravates the problem. Consequently, PTX-loaded PLGA₄-LMWC NPs showed a rapid drug release in PBS with 0.1% Tween 80 in 24 hours (Amoozgar et al., 2012a). NPs showing high initial burst release are likely to release the drug in circulation and not contribute to improving tumor-specific drug delivery; therefore, these shortcomings should be overcome for the LMWC-coated NPs to make further contribution to chemotherapy.

In an attempt to overcome this challenge, we have employed a new surface modification method based on dopamine polymerization (Lee et al., 2007), which has been used to functionalize several nanostructures including nanowires (Ryu et al., 2011), carbon nanospheres (Wang et al., 2012), gold nanoclusters (Lin et al., 2013) and gold nanorods (Black et al., 2013), and validated that the new method can effectively functionalize polymeric NPs with different types of ligands (Gullotti et al., 2013; Park et al., 2014). The dopamine polymerization method depends on oxidation of dopamine catechol, followed by formation of polydopamine (pD) layer on the NP surface, where functional ligands with amine or thiol are covalently conjugated. This method can be implemented in mild conditions such as brief exposure to pH 8.5, UV light (X. Du et al., 2014), or oxidants (Wei et al., 2010), does not require reactive reagents or lengthy reaction, and can be applied to a broad range of surface modifiers and NP platforms (Lee et al., 2007; Park et al., 2014).

Once dopamine polymerizes, it loses its dopaminergic activity (Park et al., 2014), and the resulting pD is biodegradable and biocompatible with a LD₅₀ of 483.95 mg/kg in mice after intravenous injection (S. A. Abouelmagd et al., 2014).

In this study, we use the dopamine polymerization method to produce LMWC-coated NPs (**Fig.3**) based on the flexibility in controlling drug release. Here, LMWC molecules are incorporated into the pD layer on PLGA NPs via multiple amine groups. Since LMWC is introduced as an addendum to pre-formed NPs via the pD layer, the core NPs can be prepared with polymers that serve best to load and retain drugs, not constrained by the needs for carboxyl termini or the hydrophilicity of the modified polymer. We demonstrate that PLGA NPs modified with LMWC via dopamine polymerization method overcome the previously observed limitations of PLGA₄-LMWC NPs and show the desired pH-sensitivity in cell interaction and drug delivery and the tendency to avoid phagocytic uptake, similar to PLGA₄-LMWC NPs. We also investigate NP-cell interactions at acidic pH and their intracellular trafficking and discuss their implications in drug delivery to tumor tissues.

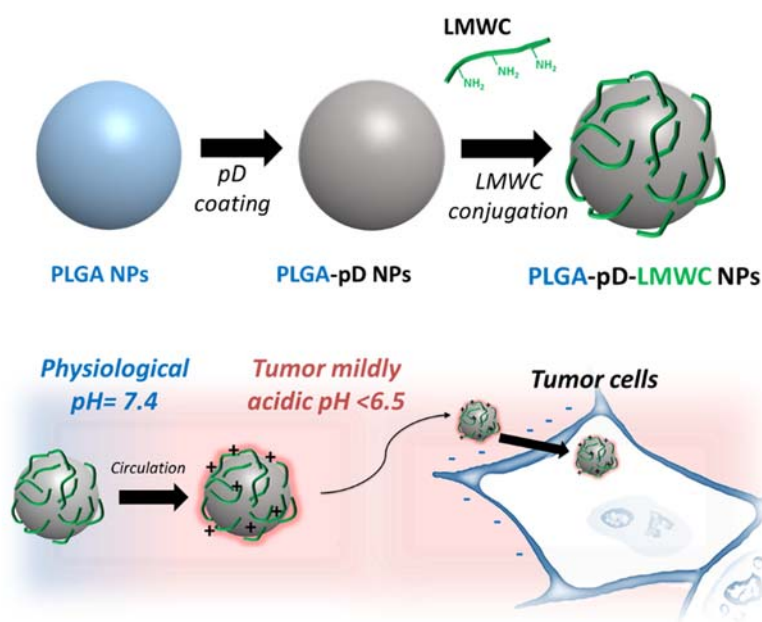


Figure 3: Schematic diagram of PLGA-pD-LMWC NP preparation and following cellular interactions.

2.2 Materials and Methods

2.2.1 Materials

Chitosan (90-150 kDa) was purchased from Sigma-Aldrich (MO, USA). PLGA (acid end cap, 4 kDa, LA:GA=50:50, PLGA₄) was purchased from Durect Corp (AL, USA). PLGA (118 kDa, LA:GA= 65:35, PLGA₁₁₈) was purchased from Lakeshore Biomaterials (AL, USA). PLGA (150 kDa, LA:GA=85:15, PLGA₁₅₀) and fluorescein-conjugated PLGA (7 kDa, LA:GA=50:50, *PLGA) were purchased from Akina Inc. (IN, USA). Paclitaxel (PTX) was a gift from Samyang Genex Corp (Seoul, Korea). LysoTracker Red DND-99, CellMask Deep Red plasma membrane stain, and Hoechst 33342 were purchased from Life Technologies (CA, USA). Methoxy PEG amine, HCl salt (5 kDa, mPEG-NH₂) was purchased from JenKem Technology USA (TX, USA). Dopamine hydrochloride was purchased from Alfa Aesar (MA, USA). Coomassie Brilliant blue G-250 protein stain and sodium dodecyl sulfate-acrylamide gel electrophoresis (SDS-PAGE) molecular weight standards were purchased from Bio-Rad (CA, USA). (3-(4,5-Dimethylthiazol-2-yl)- 2,5-diphenyltetrazolium bromide) (MTT) was purchased from Invitrogen (Eugene, OR, USA). All other materials were of analytical grade

2.2.2 Preparation of PLGA Cores

PLGA polymers with different molecular weights and LA:GA ratios (PLGA₄: 4 kD, LA:GA=50:50, PLGA₁₁₈: 118 kD, LA:GA=65:35 and PLGA₁₅₀: 150 kD, LA:GA=85:15) were formulated into NPs via the single emulsion solvent evaporation method. 20 mg of polymer and 2.2 mg of PTX were dissolved into 1 ml DCM. The organic polymer phase was emulsified in 5 mL aqueous phase containing 5% PVA at 80% amplitude and on a 4-s on and 2-s off pulse mode. Emulsion was dispersed in deionized water and stirred for 3 hours to allow evaporation of DCM. NPs were collected via centrifugation at 12,000 rpm (15,000 xg rcf) for 30 minutes and washed three times using deionized water to remove any residual DCM and PVA.

2.2.3 Preparation and Characterization of LMWC

LMWC was prepared by as previously described (Amoozgar et al., 2012a). Briefly, 25 mg/mL of chitosan solution was incubated in 33% hydrogen peroxide for 3.5 hours, dialyzed against water with a molecular weight cut-off (MWCO) of 3500 Da, and freeze-dried. The molecular weight of LMWC was estimated by matrix-assisted laser desorption ionization time-of-flight/time-of-flight (MALDI-TOF/TOF) analysis and analytical ultracentrifugation (AUC). For mass spectrometry, 1 mg/mL LMWC solution was prepared in acidified water (pH 5), filtered with a 0.2 μm syringe filter, and mixed with a matrix (sinapinic acid solution in acetonitrile/water (50:50) containing 0.1% trifluoroacetic acid) in 1:1 ratio. Mass analysis was performed with a 4800 MALDI TOF/TOF instrument (Applied Biosystems, USA) in 2000-8000 m/z range. For AUC, LMWC solution in sodium acetate buffer (pH 4.3, 10 mM) was prepared in 1, 0.5 and 0.25 mg/mL and analyzed with a Beckman Optima XL-I ultracentrifuge (Beckman Coulter Inc., CA, USA). The sedimentation coefficients and apparent molecular weights were calculated from size distribution analysis with SEDFIT v.12.0. The pH dependence of water solubility of LMWC was estimated by measuring the transmittance of LMWC solution (0.5 mg/mL) varying the pH from 2.5 to 10 with NaOH. % Transmittance (%T) was calculated as $10^{-A} \times 100$, where A was the absorbance of the solution at 500 nm.

2.2.4 Preparation of Coated Particles

PLGA₄-LMWC NPs. A covalent conjugate PLGA₄-LMWC was prepared as described previously (Amoozgar et al., 2012a). Briefly, 200 mg of LMWC was dissolved in acidified water (20 mL, pH 5) and added to 40 mL dimethyl sulfoxide (DMSO). Five hundred milligrams of PLGA₄ was dissolved in 2 mL of dichloromethane (DCM), to which hydroxybenzotriazole (HOBT) (74.3 mg), 1-Ethyl-3-(3-dimethylaminopropyl) carbodiimide (EDC) (106.2 μL), and tetramethylethylenediamine (TEMED) (269.9 μL) were sequentially added. The activated PLGA₄ was added to LMWC solution dropwise and stirred overnight. The formed conjugate, PLGA₄-LMWC, was purified by dialysis (MWCO: 3500 Da) against a mixture of DMSO and water (50:50) and then water, freeze-dried, and stored at -20°C. PLGA₄-LMWC NPs were prepared using the single emulsion

solvent evaporation method. Twenty milligrams of PLGA₄-LMWC was dissolved in a mixture of 0.5 mL DMSO, 0.5 mL DCM and 0.1 mL water, optionally with 1.2 mg of paclitaxel (PTX). The organic phase was emulsified in 5 mL of aqueous phase containing 5% polyvinyl alcohol (PVA) using a Vibra-Cell probe sonicator (Sonics, Newtown, CT, USA) at 80% amplitude with a 4-s on and 2-s off pulse mode. The emulsion was dispersed in 10 mL of deionized water and stirred for 3 hours to evaporate DCM. NPs were collected via centrifugation at 10,000 rpm for 30 minutes and washed three times. Fluorescently labeled PLGA₄-LMWC NPs (*PLGA₄-LMWC NPs) were prepared by replacing 25% of polymer with *PLGA.

PLGA-pD-LMWC and PLGA-pD-PEG particles. PLGA-pD-LMWC NPs were prepared by coating pre-formed particles with LMWC via the dopamine polymerization method (Park et al., 2014). For PLGA cores, organic phase containing 50 mg polymer (PLGA₁₁₈, PLGA₁₅₀ or PLGA₇-FITC=PLGA*) were emulsified into 10 mL of 4% PVA solution and followed by dispersion into deionized water. For PTX loaded NPs, 10 mg PTX were incorporated into the organic phase. Emulsion was stirred for 5 hours to allow DCM evaporation. NPs were collected by centrifugation and washed with water three times.

PLGA microparticles (MPs) were prepared in a similar way except that the emulsification process was performed with a Silverson L4R Laboratory Mixer (East Longmeadow, MA, USA) for 1 minute at 5,000 rpm. The core particles were then prime-coated with polymerized dopamine (pD) by incubation in 1 mg/mL dopamine solution in Tris buffer (pH 8.5, 10 mM) for 3 hours at room temperature. The pD-coated particles were collected by centrifugation, washed two times, and incubated with LMWC aqueous solution (pH 7.5, 0.5 mg/mL) for 40 minutes to produce PLGA-pD-LMWC particles. For comparison, PEG-modified (PLGA-pD-PEG) particles were created by incubating the pD-coated particles in mPEG-NH₂ solution (pH 8.5, 2 mg/mL). The particles were collected by centrifugation and washed two times to remove excess LMWC or mPEG-NH₂. Throughout this study, PLGA particles refer to PLGA₁₅₀ particles unless stated otherwise.

2.2.5 Particle Characterization

Particle size and zeta potential of particles were determined using a Malvern Zetasizer Nano ZS90 (Worcestershire, UK). The size was measured with particles dispersed in phosphate buffer (2.2 mM, pH 7.4). The zeta potential was determined at different pHs with particles dispersed in phosphate buffer (2.2 mM, pH 7.4) or MES buffer (5 mM, pH 6.2). Particle morphology was observed by transmission electron microscopy (TEM). An aqueous suspension of freshly prepared NPs (0.5-1 mg/mL) was spotted on a formvar-coated carbon grid (400 mesh) and negatively stained with 2% uranyl acetate solution. The grid was air-dried and examined with a FEI Tecnai T20 transmission electron microscope (OR, USA).

The LMWC content in PLGA-pD-LMWC NPs was quantified by the ninhydrin assay. The ninhydrin reagent was prepared by dissolving ninhydrin and hydrindantin in lithium acetate buffer (Amoozgar et al., 2012a; Leane et al., 2004). 0.5 mg of freeze-dried NPs were dispersed in 0.5 mL water and combined with 0.5 mL of fresh reagent. The mixture was heated in boiling water for 30 minutes, then cooled and quenched with 15 mL of 50% ethanol solution. The absorbance of the solution was read at 570 nm using SpectraMax M3 microplate reader (Molecular Device, Sunnyvale, CA). The amount of LMWC per NP sample was calculated after subtracting the background absorbance of PLGA-pD NPs, using a calibration curve drawn with LMWC solutions of known concentrations.

2.2.6 PTX Release from PLGA Matrices

2.2.6.1 *In Vitro* Release Study

To determine PTX loading in NPs, freeze-dried NPs were accurately weighed and dissolved in 0.5 mL acetonitrile. After precipitating polymer with the addition of 0.5 mL deionized water, the sample was centrifuged, and the supernatant analyzed via high pressure liquid chromatography (HPLC). The loading efficiency (LE%) was calculated as the amount of PTX per NP mass. For *in vitro* release studies, NPs equivalent to 8.75 μg PTX were dispersed in 1 mL of phosphate-buffered saline (PBS, pH 7.4) containing 0.2%

Tween 80 and shaken at 37°C. At regular time points, NP suspension was centrifuged at 12,000 rpm (15,000 xg rcf) for 15 min, 0.8 mL of supernatant was sampled and replaced with 0.8 mL of fresh buffer, and the pellet was resuspended and returned for continued incubation. The sampled supernatant was filtered with a 0.45 µm syringe filter and analyzed by HPLC. HPLC analysis was performed with an Agilent 1100 HPLC system (Palo Alto, CA), equipped with Ascentis C18 column (25 cm × 4.6 mm, particle size 5 µm). The mobile phase was a 50:50 mixture of water and acetonitrile run at a flow rate of 1 mL/min. PTX was detected by a UV detector (227 nm).

2.2.6.2 Cell Culture

SKOV-3 human ovarian cancer cells (ATCC, Manassas, VA, USA) were grown in RPMI-1640 medium containing 10% FBS, 100 units/mL of penicillin and 100 µg/mL of streptomycin.

2.2.6.3 Cytotoxicity of PLGA NPs

Cells were seeded in 96-well plates with the density of 8000 cells/well. Next day, PLGA NPs equivalent to 1-1000 nM PTX was incubated with the cells for 24 or 72 hours. For the former, NPs containing medium was replaced with fresh one after 24 hour incubation with treatment, and the cells were further incubated for 48 more hours. For the latter, cells were incubated with NPs for 72 hours without medium change. At the end of the incubation time, MTT (3-(4,5-dimethylthiazol-2-yl)-2,5-diphenyltetrazolium bromide) assay was used to determine cell viability. Briefly, medium was replaced with 100 µL of fresh medium and 15 µL of MTT solution (5 mg/mL), and cells were incubated for 3.5 hours, followed by addition of 100 µL of stop solution (50 % DMSO, 20% SDS and 0.02% acetic acid). Next day, wells absorbance was read using a SpectraMax M3 microplate reader (Molecular Device, Sunnyvale, CA) at 529 nm.

2.2.7 Protein Adsorption to NP surface

NPs were incubated with 50% fetal bovine serum (FBS) in PBS at 37°C with shaking for 1 or 24 hours. NPs were collected by centrifugation at 13,200 rpm and washed 3 times with water to remove excess and loosely bound proteins. To strip off hard corona

proteins from NP surface, NPs were boiled in sample buffer containing 5-mercaptoethanol and 2% SDS for 5 minutes. The sample was analyzed with SDS-PAGE. The resolved protein bands were stained with Coomassie brilliant blue G-250. The molecular weight of band of interest was determined using GelAnalyzer 2010a software (www.GelAnalyzer.com). Briefly, a calibration curve was constructed with a plot of the relative migration distance (R_f) of standard bands versus their MWs and used to determine the MW of resolved bands in each gel. The intensity of different bands was quantified using ImageJ 1.48v software densitometry analysis (National Institute of Health, MD, USA).

2.2.8 NP-Cell Interaction Studies

2.2.8.1 Cell Culture

SKOV-3 human ovarian cancer cells (ATCC, Manassas, VA, USA) were grown in RPMI-1640 medium containing 10% FBS, 100 units/mL of penicillin and 100 μ g/mL of streptomycin. J774A.1 mouse macrophages (ATCC) were grown in Dulbecco's modified Eagle medium (DMEM) medium supplemented with 10% FBS, 100 units/mL of penicillin and 100 μ g/mL of streptomycin. All cell experiments were performed in the FBS-supplemented medium.

2.2.8.2 Quantitative Analysis of Cell-Particle Interactions

SKOV-3 cells and J774A.1 macrophages were seeded in 6-well plates at a density of 500,000 cells per well and incubated overnight. Next day, the medium was replaced with fresh medium that contained 0.1 mg/mL of fluorescently labeled NPs or MPs (*NPs or *MPs). For SKOV-3 cells the medium pH was adjusted to 6.2 or 7.4. After 3 hours, cells were harvested by trypsinization (SKOV-3) or scraping (J774A.1), dispersed in fresh medium of corresponding pH, and analyzed with a FC500 flow cytometer (Beckman Coulter, Indianapolis, IN, USA). At least 10,000 gated events were acquired, and data was analyzed with the FlowJo software (Treestar, CA, USA).

2.2.8.3 Visualization of Cell-Particle Interactions

NP interaction with SKOV-3 cells was observed with confocal microscopy. SKOV-3 cells were seeded in a 35 mm glass bottomed dish (MatTek) at a density of 500,000 cells per dish. After overnight incubation, the medium was replaced with fresh RPMI medium adjusted to pH 6.2 or 7.4, which contained 0.1 mg/mL of *NPs. After 3 hours of incubation, the medium was removed, and the cells were washed with fresh medium twice to remove free and loosely-bound *NPs. Cells were incubated with Hoechst 33342 nuclear staining dye at 5 μ g/mL for 10 minutes, and imaged with a Nikon-A1R confocal microscope (Nikon America Inc., NY, USA). The *NPs were excited with a 488 nm laser, and the emission was read from 500 to 550 nm. The cell nuclei were excited with a 407 nm laser, and the emission was read from 425 to 475 nm.

To locate NPs in SKOV-3 cells, cells were further stained with CellMask Deep Red (Life Technologies) or LysoTracker Red DND-99 (Life Technologies) for labeling the plasma membrane or acidic intracellular organelles (late endosomes and lysosomes), respectively. Cells were incubated with *NPs in the same manner as above. After removing *NPs, CellMask Deep Red was added at 5 μ g/mL or LysoTracker Red at 30 nM. Cells were incubated with each marker for 40 min, washed twice with fresh medium at corresponding pH, stained with Hoechst 33342, and imaged with a Nikon A1R confocal microscope. Stained plasma membrane was excited at 639 nm, and emission was collected from 663 to 738 nm. LysoTracker stained organelles were excited at 561 nm, and the emission was collected from 570 to 620 nm.

Time-lapse confocal microscopy was performed to examine the time course of cellular uptake and intracellular trafficking of *PLGA-pD-LMWC NPs. SKOV-3 cells were seeded in a glass bottomed dish at a density of 500,000 cells per dish. After overnight incubation, the medium was replaced with 1 mL of fresh medium adjusted to pH 6.2, and cells were stained with LysoTracker Red DND-99 and Hoechst 33342. The dish was put in an environmental chamber, supplied with 5% CO₂, and mounted on Nikon A1R confocal microscope. The chamber, microscope stage, and objective lens were heated to 37°C.

*PLGA-pD-LMWC NPs (0.1 mg) was added to the dish, and the cells were imaged over 4.5 hours.

Macrophage uptake of *MPs was visualized with fluorescence microscopy. J774A.1 macrophages were seeded in a 24-well plate at a density of 100,000 cells per well and incubated overnight. The medium was replaced with fresh one containing 0.1 mg/mL *MPs. After 3 hours, the medium was removed, and cells were washed with fresh medium twice. The cells were stained with Hoechst 33342 and imaged with a Cytation-3 imaging system (BioTek, USA).

2.2.9 pH Selective PTX Delivery to Cancer Cells by NPs

Cellular uptake of PTX delivered by NPs was estimated at different pHs. SKOV-3 were seeded at a density of 200,000 cells per well in a 12-well plate. Next day, the medium was replaced with 0.8 mL of fresh medium of pH 6 or 7.4, which contained PTX-loaded PLGA-pD-LMWC- or PLGA-pD-PEG NPs equivalent to 4.8 μ g of PTX. Free PTX dissolved in DMSO solution was added at the same concentration to a control group. The total amount of DMSO added to 0.8 mL of medium was 12 μ L and non-toxic to the cells. After 2.5 hours at 37°C, the medium was removed, and cells were trypsinized, suspended in fresh medium of corresponding pH, and centrifuged at 2,000 rpm to separate cells from NPs. The cell pellet was lysed by three freeze-thaw cycles, suspended in 0.5 mL PBS, and probe sonicated. The cell lysate was spiked with 35 μ g of carbamazepine as an internal standard, extracted with 1.5 mL of ethyl acetate for 40 min, and centrifuged at 4,000 rpm for 25 minutes to separate ethyl acetate layer. 1.3 mL of ethyl acetate were dried under vacuum in a glass tube and reconstituted with 1:1 acetonitrile/water solution and analyzed with HPLC. A PTX calibration curve was drawn with different amounts of PTX added to cell suspension in PBS and treated in the same way.

2.3 Results

2.3.1 Preparation and Characterization of PLGA Cores

PTX loaded PLGA NPs with different molecular weights (4, 118 and 150 kDa) and LA: GA (50:50, 65:35 and 85:15), respectively, were prepared via the single emulsion-solvent evaporation method. The produced NPs had average diameters of ~220- 250 nm, low polydispersity indices (PDI, the width of the particle size distribution, obtained from the cumulant analysis (Amoozgar et al., 2012b)) and negative zeta potentials (**Table 2**). As the molecular weight (MW) and LA fraction in the polymer increased, the LE of PTX increased from 8.17 to 11.4%. This is likely due to the relatively high hydrophobicity of high MW polymers, which had greater affinity for hydrophobic PTX and solidified faster than lower MW polymers. To evaluate the NP's ability to retain PTX, *in vitro* release kinetics of PTX was examined in phosphate buffered saline (PBS) containing 0.2% Tween 80 at pH 7.4. Tween containing medium was chosen to provide an amphiphilic environment for PTX release, more physiologically relevant than plain PBS. As expected, MW and LA:GA had a dramatic effect on *in vitro* release profiles (**Fig. 4**).

Table 2: Particle size, zeta potential and loading efficiency of PTX loaded NPs

NP type (Polymer ^{MW} (LA:GA))	Particle size (diameter, nm)	Polydispersity index (PDI)	Zeta potential at pH 7.4 (mV)	Loading efficiency (LE %)
PLGA ₄ (50:50)	250 ± 41	0.124 ± 0.02	-8.02 ± 0.3	8.17 ± 0.6
PLGA ₁₁₈ (65:35)	230 ± 36	0.08 ± 0.013	-4.67 ± 2.5	8.25 ± 0.47
PLGA ₁₅₀ (85:15)	223 ± 12	0.06 ± 0.04	-3.91 ± 2.11	11.4 ± 0.38

Among the three types of PLGA NPs, the least hydrophobic one, PLGA4 NPs released almost all loaded PTX in a few hours. More hydrophobic PLGA118 NPs showed less burst initial release of <50% in the first 8 hours and retained PTX for a longer period of time. PLGA150 NPs had the least burst release effect. At the end of the release study, ~30% and 10% of the loaded PTX was retrieved by the end of the release from PLGA150 and PLGA118 NPs, respectively.

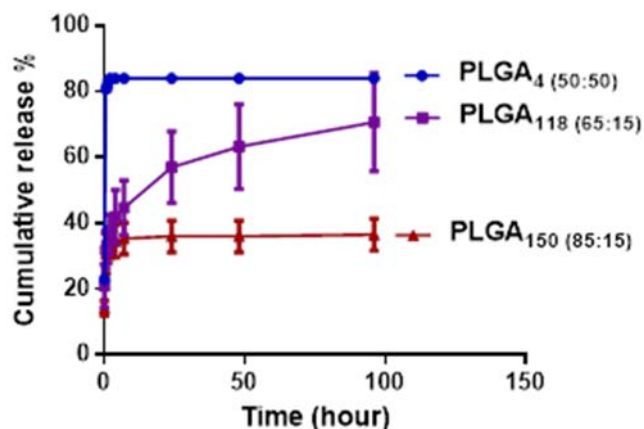


Figure 4: *In vitro* release profiles of PTX from NPs of different polymer matrices in PBS (0.2% Tween 80, pH 7.4).

To confirm the results of the *in vitro* release study and compare different polymers in a physiologically relevant serum-containing medium, cytotoxic activity of PTX loaded NPs on sensitive SKOV3 cells was evaluated as an indirect measurement of PTX release from the NPs. Since plain PLGA NPs were not taken up by the cells (Xu et al., 2009), it was expected that the killing effect would be directly proportional to the drug release. For this study, SKOV-3 cells were exposed to PTX loaded PLGA₄, PLGA₁₁₈ and PLGA₁₅₀ for 24 or 72 hours, and their mitochondrial activity was determined via the MTT assay. All NPs showed a less cytotoxic effect than free PTX (**Fig. 5a and b**) reflecting the attenuation of drug release. The cytotoxic effect trend matched that seen with the *in vitro* release study for both 24 and 72 hour exposure times; PLGA₄ > PLGA₁₁₈ > PLGA₁₅₀.

However, the extent of difference observed in this study was less than that seen with the release study. This can be explained by the effect of cell culture medium components, including serum proteins, on the release of PTX from the polymer matrix and/or stability of the released PTX. The PLGA matrix itself did not contribute to the cytotoxic effect of PTX loaded PLGA NPs (**Fig. 5c and d**).

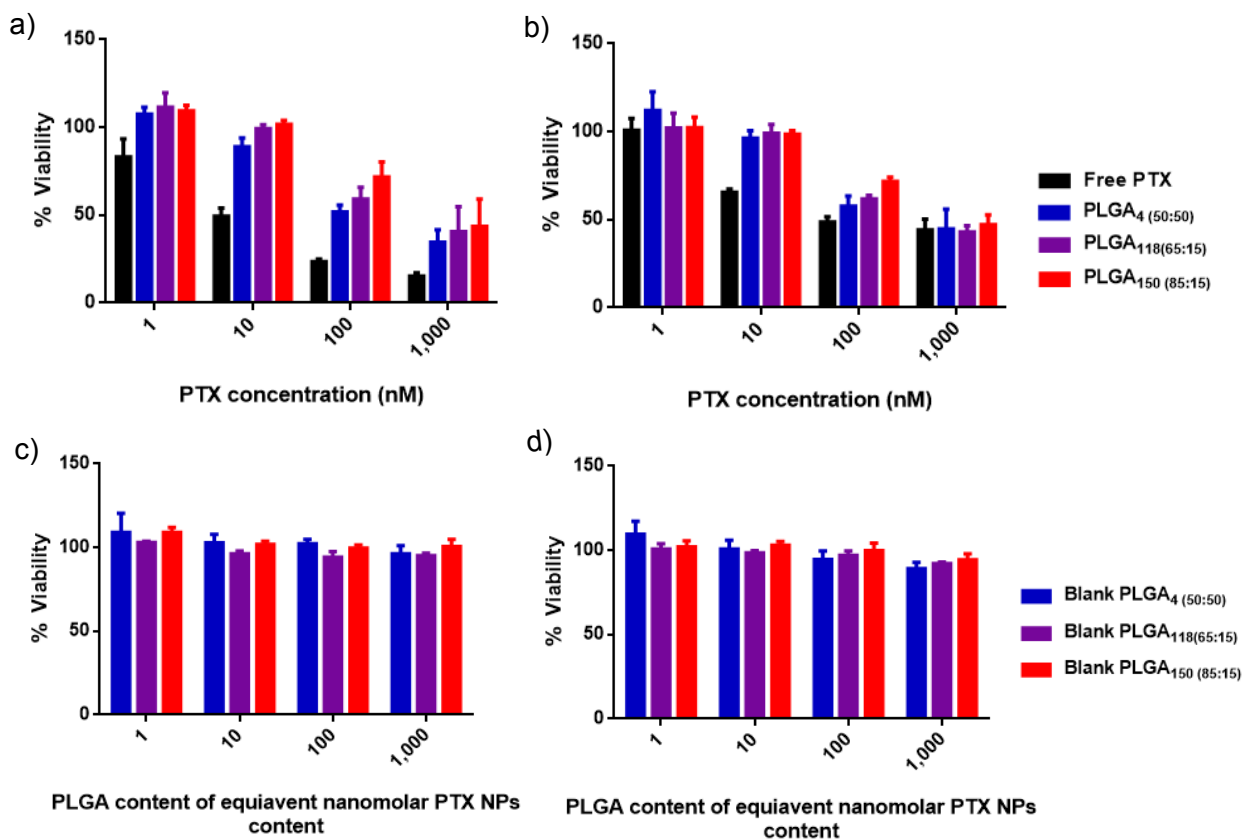


Figure 5: Viability of SKOV-3 cells exposed to free PTX and PTX loaded NPs for 24 (a) or 72 hour (b), and blank PLGA NPs for 24 (c) or 72 hour (d).

2.3.2 Preparation and Characterization of Coated NPs

LMWC was produced by H₂O₂ digestion. Three and a half hour digestion in 33% H₂O₂ reduced the chitosan molecular weight from 90-150 kDa to 4.8 kDa, consistent our

the previous study (Amoozgar et al., 2012a). The MALDI spectrum of LMWC showed a peak at ~ 4800 m/z (**Fig. 6a**). The AUC analysis confirmed the result with additional insight into the structure. The global analysis of fitted data identified two species with apparent MWs of 2.5 and 7.3 kDa, existing in a dynamic mixture in solution. The frictional coefficient ratio (f/f_0) was ~ 2.2 , which indicated that LMWC had a semi-flexible rod shape, in agreement with existing studies (Errington et al., 1993). LMWC was soluble in water over a wide range of pH including 7-9, where the parent chitosan was not soluble (**Fig. 6b**).

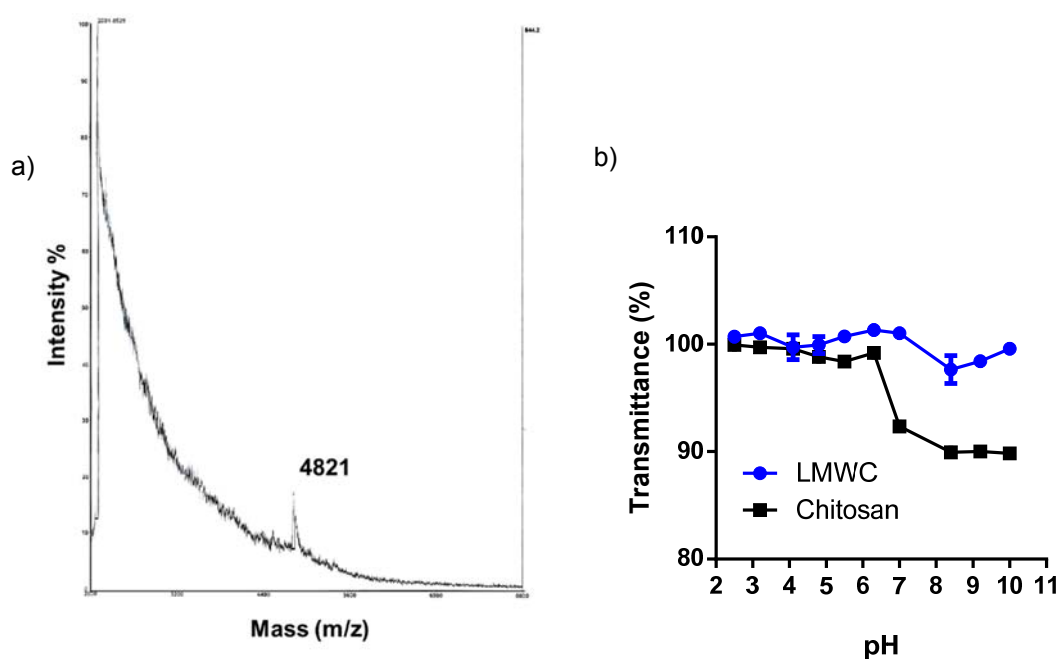


Figure 6: (a) Analysis of LMWC via MALDI-TOF/TOF using sinapinic acid as a matrix (1:1), (b) pH-dependent change in transmittance for LMWC ($n=2$) and undegraded chitosan (0.5 mg/mL in water) measured at 500 nm.

LMWC-coated NPs were produced with a polymer pre-conjugated with LMWC (PLGA₄-LMWC NPs) or by LMWC conjugation via pD to the pre-formed PLGA NPs (PLGA-pD-LMWC NPs). PLGA₄-LMWC NPs or pre-formed core PLGA NPs showed similar sizes, 160 nm and 158 nm, respectively (**Fig. 7a**). LMWC coating via pD increased the size to 209 nm (**Fig. 7a**). The size increase is likely due to aggregation by additional centrifugation rather than the thickness of the conjugated layer, given that the

polydispersity increased with coating (**Fig. 7a**), and individual NPs observed with TEM showed similar sizes irrespective of the coating (**Fig. 8**). TEM of negatively stained NPs revealed thin layer of pD coating on the NP surface. However, no other difference was observed in NPs further conjugated with LMWC or PEG-NH₂.

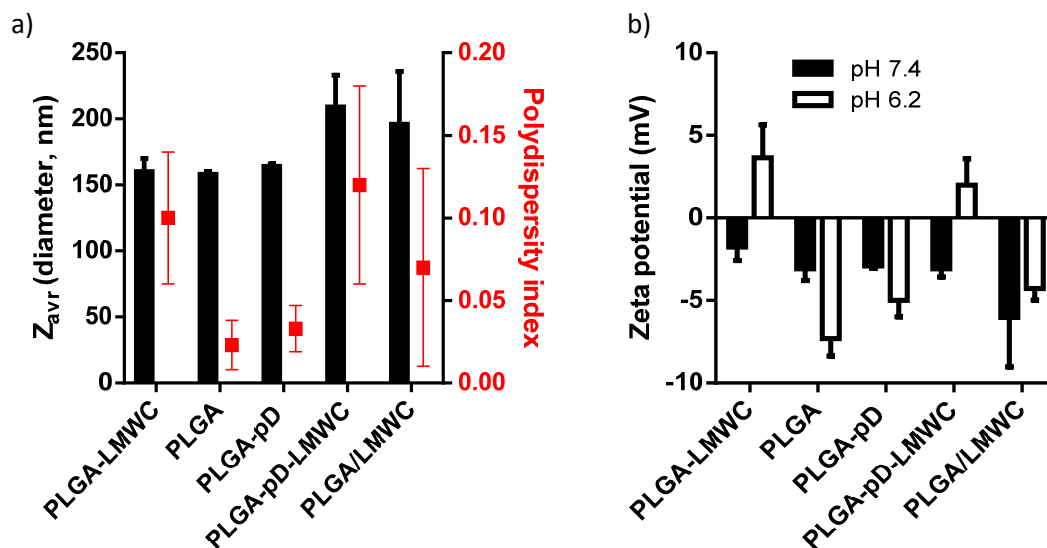


Figure 7: Particle size and surface charge analysis of different NPs: (a) Average diameter (Z_{avr}) and polydispersity index, (b) Zeta potential at pH 7.4 and 6.2.

Although the presence of LMWC or PEG conjugated to pD were not visually identified in TEM images, their immobilization was confirmed by the altered surface properties. PLGA-pD-LMWC NPs showed a characteristic pH-dependent charge profile, negative at pH 7.4 and positive at pH 6.2, similar to PLGA₄-LMWC NPs. PLGA NPs, PLGA-pD NPs, and PLGA-pD-PEG NPs remained negatively charged irrespective of the pH (**Fig. 7b**). PLGA NPs incubated with LMWC without pD prime coating (PLGA/LMWC NPs) did not show the pH-dependent charge profile, indicating that LMWC did not physically adsorb to PLGA and the LMWC immobilization depended on the pD layer. The LMWC content in PLGA-pD-LMWC NPs was determined to be $4.7\pm 3\%$ according to the ninhydrin assay, lower than the estimated value for PLGA₄-LMWC NPs ($8.7\pm 1.5\%$) (Amoozgar et al., 2012a).

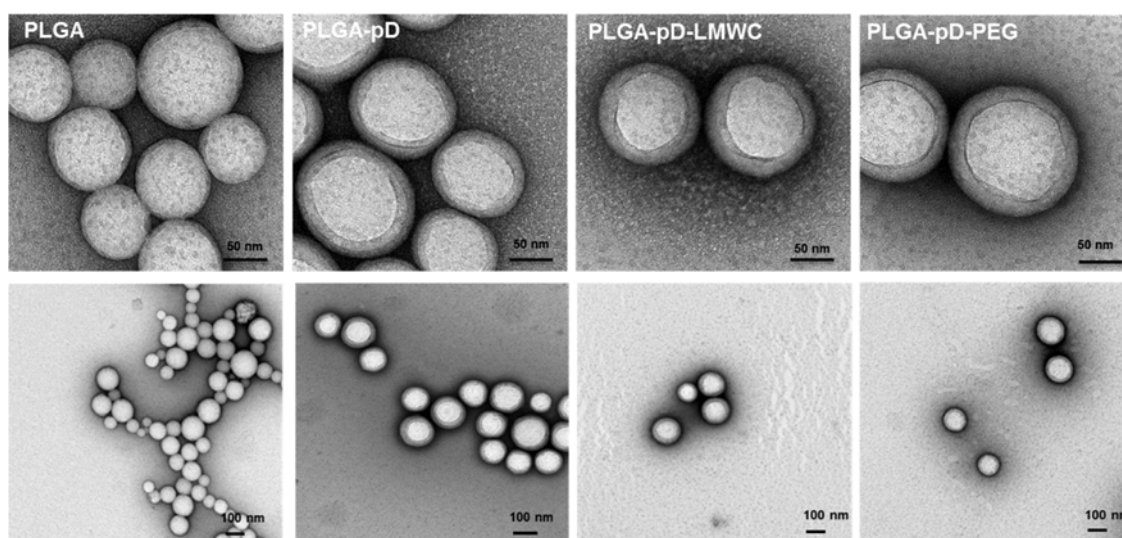


Figure 8: Transmission electron microscopy (TEM) images of NPs negatively stained with 2% uranyl acetate. Scale bar: 50 nm (top panel), 100 nm (bottom panel).

2.3.3 In Vitro PTX Release of Coated PLGA NPs

PLGA₄-LMWC NPs and PLGA-pD-LMWC NPs were compared with respect to the LE of PTX and *in vitro* PTX release. PLGA₄-LMWC NPs showed a LE of $27.9\pm 7.9\%$, higher than the theoretical LE (5.7%), which suggested partial loss of PLGA₄-LMWC

polymer during NP preparation (Amoozgar et al., 2012a). PLGA-pD-LMWC NPs made of PLGA₁₁₈ and PLGA₁₅₀ showed LE's of $12.8 \pm 5.3\%$ and $8.6 \pm 3.4\%$, corresponding to 77.0% and 51.7% of the theoretical LE (16.7%), respectively. *In vitro* PTX release kinetics study was performed in PBS containing 0.2% Tween 80 (pH 7.4). PLGA₄-LMWC showed initial burst release in this medium, releasing $90.4 \pm 8.5\%$ of the loaded dose in 7 hours. On the other hand, PLGA₁₁₈-pD-LMWC and PLGA₁₅₀-pD-LMWC NPs released PTX more slowly: $54.2 \pm 5.5\%$ and $39.9 \pm 9.0\%$ of the total dose in 7 hours, reaching ~80% release in 48 hours (**Fig. 9**). Since PLGA₁₅₀-pD-LMWC NPs retained PTX most stably, they were used in the rest of the study, referred to as PLGA-pD-LMWC NPs without a subscript.

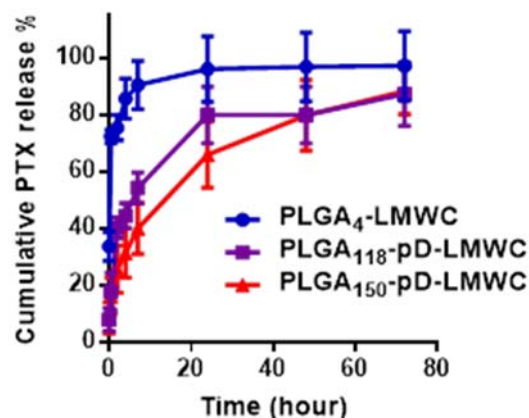


Figure 9: *In vitro* release of PTX from different NPs in PBS (0.2% Tween 80) at 37°C. At 7th hour, release % is significantly different among three types of NPs ($p < 0.05$, two-tailed T-test, $n=3$).

2.3.4 Protein Adsorption to NPs Surface

To identify proteins binding to the NPs during incubation in serum-containing medium and correlate them with NP-cell interactions, the NPs were incubated in 50% FBS solution for 1 or 24 hours, and the proteins tightly bound to NPs (“hard corona”) were analyzed by gel electrophoresis. Proteins bound to NPs were recovered with a detergent (SDS) and a reducing agent (5-mercaptoethanol), combined with heating (Docter et al., 2014; Monopoli et al., 2011), and analyzed with SDS-PAGE. The intensity of protein bands

increased with time (**Figs. 10a and b**), indicating the increase of protein binding to NPs, as previously observed (Casals et al., 2010). Three major bands were identified at 66 kDa, 61 kDa, and 52 kDa, likely corresponding to bovine serum albumin, fetuin-A (Martel et al., 2010; Young et al., 2009), and IgG (Ehrenberg et al., 2009), respectively. Albumin and fetuin-A made up dominant fractions, reflecting their abundance in FBS (**Fig. 10c**) (Wu et al., 2013).

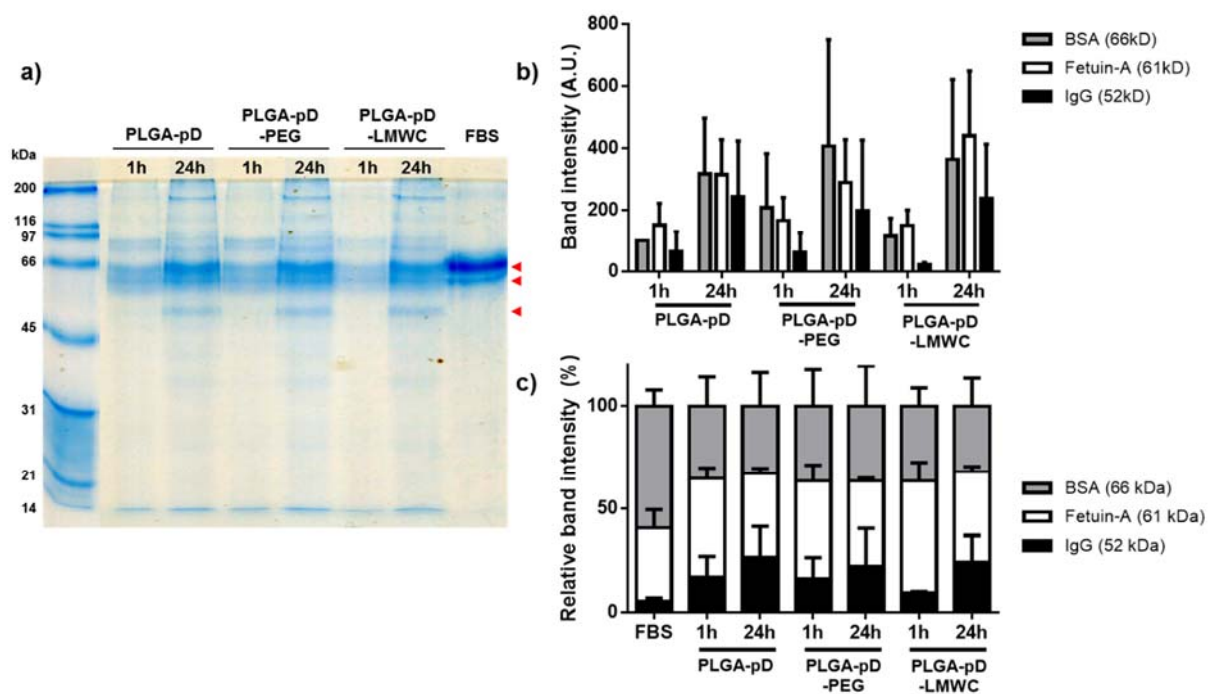


Figure 10: Analysis of NPs hard corona composition post incubation in 50% FBS. Proteins were stripped off NPs and resolved via SDS-PAGE. Protein extracts of different NPs post incubation for 1 or 24 hours were run on 12% gels and compared to standards ‘ladder’ (left) and FBS (right of gel). A representative Coomassie blue-stained gel of resolved corona proteins is shown in (a), where arrows point to bands of interest. Relative band intensity of most prominent proteins pointed with arrows in (a) was analyzed via ImageJ 1.48v software. Average of four different gels is shown in (b).

The relative intensity of IgG band increased with time in all NPs tested, irrespective of the coating polymers (LMWC vs. PEG) (**Fig. 10c**). Consistent with the protein

adsorption, the NPs with hard corona showed relatively more negative zeta potential than those in buffer (**Fig. 11**).

2.3.5 NP-Cell Interaction Studies

Given that PLGA-pD-LMWC NPs did not completely avoid protein binding in serum solution, we were curious if PLGA-pD-LMWC NPs would maintain the intended advantage of pH-sensitive surface in serum-containing medium. Fluorescently labeled NPs (*PLGA-pD-LMWC NPs and other control *NPs) had similar sizes and surface charges to those of unlabeled NPs (**Fig. 12**). The labeled *NPs were incubated with SKOV-3 cells in medium containing 10% FBS at pH 7.4 and 6.2. From flow cytometry analysis, only the cells incubated with *PLGA-pD-LMWC and *PLGA-LMWC NPs at pH 6.2 showed increased geometric mean, indicating NP-cell interaction (**Fig. 13a**). Those incubated with *PLGA-pD-LMWC or *PLGA-LMWC NPs pH 7.4 did not show such increase, which means that LMWC-coated NPs can preferentially interact with cells in mildly acidic environment such as the extracellular matrix of solid tumors but not in normal tissues. *PLGA, *PLGA-pD, and *PLGA-pD-PEG NPs had no cell interaction at either pH. Confocal microscopy confirmed this result (**Fig. 13b**).

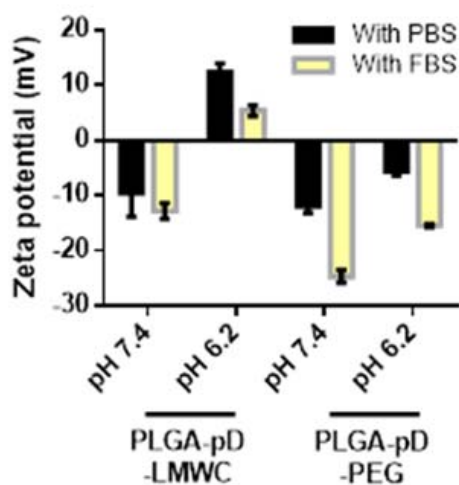


Figure 11: Zeta potential of protein coated PLGA-pD-LMWC and PLGA-pD-PEG NPs. NPs were incubated in PBS or 50% FBS in PBS. (n=3).

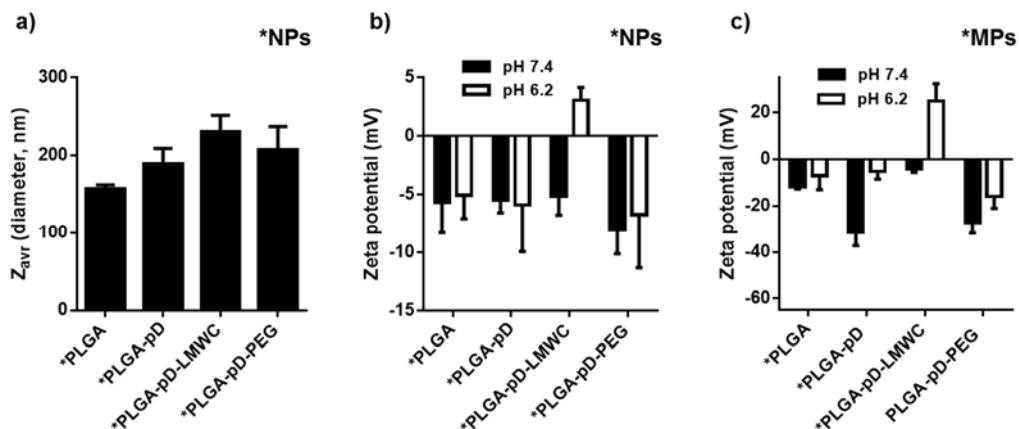


Figure 12: Analysis of different fluorescent particles: Average diameter (Z_{avr}) of fluorescent NPs (a), and Zeta potential at pH 7.4 and 6.2 of fluorescent NPs (b) and MPs (c).

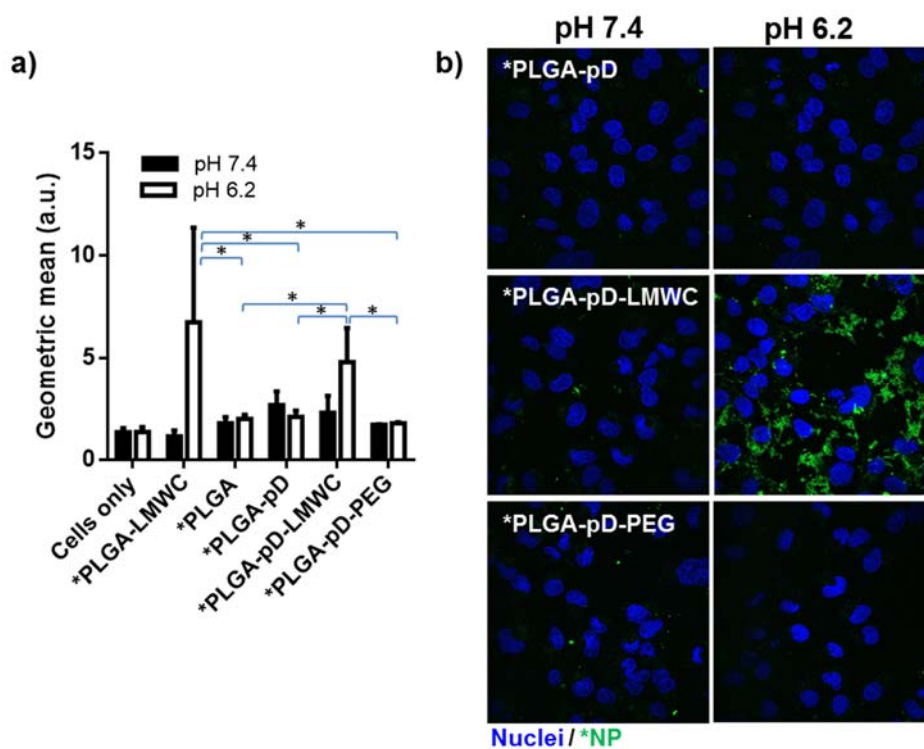


Figure 13: pH dependent cellular interaction of different fluorescently labeled NPs (*PLGA) with SKOV-3 cells as quantified by (a) Flow-cytometry (Geometric mean at pH 6.2 was significantly different for *PLGA-LMWC and *PLGA-pD-LMWC from that of *PLGA, *PLGA-pD and *PLGA-pD-PEG, two tailed t-test, $P < 0.05$) or visualized via confocal microscopy (b) after three hours of incubation (Green= NPs labeled by FITC, Blue= nuclei stained by Hoechst).

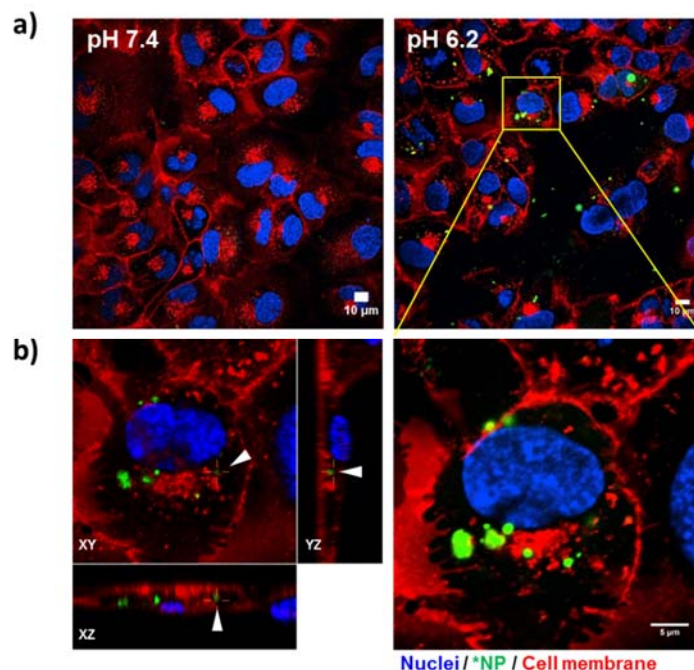


Figure 14: Cellular uptake of *PLGA-pD-LMWC NPs by SKOV-3 cells after three hours of incubation at pH 7.4 or 6.2, imaged via confocal microscopy as thin sections (a) or z-stack (b, right panel). A cross section showing XY, XZ and YZ planes demonstrates NPs intracellular localization (b, left panel) (Green= NPs labeled by FITC, Red= cell membrane labeled by CellMask deep red).

To locate *PLGA-pD-LMWC NPs with respect to cells, cell membrane or acidic intracellular organelles (late endosomes and lysosomes) were stained after removing uninternalized or loosely bound NPs. *PLGA-pD-LMWC NPs incubated with SKOV-3 cells at pH 6.2 for 3 hours were observed on the membrane or within the membrane boundary (**Figs. 14a and b**), indicating that they were partly internalized by the cells, but not at pH 7.4 (**Fig. 14a**). *PLGA-pD-LMWC NPs were not colocalized with the acidic organelles at least in 3 hours (**Fig. 15a**). According to time-lapse microscopy, cell binding of *PLGA-pD-LMWC NPs at pH 6.2 occurred in 60-75 min (**Fig. 15b**). The NP signals increased over time (**Fig. 15b and 16**), both outside and inside the cells, but NPs did not traffic into the late endosomes and lysosomes at least by 4.5 hours (**Fig. 15b**).

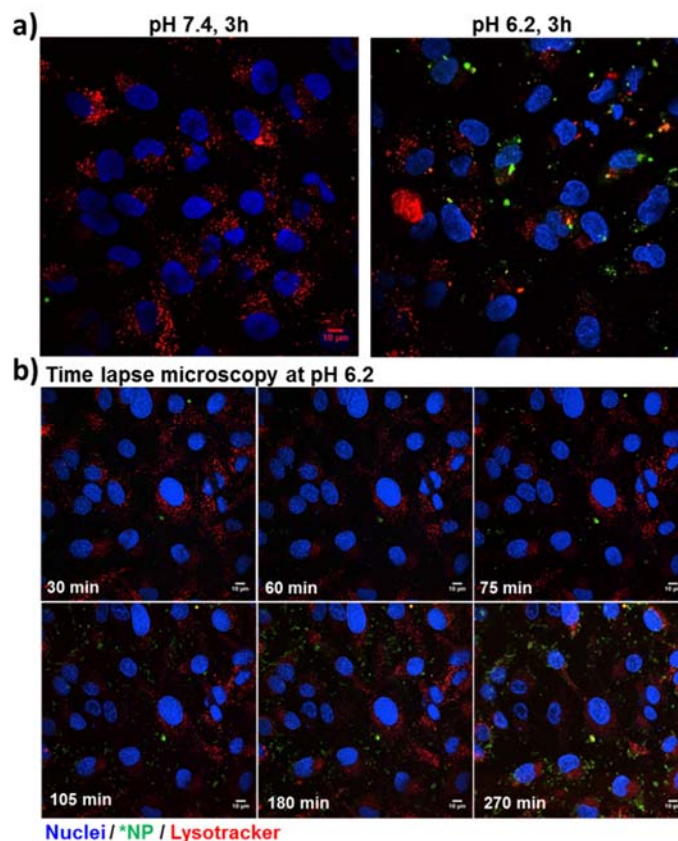


Figure 15: Intracellular trafficking of *PLGA-pD-LMWC NPs in SKOV-3 cells imaged by confocal microscopy after three hours of incubation at pH 7.4 or 6.2 (a). Time lapse imaging of *PLGA-pD-LMWC NPs incubated with SKOV-3 cells at pH 6.2 over 270 minutes (b) (Green= NPs labeled by FITC, Red= Lysotracker Red DND-99).

To test if the LMWC layer could reduce phagocytic uptake of particles despite the apparent protein binding, *PLGA-pD-LMWC MPs and control *MPs (2-3 μm in diameter), with similar surface charge profiles to those of *NPs (**Fig. 12c**), were incubated with J774A.1 macrophages in medium containing 10% FBS, and the extent of MP phagocytosis was determined by measuring the fluorescence of macrophages by flow cytometry and fluorescence microscopy. Here, MPs were used instead of NPs, as they are more readily phagocytosed than NPs (Tabata & Ikada, 1988), hence serving as a more sensitive model for evaluating macrophage uptake of particles. *PLGA MPs were taken up most avidly (**Fig. 17**). *PLGA-pD MPs were taken up less than the naked MPs due to the hydrophilicity

imparted by amine-containing pD. *PLGA-pD-LMWC MPs showed significant reduction in macrophage uptake, to even greater extent than *PLGA-pD-PEG MPs (Fig. 17).

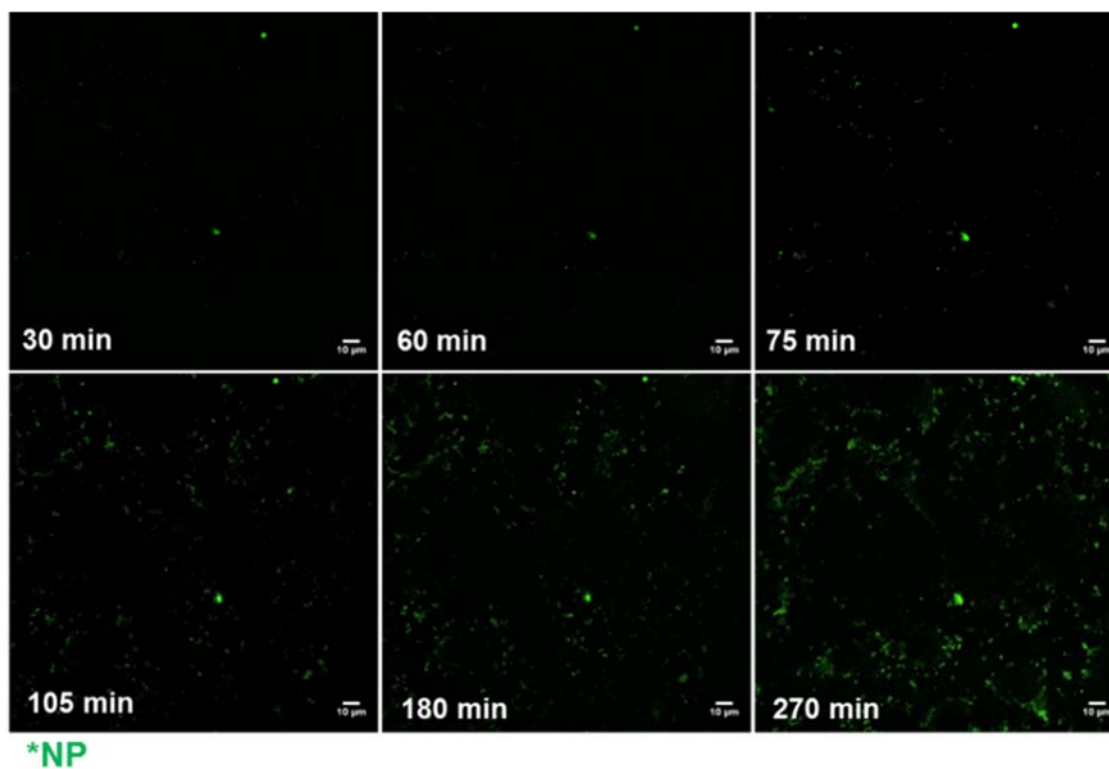


Figure 16: Time lapse imaging of *PLGA-pD-LMWC NPs after incubation with SKOV-3 cells over 270 minutes at pH 6.2 (Green= NPs labeled by FITC).

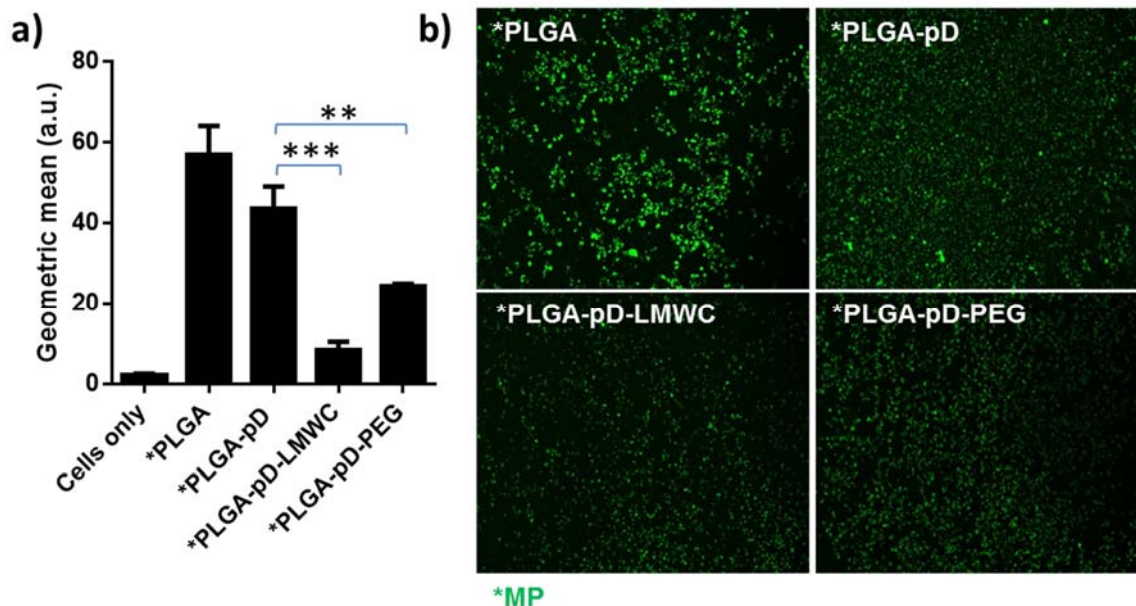


Figure 17: J774A.1 macrophage uptake of fluorescently labeled MPs at pH 7.4 after three hours analyzed via flow cytometry (a) or visualized with Cytation 3 fluorescence imaging system (b). All geometric means were significantly different from each other (One-way Anova test, $P < 0.05$). ** $p = 0.0034$ and *** $p = 0.0004$ (two-tailed t-test). (Green= MPs labeled by FITC)

We hypothesize that selective cell interaction of PLGA-pD-LMWC NPs at acidic pH would translate to superior drug delivery. To test this, PTX-loaded PLGA-pD-LMWC NPs were incubated with SKOV-3 cells at pH 7.4 and 6 for 2.5 hours, and the amount of PTX retained by the cells was quantified. Cells incubated at pH 6 had > 4-fold higher PTX content as compared to pH 7.4 (**Fig. 18**). On the other hand, there was no such difference for the cells incubated with free PTX or PTX-loaded PLGA-pD-PEG NPs. This shows that the enhanced NP-cell interaction at acidic pH leads to similar enhancement in drug delivery to the cells.

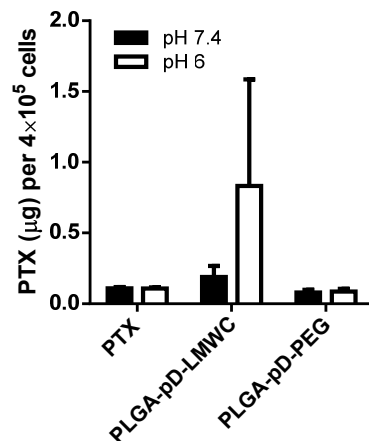


Figure 18: pH dependent PTX retention post incubation of SKOV-3 cells with PTX loaded NPs or free PTX at pH 7.4 or 6. NPs were incubated with the cells for two and half hours at either pH after which cells were harvested, separated from NPs and analyzed for PTX content (* $p=0.03$, two-tailed T-test, $n=4-8$).

2.4 Discussion

Polymeric NP systems have been pursued for decades as a way of achieving tumor-specific drug delivery (Cheng et al., 2012). One of the critical challenges in clinical translation of these systems is the increasing complexity of NP design and production methods. While the complexity is introduced to accommodate the developing knowledge of cancer biology, it also leads to increasing cost and regulatory scrutiny, making the development of a commercial product more challenging (Cheng et al., 2012; Goldberg et al., 2013). Moreover, the complicated design and synthesis can induce undesirable changes to the material properties of the NPs such as MW and hydrophobicity, which are essential for their primary roles: loading and retaining drugs. We experienced this problem in developing PLGA₄-LMWC NPs, where the LMWC conjugation allowed for specific drug delivery to acidic tissues but increased hydrophilicity of the polymer and compromised the NP's function as a carrier of PTX (Amoozgar et al., 2012a). Here, we used a new surface modification method based on dopamine polymerization to decouple the NP formation from the surface modification, enabling independent control of NP cores and surface properties for drug loading/release and specific NP-cell interactions, respectively.

The LMWC-coated PLGA NPs via dopamine polymerization (PLGA-pD-LMWC NPs) showed comparable average diameter and pH-dependent charge profile to those of PLGA₄-LMWC NPs (**Fig. 7**). The LMWC content in PLGA-pD-LMWC NPs was lower than that of PLGA₄-LMWC NPs, but it does not necessarily indicate less efficient coating because in PLGA₄-LMWC NPs a fraction of the LMWC is supposed to be buried in the NPs and not exposed on the surface. Given the extent of charge change and NP-cell interaction profiles (**Fig. 13**), the surface exposed LMWC of the two NPs is likely to be comparable.

The PTX LE of PLGA₄-LMWC NPs was apparently higher than that of PLGA-pD-LMWC NPs, but this is likely because of the hydrophilicity of PLGA₄-LMWC polymer, which was selectively washed out during the NP preparation (Amoozgar et al., 2012a). PTX-loaded PLGA-pD-LMWC NPs produced with PLGA₁₁₈ and PLGA₁₅₀ showed more prolonged drug release than PTX-loaded PLGA₄-LMWC NPs, due to the greater hydrophobicity and MW of the polymers. PTX release in the first few hours from these NPs was much slower than that from PLGA₄-LMWC NPs and sustained over three days (**Fig. 9**), suggesting that these NPs may reduce premature drug release in circulation during the critical period for NP biodistribution. The drug release from PLGA₄-LMWC NPs reported in this study appears faster than that in the previous study (Amoozgar et al., 2012a), but the two results are not directly comparable because the Tween 80 concentration in release medium was different (0.2 vs. 0.1%). We chose 0.2% Tween 80 in PBS as release medium, as we determined that it was suitable to mimic the amphiphilic feature of physiological fluid and simulate a sink condition faced *in vivo* (Sara A. Abouelmagd et al., 2015). Even though the drug release attenuation appears to be modest as compared to the previous study, the actual extent of attenuation is deemed significant given the difference of the medium. The NP core can be further optimized, if additional release control is necessary, by simple replacement of the polymer with more hydrophobic and slowly degrading ones (Mittal et al., 2007).

The LMWC layer introduced via pD layer to the pre-formed PLGA NPs provided pH-sensitive functionality necessary for desired cell-NP interactions (**Fig. 7b**). Prior to testing cellular uptake of NPs, we investigated protein binding to PLGA-pD-LMWC NPs

incubated in serum solution. As the NPs enter the blood stream, they instantaneously interact with plasma proteins to be covered with a protein corona on NPs surface. The protein coronal is composed of a tightly bound stable “hard” corona and a loosely bound “soft” corona, which can be dynamically exchanged with other proteins (Milani et al., 2012). Since NPs entering the bloodstream cannot completely avoid protein binding even with protective surface layer (Walkey et al., 2012) and the identity of bound proteins has shown to be critical to the biological fate of NPs (Salvati et al., 2013), we investigated the protein binding profile of the surface-modified NPs after incubation in 50% FBS, which mimicked the serum content in blood (Sherwood, 2011). Protein binding occurred with all tested NPs (PLGA-pD, PLGA-pD-LMWC, and PLGA-pD-PEG NPs) in a similar pattern (**Fig. 10**). It is noteworthy that all NPs were increasingly enriched with IgG, antibodies responsible for opsonization and complement activation, over time. **Figure 17** shows that pD, pD-LMWC, and pD-PEG layers helped reduce phagocytic uptake of PLGA MPs by J774.1 macrophages due to the hydrophilicity imparted by the surface polymers. However, the increasing IgG enrichment indicates that the function of LMWC or PEG in this NP system is still imperfect as a stealth layer and remains to be improved in future studies.

The surface charges of all NPs decreased after incubation in serum solution (**Fig. 11**), reflecting protein binding. Nevertheless, the protein-bound PLGA-pD-LMWC NPs maintained the pH-sensitive charge profile, allowing for acid-specific NP-cell interactions in serum-containing medium. Confocal microscopy showed that PLGA-pD-LMWC NPs established interactions with SKOV-3 cell membrane at pH 6.2 in 1 hour and entered the cells in 3 hours (**Fig. 14**), likely via adsorption-mediated endocytosis (Tahara et al., 2009). The internalized NPs did not colocalize with the late endosomes or lysosomes by 4.5 hours (**Fig. 15b**). This result is similar to an observation made with cationic NPs coated with quaternized chitosan, which were internalized by human proximal epithelial cells and showed little colocalization with lysosomes in 6 hours (Yue et al., 2011). Other types of NPs lacking LMWC (PLGA, PLGA-pD or PLGA-pD-PEG) did not show cellular uptake at 6.2. All tested NPs showed little uptake by SKOV-3 cells at pH 7.4 (**Fig. 13**). This result indicates that while PLGA-pD-LMWC NPs did not interact with cells at normal physiological pH, they were able to establish interactions with cells at <pH 6.5 as PLGA-

LMWC NPs previously did (Amoozgar et al., 2012a) and get internalized into the cells without being trafficked into the acidic organelles. Given that hard corona compositions for all pD-coated NPs (PLGA-pD, PLGA-pD-PEG, and PLGA-pD-LMWC NPs) were similar (**Fig. 10**), yet PLGA-pD-LMWC NPs showed different behavior than the other NPs, the protein corona in this NP system did not play a role significant enough to interfere with the intended NP-cell interactions. This result is contrasted with transferrin-functionalized silica NPs that lost targeting capabilities in serum-containing medium due to the formation of protein corona (Salvati et al., 2013).

The reliable drug encapsulation achieved by PLGA-pD-LMWC NPs allowed us to test the contribution of the LMWC surface to PTX delivery in acidic medium. SKOV-3 cells were exposed to PTX-loaded PLGA-pD-LMWC NPs at pH 7.4 and 6 for 2.5 hours and analyzed with respect to the amount of PTX retained by the cells (through NP binding and/or uptake). The exposure time was limited to 2.5 hours since it would better represent dynamic *in vivo* situation, where NPs would continuously flow and get gradually diluted. PTX-loaded PLGA-pD-LMWC NPs delivered a significantly greater amount of PTX to SKOV-3 cells at pH 6 compared to pH 7.4 and those delivered by free PTX treatment or PTX-loaded PLGA-pD-PEG NPs, which showed similar cellular levels of PTX at both pHs (**Fig. 18**). Since drug release from NPs was minimal (<30 %) in 2.5 hours (**Fig. 9**), the large amount of drug delivered by PLGA-pD-LMWC NPs would be readily attributable to the enhanced NP binding and uptake by the cells at acidic pH, previously observed by confocal microscopy and flow cytometry.

2.5 Conclusions

In summary, LMWC-coated PLGA NPs created by the dopamine polymerization method overcame the limitations of the earlier version based on a PLGA-LMWC covalent conjugate in loading and retaining PTX. The PLGA-pD-LMWC NPs provided pH-sensitive surface layer, which enabled acid-specific NP-cell interaction and enhanced drug delivery to cells in the weakly acidic environment. The LMWC layer did not completely prevent protein binding to the NPs incubated in serum solution but reduced phagocytic uptake. The surface remains to be further optimized to reduce IgG binding.

2.6 References

- Amoozgar, Z., Park, J. Y., Lin, Q. N., & Yeo, Y. (2012). "Low Molecular-Weight Chitosan as a pH-Sensitive Stealth Coating for Tumor-Specific Drug Delivery." Mol Pharm 9(5): 1262-1270.
- Du, H., Chandaroy, P., & Hui, S. W. (1997). "Grafted poly-(ethylene glycol) on lipid surfaces inhibits protein adsorption and cell adhesion." Biochimica et biophysica acta 1326(2): 236-248.
- Gerweck, L. E., & Seetharaman, K. (1996). "Cellular pH gradient in tumor versus normal tissue: Potential exploitation for the treatment of cancer." Cancer Res 56(6): 1194-1198.
- Hatakeyama, H., Akita, H., & Harashima, H. (2011). "A multifunctional envelope type nano device (MEND) for gene delivery to tumours based on the EPR effect: a strategy for overcoming the PEG dilemma." Adv Drug Deliv Rev 63(3): 152-160.
- Ishak, R. A. H., Awad, G. A. S., Zaki, N. M., El-Shamy, A. E. H. A., & Mortada, N. D. (2013). "A comparative study of chitosan shielding effect on nano-carriers hydrophilicity and biodistribution." Carbohydrate Polymers 94(1): 669-676.
- Parveen, S., & Sahoo, S. K. (2011). "Long circulating chitosan/PEG blended PLGA nanoparticle for tumor drug delivery." European Journal of Pharmacology 670(2-3): 372-383.
- Senior, J., Delgado, C., Fisher, D., Tilcock, C., & Gregoriadis, G. (1991). "Influence of Surface Hydrophilicity of Liposomes on Their Interaction with Plasma-Protein and Clearance from the Circulation - Studies with Poly(Ethylene Glycol)-Coated Vesicles." Biochimica et biophysica acta 1062(1): 77-82.
- Torchilin, V. P., Omelyanenko, V. G., Papisov, M. I., Bogdanov, A. A., Trubetskoy, V. S., Herron, J. N., & Gentry, C. A. (1994). "Poly(Ethylene Glycol) on the Liposome Surface - on the Mechanism of Polymer-Coated Liposome Longevity." Biochimica Et Biophysica Acta-Biomembranes 1195(1): 11-20.
- Abouelmagd, S. A., Hyun, H., & Yeo, Y. (2014). "Extracellularly activatable nanocarriers for drug delivery to tumors." Expert Opinion on Drug Delivery 11(10): 1601-1618.
- Abouelmagd, S. A., Sun, B., Chang, A. C., Ku, Y. J., & Yeo, Y. (2015). "Release kinetics study of poorly water-soluble drugs from nanoparticles: Are we doing it right?" Molecular Pharmaceutics.
- Amoozgar, Z., Park, J. Y., Lin, Q. N., & Yeo, Y. (2012a). "Low Molecular-Weight Chitosan as a pH-Sensitive Stealth Coating for Tumor-Specific Drug Delivery." Mol Pharm 9(5): 1262-1270.
- Amoozgar, Z., Park, J. Y., Lin, Q. N., & Yeo, Y. (2012b). "Low Molecular-Weight Chitosan as a pH-Sensitive Stealth Coating for Tumor-Specific Drug Delivery." Molecular Pharmaceutics 9(5): 1262-1270.
- Black, K. C. L., Yi, J., Rivera, J. G., Zelasko-Leon, D. C., & Messersmith, P. B. (2013). "Polydopamine-enabled surface functionalization of gold nanorods for cancer cell-targeted imaging and photothermal therapy." Nanomedicine 8(1): 17-28.

- Casals, E., Pfaller, T., Duschl, A., Oostingh, G. J., & Puntès, V. (2010). "Time Evolution of the Nanoparticle Protein Corona." *Acs Nano* 4(7): 3623-3632.
- Cheng, Z. L., Al Zaki, A., Hui, J. Z., Muzykantov, V. R., & Tsourkas, A. (2012). "Multifunctional Nanoparticles: Cost Versus Benefit of Adding Targeting and Imaging Capabilities." *Science* 338(6109): 903-910.
- Docter, D., Distler, U., Storck, W., Kuharev, J., Wunsch, D., Hahlbrock, A., Knauer, S. K., Tenzer, S., & Stauber, R. H. (2014). "Quantitative profiling of the protein coronas that form around nanoparticles." *Nat Protoc* 9(9): 2030-2044.
- Du, H., Chandaroy, P., & Hui, S. W. (1997). "Grafted poly-(ethylene glycol) on lipid surfaces inhibits protein adsorption and cell adhesion." *Biochimica et biophysica acta* 1326(2): 236-248.
- Du, X., Li, L. X., Li, J. S., Yang, C. W., Frenkel, N., Welle, A., Heissler, S., Nefedov, A., Grunze, M., & Levkin, P. A. (2014). "UV-Triggered Dopamine Polymerization: Control of Polymerization, Surface Coating, and Photopatterning." *Advanced Materials* 26(47): 8029-+.
- Ehrenberg, M. S., Friedman, A. E., Finkelstein, J. N., Oberdorster, G., & McGrath, J. L. (2009). "The influence of protein adsorption on nanoparticle association with cultured endothelial cells." *Biomaterials* 30(4): 603-610.
- Errington, N., Harding, S. E., Varum, K. M., & Illum, L. (1993). "Hydrodynamic Characterization of Chitosans Varying in Degree of Acetylation." *International Journal of Biological Macromolecules* 15(2): 113-117.
- Gerweck, L. E., & Seetharaman, K. (1996). "Cellular pH gradient in tumor versus normal tissue: Potential exploitation for the treatment of cancer." *Cancer Res* 56(6): 1194-1198.
- Goldberg, M. S., Hook, S. S., Wang, A. Z., Bulte, J. W. M., Patri, A. K., Uckun, F. M., Cryns, V. L., Hanes, J., Akin, D., Hall, J. B., Gharkholo, N., & Mumper, R. J. (2013). "Biotargeted nanomedicines for cancer: six tenets before you begin." *Nanomedicine* 8(2): 299-308.
- Gullotti, E., Park, J., & Yeo, Y. (2013). "Polydopamine-Based Surface Modification for the Development of Peritumorally Activatable Nanoparticles." *Pharmaceutical Research* 30(8): 1956-1967.
- Hatakeyama, H., Akita, H., & Harashima, H. (2011). "A multifunctional envelope type nano device (MEND) for gene delivery to tumours based on the EPR effect: a strategy for overcoming the PEG dilemma." *Adv Drug Deliv Rev* 63(3): 152-160.
- Ishak, R. A. H., Awad, G. A. S., Zaki, N. M., El-Shamy, A. E. H. A., & Mortada, N. D. (2013). "A comparative study of chitosan shielding effect on nano-carriers hydrophilicity and biodistribution." *Carbohydrate Polymers* 94(1): 669-676.
- Leane, M. M., Nankervis, R., Smith, A., & Illum, L. (2004). "Use of the ninhydrin assay to measure the release of chitosan from oral solid dosage forms." *International Journal of Pharmaceutics* 271(1-2): 241-249.
- Lee, H., Dellatore, S. M., Miller, W. M., & Messersmith, P. B. (2007). "Mussel-inspired surface chemistry for multifunctional coatings." *Science* 318(5849): 426-430.

- Lin, M. H., Liu, Y. J., Chen, X. F., Fei, S. D., Ni, C. L., Fang, Y. P., Liu, C. B., & Cai, Q. Y. (2013). "Poly(dopamine) coated gold nanocluster functionalized electrochemical immunosensor for brominated flame retardants using multienzyme-labeling carbon hollow nanochains as signal amplifiers." Biosensors & Bioelectronics 45: 82-88.
- Martel, J., Wu, C. Y., & Young, J. D. (2010). "Critical evaluation of gamma-irradiated serum used as feeder in the culture and demonstration of putative nanobacteria and calcifying nanoparticles." PLoS One 5(4): e10343.
- Milani, S., Bombelli, F. B., Pitek, A. S., Dawson, K. A., & Radler, J. (2012). "Reversible versus Irreversible Binding of Transferrin to Polystyrene Nanoparticles: Soft and Hard Corona." Acs Nano 6(3): 2532-2541.
- Mittal, G., Sahana, D. K., Bhardwaj, V., & Kumar, M. N. V. R. (2007). "Estradiol loaded PLGA nanoparticles for oral administration: Effect of polymer molecular weight and copolymer composition on release behavior in vitro and in vivo." Journal of Controlled Release 119(1): 77-85.
- Monopoli, M. P., Walczyk, D., Campbell, A., Elia, G., Lynch, I., Bombelli, F. B., & Dawson, K. A. (2011). "Physical-chemical aspects of protein corona: relevance to in vitro and in vivo biological impacts of nanoparticles." J Am Chem Soc 133(8): 2525-2534.
- Park, J., Brust, T. F., Lee, H. J., Lee, S. C., Watts, V. J., & Yeo, Y. (2014). "Polydopamine-Based Simple and Versatile Surface Modification of Polymeric Nano Drug Carriers." ACS Nano.
- Parveen, S., & Sahoo, S. K. (2011). "Long circulating chitosan/PEG blended PLGA nanoparticle for tumor drug delivery." European Journal of Pharmacology 670(2-3): 372-383.
- Ryu, J., Ku, S. H., Lee, M., & Park, C. B. (2011). "Bone-like peptide/hydroxyapatite nanocomposites assembled with multi-level hierarchical structures." Soft Matter 7(16): 7201-7206.
- Salvati, A., Pitek, A. S., Monopoli, M. P., Prapainop, K., Bombelli, F. B., Hristov, D. R., Kelly, P. M., Aberg, C., Mahon, E., & Dawson, K. A. (2013). "Transferrin-functionalized nanoparticles lose their targeting capabilities when a biomolecule corona adsorbs on the surface." Nat Nanotechnol 8(2): 137-143.
- Senior, J., Delgado, C., Fisher, D., Tilcock, C., & Gregoriadis, G. (1991). "Influence of Surface Hydrophilicity of Liposomes on Their Interaction with Plasma-Protein and Clearance from the Circulation - Studies with Poly(Ethylene Glycol)-Coated Vesicles." Biochimica et biophysica acta 1062(1): 77-82.
- Sherwood, L. (2011). Human Physiology: From Cells to Systems, Cengage Learning.
- Tabata, Y., & Ikada, Y. (1988). "Effect of the Size and Surface-Charge of Polymer Microspheres on Their Phagocytosis by Macrophage." Biomaterials 9(4): 356-362.
- Tahara, K., Sakai, T., Yamamoto, H., Takeuchi, H., Hirashima, N., & Kawashima, Y. (2009). "Improved cellular uptake of chitosan-modified PLGA nanospheres by A549 cells." Int J Pharm 382(1-2): 198-204.

- Torchilin, V. P., Omelyanenko, V. G., Papisov, M. I., Bogdanov, A. A., Trubetsky, V. S., Herron, J. N., & Gentry, C. A. (1994). "Poly(Ethylene Glycol) on the Liposome Surface - on the Mechanism of Polymer-Coated Liposome Longevity." Biochimica Et Biophysica Acta-Biomembranes 1195(1): 11-20.
- Walkey, C. D., Olsen, J. B., Guo, H., Emili, A., & Chan, W. C. (2012). "Nanoparticle size and surface chemistry determine serum protein adsorption and macrophage uptake." J Am Chem Soc 134(4): 2139-2147.
- Wang, G. F., Huang, H., Zhang, X. J., & Wang, L. (2012). "Electrically contacted enzyme based on dual hairpin DNA structure and its application for amplified detection of Hg²⁺." Biosensors & Bioelectronics 35(1): 108-114.
- Wei, Q., Zhang, F. L., Li, J., Li, B. J., & Zhao, C. S. (2010). "Oxidant-induced dopamine polymerization for multifunctional coatings." Polymer Chemistry 1(9): 1430-1433.
- Wu, C.-Y., Young, L., Young, D., Martel, J., & Young, J. D. (2013). "Bions: A Family of Biomimetic Mineralo-Organic Complexes Derived from Biological Fluids." PLoS ONE 8(9): e75501.
- Xu, P. S., Gullotti, E., Tong, L., Highley, C. B., Errabelli, D. R., Hasan, T., Cheng, J. X., Kohane, D. S., & Yeo, Y. (2009). "Intracellular Drug Delivery by Poly(lactic-co-glycolic acid) Nanoparticles, Revisited." Molecular Pharmaceutics 6(1): 190-201.
- Young, J. D., Martel, J., Young, L., Wu, C. Y., Young, A., & Young, D. (2009). "Putative nanobacteria represent physiological remnants and culture by-products of normal calcium homeostasis." PLoS One 4(2): e4417.
- Yue, Z. G., Wei, W., Lv, P. P., Yue, H., Wang, L. Y., Su, Z. G., & Ma, G. H. (2011). "Surface charge affects cellular uptake and intracellular trafficking of chitosan-based nanoparticles." Biomacromolecules 12(7): 2440-2446.

CHAPTER 3. *IN VIVO* EVALUATION OF LMWC-COATED NPS IN TUMOR BEARING MICE

3.1 Introduction

Through *in vitro* studies described in Chapter 2, I have demonstrated that PLGA-pD-LMWC NPs enabled acid-specific NP-cell interaction via pH-sensitive surface layer (Abouelmagd et al., 2015). Based on this outcome, I hypothesized that LMWC coated NPs would have superior tumor accumulation and retention to PEG coated NPs, leading to an enhanced antitumor effect. The purpose of this chapter is to evaluate *in vivo* efficacy of systemically administered the PLGA-pD-LMWC NPs in tumor-bearing mice in comparison with pH-insensitive PLGA-pD-LMWC NPs. Ideally, *in vitro* tests of prepared NPs for tumor drug delivery should help characterize different formulations and optimize their properties for *in vivo* efficacy. However, current *in vitro* tests can only examine one parameter at a time, such as surface charge, protein adsorption profile, drug release kinetics, or cellular interactions with tumor cells. Most importantly, *in vitro* tests do not replace *in vivo* test, where the outcome is the net result of all parameters: opsonization, drug release in blood, macrophage uptake, biodistribution, tumor accumulation and retention (Cho et al., 2013).

A mouse model of subcutaneous xenograft is the most widely used *in vivo* model. In the subcutaneous xenograft model, human tumor cells are inoculated under the skin of immunocompromised mice and allowed to grow to a visible tumor mass. Although this model is not a close representation of natural human primary tumors, it provides a convenient tool to study and compare the biodistribution and anti-tumor effect of different formulations in a relatively short time period due to the fast growth rate and the ease of size measurement (Cho et al., 2013).

In particular, selected tumor models show high vascularization, one of the most important pathological features of tumors, almost always exploited by NP drug carriers (Maeda, 2012). In this study, the *in vivo* behaviors of LMWC and PEG coated NPs were evaluated in two mouse models of subcutaneous tumor xenograft: MCF-7 and LS174T. MCF-7 is a human breast adenocarcinoma cell line, known to be non-invasive and weakly angiogenic due to the poor expression of VEGF (Pathak et al., 2013). LS174T is a human colorectal adenocarcinoma cell line, expressing high amounts of VEGF, and therefore well vascularized (Dang et al., 2008).

The anti-tumor effect of PTX-loaded NPs was evaluated in MCF-7 and LS174T tumor models. To elucidate on the results of tumor suppression profiles, whole-body imaging was performed using NPs loaded with indocyanine green (ICG), in lieu of PTX, in MCF-7 model. ICG is a near-infrared fluorescence dye, conducive to non-invasive *in vivo* imaging due to the negligible tissue background (Frangioni, 2003). ICG was chosen as a proxy of PTX due to the similarity in molecular weight (ICG: 775 Da vs. PTX: 853 Da) and high plasma protein binding. Both ICG and PTX have high affinity for serum albumin (Cherrick et al., 1960; Kumar et al., 1993; Paal et al., 2001). The imaging study was repeated with additional enhancement of tumor acidity via intraperitoneal (IP) injection of glucose and *meta*-iodo-benzylguanidine (MIBG), a mitochondrial respiration inhibitor.

3.2 Materials and Methods

3.2.1 Materials

PLGA (150 kDa, LA:GA=85:15, PLGA₁₅₀) was purchased from Akina Inc. (IN, USA). Paclitaxel (PTX) was a gift from Samyang Genex Corp (Seoul, Korea). Methoxy PEG amine, HCl salt (5 kDa, mPEG-NH₂) was purchased from JenKem Technology USA (TX, USA). Dopamine hydrochloride was purchased from Alfa Aesar (MA, USA). Indocyanine green (ICG) was purchased from MP Biomedical (CA, USA). Human serum albumin (HSA) and *meta*-iodo-benzylguanidine hemisulfate salt (MIBG) were purchased from Sigma-Aldrich (MO, USA). Abraxane was purchased from Celgene (NJ, USA).

Cremonophor EL was purchased from BASF (IL, USA). All other materials were of analytical grade.

3.2.2 Preparation of NPs

3.2.2.1 Preparation of NP Cores

PTX loaded NPs. NPs were prepared via the single emulsion-solvent evaporation method, where PTX was incorporated in the organic phase with PLGA. Briefly, 70 mg of PTX was dissolved with 350 mg of PLGA₁₅₀ in 35 mL DCM, then emulsified in an aqueous phase of PVA (4%, 60 mL) using probe sonication (2 minutes, 4s on/2s off). Emulsion was dispersed in 67 mL of water and stirred for 1 hour followed by rotary evaporation for 1.5 hour to allow complete evaporation of DCM. Finally, NPs were collected via centrifugation (20,000 rpm (30,000 xg rcf)) and washed twice with water.

ICG labeled NPs. NPs were produced by the double emulsion-solvent evaporation method with modification of a previously reported method (Hwang et al., 2014). An aqueous phase of 625 μ L containing 19 mg of human serum albumin (HSA) and 6.3 mg of ICG was emulsified in 6.3 mL of an organic phase of PLGA₁₅₀ (130 mg) in DCM via probe sonication (1 minutes, 1s on/1s off). Resulting emulsion was further emulsified in the second aqueous phase of PVA solution (24 mL, 2.5%) via sonication (2 minutes, 4s on/2s off). Final NP suspension was dispersed in 42 mL of water and stirred for 1 hour to allow DCM evaporation, followed by rotary evaporation for 2 hour to completely remove any DCM trace. NPs were collected by centrifugation at 13,200 rpm (16,000 xg rcf) for 30 minutes, and washed with water twice to remove any remaining PVA and excess ICG.

3.2.2.2 *In Vitro* Release of ICG from NP Cores

To test the stability of ICG-loaded NPs in serum-containing medium, 0.2 mg of freeze-dried NPs contained in 40 μ L of water was dispersed in 1 mL of FBS/PBS solution (50:50). Multiple samples were prepared identically and incubated at 37 °C with agitation. At different time points, samples were removed and centrifuged at 13,000 rpm for 15 minutes. Top 500 μ L of the supernatant were stored in -20°C. The pellet was briefly rinsed

with water and also stored at -20°C . After the last time point (72 hr), all samples were thawed and dissolved in acetonitrile/PBS solution (50:50). The dissolved samples were diluted to avoid signal saturation (10 folds for supernatant and 20 folds for pellet) and transferred to a black 96-well plate. The fluorescence intensity was measured using an IVIS Lumina II imaging system (PerkinElmer, MA, USA) using 745 nm excitation filter, ICG emission filter, 1 second exposure, medium binning. ICG was quantified using a calibration curve of standard ICG concentrations in same medium (FBS/PBS).

3.2.2.3 Coating of NP Cores

Different types of NP cores were coated with pD-PEG or pD-LMWC using the same method reported in Chapter 2. Briefly, NPs were dispersed at 1 mg/mL in Tris buffer (10 mM, pH 8.5) containing 1 mg/mL dopamine HCl and shaken for three hours. Dopamine polymerized on NPs surface resulting in formation of NP-pD, which were collected by centrifugation, and washed once with water. To coat NP-pD with LMWC, they were further incubated in LMWC aqueous solution (0.5 mg/mL, pH 7.5) for 30 minutes, followed by purging using nitrogen gas for 5 minutes to stop polymerization reaction. LMWC coated NPs (NP-pD-LMWC) were collected via centrifugation and washed with water twice to remove excess LMWC. Alternatively, to coat NP-pD with PEG, LMWC solution was replaced with mPEG-NH₂ solution in Tris buffer (2 mg/mL, pH 8.5), keeping the rest of the method the same. After washing, NPs were freeze-dried with trehalose as a cryoprotectant to help redispersion: stock solution of trehalose (50 mg/mL) was added to make a final ratio of NP: trehalose 1:1. In this chapter, PLGA-pD-LMWC and PLGA-pD-PEG refer to PTX-loaded NPs prepared with PLGA₁₅₀ polymer cores and respective coatings, while *PLGA-PD-LMWC and *PLGA-pD-PEG refer to ICG-loaded NPs. Particle size and zeta potential of different types of NPs were measured as described in section 2.2.5

3.2.3 Development of Xenograft Tumor Model

3.2.3.1 Cell Culture

MCF-7 cells (human breast adenocarcinoma, ATCC, VA, USA) were grown in RPMI-1640 medium containing 10% FBS, 100 units/mL of penicillin, 100 µg/mL of streptomycin, L-glutamine (2 mM), sodium pyruvate (1 mM), HEPES buffer (10 mM) and 2-mercaptoethanol (55 µM). LS174T cells (ATCC, VA, USA) were grown in Eagle's Minimal Essential Medium (EMEM) containing 10% FBS, 100 units/mL of penicillin and 100 µg/mL of streptomycin.

3.2.3.2 Tumor Inoculation

All animal procedures were approved by Purdue Animal Care and Use Committee, in conformity with the NIH guidelines for the care and use of laboratory animals. Female athymic Foxn1nu nude mice (20-24 g) were purchased from Harlan Laboratories (Indianapolis, IN) and housed for a minimum of one week prior to tumor inoculation.

LS174T tumor model. Fifty microliters of LS174T suspension in PBS (20 million cells/mL) was mixed with 50 µL matrigel and subcutaneously inoculated in the right flank. Mice were monitored daily for tumor size and body weight.

MCF-7 tumor model. A hundred microliters of MCF-7 suspension in PBS (50 million cells/mL) was mixed with 100 µL matrigel and subcutaneously inoculated on the neck (for whole body imaging), or in the right flank (for anti-tumor study). Mice were monitored every other day for tumor size and body weight.

3.2.3.3 Tumor Measurement

Two dimensions of the tumor were measured using a digital caliper, where L is longest dimension and W is the shorter dimension. Tumor volume was calculated from the equation (Tomayko & Reynolds, 1989):

$$Tumor\ volume = \frac{L \times W^2}{2}$$

As tumor grew larger, some developed ulcerations, similar to that observed with previous reports (Bryan et al., 2011; Hollis et al., 2013). Ulceration caused a change in tumor growth rate; therefore, mice that developed ulcerations were excluded from the study once observed and were monitored regularly and sacrificed if ulcerations became severe. Additionally, mice were sacrificed when they lost >20% body weight, or when tumors grew >2000 mm³.

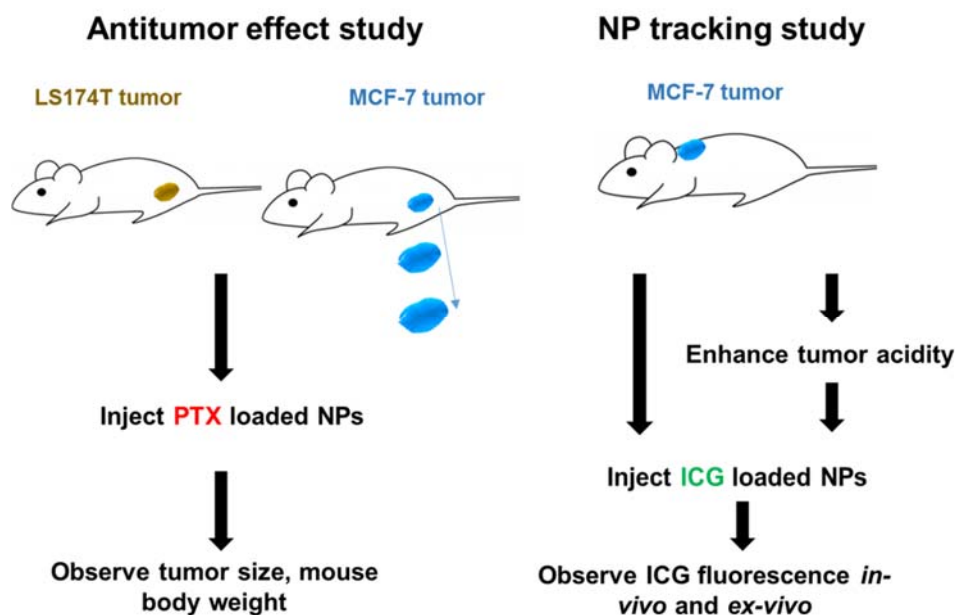


Figure 19: Outline of *in vivo* studies carried out using LS174T and MCF-7 subcutaneous tumor models.

3.2.4 Antitumor Effect of PTX-Loaded NPs on LS174T Tumor-Bearing Mice

Once subcutaneous tumor xenografts reached an average size of ~150 mm³, mice were randomized into 5 groups (n=5, except for control group, where n=4), receiving: PBS (control), Taxol, Abraxane, PLGA-pD-PEG and PLGA-pD-LMWC on days 0, 3 and 7.

PTX content of NP formulations was determined using the method detailed in section 2.2.6. For standard Abraxane formulation, PTX content was determined via HPLC

after PTX extraction. Briefly, 1 mL of aqueous solution of a known amount of Abraxane spiked with 10 μg of carbamazepine as an internal standard was mixed with 3 mL of ethyl acetate and shaken on a rotating shaker for 40 minutes. The mixture was then centrifuged at 4,000 rpm (4,500 $\times\text{g}$ rcf) for 15 minutes to separate the organic layer, which was transferred to a glass vial and dried under vacuum. The dried sample was resuspended in the HPLC mobile phase, filtered through 0.45 μm syringe filter, and analyzed with HPLC. A calibration curve was drawn with PTX solutions of known concentrations treated similarly.

Freeze-dried formulations (PLGA-pD-LMWC, PLGA-pD-PEG and Abraxane) were dispersed in 200 μL of sterile PBS at a dose equivalent to PTX 10 mg/kg. Taxol was prepared by dissolving PTX in equal parts of Cremphor EL vehicle and ethanol at concentration of 6 mg/mL, followed by dilution with PBS to a comparable dose. Mice received each treatment (10 mg/kg per treatment) on days 1, 4 and 7 (total of 30 mg/kg) via tail vein injection. For the control group, mice received 200 μL of sterile PBS.

3.2.5 Antitumor Effect of PTX-Loaded NPs on MCF-7 Tumor-Bearing Mice

A similar procedure was followed for the MCF-7 model, except that (i) the treatment was started when tumor reached $\sim 280\text{ mm}^3$ ($n=5$); (ii) the treatment groups were PBS (control), Abraxane, PLGA-pD-PEG and PLGA-pD-LMWC (no Taxol group); (iii) treatments were injected intravenously via retro-orbital injection. One of the mice in PLGA-pD-LMWC group was sacrificed at day 7 of the treatment initiation due to eye damage. All mice were sacrificed at day 19 of the study.

3.2.6 Tracking of ICG-Labeled NPs in MCF-7 Tumor-Bearing Mice

In this study, tumor xenografts were grown on the neck to avoid background signals from internal organs during whole body imaging. When tumors reached an average size of 380 mm^3 , mice were randomized into two groups ($n=5$): *PLGA-pD-LMWC, and *PLGA-pD-PEG. Each mouse received 100 μL of NP suspension in sterile PBS (30 mg/kg) via retro-orbital injection, and the ICG fluorescence was monitored at different time points

using the IVIS Lumina II system (PerkinElmer, MA, USA) using 745/ICG filters, 1s exposure time and medium binning. At the end of the experiment (48 hours after injection), mice were sacrificed, different organs extracted, and their fluorescence quantified using the IVIS Lumina system (*ex-vivo* imaging). For quantification of ICG contents in tumor and liver tissues, ICG was extracted from the tissues according to the reported method (Saxena et al., 2006). Briefly, the weighed tissue was homogenized in 20 volume of DMSO and incubated for five hours. The tissue homogenate was centrifuged at 4,000 rpm (4,500 xg rcf) for 20 minutes, then 13,200 rpm (16,000 xg rcf) for 20 minutes to remove all tissue particles. Obtained supernatant was scanned via the IVIS Lumina system.

For the acidity-enhanced tumor model, tumors averaging at 225 mm³ were randomized into 2 groups (n=6): *PLGA-pD-LMWC, and *PLGA-pD-PEG. Three mice in each group received a combination of glucose and MIBG IP, and the other three received PBS IP, according to the schedule illustrated in **Figure 20**.

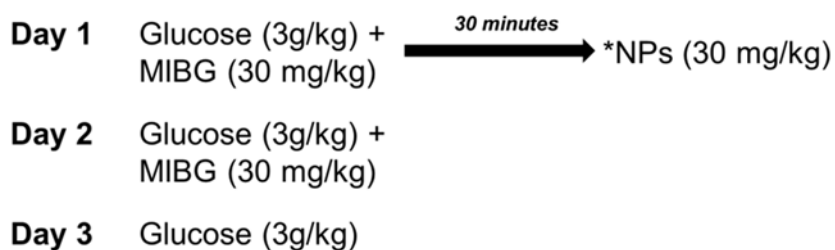


Figure 20: Dosing schedule of glucose and MIBG for the acidity-enhanced tumor model. Glucose and MIBG were injected IP once daily for three days, while *NPs were delivered via the retro-orbital injection on the first day.

3.3 Results

3.3.1 NP preparation and Characterization

Freeze-dried NPs with PTX-loaded cores restored their size after redispersion in phosphate buffer (~ 200 nm) with a good polydispersity index < 0.2 (**Fig. 21a**). PTX LE% of both PEG and LMWC coated NPs was $6.4\% \pm 1.6$ and $6.5\% \pm 1.4$, respectively. PTX loaded PLGA-pD-LMWC NPs had the same pH-sensitive surface charge previously reported (**Fig. 21b**). PTX content of Abraxane was determined to be $10.3\% \pm 1.3$, in agreement with the manufacturer's description (Celgene, 2015).

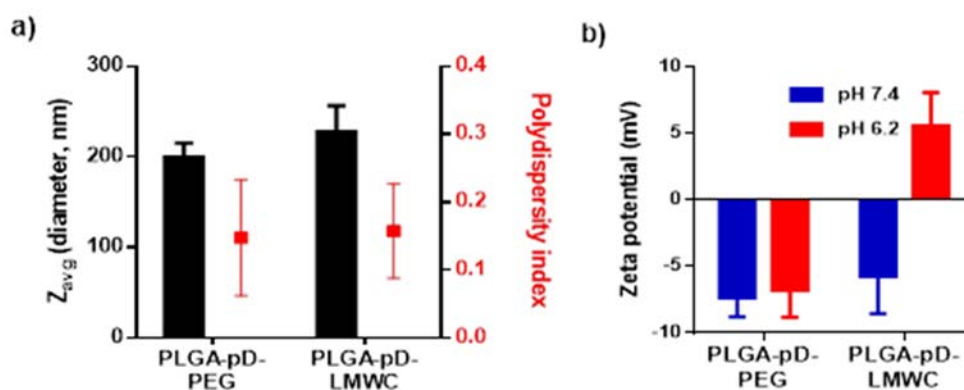


Figure 21: Characterization of freeze-dried PTX loaded NPs after redispersion: a) Particle size and polydispersity index, b) Zeta potential at pH 7.4 and 6.2 (n=4).

3.3.2 Antitumor Effect of PTX-Loaded NPs on LS174T and MCF-7 Tumor-Bearing Mice

Antitumor activity of different formulations was tested in two different tumor models, MCF-7 and LS174T. These two tumor models had different vascularization and growth rates. LS174T tumors grew faster (data not shown) and had greater vascularization than MCF-7 tumors (**Fig. 22**).

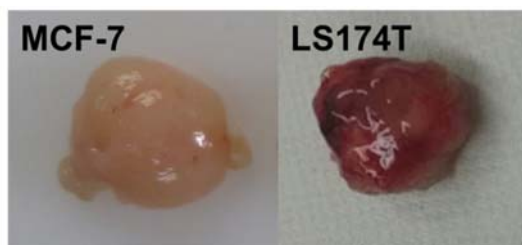


Figure 22: Subcutaneous xenografts of MCF-7 and LS174T tumors post extraction.

Fold increase in tumor volume was used to express the effectiveness of different treatments in suppressing tumor growth. Additionally, fold change of mice body weight was to evaluate systemic toxicity of the formulation.

In the LS174T model, ulceration occurred in 28% of the mice. Since the ulcerated tumors were excluded from the data analysis, average tumor sizes could not be compared beyond 10 days after the treatment initiation. By statistical analysis of all tumors growth curves, all PTX formulations suppressed tumor growth as compared to the PBS control (**Fig. 23a and b, $p < 0.05$, see appendix for statistical analysis**). However, there was no significant difference among the formulations.

In the MCF-7 model, no ulcerations were developed, and tumor growth could be observed over a longer period of time (19 days). As in the LS174T model, Abraxane and PLGA-pD-PEG suppressed the tumor growth, but PLGA-pD-LMWC did not. PLGA-pD-LMWC was significantly less effective than PLGA-pD-PEG NPs (**Fig. 24a and b, $p < 0.05$, see appendix for statistical analysis**). For both tumor models, no significant change in body weight was observed over the course of treatment, indicating that formulations were well tolerated by the mice (**Fig. 25a and b, ANOVA test**).

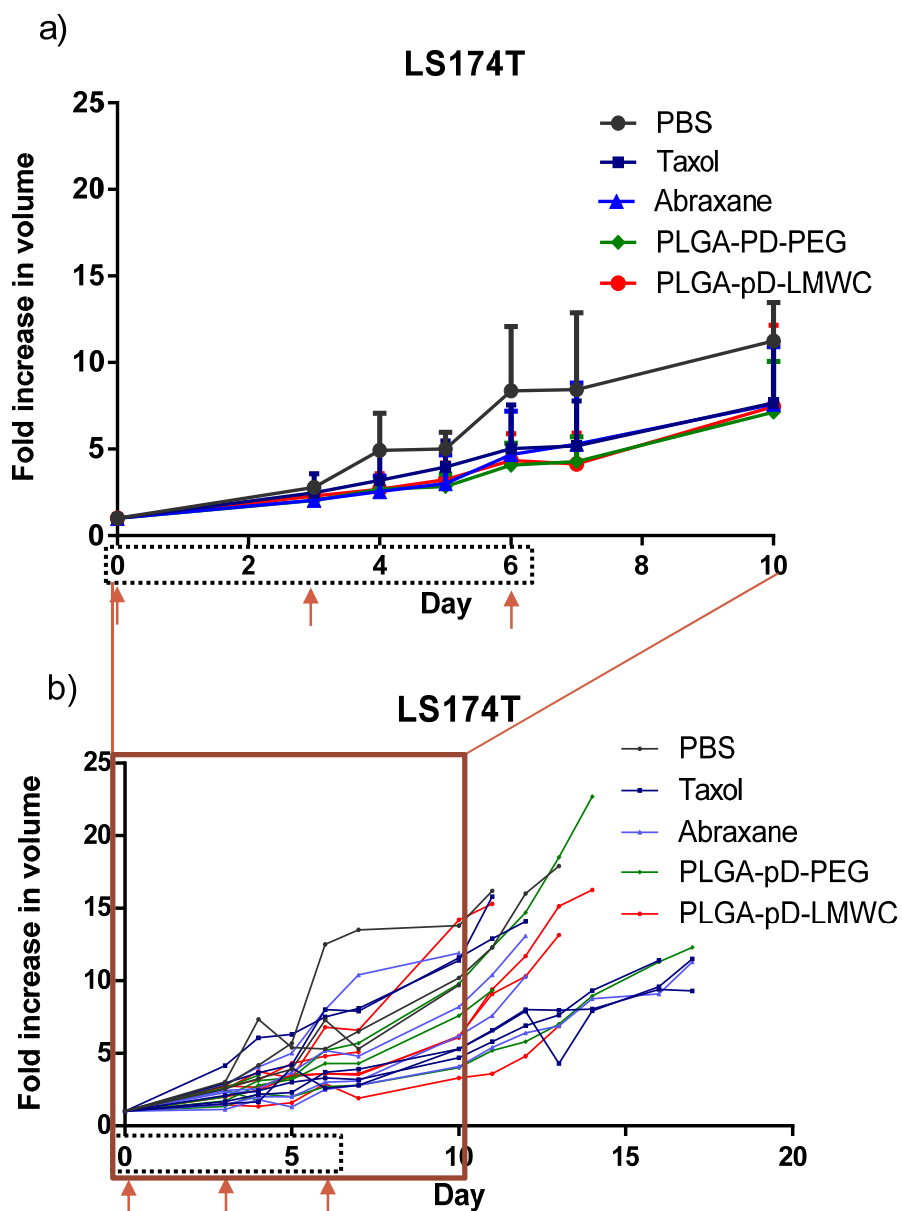


Figure 23: Growth profile of LS174T tumors receiving different treatments over time (a) average fold increase in tumor volume (average \pm SD), (b) growth profiles of individual tumors. Arrows indicate the days treatments were administered.

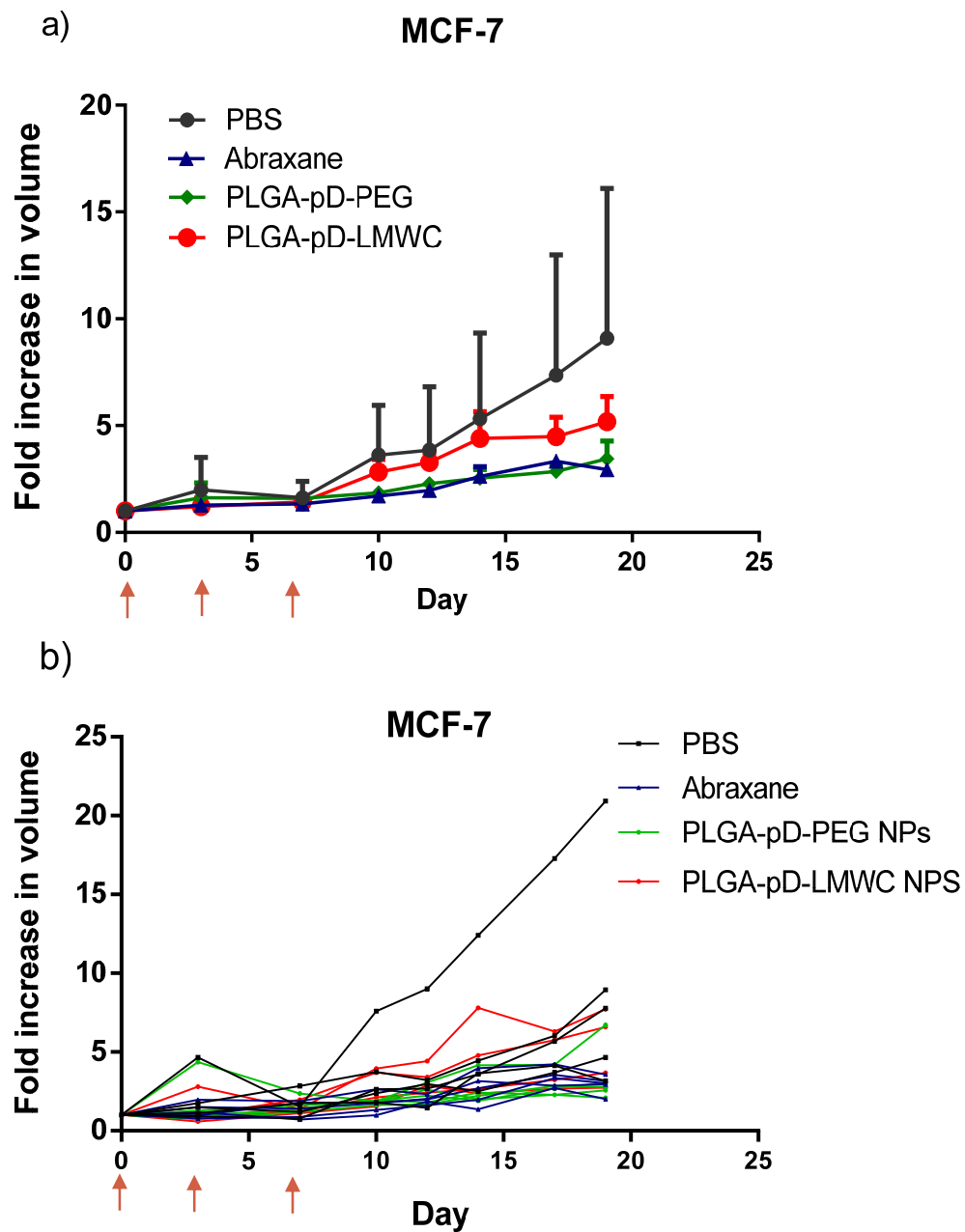


Figure 24: Growth profile of MCF-7 tumors receiving different treatments over time (a) average fold increase in tumor volume (average \pm SD), (b) growth profiles of individual tumors. Arrows indicate the days treatments were administered.

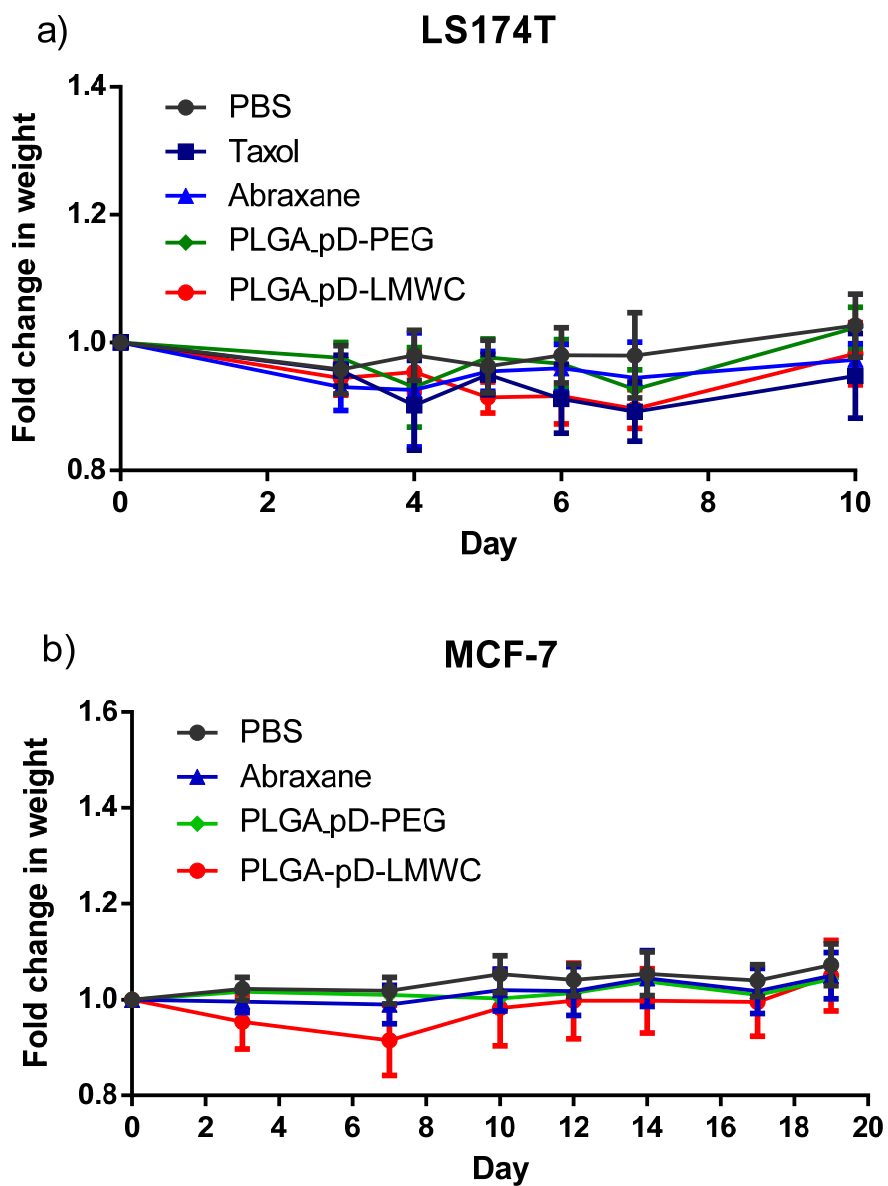


Figure 25: Average fold change in body weight of (a) LS174T and (b) MCF-7 tumor xenograft model after intravenous administration of different formulations (average \pm SD).

3.3.3 Tracking of ICG-Loaded NPs in MCF-7 Tumor-Bearing Mice

Loading of ICG in PLGA NPs (*PLGA) was confirmed by their green color (**Fig. 26**). After coating with pD-LMWC or pD-PEG, *PLGA NPs had a particle size of ~ 220 nm (**Fig. 27a**), and maintained the same surface charge profile as NPs with non-fluorescent cores (**Fig. 27b**). When the stability of loaded ICG was tested in serum containing medium, 60% of loaded ICG was released in the first 24 hours (**Fig. 28**), while $\sim 30\%$ of the dose was retained until 72 hours. This indicates that within the first day, most of ICG is released, while NP cores maintained remaining ICG throughout the following 2 days.



Figure 26: ICG loaded PLGA NPs (*PLGA) and pD coated *PLGA (*PLGA-pD).

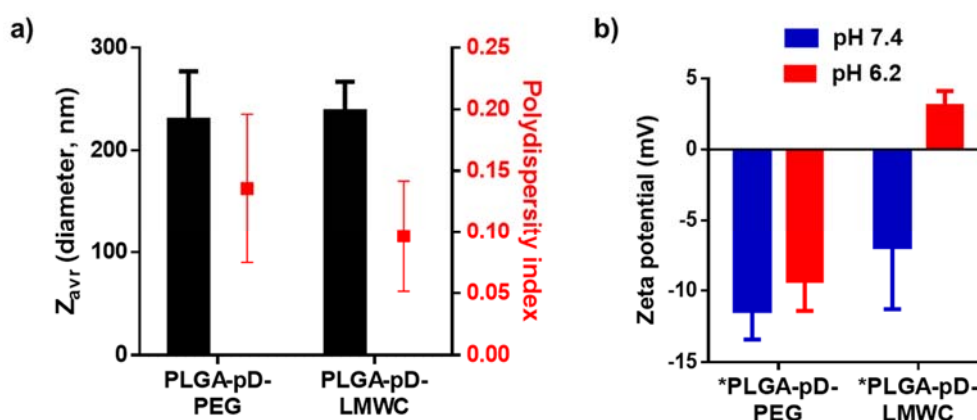


Figure 27: Characterization of freeze-dried ICG loaded NPs after redispersion: (a) Particle size and polydispersity index, (b) Zeta potential at pH 7.4 and 6.2 (average \pm SD, n=3-4).

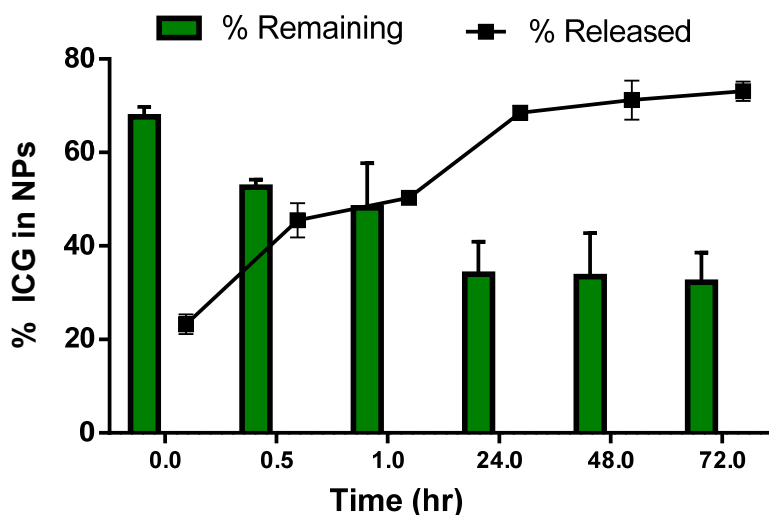


Figure 28: *In vitro* release of ICG from PLGA cores (*PLGA) dispersed in serum containing medium at 37°C at different time points (average \pm SD, n=3).

When ICG loaded NPs (*PLGA-pD-LMWC and *PLGA-pD-PEG) were intravenously injected to mice with MCF-7 xenografts, strong fluorescent signal of ICG appeared in the whole body in the first 2 hours, then disseminated and appeared strongest in the tumors at 24 hours and beyond (**Fig. 29a**). Tumor ICG signal was observed for 48 hours post injection. There was no difference in tumor fluorescence intensity between *PLGA-pD-LMWC and *PLGA-pD-PEG NPs throughout the time course of observation (**Fig. 29b**). At the end of the study, organs were examined *ex vivo* (**Fig. 30**). The excised tumors and livers appeared fluorescent when imaged with the Lumina system (**Fig. 30a**). ICG was extracted from organs and quantified. In animals treated with *PLGA-pD-LMWC NPs, ICG content per 10 mg tumor was significantly higher than ICG in 10 mg liver (**Fig. 30b**). In animals treated with *PLGA-pD-PEG NPs, the ICG content in tumor was similar to those with *PLGA-pD-LMWC NPs, but the ICG content in liver was higher (**Fig. 30b**). However, there was no overall significant difference in tumor/liver ratio between *PLGA-pD-LMWC NPs and *PLGA-pD-PEG NPs (**Fig. 30c**).

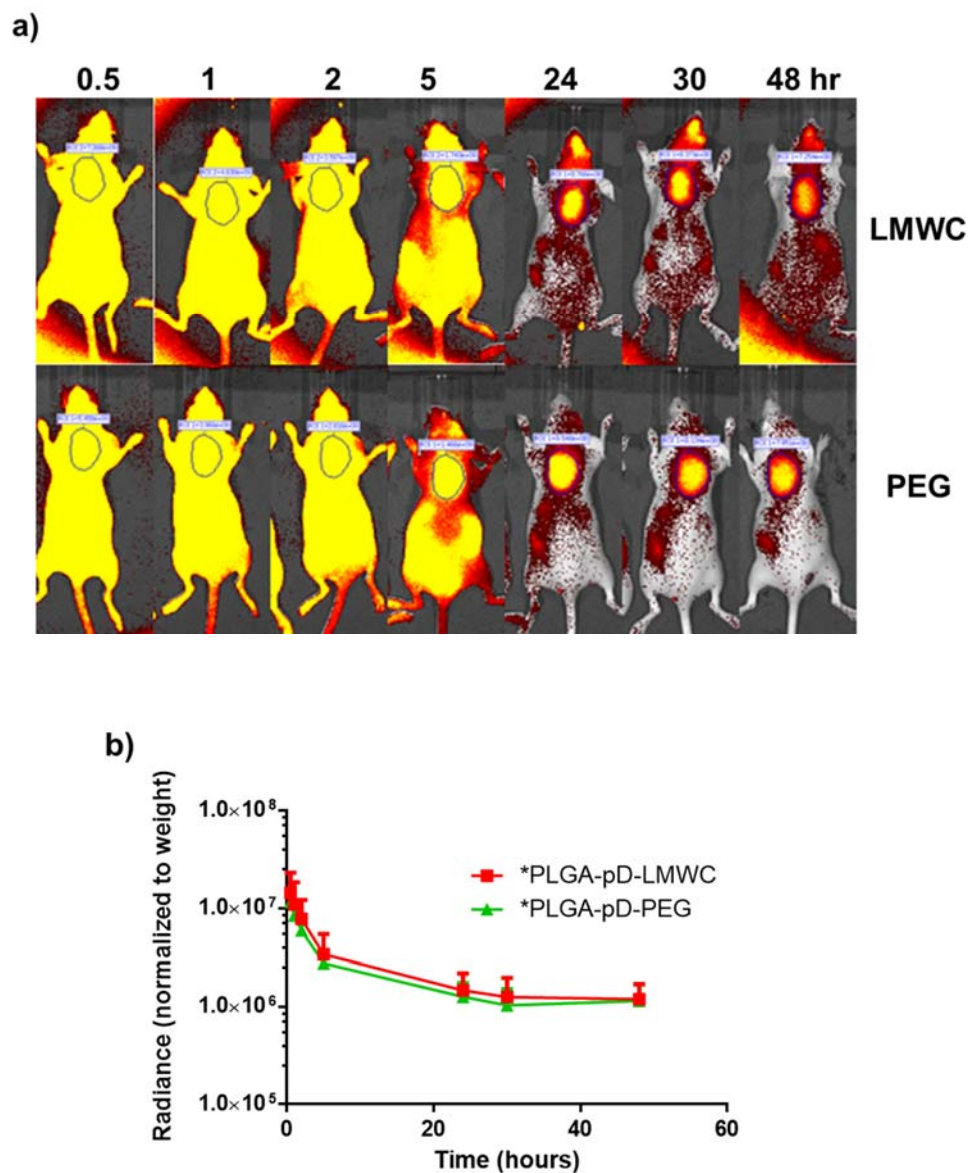


Figure 29: Tracking of ICG loaded NPs in MCF-7 xenograft model (n=5), (a) Representative image of whole body imaging performed, using IVIS Lumina system, on mice after injection of ICG loaded NPs, *PLGA-pD-LMWC and *PLGA-pD-PEG. Fluorescence signal was quantified throughout the 48 hour of the study (tumor tissue outlined), (b) Corresponding fluorescence signal (total radiance efficiency) of tumors after subtraction of background signal (signal prior to NP injection) and normalization to tumor weight (average \pm SD).

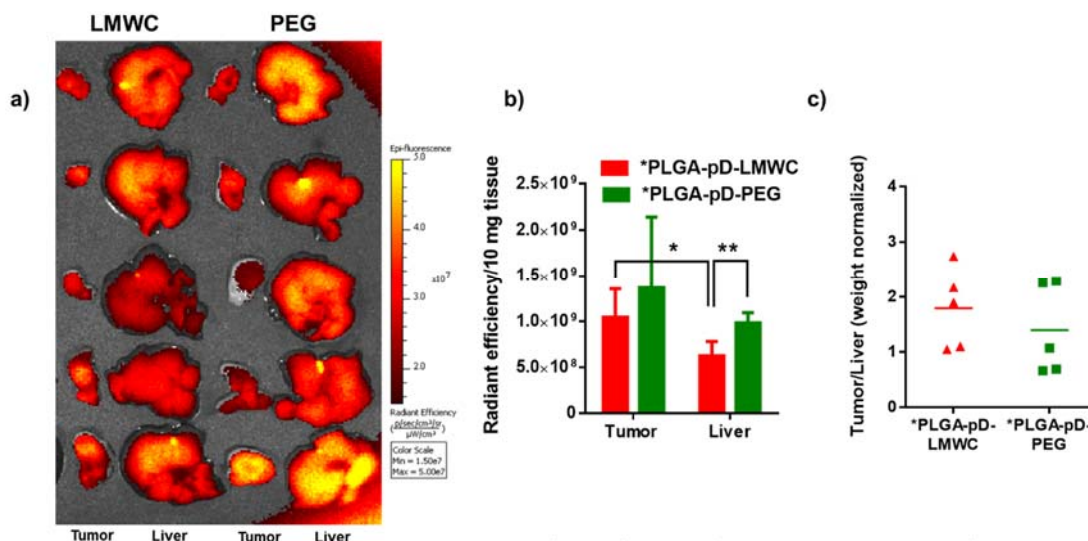


Figure 30: Fluorescence imaging and quantification of ICG content of extracted MCF-7 tumors and livers, (a) *Ex-vivo* fluorescence imaging of extracted organs at the end of the study, (b) Weight-normalized fluorescence signal of tumors and livers for LMWC and PEG coated NPs post ICG extraction, (c) Weight-normalized tumor/liver ratio of ICG fluorescence for LMWC and PEG coated NPs (average \pm SD, $n=5$, $*p<0.05$, $**p<0.005$, Two-tailed T-test).

Since the results were contrary to the expectation, the imaging experiment was repeated with enhancement of tumor acidity. This was achieved by multiple IP injections of a glucose and MIBG combination. The combination of hyperglycemia and MIBG stimulates the production of lactic acid in tumors and consequently enhances their acidity (Jahde et al., 1992; McCarty & Whitaker, 2010). MIBG also helps produce more homogenous tumor acidification (Kuin et al., 1994). The tumor extracellular pH was not experimentally determined in this study, but several studies reported acidity enhancement in murine and human xenograft tumors via glucose-MIBG combination (Jahde et al., 1992; Kalliomaki & Hill, 2004). Tumor accumulation in the acidity enhanced model was compared with that of control model (no glucose/MIBG injections). Nonetheless, the glucose-MIBG treatment did not make any difference in ICG accumulation patterns in tumor and liver for both NPs during in situ whole body imaging (Fig. 31a) or *ex-vivo* assessment (Fig. 31b).

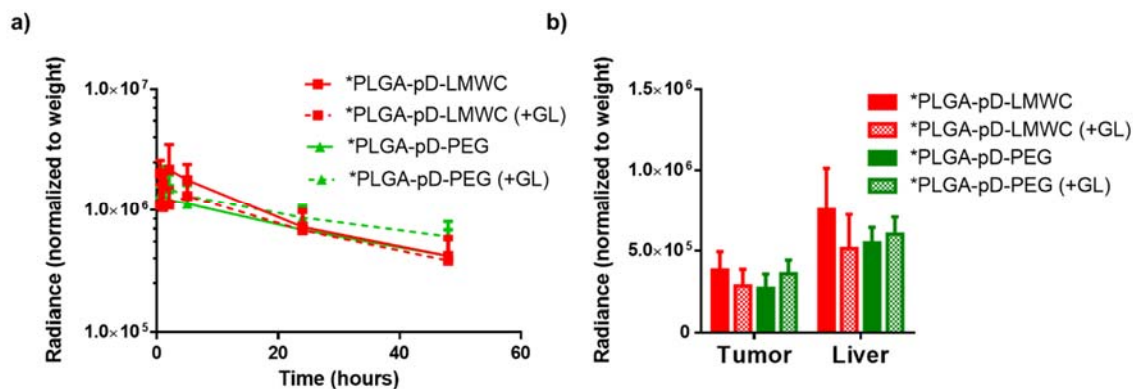


Figure 31: Tracking of ICG loaded NPs in acidity-enhanced MCF-7 tumor models versus normal model, (a) Fluorescence signal (total radiance efficiency) of tumors after subtraction of background signal (signal prior to NP injection) and normalization to tumor weight, (b) Weight-normalized *ex-vivo* fluorescence signal of tumors and livers for LMWC and PEG coated NPs in both tumor models (averages \pm SD, $n=3$).

3.4 Discussion

The goal of developing NP formulations for delivery of chemotherapeutic agents is to enhance the tumor delivery of such agents and minimize their off-target exposure. Mostly, these effects are attributed to the improved biodistribution profile of drug loaded NPs and/or the modified NP-cell interactions favoring NP uptake.

We have developed LMWC-coated NPs with pH-sensitive cellular interactions. *In vitro* studies (Chapter 2) have demonstrated that NPs can be selectively taken up by cancer cells at mildly acidic pH, similar to that of tumor microenvironment, while avoiding cellular interactions and macrophage uptake at neutral pH. Based on these promising results, we hypothesized that, LMWC-coated NPs would avoid the macrophage uptake, achieve long circulation to reach tumors via the leaky vasculature similar to PEG-coated NPs, yet show greater tumor retention than PEG-coated NPs due to the increased cellular interaction in acidic tumor microenvironment, delivering a greater amount of PTX to tumors. The antitumor effect of PTX-loaded NPs was tested in two tumor models, LS174T and MCF-7, with different vascularization and growth rates. The injected NPs were all well tolerated in mice, resulting in no significant weight loss (**Fig. 25**) or mortality. On the other hand, LMWC- and PEG-coated NPs showed similar tumor suppression, comparable to

Abraxane, the current commercial gold standard formulation for PTX. No significant difference was observed between PEG and LMWC NPs (**Fig. 23 and 24**), which suggests that both NPs delivered the same amount of PTX to the tumors, contrary to the expectation. The whole body imaging using a fluorescent dye, ICG, as a surrogate for PTX corroborated this speculation (**Fig. 29 and 30**).

The observed antitumor effect results may be explained in three potential scenarios: In the first scenario, the tumor xenografts were not sufficiently acidic for LMWC-coated NPs to achieve anticipated tumor retention. Second, tumors were acidic, but PLGA cores did not hold PTX stably during circulation; therefore, the drug reached tumors irrespective of the carriers. Third, NPs entering the circulation were immediately coated with plasma proteins and lost differential surface properties (**Fig. 10**).

To investigate the first scenario, whole body imaging was repeated with acidity-enhanced MCF-7 tumor model. The trend remained the same (**Fig. 31**), which suggests that poor development of tumor acidity may not have been the main reason. The second and third scenarios remain to be confirmed. This will be investigated in another whole-body imaging study using NPs made of an ICG-conjugated PLGA (instead of physical encapsulation of ICG in NPs). Unlike current imaging, the fluorescence signal will represent the trajectory of NPs rather than the dye payload. If the NP distribution profiles coincide with payload distribution seen in this study, it is likely that protein coronas forming on NPs have eliminated their differential surface properties. If the NPs show expected distribution profile (i.e., LMWC-coated NPs show greater retention in tumors than PEG-coated NPs), the main cause may be the premature release of the payload. Our *in vitro* studies suggest both are possible, given that PLGA NPs showed a high initial burst albeit to a lesser extent than low MW PLGA NPs and LMWC- and PEG-coated NPs had similar protein binding patterns in serum (Chapter 2).

Finally, the limitation of current tumor models may be noted. Since the selectivity of NPs in tumor accumulation primarily depend on the leakiness of tumor vasculature, the nature and distribution of blood vessels dictate NP accumulation and extravasation in the tumor tissues (Chauhan et al., 2012; Ruoslahti et al., 2010). Therefore, NPs are typically

tested in animal models of tumor xenografts based on established cell lines, which grow rapidly and develop imperfect vasculature structure, as done in this study. However, the clinical utility of these models are currently in question, because they do not reflect other factors dictating tumor microenvironment, such as heterogeneity of tumor tissues (Nichols & Bae, 2014) and supporting cells such as stromal cells and immune cells (Yip & Cho, 2013) (Chia et al., 2005).

3.5 Conclusions

In summary, this study investigated the tumor suppression effect of PTX loaded NPs coated with PEG or LMWC and visualized the payload (ICG) delivery to tumors. Although *in vitro* studies predicted superior performance of LMWC-coated NPs, in terms of tumor growth suppression and tumor ICG delivery, there was no significant difference between LMWC and PEG-coated NPs. The specific reasons behind the poor *in vitro-in vivo* correlation remain to be confirmed. Whether it is premature drug release or protein corona formation, this study highlights the importance of controlling nanocarrier stability during circulation.

3.6 References

- Abouelmagd, S. A., Ku, Y. J., & Yeo, Y. (2015). "Low molecular weight chitosan-coated polymeric nanoparticles for sustained and pH-sensitive delivery of paclitaxel." Journal of Drug Targeting 23(7-8): 725-735.
- Bryan, J. N., Jia, F., Mohsin, H., Sivaguru, G., Anderson, C. J., Miller, W. H., Henry, C. J., & Lewis, M. R. (2011). "Monoclonal antibodies for copper-64 PET dosimetry and radioimmunotherapy." Cancer Biology & Therapy 11(12): 1001-1007.
- Celgene. (2015). Abraxane Prescribing Information October 25, 2015, from http://www.abraxane.com/downloads/Abraxane_PrescribingInformation.pdf
- Chauhan, V. P., Stylianopoulos, T., Martin, J. D., Popovic, Z., Chen, O., Kamoun, W. S., Bawendi, M. G., Fukumura, D., & Jain, R. K. (2012). "Normalization of tumour blood vessels improves the delivery of nanomedicines in a size-dependent manner." Nat Nanotechnol 7(6): 383-388.
- Cherrick, G. R., Stein, S. W., Leevy, C. M., & Davidson, C. S. (1960). "Indocyanine Green - Observations on Its Physical Properties, Plasma Decay, and Hepatic Extraction." Journal of Clinical Investigation 39(4): 592-600.
- Chia, S. M., Lin, P. C., & Yu, H. (2005). "TGF-beta 1 regulation in hepatocyte-NIH3T3 co-culture is important for the enhanced hepatocyte function in 3D microenvironment." Biotechnology and Bioengineering 89(5): 565-573.
- Cho, E. J., Holback, H., Liu, K. C., Abouelmagd, S. A., Park, J., & Yeo, Y. (2013). "Nanoparticle characterization: state of the art, challenges, and emerging technologies." Mol Pharm 10(6): 2093-2110.
- Dang, D. T., Chun, S. Y., Burkitt, K., Abe, M., Chen, S., Havre, P., Mabweesh, N. J., Heath, E. I., Vogelzang, N. J., Cruz-Correa, M., Blayney, D. W., Ensminger, W. D., Croix, B. S., Dang, N. H., & Dang, L. H. (2008). "Hypoxia-inducible factor-1 target genes as indicators of tumor vessel response to vascular endothelial growth factor inhibition." Cancer Research 68(6): 1872-1880.
- Frangioni, J. V. (2003). "In vivo near-infrared fluorescence imaging." Curr Opin Chem Biol 7(5): 626-634.
- Hollis, C. P., Weiss, H. L., Leggas, M., Evers, B. M., Gemeinhart, R. A., & Li, T. (2013). "Biodistribution and bioimaging studies of hybrid paclitaxel nanocrystals: lessons learned of the EPR effect and image-guided drug delivery." Journal of Controlled Release 172(1): 12-21.
- Hwang, J. H., Noh, Y. W., Choi, J. H., Noh, J. R., Kim, Y. H., Gang, G. T., Kim, K. S., Park, H. S., Lim, Y. T., Moon, H., Hong, K. S., Lee, H. G., Chung, B. H., & Lee, C. H. (2014). "In Vivo Imaging of Islet Transplantation Using PLGA Nanoparticles Containing Iron Oxide and Indocyanine Green." Magnetic Resonance in Medicine 71(3): 1054-1063.

- Jahde, E., Volk, T., Ateman, A., Smets, L. A., Glusenkamp, K. H., & Rajewsky, M. F. (1992). "pH in human tumor xenografts and transplanted rat tumors: effect of insulin, inorganic phosphate, and m-iodobenzylguanidine." Cancer Research 52(22): 6209-6215.
- Kalliomaki, T., & Hill, R. P. (2004). "Effects of tumour acidification with glucose plus MIBG on the spontaneous metastatic potential of two murine cell lines." British Journal of Cancer 90(9): 1842-1849.
- Kuin, A., Smets, L., Volk, T., Paans, A., Adams, G., Ateman, A., Jahde, E., Maas, A., Rajewsky, M. F., Visser, G., & Wood, P. (1994). "Reduction of Intratumoral Ph by the Mitochondrial Inhibitor M-Iodobenzylguanidine and Moderate Hyperglycemia." Cancer Research 54(14): 3785-3792.
- Kumar, G. N., Walle, U. K., Bhalla, K. N., & Walle, T. (1993). "Binding of Taxol to Human Plasma, Albumin and Alpha-1-Acid Glycoprotein." Research Communications in Chemical Pathology and Pharmacology 80(3): 337-344.
- Maeda, H. (2012). "Vascular permeability in cancer and infection as related to macromolecular drug delivery, with emphasis on the EPR effect for tumor-selective drug targeting." Proc Jpn Acad Ser B Phys Biol Sci 88(3): 53-71.
- McCarty, M. F., & Whitaker, J. (2010). "Manipulating Tumor Acidification as a Cancer Treatment Strategy." Alternative Medicine Review 15(3): 264-272.
- Nichols, J. W., & Bae, Y. H. (2014). "EPR: Evidence and fallacy." Journal of Controlled Release 190: 451-464.
- Paal, K., Muller, J., & Hegedus, L. (2001). "High affinity binding of paclitaxel to human serum albumin." European Journal of Biochemistry 268(7): 2187-2191.
- Pathak, A. P., McNutt, S., Shah, T., Wildes, F., Raman, V., & Bhujwala, Z. M. (2013). "In vivo "MRI phenotyping" reveals changes in extracellular matrix transport and vascularization that mediate VEGF-driven increase in breast cancer metastasis." Plos One 8(5): e63146.
- Ruoslahti, E., Bhatia, S. N., & Sailor, M. J. (2010). "Targeting of drugs and nanoparticles to tumors." J Cell Biol 188(6): 759-768.
- Saxena, V., Sadoqi, M., & Shao, J. (2006). "Polymeric nanoparticulate delivery system for Indocyanine green: Biodistribution in healthy mice." Int J Pharm 308(1-2): 200-204.
- Tomayko, M. M., & Reynolds, C. P. (1989). "Determination of Subcutaneous Tumor Size in Athymic (Nude) Mice." Cancer Chemotherapy and Pharmacology 24(3): 148-154.
- Yip, D., & Cho, C. H. (2013). "A multicellular 3D heterospheroid model of liver tumor and stromal cells in collagen gel for anti-cancer drug testing." Biochemical and Biophysical Research Communications 433(3): 327-332.

CHAPTER 4. EXPERIMENTAL DESIGN OF RELEASE STUDIES FOR NANOPARTICLE FORMULATIONS

4.1 Introduction

The evaluation of drug release from NP carriers intended for systemic delivery is one of the most important characterizations in terms of predicting their *in vivo* efficiency. Specifically for NPs intended for tumor drug delivery, due to the prolonged circulation of the NPs prior to tumor accumulation. It is predicted that significant drug load can be lost during that stage, leading to delivery of near empty NP carrier. Therefore, it is critical to characterize the *in vitro* release kinetics of drugs from different carriers accurately.

Irrespective of the test method, the assumption underlying the release kinetics studies is that the dose range of the NP products and the volume of release medium satisfy sink conditions (defined as the volume of medium at least three times that required to form a saturated solution of a drug (The United States Pharmacopeia: The National Formulary (USP37/NF32), 2014)): i.e., the drug release is not limited by the solubility, and the difference in release kinetics profile reflects the performance of NPs as a drug carrier *in vivo*. To meet this requirement, it is important that one use a sufficient volume of release medium for the NPs. However, in the case of poorly water-soluble drugs, like PTX, satisfying the sink condition can be quite challenging as it means a very low ratio of NP mass to the volume of release medium. A disadvantage of using a large volume of release medium is that drug analysis gets difficult due to the low concentration. In order to alleviate this difficulty, the sampled solution is concentrated prior to analysis or a dissolution aid such as surfactants or co-solvents is included in the release medium (Daniel J. Phillips et al., 2012; The United States Pharmacopeia: The National Formulary (USP37/NF32), 2014).

Given these requirements and constraints in fulfilling a sink condition, it is very important to know an accurate solubility value of a drug and set up appropriate experimental conditions in studying drug release kinetics from NPs.

For PTX, the solubility values reported in the literature vary over a range of orders of magnitude (Table 3). In this study, we look into the solubility of PTX in potential release media (PBS, PBS with 0.2% Tween 80, and PBS with 50% fetal bovine serum (FBS)) and perform release kinetics studies of PTX loaded NP formulations.

Table 3: Reported PTX solubility in different media (Abouelmagd et al., 2015).

Medium	PTX solubility ($\mu\text{g/mL}$)	References
Deionized water	0.3	(Lee et al., 2003)
Deionized water	0.7	(Mathew et al., 1992)
Deionized water	1.0	(Zhang et al., 2005)
Deionized water	6	(Tarr & Yalkowsky, 1987)
Deionized water	30	(Swindell et al., 1991)
Phosphate buffered saline (PBS, pH 7.4)	0.3	(Kilfoyle et al., 2012)
PBS	0.95	(Zhang et al., 2005)
PBS	3	(Lovich et al., 2001)
PBS	6-10	(Y. S. Wang et al., 2008)
PBS with 0.05% Tween 80	3	(Yang et al., 2007)
PBS with 0.1% Tween 80	2.7	(Kilfoyle et al., 2012)
PBS with 0.1% Tween 80	6.32	(Yang et al., 2007)
PBS with 0.15% Tween 80	6.8	(Yang et al., 2007)
PBS with 0.2% Tween 80	8.75	(Yang et al., 2007)
PBS with 1% Tween 80	13.8	(Kilfoyle et al., 2012)
PBS with 1% Tween 80	37	(Yang et al., 2007)
PBS with 2% Tween 80	20	(Steele et al., 2011)
PBS with 2% Tween 80	70	(Yang et al., 2007)
PBS with 3% Tween 80	115	(Yang et al., 2007)
Calf serum	171	(Lovich et al., 2001)

4.2 Materials and Methods

4.2.1 Materials

PLGA (150 kDa, LA:GA=85:15, PLGA₁₅₀) and fluorescein-conjugated PLGA (7 kDa, LA:GA=50:50, *PLGA) were purchased from Akina Inc. (IN, USA). Paclitaxel (PTX) was a gift from Samyang Genex Corp (Seoul, Korea). Tween-80 was purchased from VWR Life Science (PA, USA). All other materials were of analytical grade.

4.2.2 PTX Solubility Studies

PTX solubility in PBS containing 0.2v/v% Tween 80 (Tween/PBS), and PBS containing 50 v/v% FBS (FBS/PBS) were determined by incubating excess PTX (0.6 – 2.4 mg) in 1 mL of each medium at 37°C for 7 or 24 hours with agitation. Samples were centrifuged at 10,000 rpm for 20 min to separate a supernatant. PTX dissolved in Tween/PBS was analyzed with HPLC. PTX dissolved in FBS/PBS was first extracted with ethyl acetate and reconstituted in the HPLC mobile phase prior to HPLC analysis (as described in section 2.2.9).

PTX solubility was alternatively determined by diluting 10 mg/mL PTX DMSO stock solution in each medium. To determine PTX solubility in Tween/PBS and PTX/DMSO solution (10 mg/mL) was first diluted with Tween/PBS to make 1 mg/mL of PTX solution, which was further diluted with Tween/PBS to 1-70 µg/mL (n=3). Samples were incubated at 37°C for 24 hours with shaking. Finally, samples were filtered with 0.45 µm PVDF syringe filters and directly analyzed with HPLC. To determine PTX solubility in FBS/PBS, PTX/DMSO solution (10 mg/mL) was sequentially diluted with FBS/PBS to yield final concentrations of 25-300 µg/mL (n=3). Samples were incubated at 37°C for 7 or 24 hours with shaking. At the end of the incubation, the samples were centrifuged at 10,000 rpm for 20 min, and the supernatant was filtered with 0.45 µm PVDF syringe filters, extracted with ethyl acetate as described in Section 2.7, and analyzed with HPLC (as described in section 2.2.9).

4.2.3 PLGA NP Preparation and Characterization

PLGA NPs loaded with PTX (PTX/NPs) were prepared by the single emulsion solvent evaporation method. Briefly, 20 mg of PLGA and 2.5 mg of PTX were dissolved in 1 mL of dichloromethane (DCM) and emulsified in 4 mL of 4% polyvinyl alcohol (PVA) solution by probe sonication. The o/w emulsion was dispersed in deionized water and stirred for 1 hour, followed by rotary evaporation for another hour to ensure DCM evaporation. Finally, NPs were collected by centrifugation and washed three times with water. The NPs were lyophilized with trehalose as a lyoprotectant. NP Particle size was characterized as detailed in section 2.2.5.

4.2.4 *In Vitro* Release of PTX from PLGA NPs

To determine the PTX content in NPs, the freeze-dried PTX/NPs was dissolved in a mixture of acetonitrile:water (50:50) for 2 hours, and the supernatant was analyzed with HPLC. For release kinetics studies of PTX/NPs, the freeze-dried PTX/NPs equivalent to 4.4 or 27 μg of PTX were suspended in 1 mL of release medium (PBS, Tween/PBS, or FBS/PBS) and incubated at 37°C with constant agitation. At predetermined time points, the suspension was centrifuged at 10,000 rpm for 10 minutes at room temperature to separate NP pellets and supernatants. 0.8 mL of supernatant was sampled and replaced with the same volume of fresh medium, in which the NP pellet was resuspended and returned for further incubation. The sampled supernatant was analyzed immediately (PBS and Tween/PBS) or stored frozen (FBS/PBS) until HPLC analysis. At the end of the release experiment, the remaining NPs were dissolved in 1 mL of acetonitrile:water (50:50) for 2 hours (PBS and Tween/PBS) or processed with the same extraction method as release samples (FBS/PBS) to determine the unreleased PTX.

4.3 Results

4.3.1 PTX Solubility in Different Media

The reported values of PTX solubility in deionized water or phosphate-buffered saline (PBS, pH 7.4) range from 0.3 to 30 $\mu\text{g/mL}$ (**Table 3**). PTX solubility in a medium containing a surfactant such as Tween 80 is reported to be much higher: up to $>100 \mu\text{g/mL}$ (3% Tween 80)(Yang et al., 2007). PTX solubility in calf serum is defined as 171 $\mu\text{g/mL}$.(Lovich et al., 2001) We evaluated PTX solubility in different media by suspending excess amounts of PTX in each medium and measuring the concentration of dissolved PTX. The results showed a similar trend as those in the literature, although the values fell in lower ends of the reported ranges. PTX solubility in Tween/PBS was measured to be 3.3 $\mu\text{g/mL}$ irrespective of the incubation time (**Fig. 32a**). PTX solubility in FBS/PBS was measured at 45 $\mu\text{g/mL}$ after 24 hour incubation at 37 °C, much higher than those in PBS or Tween/PBS, which confirmed solubilizing effect of serum proteins (**Fig. 32b**).

PTX solubility was alternatively measured with solutions prepared by diluting a concentrated PTX/DMSO stock solution with each medium. This method helped handle small quantities of PTX with greater accuracy than the previous method. However, a small trace of DMSO in the solution (maximum 0.7% in Tween/PBS, and 3% in FBS/PBS) seemed to have affected PTX dissolution, resulting in slightly higher solubility values after 24 hour incubation in 37°C (4 $\mu\text{g/mL}$ in Tween/PBS, **Fig. 33a**). In FBS/PBS, PTX concentration increased linearly with the PTX input and never reached a limit at least by 300 $\mu\text{g/mL}$ (**Fig. 33b**). PTX concentrations measured after 24h incubation at 37°C were about 50% of those incubated for 7h, confirming the instability of PTX in FBS/PBS reported previously (Bajaj et al., 2012; Ringel & Horwitz, 1987; Willey et al., 1993). This indicates that, if PTX release kinetics studies are performed in serum-containing medium and the medium is not sampled and analyzed frequently, one may not recover 100% of PTX from the formulation due to the degradation of released PTX. In contrast, PTX was relatively more stable in Tween/PBS (Abouelmagd et al., 2015). This means that, as long as the medium is sampled at least once a day, PTX stability in Tween/PBS is less likely to

be a problem. Of note, PTX solubility in Tween/PBS showed interesting variability across the measurements repeated four times (data not shown, (Abouelmagd et al., 2015)). While the saturation solubility was measured to be 4 $\mu\text{g}/\text{mL}$ in the presence of far excess PTX, PTX solutions prepared in the range of 4-18 $\mu\text{g}/\text{mL}$ in Tween/PBS showed concentrations greater than the saturation solubility to varying degrees in each experiment, indicating the formation of supersaturated solutions. This result indicates that one may observe variable solubility values in Tween/PBS, depending on the degree of supersaturation.

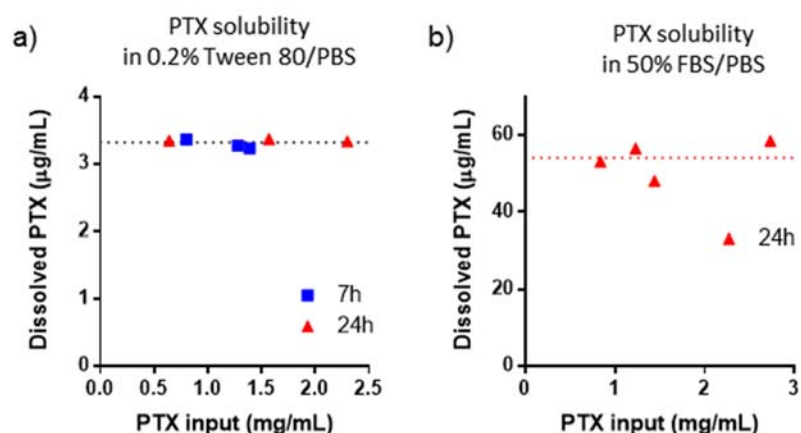


Figure 32: PTX solubility in 0.2% Tween 80/PBS (a) and 50% FBS in PBS (b) was determined by incubating excess PTX in 1 mL of the medium at 37 °C for 7 and/or 24 h with agitation (Adapted from Abouelmagd et al., 2015).

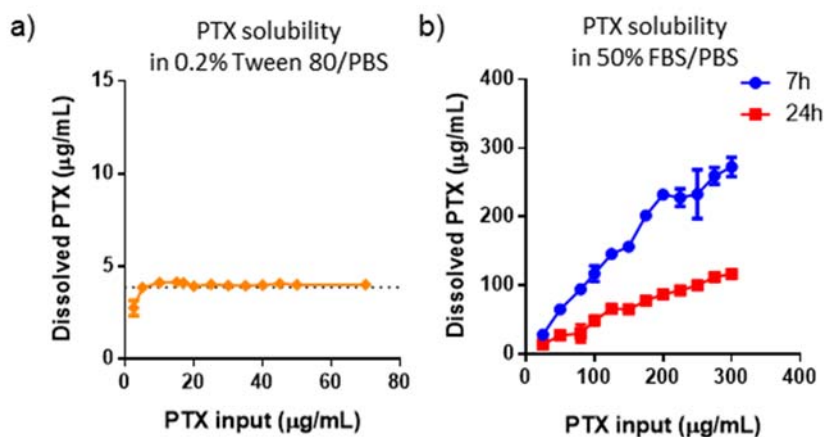


Figure 33: PTX solubility in 0.2% Tween 80/PBS (24 hr) (a) and 50% FBS in PBS (7 and 24 hr) (b) was determined by an alternative method. PTX was added to each medium in the amount indicated in the x-axis from a 10 mg/mL stock in DMSO. Samples were incubated for different times at 37 °C with agitation (Adapted from Abouelmagd et al., 2015).

4.3.2 *In Vitro* Release of PTX from PLGA NPs

For this study, polymeric PLGA NPs were loaded with PTX and tested for release kinetics with centrifugation method. PTX loaded PLGA NPs (PTX/NPs) were prepared using the single emulsion method. NPs were spherical and had an average diameter of 161 nm. PTX release from PTX/NPs was tested using PBS, Tween/PBS, or FBS/PBS as release media. NPs equivalent to 4.4 μg of PTX was suspended in 1 mL of each release medium, creating a condition exceeding the solubility limit (in PBS), close to the solubility (in Tween/PBS), or satisfying the sink condition (in FBS/PBS). At regular intervals, 80% of the release medium (0.8 mL) was sampled after centrifugation and replaced with fresh buffers, and the sampled medium was filtered and analyzed by HPLC. In FBS/PBS which satisfied a sink condition from the initial time point, NPs released $50.7 \pm 9.1\%$ of the loaded PTX upon the addition of the release medium and $98.7 \pm 11.0\%$ in 72 hours (**Fig. 34a**). Similarly, in Tween/PBS, NPs released $56.6 \pm 1.2\%$ of the loaded PTX immediately and $83.9 \pm 1.3\%$ in 72 hours (**Fig. 34a**). It is worth mentioning that NPs in Tween/PBS did not satisfy the sink condition at the initial time point but resulted in a similar trend as in FBS/PBS. On the other hand, PTX release in PBS was relatively small, reaching a cumulative release of $34.2 \pm 6.4\%$ in 72 hours (**Fig. 34a**). Since the total amount of PTX dispersed as NPs in PBS ($4.4 \mu\text{g}/\text{mL}$) was above the PTX solubility ($0.2 \mu\text{g}/\text{mL}$), we initially thought that PTX release was inhibited due to the low PTX solubility. However, the sum of total release (34.2%) and unreleased PTX (3.8%) fell far short of 100%, unlike those in Tween/PBS or FBS/PBS (**Fig. 35**), suggesting a potential sample loss during the sampling or sample treatment. We thus added acetonitrile to the sampled PBS medium in 1:1 volume ratio and reanalyzed the samples. We found that a much greater amount of PTX was present in the sampled medium ($46.1 \pm 1.4\%$ as immediate release and $78.7 \pm 3.2\%$ as cumulative release by 72h) than initially measured. This indicates that PTX was released in PBS to a similar level as in Tween/PBS and FBS/PBS but quickly precipitated out in the sampled medium due to the low solubility in PBS. When analyzed as sampled (without additional acetonitrile), the precipitated PTX was removed during the HPLC sample preparation (i.e., filtration) and excluded from the analysis, which was avoided in the

second analysis by the addition of acetonitrile. This result underscores the importance of keeping the ratio of total drug in NPs to medium volume below the drug solubility limit in the release kinetics studies. If this condition is not met (as in PBS in our case), one may observe low drug levels in the medium and incorrectly interpret them as sustained drug release, when in reality the drug has already been released and precipitated out in the sampled medium.

The release kinetics of PTX/NPs was also studied using a greater amount of NPs per release medium (NPs equivalent to 27 μg of PTX in 1 mL of release medium), which was comparable to typical conditions described in the literature (Abouelmagd et al., 2015) (hence ending up violating sink conditions for all samples at the initial time point). A similar trend was observed (**Fig. 34b**), with the cumulative release in PBS being the least when directly measured but similar to those in Tween/PBS and FBS/PBS when analyzed with additional acetonitrile. Interestingly, PTX concentrations in sampled media (4.0 $\mu\text{g}/\text{mL}$ in PBS, 13.1 $\mu\text{g}/\text{mL}$ in Tween/PBS at the first sampling time point) were much greater than its solubility limit in each medium (0.2 $\mu\text{g}/\text{mL}$ in PBS and 3.3 $\mu\text{g}/\text{mL}$ in Tween/PBS). This may be explained by temporary supersaturation of PTX in the release medium. However, since the extent of supersaturation may vary, one cannot be sure that the result will be reproducible (Abouelmagd et al., 2015).

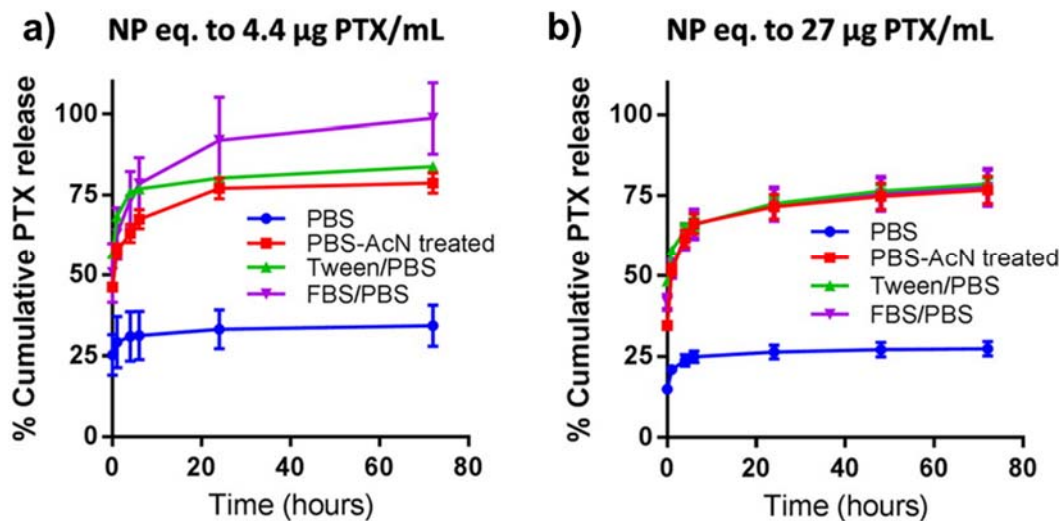


Figure 34: Release kinetics of PTX/NPs in media containing PBS, FBS, or Tween 80. PTX/NPs equivalent to (a) 4.4 µg or (b) 27 µg of PTX were suspended in 1 mL of release medium and incubated at 37°C with constant agitation (Adapted from Abouelmagd et al., 2015).

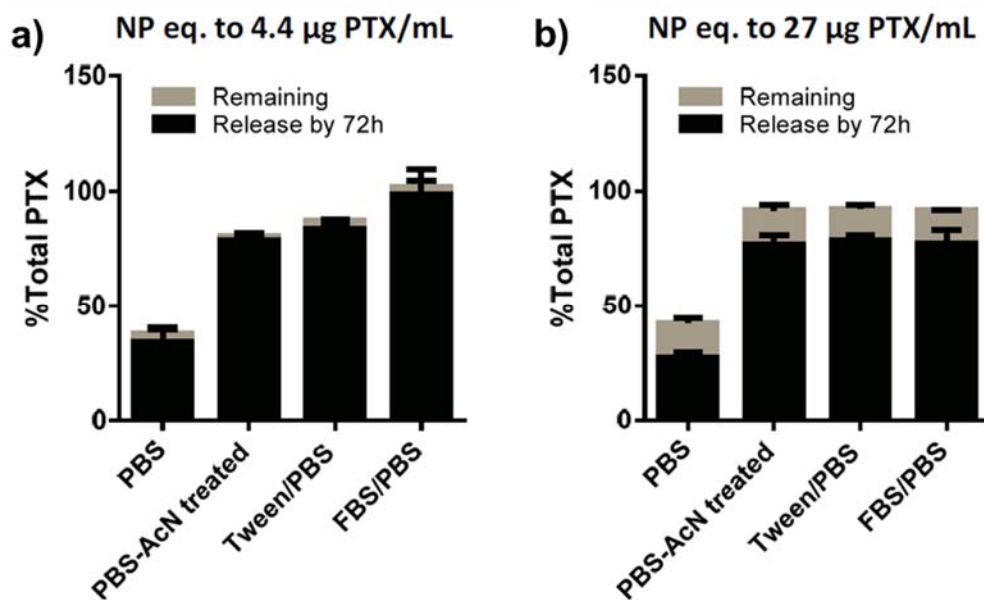


Figure 35: Mass balance after release kinetic studies of PTX/NPs in media containing PBS, FBS or Tween 80 (Adapted from Abouelmagd et al., 2015).

4.4 Discussion

This study demonstrates that release kinetics of a poorly water-soluble drug may be much underestimated when the ratio of the NP mass to release medium is not sufficiently low, because the released drug precipitated in the sampled medium (**Fig. 34**). From reported review of *in vitro* release kinetics of PTX from NPs or other sustained delivery formulations, (Abouelmagd et al., 2015), studies using the centrifugation method, PTX concentration in a test tube ranged from 25 to 1000 $\mu\text{g/mL}$. These studies conclude that their NP formulations achieve sustained PTX release over various time periods. However, given that these concentration ranges are far above the solubility (0.2 $\mu\text{g/mL}$), we suspect that even if the drug release had been much faster in reality they would not have been able to detect it. As the release kinetics studied show, when PTX is present in excess of the solubility limit in the medium, the drug can precipitate out in the system shortly after it is released out of the formulation. This translates to a low drug level in the release medium, which can be incorrectly interpreted as sustained drug release. From this perspective, revisiting some of the previous studies with conflicting bioactivity results. For example, with slow *in vitro* drug release kinetics, one may expect that a NP formulation will be less effective than a free drug control. Some studies do report the attenuated bioactivity of NPs relative to free PTX.(J. H. Kim et al., 2006; Liang et al., 2006; Malavaud et al., 2004; Saravanakumar et al., 2009; Yang et al., 2007; Z. P. Zhang & S. S. Feng, 2006) However, in many cases, PTX NP formulations are not any less toxic than a free drug control (Gu et al., 2013; Jiang et al., 2012; S. H. Kim et al., 2011; Liu et al., 2005; Song et al., 2011; Tang et al., 2013; X. Wang et al., 2014; Z. Zhang & S. S. Feng, 2006). This may be interpreted as a consequence of enhanced cellular drug uptake or retention of NPs (Jiang et al., 2012; Liu et al., 2005; Song et al., 2011; Tang et al., 2013), but it could also be premature drug release, which has been ignored in the release kinetics study. A potential hazard of underestimating *in vitro* drug release is that it can mislead to a prediction that a NP formulation will attenuate the drug activity during circulation and, thus, help reduce its side effects on non-target tissues. However, unlike *in vitro*, NPs face an ultimate sink condition in the body, where the released drug is continuously diluted and undergoes protein binding,

and can thus show very different drug release behaviors and biological performances than expected from the *in vitro* release studies. This may partly explain why many NPs expected to be effective *in vitro* do not readily translate to clinically effective products.

In order for *in vitro* release kinetics to provide some predictive potential, it is necessary that the release studies be performed with release media that simulate critical features of *in vivo* systems while maintaining simplicity and convenience of *in vitro* tests. PBS is the most simple and common medium for the release kinetics studies, but it requires a very low ratio of NPs to medium volume especially for poorly water-soluble drugs, which is met at the price of accuracy of the analysis. To avoid analytical limitation, some have measured drug remaining as NPs in the system at regular time points as an indirect estimate of drug release, where the difference between the initial and remaining dose is considered the released drug (Modi & Anderson, 2013). This is a good alternative to measuring the released drug, as long as the released drug remains stable in the medium. Serum-containing buffers may be a reasonable choice of release medium for mimicking a physiological fluid with a complex composition that affects drug release. Due to the solubilizing effect of serum proteins, these media are also good for achieving a sink condition at a reasonably high concentration. However, PTX in serum-containing medium requires additional extraction step to separate PTX from the proteins prior to analysis. Moreover, PTX is unstable in serum-containing solution; thus, the drug release may be underestimated unless the medium is exchanged frequently. Hence, Tween/PBS is most recommendable among those tested in this study, as PTX in Tween/PBS are more stable than in FBS/PBS, do not require extra sample treatment for HPLC analysis, and generates a similar release profile as that in FBS/PBS when used in the centrifugation method.

Centrifugation and dialysis are most widely used for sampling the release medium, but both have critical limitations. Centrifugation method requires centrifugation at a high speed for separating NPs from the free drug at each sampling. The pressure generated during the centrifugation can disturb the equilibrium between released drug and NPs and make it difficult to resuspend the NPs for further incubation. In addition, the separation is often incomplete, leading to cumulative errors in measurement of the released drug. Dialysis method eliminates the need for separation step, but the fact that the dialysis

membrane itself functions as a diffusion barrier creates a different problem, especially for the poorly water-soluble drugs. As observed in this study, a poorly water-soluble drug, accumulating in the bag due to the delay in diffusion across the membrane, can reprecipitate into larger aggregates, which then drive the apparent release kinetics. A similar concern has been raised by Anderson et al, who studied release kinetics of lipophilic drug-loaded liposomes with the dialysis method and observed reversible binding of the released drug to the liposomes (Modi & Anderson, 2013). Given these disadvantages, it is worthwhile to consider alternative methods. For example, Szoka et al used agarose hydrogel to accommodate liposomes for non-invasive separation of the released drug from the carrier (Peschka et al., 1998). Alternatively, a biphasic dissolution model is a conceivable option for studying the release kinetics of poorly water-soluble drugs (D. J. Phillips et al., 2012). Here, a water-immiscible organic solvent with a low density (e.g., octanol) is laid over an aqueous release medium that contains the formulation. A drug released into the medium partitions into the organic layer due to the lipophilicity, keeping the aqueous medium from saturation (D. J. Phillips et al., 2012). This method can, at least in theory, maintain the sink condition without excessive dilution and/or invasive sampling.

4.5 Conclusions

Overall, this study demonstrates the importance of choosing both optimum drug concentration and release medium when designing *in vitro* release experiments of poorly water soluble drugs from NPs. *In vitro* release kinetics studies of poorly water-soluble drugs designed without considering the solubility limitation can result in underestimation of drug release. To reasonably simulate *in vivo* conditions in which NPs are administered, the ratio of NPs to the initial volume of the release medium should be sufficiently lower than the saturation solubility. Inclusion of a dissolution aid in the release medium can help meet this requirement without compromising sample detection as long as it is in direct contact with NPs. In any combinations of release media and sampling methods, it is desirable to analyze the remaining NPs at the end of the study and check the mass balance, in order to exclude potential underestimation of drug release.

4.6 References

- Abouelmagd, S. A., Sun, B., Chang, A. C., Ku, Y. J., & Yeo, Y. (2015). "Release kinetics study of poorly water-soluble drugs from nanoparticles: are we doing it right?" Mol Pharm 12(3): 997-1003.
- Bajaj, G., Kim, M. R., Mohammed, S. I., & Yeo, Y. (2012). "Hyaluronic acid-based hydrogel for regional delivery of paclitaxel to intraperitoneal tumors." Journal of Controlled Release 158(3): 386-392.
- Gu, Q., Xing, J. Z., Huang, M., Zhang, X., & Chen, J. (2013). "Nanoformulation of paclitaxel to enhance cancer therapy." J Biomater Appl 28(2): 298-307.
- Jiang, X., Li, L., Liu, J., Hennink, W. E., & Zhuo, R. (2012). "Facile fabrication of thermo-responsive and reduction-sensitive polymeric micelles for anticancer drug delivery." Macromol Biosci 12(5): 703-711.
- Kilfoyle, B. E., Sheihet, L., Zhang, Z., Laohoo, M., Kohn, J., & Michniak-Kohn, B. B. (2012). "Development of paclitaxel-TyroSpheres for topical skin treatment." J Control Release 163(1): 18-24.
- Kim, J. H., Kim, Y. S., Kim, S., Park, J. H., Kim, K., Choi, K., Chung, H., Jeong, S. Y., Park, R. W., Kim, I. S., & Kwon, I. C. (2006). "Hydrophobically modified glycol chitosan nanoparticles as carriers for paclitaxel." J Control Release 111(1-2): 228-234.
- Kim, S. H., Tan, J. P., Fukushima, K., Nederberg, F., Yang, Y. Y., Waymouth, R. M., & Hedrick, J. L. (2011). "Thermoresponsive nanostructured polycarbonate block copolymers as biodegradable therapeutic delivery carriers." Biomaterials 32(23): 5505-5514.
- Lee, J., Lee, S. C., Acharya, G., Chang, C. J., & Park, K. (2003). "Hydrotropic solubilization of paclitaxel: analysis of chemical structures for hydrotropic property." Pharm Res 20(7): 1022-1030.
- Liang, H. F., Chen, C. T., Chen, S. C., Kulkarni, A. R., Chiu, Y. L., Chen, M. C., & Sung, H. W. (2006). "Paclitaxel-loaded poly(γ -glutamic acid)-poly(lactide) nanoparticles as a targeted drug delivery system for the treatment of liver cancer." Biomaterials 27(9): 2051-2059.
- Liu, S. Q., Tong, Y. W., & Yang, Y. Y. (2005). "Thermally sensitive micelles self-assembled from poly(N-isopropylacrylamide-co-N,N-dimethylacrylamide)-b-poly(D,L-lactide-co-glycolide) for controlled delivery of paclitaxel." Mol Biosyst 1(2): 158-165.
- Lovich, M. A., Creel, C., Hong, K., Hwang, C. W., & Edelman, E. R. (2001). "Carrier proteins determine local pharmacokinetics and arterial distribution of paclitaxel." J Pharm Sci 90(9): 1324-1335.
- Malavaud, B. A., LeVisage, C., Rioux-Leclercq, N., Haller, M., Breton, P., & Leong, K. (2004). "Efficacy of paclitaxel released from bio-adhesive polymer microspheres on model superficial bladder cancer." Journal of Urology 171(4): 188-188.

- Mathew, A. E., Mejillano, M. R., Nath, J. P., Himes, R. H., & Stella, V. J. (1992). "Synthesis and evaluation of some water-soluble prodrugs and derivatives of taxol with antitumor activity." J Med Chem 35(1): 145-151.
- Modi, S., & Anderson, B. D. (2013). "Determination of drug release kinetics from nanoparticles: overcoming pitfalls of the dynamic dialysis method." Mol Pharm 10(8): 3076-3089.
- Peschka, R., Dennehy, C., & Szoka, F. C., Jr. (1998). "A simple in vitro model to study the release kinetics of liposome encapsulated material." Journal of Controlled Release 56(1-3): 41-51.
- Phillips, D. J., Pygall, S. R., Cooper, V. B., & Mann, J. C. (2012). "Overcoming sink limitations in dissolution testing: a review of traditional methods and the potential utility of biphasic systems." Journal of Pharmacy and Pharmacology 64(11): 1549-1559.
- Phillips, D. J., Pygall, S. R., Cooper, V. B., & Mann, J. C. (2012). "Overcoming sink limitations in dissolution testing: a review of traditional methods and the potential utility of biphasic systems." J Pharm Pharmacol 64(11): 1549-1559.
- Ringel, I., & Horwitz, S. B. (1987). "Taxol is converted to 7-epitaxol, a biologically active isomer, in cell culture medium." Journal of Pharmacology and Experimental Therapeutics 242(2): 692-698.
- Saravanakumar, G., Min, K. H., Min, D. S., Kim, A. Y., Lee, C. M., Cho, Y. W., Lee, S. C., Kim, K., Jeong, S. Y., Park, K., Park, J. H., & Kwon, I. C. (2009). "Hydrotropic oligomer-conjugated glycol chitosan as a carrier of paclitaxel: synthesis, characterization, and in vivo biodistribution." J Control Release 140(3): 210-217.
- Song, N., Liu, W., Tu, Q., Liu, R., Zhang, Y., & Wang, J. (2011). "Preparation and in vitro properties of redox-responsive polymeric nanoparticles for paclitaxel delivery." Colloids Surf B Biointerfaces 87(2): 454-463.
- Steele, T. W. J., Huang, C. L., Kumar, S., Widjaja, E., Boey, F. Y. C., Loo, J. S. C., & Venkatraman, S. S. (2011). "High-Throughput Screening of PLGA Thin Films Utilizing Hydrophobic Fluorescent Dyes for Hydrophobic Drug Compounds." Journal of Pharmaceutical Sciences 100(10): 4317-4329.
- Swindell, C. S., Krauss, N. E., Horwitz, S. B., & Ringel, I. (1991). "Biologically active taxol analogues with deleted A-ring side chain substituents and variable C-2' configurations." J Med Chem 34(3): 1176-1184.
- Tang, X. L., Cai, S. Y., Zhang, R. B., Liu, P., Chen, H. B., Zheng, Y., & Sun, L. L. (2013). "Paclitaxel-loaded nanoparticles of star-shaped cholic acid-core PLA-TPGS copolymer for breast cancer treatment." Nanoscale Research Letters 8.
- Tarr, B. D., & Yalkowsky, S. H. (1987). "A new parenteral vehicle for the administration of some poorly water soluble anti-cancer drugs." J Parenter Sci Technol 41(1): 31-33.
- The United States Pharmacopeia: The National Formulary (USP37/NF32) (2014). Rockville, MD, The United States Pharmacopeial Convention, Inc.

- Wang, X., Chen, Y., Dahmani, F. Z., Yin, L., Zhou, J., & Yao, J. (2014). "Amphiphilic carboxymethyl chitosan-quercetin conjugate with P-gp inhibitory properties for oral delivery of paclitaxel." Biomaterials 35(26): 7654-7665.
- Wang, Y. S., Jiang, Q., Li, R. S., Liu, L. L., Zhang, Q. Q., Wang, Y. M., & Zhao, J. (2008). "Self-assembled nanoparticles of cholesterol-modified O-carboxymethyl chitosan as a novel carrier for paclitaxel." Nanotechnology 19(14): 145101.
- Willey, T. A., Bekos, E. J., Gaver, R. C., Duncan, G. F., Tay, L. K., Beijnen, J. H., & Farmen, R. H. (1993). "High-performance liquid chromatographic procedure for the quantitative determination of paclitaxel (Taxol) in human plasma." J Chromatogr 621(2): 231-238.
- Yang, T., Cui, F. D., Choi, M. K., Cho, J. W., Chung, S. J., Shim, C. K., & Kim, D. D. (2007). "Enhanced solubility and stability of PEGylated liposomal paclitaxel: In vitro and in vivo evaluation." International Journal of Pharmaceutics 338(1-2): 317-326.
- Zhang, J. A., Anyarambhatla, G., Ma, L., Ugwu, S., Xuan, T., Sardone, T., & Ahmad, I. (2005). "Development and characterization of a novel Cremophor EL free liposome-based paclitaxel (LEP-ETU) formulation." Eur J Pharm Biopharm 59(1): 177-187.
- Zhang, Z., & Feng, S. S. (2006). "Self-assembled nanoparticles of poly(lactide)--Vitamin E TPGS copolymers for oral chemotherapy." Int J Pharm 324(2): 191-198.
- Zhang, Z. P., & Feng, S. S. (2006). "In vitro investigation on poly(lactide)-Tween 80 copolymer nanoparticles fabricated by dialysis method for chemotherapy." Biomacromolecules 7(4): 1139-1146.

CHAPTER 5. APPLICATION OF TANNIC ACID FOR SURFACE FUNCTIONALIZATION OF NANOPARTICLES

5.1 Introduction

The development of simple techniques for functionalizing NPs with different ligands and molecules is a topic of wide interest. Polydopamine (pD) represents a universal technique for easy functionalization of polymeric nanocarriers with different ligands, including small molecules, like folate and fluoresceinamine, and macromolecules like LMWC (discussed in Chapter 2), PEG, TAT peptide and polycarboxybetaine (Gullotti et al., 2013; Park et al., 2014). Successful conjugation of these ligands resulted in changes in NP surface properties and corresponding NP-cell interactions. Furthermore, the use of pD as a prime coating for polymeric NP cores did not compromise the drug loading function of the core (Abouelmagd et al., 2015).

However, in spite of the simplicity and efficiency of pD as a universal coating material, its chemical and optical nature limits broader application of this technique: (1) pD is black in color and has a broadband absorbance profile, which interferes with the optical properties of the core (Quignard et al., 2014); (2) Amine groups in pD give significant background signals in spectroscopic analysis and quantification of functionalized ligands (specially proteins and peptides); (3) Dopamine polymerization requires alkaline conditions, unless an oxidation aid (external ultraviolet light, or oxidants like sodium periodate) is provided, (Du et al., 2014; Wei et al., 2010), while such alkaline pH is not compatible with selected drugs and polymers; and (4) Dopamine is relatively expensive.

In an effort to overcome these challenges, alternative coating substrates are considered. These substrates “monomers” mostly have the same characteristic catechol and amine groups of dopamine, and therefore can polymerize on a solid platform like dopamine, but have additional functional groups to produce a surface coating with different properties than pD (Lynge et al., 2011).

Among the monomers is norepinephrine, which shares the same catechol and terminal primary amine group with dopamine. Reportedly, Norepinephrine forms coatings universally in a manner similar to dopamine. However, unlike pD, polymerized norepinephrine coatings facilitates additional ring polymerization reactions for polyester monomers on the surface, due to the additional alkyl hydroxyl group of norepinephrine (Kang et al., 2009). In another study, azide group was introduced into dopamine. The presence of azide group in the polymerized coating mediated introduction of alkynyl terminated molecules via click chemistry, enabling simple conjugation of a new range of molecules to azide-dopamine coated surfaces (Barras et al., 2011).

Recently, a whole new class of multifunctional coatings was introduced. Sileika et al recently proposed a group of coatings derived from natural products (Sileika et al., 2013). Molecules like tannic acid (TA), pyrogallol (PG), and epigallocatechins gallate (EGCG) are known phenolic and polyphenolic compounds of plant origin. They are not catecholamine compounds but possess abundant catechol (dihydroxyphenyl) and galloyl (trihydroxybenzoyl) groups (**Fig. 36**). These natural precursors formed coatings similar to pD on organic and inorganic substrates, including polycarbonate and titanium dioxide (Sileika et al., 2013). It appears that the coating formation was driven by oxidation reactions, as the thickness dramatically decreased in the absence of oxygen. Phenolic compounds are known to polymerize under oxidative conditions “oxidative polymerization”, for example, PG is known to dimerize via oxidative coupling to form PG-PG dimer (Appel, 1993; Drynan et al., 2010).

Unlike pD coating, the polyphenolic coatings spontaneously formed at neutral pH, were colorless at same thickness with minimum alteration of the optical properties of the coated substrate (Sileika et al., 2013). Additionally, phenols and polyphenols like PG, TA

and EGCG are much cheaper than dopamine (Barrett et al., 2014). These differences provide a good opportunity to overcome the previously mentioned limitations of dopamine.

PG and TA coatings had no cytotoxic effects on NIH/3T3 fibroblasts but favorably decreased the formation of reactive oxygen species (ROS) due to their antioxidant properties. The same group further investigated the coating-formation ability of many structurally related phenols and polyphenols and concluded that precursors with a minimum of one aromatic vicinal diol were most successful in coating formation (Barrett et al., 2014).

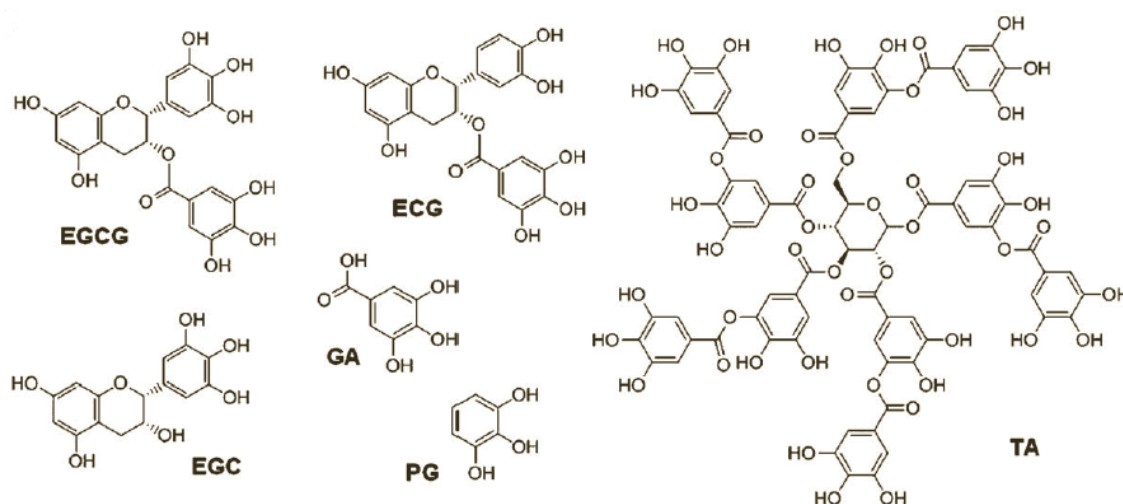


Figure 36: Plant derived phenolic and polyphenolic compounds investigated for formation of colorless multifunctional coatings (adapted from Sileika et al, 2013).

Among all the polyphenolic precursors shown in **Figure 36**, TA stands out as multifunctional coating material. According to the literature (Barrett et al., 2014; Sileika et al., 2013), TA is water soluble and able to spontaneously form a colorless coating via oxidation at pH 7 with a thickness comparable to that of pD (Sileika et al., 2013). As a polyphenol with 10 units of gallic acid, it has a lot of hydroxyl groups, which enables interaction with different molecules via hydrogen bonding (S. Kim et al., 2015). The high

number of galloyl groups also makes the molecule negatively charged, driving strong electrostatic interactions with cationic molecules. Moreover, multiple aromatic rings can mediate hydrophobic interactions with hydrophobic molecules. Due to this unique combination of intermolecular interactions, TA is expected to be more versatile than dopamine as a precursor.

Accordingly, TA has repeatedly been used to crosslink collagen scaffolds, resulting in dramatically higher stability and resistance to degradation than TA-free collagen scaffolds (Heijmen et al., 1997; Natarajan et al., 2013). This was mainly attributed to TA's significant hydrogen bonding with collagen carbonyl groups, in addition to hydrophobic interaction with collagen hydrophobic domains (Jackson et al., 2010). In another study, Wang et al described the adsorption of TA to the surface of amine functionalized mesoporous silica NPs and confirmed covalent conjugation between TA and amine groups of the silica NPs via X-ray photoelectron spectroscopy (XPS) (Wang et al., 2010). Additionally, TA was employed as a "molecular glue" to interact with DNA forming a mucoadhesive and biodegradable hydrogel for biomedical applications (Shin et al., 2015). Hydrogel formation was attributed to the interaction between phosphate groups of DNA and phenolic groups of TA. It is worth mentioning that TA was frequently utilized as a building block for fabrication of NPs and MPs, but it was mainly used as a polyanion in Layer-by-Layer (LbL) composites (B. S. Kim et al., 2009; Kozlovskaya et al., 2010; Lomova et al., 2015; Shutava & Lvov, 2006). The application of polymerized TA as multifunctional coating material of polymeric NPs has not been fully explored.

In this study, the application of TA as a multifunctional coating for polymeric NPs is investigated. In addition to its biocompatibility and favorable optical properties, we hypothesize that, given the multitude of molecular interaction capabilities, TA will enable functionalization of PLGA NPs with a unique array of (macro) molecules which would be challenging to conjugate with pD. Two different coating methods were explored, and its utility in surface functionalization with different types of ligands was evaluated.

5.2 Materials and Methods

5.2.1 Materials

PLGA (150 kDa, LA:GA=85:15, PLGA₁₅₀) was purchased from Akina Inc. (IN, USA). Paclitaxel (PTX) was a gift from Samyang Genex Corp (Seoul, Korea). Tannic acid (Pure) and albumin from human serum were purchased from Sigma-Aldrich (MO, USA). Dopamine HCl was purchased from Alfa-Aesar (MA, USA). Pierce BCA protein assay and CBQCA protein assay kit were purchased from Thermo Scientific (NY, USA). (3-(4,5-Dimethylthiazol-2-yl)- 2,5-diphenyltetrazolium bromide) (MTT) was purchased from Invitrogen (Eugene, OR, USA). All other materials were of analytical grade.

5.2.2 Preparation and Characterization of NPs

Conventional method. PLGA NP cores were prepared via single emulsion-solvent evaporation method. Briefly 100 mg of PLGA and 10 mg of PTX were dissolved in an organic phase of DCM (10 mL) were sonicated into an aqueous phase of PVA (4%, 20 mL) using Vibra-Cell probe sonicator (Sonics, Newtown, CT, USA) with 45% amplitude at a pulse of 4-s on and 2-s off. Formed emulsion was dispersed into 30 mL of water and stirred for 5 hours to allow evaporation of DCM. NPs were collected by centrifugation at 25,000 rpm (33,000 xg rcf) and washed 3 times with water to remove any remaining traces of DCM and PVA. To coat NPs with TA, PLGA NPs were dispersed in 0.07 mg/mL of TA solution in bicine buffer (0.1 M, pH 7.4) at a concentration of 0.5 mg NP/mL. The suspension was shaken for three hours, after which the formed PLGA-TA NPs were collected by centrifugation and further washed with water. The pD coated NPs were prepared as described in section 2.2.4. To functionalize PLGA-TA or PLGA-PD NPs with a certain ligand (albumin or fluoresceinamine (FA)), they were further incubated in ligand solution in bicine buffer (0.1 M, pH 7.4) with specified concentration and time, followed by NPs collection and washing. The washed NPs were freeze-dried and stored in 4 °C until needed.

One-pot method. PLGA emulsion was prepared in a manner similar as in the conventional method, replacing 4% PVA/water with 4% PVA in bicine buffer (0.1 M, pH 7.4). After DCM evaporation, TA was directly added to the continuous phase in a ratio of 1:1 (TA: NP), followed by addition of sodium periodate at a final concentration of 0.2 mg/mL. NP suspension was shaken for 1.5 hour to form PLGA-TA NPs, collected and conjugated with ligands in the same as detailed in the conventional method section.

5.2.3 NP Characterization

Size, zeta potential, and morphology. Different types of NPs were evaluated for particle size and zeta potential as described in section 2.2.5. NP morphology was observed by transmission electron microscopy (TEM) using the method described in section 2.2.5, employing different stains.

TA-induced AgNO₃ deposition. The presence of TA was detected by deposition of Ag metal on TA surface. (Sileika et al., 2013). Briefly, PLGA or PLGA-TA NPs were incubated overnight in AgNO₃ aqueous solution (17 mg/mL) with shaking and collected by centrifugation. The NPs were washed once with water to remove excess AgNO₃. Finally, NPs were visualized with TEM using 1% phosphotungstic acid as a negative stain.

TA content. To examine the efficiency of TA coating on PLGA NP surfaces, TA content was directly and indirectly quantified by bicinchoninic acid (BCA) assay. TA is a reducing agent and can reduce cupric ions in the assay reagent to cuprous, which form colored complexes with BCA (Marino et al., 2009). This reaction is sensitive and linear. To *directly* determine TA content, TA coated NPs of a known weight were incubated with BCA working reagent for an hour at 37 °C. A supernatant was separated from the suspension via centrifugation, and its absorbance was read at 562 nm using a SpectraMax M3 microplate reader (Molecular Device, Sunnyvale, CA). The amount of TA per NP sample was calculated after subtracting the background absorbance of uncoated PLGA NPs, using a calibration curve drawn with TA solutions of known concentrations. Alternatively, TA content of PLGA-TA NPs was determined *indirectly* by quantification of TA in bicine buffer after incubation of PLGA NPs and separation of NPs by centrifugation. The amount

of TA in the supernatant was measured using BCA assay and compared to control samples (100% TA, no PLGA NPs). The TA content of PLGA NPs (%w/w) was calculated as:

$$TA\ NP\ content\ \% = \frac{Original\ TA\ amount - remaining\ TA\ amount\ after\ NP\ incubation}{Incubated\ NP\ amount} \%$$

Human Serum Albumin content. To determine the amount of albumin conjugated to NPs surface, NPs were dispersed in water (10 mg/mL), and albumin content was determined via CBQCA fluorescence protein assay (Life Science, NY, USA) per vendor's instruction. A calibration curve was constructed using known concentrations of albumin. Fluorescence of different samples was measured at Excitation/Emission of 465/550 nm using a SpectraMax M3 microplate reader (Molecular Device, Sunnyvale, CA). The amount of albumin per NP sample was calculated after subtracting the background fluorescence level of corresponding NPs before albumin conjugation.

Fluoresceinamine content. The amount of Fluoresceinamine (FA) conjugated to different types of NPs was quantified indirectly by measuring the absorbance of FA in supernatant before and after NPs incubation. Briefly, 0.4 mg of NPs was dispersed in 1 mL of FA solution (15 ug/mL) in Tris buffer (10 mM, pH 8.5) for 40 minutes. Then, NPs were centrifuged, and the FA absorbance in the supernatant was measured at 497 nm using a SpectraMax M3 microplate reader (Molecular Device, Sunnyvale, CA) and compared to that of original FA solution. The amount of FA per NP weight was determined using a standard calibration curve of FA in the same buffer solution.

5.2.4 *In vitro* Cytotoxicity of TA coated NPs

To evaluate the cytotoxic effect of TA coated NPs. An *in vitro* cytotoxicity study was performed using NIH/3T3 fibroblast cell line (ATCC, Manassas, VA, USA). Cells were cultured in Dulbecco's modified Eagle medium (DMEM) medium supplemented with 10% fetal calf serum and 100 units/ml of penicillin and 100 ug/ml of streptomycin. Cells were seeded in 96-well plate at a density of 10,000 cell/well (200 μ L). Next day, concentrated NP suspension was added (20 μ L) to a final concentration of 0.1, 0.01, 0.001,

or 0.0001 mg/mL. After 72 hours, mitochondrial activity of the cells was evaluated using the MTT assay. NP containing medium was replaced with that containing MTT solution (115 μ L) and cells were incubated for 3.5 hours, after which 100 μ L of stop solution (50 % DMSO, 20% SDS and 0.02% acetic acid) was added. Next day, wells absorbance was read using a SpectraMax M3 microplate reader at 529 nm. % viability of the cells was determined in comparison to control cells that did not receive NP treatment.

5.3 Results

5.3.1 NPs Preparation and Characterization

Freeze-dried PLGA NPs had an average particle size of 200 nm after redispersion, maintaining a good polydispersity index (<0.2) (**Fig. 37a**). TA coating was achieved using two methods, conventional and one-pot method. The former approach was similar to that of pD coating, where PLGA NPs are first formed in PVA solution, washed, then incubated in TA solution. In the one-pot method, PLGA NPs were directly formed in TA buffer solution. The main difference was that PVA was removed prior to TA deposition in the original method, whereas TA deposition occurred in the presence of PVA emulsifier in the one pot method.

Unlike pD coating, which imparted a black color to the NPs, TA deposition on PLGA surface did not induce color change of the NPs (**Fig. 38**). Nevertheless, TA deposition was evident due to the increased net surface negative charge (**Fig. 37b**). Coating of NPs with TA via either conventional, or one-pot method, did not increase the particle size compared to uncoated PLGA NPs (**Fig.37a**), which indicates that TA existed in a thin layer not contributing to NP diameter, similar to that observed with pD coated NPs (Abouelmagd et al., 2015). Overall, all coated NPs had a good polydispersity index after freeze-drying without prior addition of cryoprotectants (**Fig. 37a**).

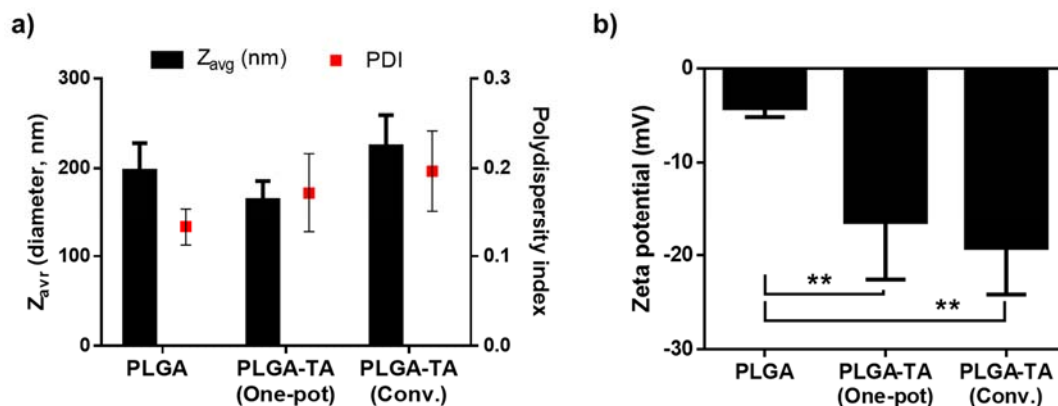


Figure 37: Particle size and surface charge of different NPs: (a) Particle size and polydispersity index, (b) Zeta potential of NPs in pH 7.4 phosphate buffer (average \pm SD, $n=4-5$, Anova test, ** $p<0.005$).

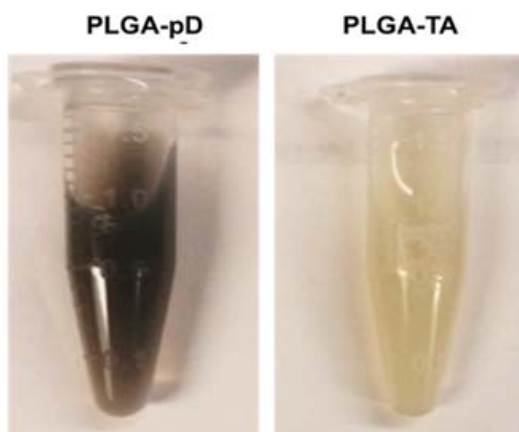


Figure 38: Suspension of PLGA NPs post coating with pD or TA (conventional method) showing the different colors of the coated NPs.

Although TA itself did not have color, its presence on NP surface was indirectly indicated by the color change of PLGA-TA NP suspension after incubation in AgNO_3 solution (**Fig. 39a**), due to the reducing effect of TA on AgNO_3 localized at NPs surface leading to deposition of metallic silver on NPs. Uncoated PLGA NPs did not show change after overnight incubation with AgNO_3 . Deposited Ag was also visualized by TEM as electron dense aggregates on the surface of PLGA-TA NPs (**Fig. 39b**).

Although both preparation methods, conventional and one-pot, seemed to result in TA coating, as indicated by negative charges of NPs, conventional method was more preferable, as TA coating was carried out in absence of an emulsifier (PVA) or excess drug (PTX), which might interfere with intimate interactions between the coating and PLGA NP surface and be entrapped in the deposited TA layer. All NPs used in the rest experiments were prepared via the conventional method. 'PLGA-TA' should refer to NPs prepared using the conventional method, unless stated otherwise.

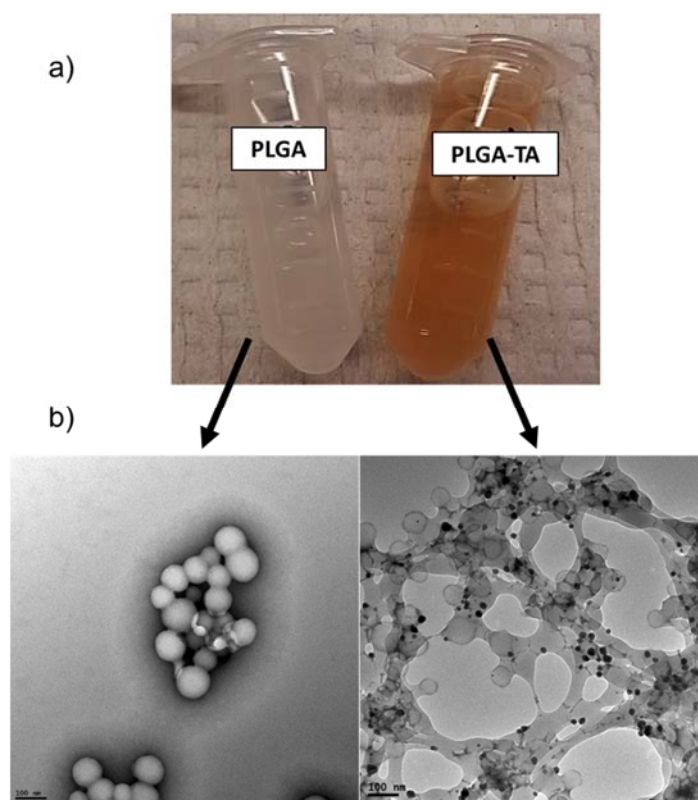


Figure 39: PLGA and PLGA-TA NPs (conventional method) post incubation in AgNO_3 aqueous solution (17 mg/mL) overnight. TA presence is indicated by the darkening of NP suspension due to reduction of AgNO_3 and deposition of metallic Ag (a). When visualized using TEM (1% PTA negative stain) (b), electron dense Ag can be seen depositing on PLGA-TA NP surface, but not on PLGA NPs.

5.3.2 Quantification of TA Coating

The TA content in NP-TA was quantified by BCA assay. TA reacts linearly with BCA working reagent resulting in characteristic formation of a colored complex (Marino et al., 2009) (**Fig. 40a**). The direct or indirect methods showed consistent results, with an average of $2.84\% \pm 0.25$ and $3.2\% \pm 0.6$, respectively (**Fig. 40b and c**).

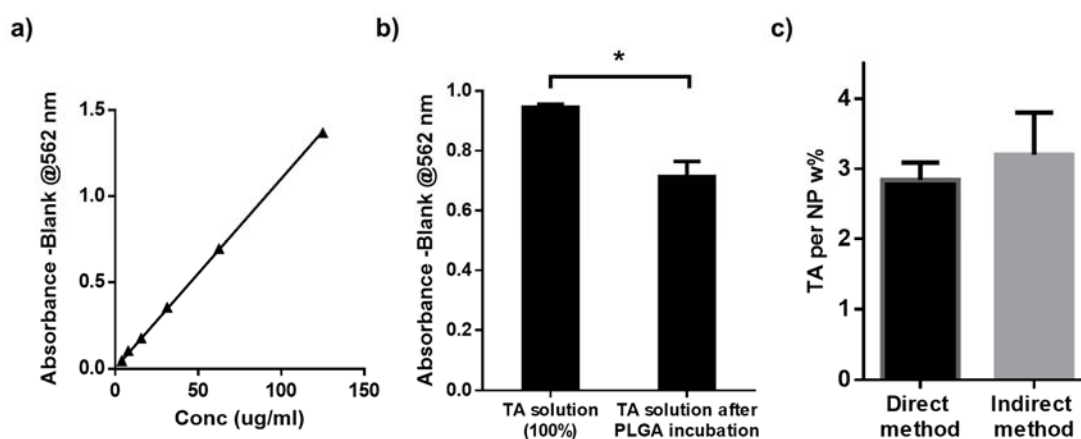


Figure 40: Quantification of TA using BCA assay. (a) Calibration curve of TA in bicine buffer (pH 7.4, 0.1 M), (b) Consumption of TA in solution by PLGA coating. Decrease in absorbance post incubation of PLGA NPs for 3 hours in comparison to control (100% TA incubated for 3 hours in absence of NPs) was used to indirectly quantify amount of TA in PLGA-TA NPs, (c) TA weight% per NP as determined by both direct and indirect methods (average \pm SD, Two-tailed T-test, * $p < 0.05$).

5.3.3 Functionalization of PLGA-TA NPs

The functionalization potential of TA as a NP coating was evaluated in comparison with pD. Fluoresceinamine (FA) (**Fig. 41a**) was chosen as a small ligand and could be easily detect via fluorescence (Duarte & da Silva, 2010). FA was readily conjugated to pD-coated NPs due to the amine group (Park et al., 2014). TA was as efficient as pD in

conjugating FA to PLGA NPs, with an average of 2.2 (TA) and 1.7 $\mu\text{g}/\text{mg}$ NPs (pD), respectively (**Fig. 41b**).

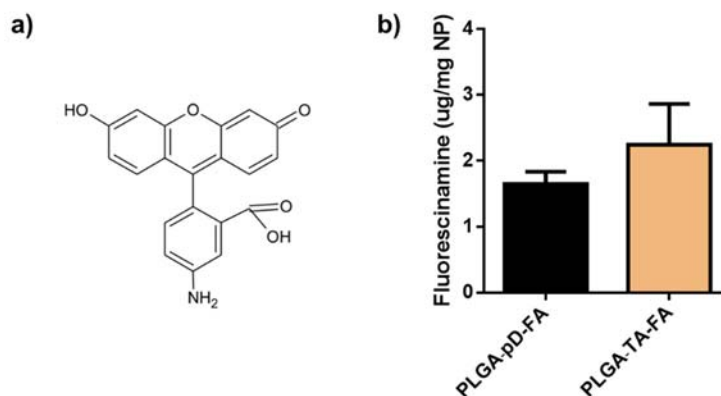


Figure 41: FA was conjugated to PLGA-pD and PLGA-TA NPs. FA is a small molecule with a free amine group (a) (Adapted from Durate et al, 2015). Amount of FA conjugated to the surface in PLGA-pD-FA and PLGA-TA-FA NPs after NPs incubation in 15 $\mu\text{g}/\text{mL}$ solution of FA (b) (average \pm SD).

Successful conjugation of FA indicated the potential of TA as a coating material for NPs. This potential was further evaluated with a large protein molecule such as albumin, a \sim 67 kDa serum protein with an isoelectric point of pH 4.7 (**Fig. 42a**) (Abou-Zied et al., 2013; Vlasova & Saletsky, 2009), which has been popularly used as a NP coating material (Peng et al., 2015; Peng et al., 2013). Albumin coating was achieved by incubation of PLGA-TA NPs with human serum albumin solution (5 mg/mL) at 2 mg/mL NP concentration for three hours. From the particle size and zeta potential analysis, PLGA-TA-Al NPs had less negative charge than that of original PLGA-TA NPs (**Fig. 42c**) but maintained a similar particle size (**Fig. 42b**). The decrease of negative charge could be explained by masking of TA layer with albumin.

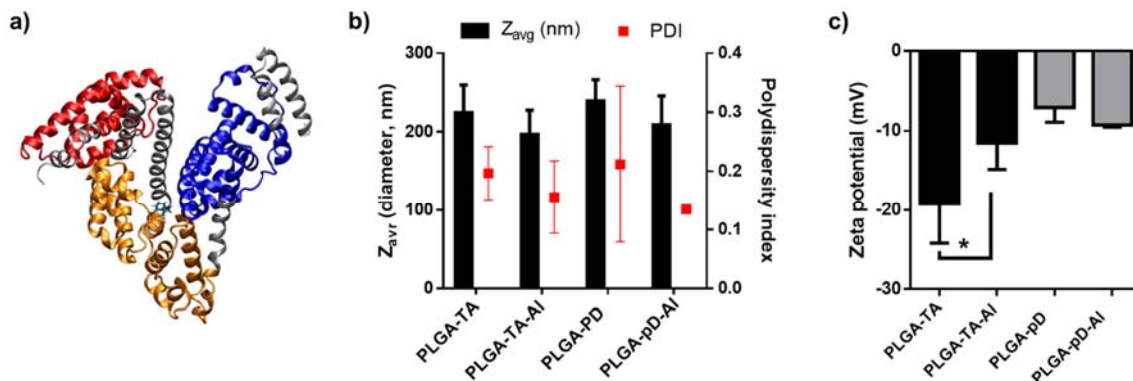


Figure 42: The functionalization of PLGA-TA NPs with human serum albumin: (a) The 3D structure of human serum albumin (Adapted from Abou-Zeid et al, 2013), (b) The particle size and polydispersity of PLGA-TA and PLGA-TA-AI NPs, (c) Zeta potential of the same NPs measured in phosphate buffer (pH 7.4) (average \pm SD, $n=3-6$, Two-tailed T-test, $*p<0.05$).

the CBQCA protein fluorescence assay (Thermo Scientific). PLGA-TA-AI NPs had $\sim 1.12\%$ albumin per NP weight (**Fig. 43**). In contrast, control PLGA-AI, where albumin was physically adsorbed to the PLGA NPs in the same conditions, had $\sim 0.39\%$ albumin per NP weight, significantly less than that conjugated on PLGA-TA-AI NPs.

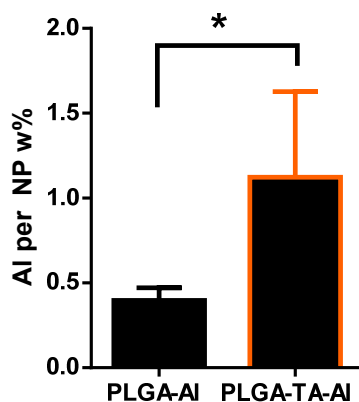


Figure 43: Albumin content of PLGA-AI and PLGA-TA-AI represented as Albumin per NP w%. PLGA-TA-AI (average \pm SD, $n=5-8$, Two-tailed T-test, $*p<0.05$).

When visualized using TEM after negative staining with 2% uranyl acetate solution, PLGA-TA-Al NPs showed a thin coating layer on the surface (**Fig. 44**), which appeared to be the combination of TA and albumin.

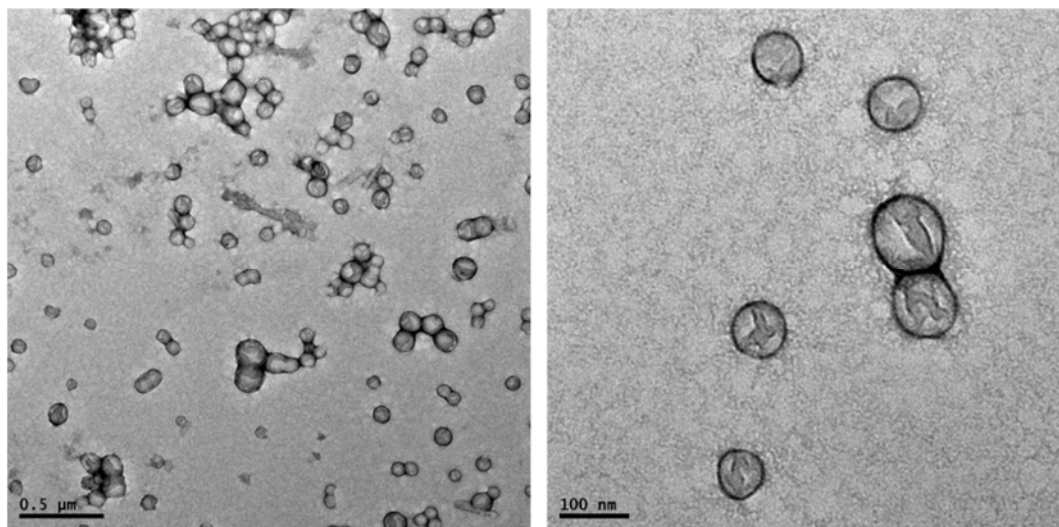


Figure 44: Transmission electron microscopy (TEM) images of PLGA-TA-Al NPs negatively stained with 2% uranyl acetate at low and high magnification levels (left and right images, respectively).

5.3.4 Cytotoxicity of PLGA-TA NPs

Finally, in order to establish TA as a coating material for NPs delivered systemically, it should not exert any cytotoxic effect. When PLGA-TA NPs (PTX free), were incubated with NIH/3T3 fibroblasts for 72 hours, no cytotoxic effect was observed in comparison with uncoated PLGA NPs, at concentrations as high as 0.1 mg/mL (**Fig. 45**).

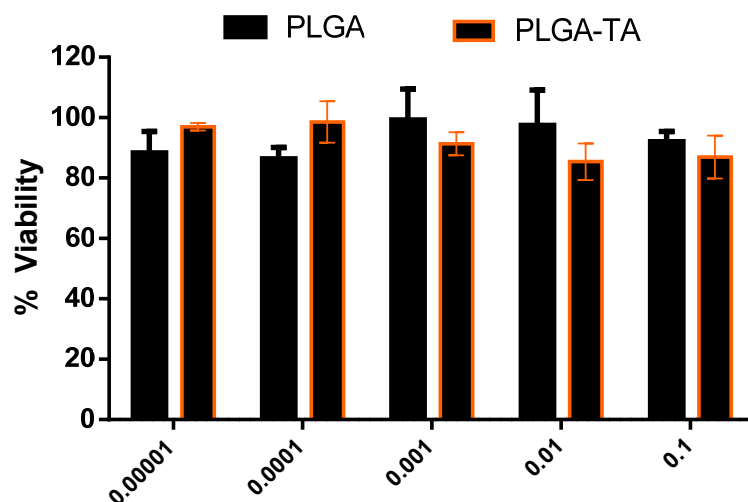


Figure 45: Viability of NIH/3T3 fibroblasts after incubation with different concentrations (mg/mL) of PTX-free PLGA-TA or PLGA NPs for 72 hours as determined with MTT assay.

5.4 Discussion

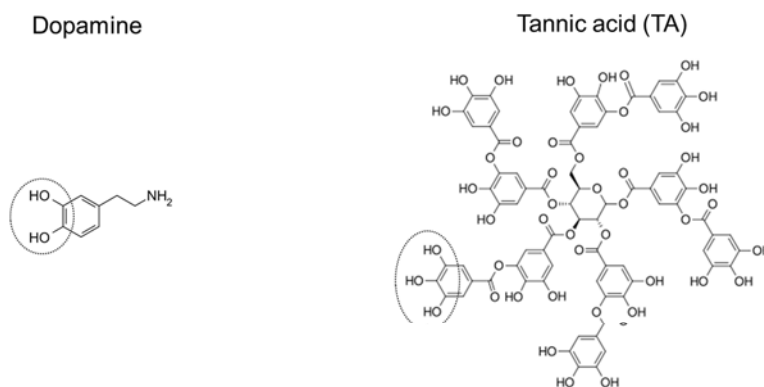
Surface properties of NPs determines their cellular interaction *in vivo* and dictates their biodistribution (Blanco et al., 2015). Therefore, controlling NP surface chemistry and properties is of great importance in the development of NPs as a drug carrier. The pD coating simplified the process of surface functionalization of polymeric nanocarriers, enabling manipulation of surface charge and cellular interactions (Abouelmagd et al., 2015; Park et al., 2014), yet with limitations identified earlier. The introduction of polyphenolic coatings as a new class of multifunctional coatings can overcome pD limitations and expand the scope of conjugated molecules as well as coated substrates. Previously discussed properties of TA and dopamine (and their corresponding coatings) are shown in **Figure 46**.

In this preliminary study, the use of TA as a coating material for PLGA NPs was investigated. Incubating PLGA NPs in low concentration of TA (0.07 mg/mL) was enough to coat NPs with TA. Two methods were attempted to prepare PLGA-TA NPs, conventional (PLGA NP purification, followed by coating) and one-pot (PLGA NP form

in TA containing medium). Although both methods formed TA-coated NPs (As indicated by NP surface charge, **Fig. 38b**), one-pot method was excluded due to the potential interference of the emulsifier. PLGA-TA NPs prepared by the conventional method had ~3% TA content per NP weight (**Fig.40**), reflected by significant increase in negative charge of the NPs and deposition of metallic Ag after incubation in AgNO₃ solution (**Fig. 39**).

The functionalization efficiency with TA was tested using two different surface ligands: FA, a small molecular weight fluorescent dye with an amine terminus, and human serum albumin, a large 67 kDa globular protein. TA successfully mediated FA conjugation to NP surface, in a similar level as pD coating (**Fig. 41**). Similarly, TA mediated surface functionalization with albumin. PLGA-TA-Al NPs had ~1.12% albumin per NP weight (**Fig. 43**), showing a decrease of the noticeably negative charge of PLGA-TA NPs (**Fig. 42c**). The interaction of TA with proteins in general, and albumin in particular, is inherent to the nature of TA as a tannin compound. Tannins are plant products long known to precipitate proteins, and therefore responsible for the astringent taste of some plant products (Soares et al., 2007). Soares et al. studied the interaction of TA, among other phenolic compounds, with bovine serum albumin. TA was shown to have the highest quenching effect on the fluorescence of albumin in solution indicating significant changes in the environment of tryptophan residues of the protein. Nevertheless, there was no blue or red shifts were observed in the fluorescence spectrum, indicating that the change in tryptophan fluorescence was not due to protein unfolding or burial (no change in protein conformation) but rather to the presence of TA in proximity (Soares et al., 2007). High molecular weight of TA and presence of repeating gallic acid units is believed to be responsible for this strong interaction with proteins mediated by hydrophobic and hydrogen bonding, as compared to other phenolic compounds, such as gallic acid and ellagic acid (Labieniec & Gabryelak, 2006; Soares et al., 2007).

This strong interaction of TA with proteins, specifically albumin was repeatedly reported in the literature (Labieniec & Gabryelak, 2006). In another study, TA was shown to react with amine-functionalized silica NPs and form stable covalent bonds, suggesting that TA molecules could also interact via covalent conjugation (Wang et al., 2010). However, it is important to consider that specific interactions of TA with albumin in solution could be different in nature from that of TA polymerized and immobilized on NPs, where TA is not mobile enough to interact with amino acids within certain pockets in the 3D structure of the protein.



Molecular weight (g/mol)	189.6	1701.19
Terminal amine	√	-
Polymerization pH	8.5 ¹	7-7.8 ²
Polymerized coating color	Dark grey	Colorless
Coating interference with optical substrate properties	√	-

Figure 46: Comparison of chemical and physical properties of different precursors (dopamine and TA), and the polymerized coatings they form. Circles in top panel point to catechol and trihydroxyphenyl groups of dopamine and TA. References: ¹ = (Park et al, 2014), ² = (Barette et al, 2014).

5.5 Conclusion

In summary, this preliminary study shows that TA can be used as an alternative coating to pD for functionalizing PLGA NPs with small ligands (FA) or macromolecules (albumin). Given the strong interactions of TA with different macromolecules (e.g.

proteins and nucleic acids), TA is expected to be an ideal coating material to functionalize NPs for drug delivery applications. However, further investigation is needed to optimize the conditions for stable conjugation of these macromolecules and to test the stability of coated NPs under physiologically relevant conditions.

5.6 References

- Abou-Zied, O. K., Al-Lawatia, N., Elstner, M., & Steinbrecher, T. B. (2013). "Binding of hydroxyquinoline probes to human serum albumin: combining molecular modeling and Forster's resonance energy transfer spectroscopy to understand flexible ligand binding." *J Phys Chem B* 117(4): 1062-1074.
- Abouelmagd, S. A., Ku, Y. J., & Yeo, Y. (2015). "Low molecular weight chitosan-coated polymeric nanoparticles for sustained and pH-sensitive delivery of paclitaxel." *Journal of Drug Targeting* 23(7-8): 725-735.
- Appel, H. M. (1993). "Phenolics in ecological interactions: The importance of oxidation." *J Chem Ecol* 19(7): 1521-1552.
- Barras, A., Lyskawa, J., Szunerits, S., Woisel, P., & Boulcherroub, R. (2011). "Direct Functionalization of Nanodiamond Particles Using Dopamine Derivatives." *Langmuir* 27(20): 12451-12457.
- Barrett, D. G., Sileika, T. S., & Messersmith, P. B. (2014). "Molecular diversity in phenolic and polyphenolic precursors of tannin-inspired nanocoatings." *Chem Commun (Camb)* 50(55): 7265-7268.
- Blanco, E., Shen, H., & Ferrari, M. (2015). "Principles of nanoparticle design for overcoming biological barriers to drug delivery." *Nat Biotechnol* 33(9): 941-951.
- Drynan, J. W., Clifford, M. N., Obuchowicz, J., & Kuhnert, N. (2010). "The chemistry of low molecular weight black tea polyphenols." *Nat Prod Rep* 27(3): 417-462.
- Duarte, A. J., & da Silva, J. C. G. E. (2010). "Reduced Fluoresceinamine as a Fluorescent Sensor for Nitric Oxide." *Sensors* 10(3): 1661-1669.
- Heijmen, F. H., duPont, J. S., Middelkoop, E., Kreis, R. W., & Hoekstra, M. J. (1997). "Cross-linking of dermal sheep collagen with tannic acid." *Biomaterials* 18(10): 749-754.
- Jackson, J. K., Zhao, J., Wong, W., & Burt, H. M. (2010). "The inhibition of collagenase induced degradation of collagen by the galloyl-containing polyphenols tannic acid, epigallocatechin gallate and epicatechin gallate." *J Mater Sci Mater Med* 21(5): 1435-1443.
- Kang, S. M., Rho, J., Choi, I. S., Messersmith, P. B., & Lee, H. (2009). "Norepinephrine: material-independent, multifunctional surface modification reagent." *Journal of the American Chemical Society* 131(37): 13224-13225.
- Kim, B. S., Lee, H. I., Min, Y., Poon, Z., & Hammond, P. T. (2009). "Hydrogen-bonded multilayer of pH-responsive polymeric micelles with tannic acid for surface drug delivery." *Chem Commun (Camb)*(28): 4194-4196.
- Kim, S., Gim, T., & Kang, S. M. (2015). "Versatile, tannic acid-mediated surface PEGylation for marine antifouling applications." *ACS Appl Mater Interfaces* 7(12): 6412-6416.
- Kozlovskaya, V., Kharlampieva, E., Drachuk, I., Cheng, D., & Tsukruk, V. V. (2010). "Responsive microcapsule reactors based on hydrogen-bonded tannic acid layer-by-layer assemblies." *Soft Matter* 6(15): 3596-3608.

- Labieniec, M., & Gabryelak, T. (2006). "Interactions of tannic acid and its derivatives (ellagic and gallic acid) with calf thymus DNA and bovine serum albumin using spectroscopic method." *J Photochem Photobiol B* 82(1): 72-78.
- Lomova, M. V., Brichkina, A. I., Kiryukhin, M. V., Vasina, E. N., Pavlov, A. M., Gorin, D. A., Sukhorukov, G. B., & Antipina, M. N. (2015). "Multilayer Capsules of Bovine Serum Albumin and Tannic Acid for Controlled Release by Enzymatic Degradation." *ACS Appl Mater Interfaces* 7(22): 11732-11740.
- Lynge, M. E., van der Westen, R., Postma, A., & Stadler, B. (2011). "Polydopamine--a nature-inspired polymer coating for biomedical science." *Nanoscale* 3(12): 4916-4928.
- Marino, D. C., Sabino, L. Z. L., Armando, J., Ruggiero, A. D., & Moya, H. D. (2009). "Analysis of the Polyphenols Content in Medicinal Plants Based on the Reduction of Cu(II)/Bicinchoninic Complexes." *Journal of Agricultural and Food Chemistry* 57(23): 11061-11066.
- Natarajan, V., Krithica, N., Madhan, B., & Sehgal, P. K. (2013). "Preparation and properties of tannic acid cross-linked collagen scaffold and its application in wound healing." *J Biomed Mater Res B Appl Biomater* 101(4): 560-567.
- Park, J., Brust, T. F., Lee, H. J., Lee, S. C., Watts, V. J., & Yeo, Y. (2014). "Polydopamine-based simple and versatile surface modification of polymeric nano drug carriers." *Acs Nano* 8(4): 3347-3356.
- Peng, Q., Wei, X. Q., Yang, Q., Zhang, S., Zhang, T., Shao, X. R., Cai, X. X., Zhang, Z. R., & Lin, Y. F. (2015). "Enhanced biostability of nanoparticle-based drug delivery systems by albumin corona." *Nanomedicine* 10(2): 205-214.
- Peng, Q., Zhang, S., Yang, Q., Zhang, T., Wei, X. Q., Jiang, L., Zhang, C. L., Chen, Q. M., Zhang, Z. R., & Lin, Y. F. (2013). "Preformed albumin corona, a protective coating for nanoparticles based drug delivery system." *Biomaterials* 34(33): 8521-8530.
- Shin, M., Ryu, J. H., Park, J. P., Kim, K., Yang, J. W., & Lee, H. (2015). "DNA/Tannic Acid Hybrid Gel Exhibiting Biodegradability, Extensibility, Tissue Adhesiveness, and Hemostatic Ability." *Advanced Functional Materials* 25(8): 1270-1278.
- Shutava, T. G., & Lvov, Y. M. (2006). "Nano-engineered microcapsules of tannic acid and chitosan for protein encapsulation." *J Nanosci Nanotechnol* 6(6): 1655-1661.
- Sileika, T. S., Barrett, D. G., Zhang, R., Lau, K. H. A., & Messersmith, P. B. (2013). "Colorless Multifunctional Coatings Inspired by Polyphenols Found in Tea, Chocolate, and Wine." *Angewandte Chemie-International Edition* 52(41): 10766-10770.
- Soares, S., Mateus, N., & Freitas, V. (2007). "Interaction of different polyphenols with bovine serum albumin (BSA) and human salivary alpha-amylase (HSA) by fluorescence quenching." *J Agric Food Chem* 55(16): 6726-6735.
- Vlasova, I. M., & Saletsky, A. M. (2009). "Study of the Denaturation of Human Serum Albumin by Sodium Dodecyl Sulfate Using the Intrinsic Fluorescence of Albumin." *Journal of Applied Spectroscopy* 76(4): 536-541.
- Wang, J. H., Zheng, S. R., Liu, J. L., & Xu, Z. Y. (2010). "Tannic acid adsorption on amino-functionalized magnetic mesoporous silica." *Chemical Engineering Journal* 165(1): 10-16.

APPENDIX

Statistical analysis was performed using SAS software (v. 9.4, NC, USA).

Logarithm of tumor volume change (fold) was analyzed over time using a mixed model based on variance being significantly different among treatments and mice.

Applied codes:

```
proc mixed data = sample;
class animalID trt;
model logy = trt day trt*day/solution;
random animalID;
```

Where 'animalID' indicates individual mice of each group, 'y' is fold tumor volume change, 'trt' represent treatment group (PBS, Abraxane,..etc)

By analyzing significant change in slope of tumor growth curve, with 'day' and 'trt' being variables, following results were obtained (significance at 'Pr > |t|' <0.05):

LS174-T					
Label	Estimate	Standard Error	DF	t Value	Pr > t
compare the slope: Abraxane vs PBS	0.02158	0.008115	203	2.66	0.0085
compare the slope: LMWC vs PBS	0.01991	0.008134	203	2.45	0.0152
compare the slope: PEG vs PBS	0.02190	0.008111	203	2.70	0.0075
compare the slope: Taxol vs PBS	0.03436	0.007526	203	4.57	<.0001
compare the slope: LMWC vs PEG	0.001986	0.006671	203	0.30	0.7662
MCF-7					
Label	Estimate	Standard Error	DF	t Value	Pr > t
compare the slope: Abraxane vs PBS	0.01769	0.004795	163	3.69	0.0003
compare the slope: LMWC vs PBS	0.004533	0.005146	163	0.88	0.3797
compare the slope: PEG vs PBS	0.01931	0.004795	163	4.03	<.0001
compare the slope: LMWC vs PEG	0.01478	0.005146	163	2.87	0.0046

VITA

VITA

Sara Ahmed grew up in Assiut, Egypt. In 2008, she obtained her Bachelor degree in Pharmaceutical Sciences, ranking first on class, from the Faculty of Pharmacy, Assiut University. After which, she was awarded a position in Pharmaceutics Department in the same Faculty, where she worked as a teaching and research assistant for three years, through which she worked closely with undergraduate students, and carried out research in the area of drug delivery.

In 2011, Sara was awarded a full PhD scholarship from the Egyptian Government, and in January 2012, she joined Dr. Yoon Yeo's lab in Industrial and Physical Pharmacy Department, College of Pharmacy, Purdue University. Throughout her PhD study, she worked on developing nanocarriers for tumor drug delivery. With completion of her PhD, Sara intends to pursue her academic career in Egypt, accepting a Lecturer position in the Pharmaceutics Department, Faculty of Pharmacy, Assiut University.

PUBLICATIONS

ORIGINAL ARTICLE

Low molecular weight chitosan-coated polymeric nanoparticles for sustained and pH-sensitive delivery of paclitaxel

Sara A. Abouelmagd^{1,2}, Youn Jin Ku¹, and Yoon Yeo^{1,3}

¹Department of Industrial and Physical Pharmacy, Purdue University, West Lafayette, IN, USA, ²Department of Pharmaceutics, Faculty of Pharmacy, Assiut University, Assiut, Egypt, and ³Weldon School of Biomedical Engineering, Purdue University, West Lafayette, IN, USA

Abstract

Low molecular weight chitosan (LMWC) is a promising polymer for surface modification of nanoparticles (NPs), which can impart both stealth effect and electrostatic interaction with cells at mildly acidic pH of tumors. We previously produced LMWC-coated NPs via covalent conjugation to poly(lactic-co-glycolic) acid (PLGA-LMWC NPs). However, this method had several weaknesses including inefficiency and complexity of the production as well as increased hydrophilicity of the polymer matrix, which led to poor drug release control. Here, we used the dopamine polymerization method to produce LMWC-coated NPs (PLGA-pD-LMWC NPs), where the core NPs were prepared with PLGA that served best to load and retain drugs and then functionalized with LMWC via polydopamine layer. The PLGA-pD-LMWC NPs overcame the limitations of PLGA-LMWC NPs while maintaining their advantages. First of all, PLGA-pD-LMWC NPs attenuated the release of paclitaxel to a greater extent than PLGA-LMWC NPs. Moreover, PLGA-pD-LMWC NPs had a pH-dependent surface charge profile and cellular interactions similar to PLGA-LMWC NPs, enabling acid-specific NP-cell interaction and enhanced drug delivery to cells in weakly acidic environment. Although the LMWC layer did not completely prevent protein binding in serum solution, PLGA-pD-LMWC NPs showed less phagocytic uptake than bare PLGANPs.

Keywords

Dopamine polymerization, drug delivery, low molecular weight chitosan, nanoparticles, pH-sensitive, sustained release

History

Received 11 April 2015
Revised 20 May 2015
Accepted 21 May 2015
Published online 5 October 2015

Introduction

Delivering drugs specifically to tumors remains a major challenge in chemotherapy. Once administered intravenously, chemotherapeutic agents spread to the whole body, causing adverse effects to healthy tissues [1]. Polymeric nanoparticles (NPs) have been developed for improving tumor-specificity of drug delivery. The popularity of NPs is mainly attributable to the so-called 'enhanced permeability and retention (EPR) effect' based on the leaky vasculature and impaired lymphatic drainage of tumors, which provides a selective advantage for small particles in accessing tumors compared with free drugs [2-4]. To take advantage of the EPR effect, NPs should be able to circulate avoiding immune surveillance, until they reach tumors. Upon arrival at target tumors, NPs should be stably retained in the tissues and/or taken up by cancer cells to release the loaded drug. Traditionally, NPs are coated with hydrophilic neutral polymers such as polyethylene glycol (PEG), which sterically stabilizes the NPs and delays adsorption of plasma proteins to the surface [5,6], to achieve long-term circulation. However, the PEG surface can also

limit cellular interactions with target cells and cellular internalization, creating a 'PEG dilemma' [7,8].

For overcoming the dilemma, we previously proposed a low molecular weight chitosan (LMWC) as an alternative surface layer [9]. Chitosan is a linear polyaminosaccharide with a p*K*_a value close to 6.5, which helps establish electrostatic interactions with negatively charged cell membrane in weakly acidic microenvironment of tumors (pH 6.8-7.2) [10]. At neutral pH, chitosan coated on polymeric NPs protects them from phagocytic uptake [11] and prolongs their circulation time [12]. By reducing the MW to 56.5 kDa, we intended to increase hydrophilicity of the polymer and reduce pH-independent interactions with cells mediated by polymer chain entanglement, further improving its protective effect at neutral pH [9]. We obtained the proof of concept in the previous study, using NPs produced with poly(lactic-co-glycolic) acid (PLGA) covalently conjugated to LMWC via an amide bond (PLGA-LMWC) [9]. The PLGA-LMWC NPs, consisting of PLGA core and LMWC surface, showed a pH-sensitive surface charge profile, which translated to NP-cell interactions at weakly acidic pH with reduced phagocytic uptake and little non-specific NP-cell interactions at neutral pH [9].

However, the covalent conjugation of LMWC to PLGA had several drawbacks. First, the chemical conjugation procedure is lengthy and inefficient and requires reactive

Address for correspondence: Yoon Yeo, PhD, Department of Industrial and Physical Pharmacy, Purdue University, 575 Stadium Mall Drive, West Lafayette, IN 47907, USA. Tel: +1 765 496 9608. Fax: +1 765 494 6545. E-mail: yyeo@purdue.edu

reagents and catalysts that need to be completely removed after the reaction. Moreover, the conjugation process reduces the potential of NPs as a drug carrier. LMWC conjugation requires a sufficient number of carboxyl termini, which necessitates the use of a low molecular weight PLGA (4 kDa, PLGA₄). This polymer is relatively hydrophilic and, thus, has an inherent limitation in encapsulating hydrophobic drugs. Covalent conjugation of LMWC makes the product even more hydrophilic, further compromising the ability of the formed NPs to load and retain a drug. Prolonged reaction in basic pH also accelerates degradation of the polymer and aggravates the problem. Consequently, PTX-loaded PLGA₄-LMWC NPs showed a rapid drug release in PBS with 0.1% Tween 80 in 24 h [9]. NPs showing high initial burst release are likely to release the drug in circulation and not contribute to improving tumor-specific drug delivery; therefore, these shortcomings should be overcome for the LMWC-coated NPs to make further contribution to chemotherapy.

In an attempt to overcome this challenge, we have employed a new surface modification method based on dopamine polymerization [13], which has been used to functionalize several nanostructures including nanowires [14], carbon nanospheres [15], gold nanoclusters [16] and gold nanorods [17], and validated that the new method can effectively functionalize polymeric NPs with different types of ligands [18,19]. The dopamine polymerization method depends on oxidation of dopamine catechol, followed by the formation of polydopamine (pD) layer on the NP surface, where functional ligands with amine or thiol are covalently conjugated. This method can be implemented in mild conditions such as brief exposure to pH 8.5, UV light [20] or oxidants [21], does not require reactive reagents or lengthy reaction, and can be applied to a broad range of surface modifiers and NP platforms [13,18]. Once dopamine polymerizes, it loses its dopaminergic activity [18], and the resulting pD is biodegradable and biocompatible with a LD₅₀ of 483.95 mg/kg in mice after intravenous injection [22].

In this study, we use the dopamine polymerization method to produce LMWC-coated NPs (Figure 1) based on the flexibility in controlling drug release. Here, LMWC

molecules are incorporated into the pD layer on PLGA NPs via multiple amine groups. Since LMWC is introduced as an addendum to pre-formed NPs via the pD layer, the core NPs can be prepared with polymers that serve best to load and retain drugs, not constrained by the needs for carboxyl termini or the hydrophilicity of the modified polymer. We demonstrate that PLGA NPs modified with LMWC via dopamine polymerization method overcome the previously observed limitations of PLGA₄-LMWC NPs and show the desired pH-sensitivity in cell interaction and drug delivery and the tendency to avoid phagocytic uptake, similar to PLGA₄-LMWC NPs. We also investigate NP-cell interactions at acidic pH and their intracellular trafficking and discuss their implications in drug delivery to tumor tissues.

Material and methods

Materials

Chitosan (90–150 kDa) was purchased from Sigma-Aldrich (St. Louis, MO). PLGA (acid end cap, 4 kDa, LA:GA ¼ 50:50, PLGA₄) was purchased from Durect Corp (Birmingham, AL). PLGA (118 kDa, LA:GA ¼ 65:35, PLGA₁₁₈) was purchased from Lakeshore Biomaterials (Birmingham, AL). PLGA (150 kDa, LA:GA ¼ 85:15, PLGA₁₅₀) and fluorescein-conjugated PLGA (7 kDa, LA:GA ¼ 50:50, *PLGA) were purchased from Akina Inc. (West Lafayette, IN). Paclitaxel (PTX) was a gift from Samyang Genex Corp (Seoul, Korea). LysoTracker Red DND-99, CellMask Deep Red plasma membrane stain and Hoechst 33342 were purchased from Life Technologies (Carlsbad, CA). Methoxy PEG amine, HCl salt (5 kDa, mPEG-NH₂) was purchased from JenKem Technology USA (Plano, TX). Dopamine hydrochloride was purchased from Alfa Aesar (Ward Hill, MA). Coomassie Brilliant blue G-250 protein stain and sodium dodecyl sulfate-acrylamide gel electrophoresis (SDS-PAGE) molecular weight standards were purchased from Bio-Rad (Berkeley, CA).

Preparation and characterization of LMWC

LMWC was prepared as previously described [9]. Briefly, 25 mg/mL of chitosan solution was incubated in 33% hydrogen peroxide for 3.5 h, dialyzed against water with a molecular weight cut-off (MWCO) of 3500 Da, and freeze-dried. The molecular weight of LMWC was estimated by matrix-assisted laser desorption ionization time-of-flight/ time-of-flight (MALDI-TOF/TOF) analysis and analytical ultracentrifugation (AUC). For mass spectrometry, 1 mg/mL LMWC solution was prepared in acidified water (pH 5), filtered with a 0.2 mm syringe filter, and mixed with a matrix (sinapinic acid solution in acetonitrile/water (50:50) containing 0.1% trifluoroacetic acid) in 1:1 ratio. Mass analysis was performed with a 4800 MALDI TOF/TOF instrument (Applied Biosystems, Foster City, CA) in 2000–8000 *m/z* range. For AUC, LMWC solution in sodium acetate buffer (pH 4.3, 10 mM) was prepared in 1, 0.5 and 0.25 mg/mL and analyzed with a Beckman Optima XL-I ultracentrifuge (Beckman Coulter Inc., Brea, CA). The sedimentation coefficients and apparent molecular weights were calculated from size distribution analysis with SEDFIT version 12.0.

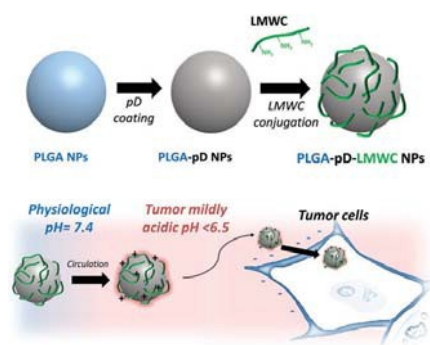


Figure 1. Schematic diagram of PLGA-pD-LMWC NPs preparation and pH-dependent NP-cell interaction.

DOI: 10.3109/1061186X.2015.1054829

LMWC-coated polymeric NPs 727

(National Institute of Health, Bethesda, MD). The pH dependence of water solubility of LMWC was estimated by measuring the transmittance of LMWC solution (0.5 mg/mL) varying the pH from 2.5 to 10 with NaOH. The percentage transmittance (%T) was calculated as $10^{-A} \times 100$, where A was the absorbance of the solution at 500 nm.

Preparation of particles

PLGA₄-LMWC NPs

A covalent conjugate PLGA₄-LMWC was prepared as described previously [9]. Briefly, 200 mg of LMWC was dissolved in acidified water (20 mL, pH 5) and added to 40 mL of dimethyl sulfoxide (DMSO). Five hundred milligrams of PLGA₄ was dissolved in 2 mL of dichloromethane (DCM), to which hydroxybenzotriazole (HOBT; 74.3 mg), 1-ethyl-3-(3-dimethylaminopropyl) carbodiimide (EDC; 106.2 mL) and tetramethylethylenediamine (TEMED; 269.9 mL) were sequentially added. The activated PLGA₄ was added to LMWC solution dropwise and stirred overnight. The formed conjugate, PLGA₄-LMWC, was purified by dialysis (MWCO: 3500 Da) against a mixture of DMSO and water (50:50) and then water, freeze-dried and stored at -20 °C.

PLGA₄-LMWC NPs were prepared using the single emulsion solvent evaporation method. Twenty milligrams of PLGA₄-LMWC were dissolved in a mixture of 0.5 mL DMSO, 0.5 mL DCM and 0.1 mL water, optionally with 1.2 mg of paclitaxel (PTX). The organic phase was emulsified in 5 mL of aqueous phase containing 5% polyvinyl alcohol (PVA) using a Vibra-Cell probe sonicator (Sonics, Newtown, CT) at 80% amplitude with a 4-s on and 2-s off pulse mode. The emulsion was dispersed in 10 mL of deionized water and stirred for 3 h to evaporate DCM. NPs were collected via centrifugation at 10 000 rpm for 30 min and washed thrice. Fluorescently labeled PLGA₄-LMWC NPs (*PLGA₄-LMWC NPs) were prepared by replacing 25% of polymer with *PLGA.

PLGA-pD-LMWC and PLGA-pD-PEG particles

PLGA-pD-LMWC NPs were prepared by coating pre-formed particles with LMWC via the dopamine polymerization method [18]. First, the core NPs were prepared with PLGA polymers with different molecular weights and LA:GA ratios (PLGA₁₁₈: 118 kD, LA:GA ¼ 65:35 and PLGA₁₅₀: 150 kD, LA:GA ¼ 85:15) by the single emulsion solvent evaporation method as described in the 'PLGA₄-LMWC NPs' section. PLGA microparticles (MPs) were prepared in a similar way except that the emulsification process was performed with a Silverson L4R Laboratory Mixer (East Longmeadow, MA) for 1 min at 5000 rpm. The core particles were then prime-coated with polymerized dopamine (pD) by incubation in 1 mg/mL dopamine solution in Tris buffer (pH 8.5, 10 mM) for 3 h at room temperature. The pD-coated particles were collected by centrifugation, washed twice and incubated with LMWC aqueous solution (pH 7.5, 0.5 mg/mL) for 40 min to produce PLGA-pD-LMWC particles. For comparison, PEG-modified (PLGA-pD-PEG) particles were created by incubating the pD-coated particles in mPEG-NH₂ solution (pH 8.5, 2 mg/mL). The particles were collected by centrifugation

and washed twice to remove excess LMWC or mPEG-NH₂. Throughout this study, PLGA particles refer to PLGA₁₅₀ particles unless stated otherwise.

Particle characterization

Particle size and zeta potential of particles were determined using a Malvern Zetasizer Nano ZS90 (Worcestershire, UK). The size was measured with particles dispersed in phosphate buffer (2.2 mM, pH 7.4). The zeta potential was determined at different pHs with particles dispersed in phosphate buffer (2.2 mM, pH 7.4) or MES buffer (5 mM, pH 6.2). Particle morphology was observed by transmission electron microscopy (TEM). An aqueous suspension of freshly prepared NPs (0.5 - 1 mg/mL) was spotted on a formvar-coated carbon grid (400 mesh) and negatively stained with 2% uranyl acetate solution. The grid was air-dried and examined with a FEI Tecnai T20 transmission electron microscope (FEI, Hillsboro, OR).

The LMWC content in PLGA-pD-LMWC NPs was quantified by the ninhydrin assay. The ninhydrin reagent was prepared by dissolving ninhydrin and hydrindantin in lithium acetate buffer [9,23]. 0.5 mg of freeze-dried NPs were dispersed in 0.5 mL water and combined with 0.5 mL of fresh reagent. The mixture was heated in boiling water for 30 min, then cooled and quenched with 15 mL of 50% ethanol solution. The absorbance of the solution was read at 570 nm using SpectraMax M3 microplate reader (Molecular Device, Sunnyvale, CA). The amount of LMWC per NP sample was calculated after subtracting the background absorbance of PLGA-pD NPs, using a calibration curve drawn with LMWC solutions of known concentrations.

In vitro PTX release kinetics from PLGA₄-LMWC and PLGA-pD-LMWC NPs

To determine PTX loading in NPs, freeze-dried NPs were accurately weighed and dissolved in 0.5 mL acetonitrile. After precipitating polymer with the addition of 0.5 mL deionized water, the sample was centrifuged, and the supernatant analyzed via high pressure liquid chromatography (HPLC). The drug loading in NPs (DL%) was calculated as the amount of PTX per NP mass. For *in vitro* release studies, NP equivalent to 8.75 mg PTX were dispersed in 1 mL of phosphate-buffered saline (PBS, pH 7.4) containing 0.2% Tween 80 and shaken at 37 °C. At regular time points, NP suspension was centrifuged at 12 000 rpm for 15 min, 0.8 mL of supernatant was sampled and replaced with 0.8 mL of fresh buffer, and the pellet was resuspended and returned for continued incubation. The sampled supernatant was filtered with a 0.45 mm syringe filter and analyzed by HPLC. HPLC analysis was performed with an Agilent 1100 HPLC system (Palo Alto, CA), equipped with Ascentis C18 column (25 cm x 4.6 mm, particle size 5 mm). The mobile phase was a 50:50 mixture of water and acetonitrile run at a flow rate of 1 mL/min. PTX was detected by a UV detector (227 nm).

Protein adsorption to NP surface

Nanoparticles (NPs) were incubated with 50% fetal bovine serum (FBS) in PBS at 37 °C with shaking for 1 or 24 h.

NPs were collected by centrifugation at 13 200 rpm and washed thrice with water to remove excess and loosely bound proteins. To strip off hard corona proteins from NP surface, NPs were boiled in sample buffer containing 5-mercaptoethanol and 2% SDS for 5 min. The sample was analyzed with SDS-PAGE. The resolved protein bands were stained with Coomassie brilliant blue G-250. The molecular weight of a band of interest was determined using GelAnalyzer 2010a software (www.GelAnalyzer.com). Briefly, a calibration curve was constructed with a plot of the relative migration distance (R_i) of standard bands versus their MWs and used to determine the MW of resolved bands in each gel. The intensity of different bands was quantified using ImageJ 1.48v software densitometry analysis (National Institute of Health, Bethesda, MD).

NP-cell interactions

Cell culture

SKOV-3 human ovarian cancer cells (ATCC, Manassas, VA) were grown in RPMI-1640 medium containing 10% FBS, 100 U/mL of penicillin and 100 mg/mL of streptomycin. J774A.1 mouse macrophages (ATCC) were grown in DMEM medium supplemented with 10% FBS, 100 U/mL of penicillin and 100 mg/mL of streptomycin. All cell experiments were performed in the FBS-supplemented medium.

Quantitative analysis of cell-particle interactions

SKOV-3 cells and J774A.1 macrophages were seeded in 6-well plates at a density of 500 000 cells per well and incubated overnight. Next day, the medium was replaced with fresh medium that contained 0.1 mg/mL of fluorescently labeled NPs or MPs (*NPs or *MPs). For SKOV-3 cells the medium pH was adjusted to 6.2 or 7.4. After 3 h, cells were harvested by trypsinization (SKOV-3) or scraping (J774A.1), dispersed in fresh medium of corresponding pH and analyzed with a FC500 flow cytometer (Beckman Coulter, Indianapolis, IN). At least 10 000 gated events were acquired, and data was analyzed with the FlowJo software (Treestar, CA).

Visualization of cell-particle interactions

NP interaction with SKOV-3 cells was observed with confocal microscopy. SKOV-3 cells were seeded in a 35 mm glass bottomed dish (MatTek) at a density of 500 000 cells per dish. After overnight incubation, the medium was replaced with fresh RPMI medium adjusted to pH 6.2 or 7.4, which contained 0.1 mg/mL of *NPs. After 3 h of incubation, the medium was removed, and the cells were washed with fresh medium twice to remove free and loosely bound *NPs. Cells were incubated with Hoechst 33342 nuclear staining dye at 5 mg/mL for 10 minutes, and imaged with a Nikon-A1R confocal microscope (Nikon America Inc., Melville, NY). The *NPs were excited with a 488 nm laser, and the emission was read from 500 to 550 nm. The cell nuclei were excited with a 407 nm laser, and the emission was read from 425 to 475 nm.

To locate NPs in SKOV-3 cells, cells were further stained with CellMask Deep Red (Life Technologies) or LysoTracker Red DND-99 (Life Technologies) for labeling the plasma membrane or acidic intracellular organelles (late endosomes and lysosomes), respectively. Cells were incubated with *NPs in the same manner as above. After removing *NPs, CellMask Deep Red was added at 5 mg/mL or LysoTracker Red at 30 nM. Cells were incubated with each marker for 40 min, washed twice with fresh medium at corresponding pH, stained with Hoechst 33342, and imaged with a Nikon A1R confocal microscope. Stained plasma membrane was excited at 639 nm, and emission was collected from 663 to 738 nm. LysoTracker stained organelles were excited at 561 nm, and the emission was collected from 570 to 620 nm.

Time-lapse confocal microscopy was performed to examine the time course of cellular uptake and intracellular trafficking of *PLGA-pD-LMWC NPs. SKOV-3 cells were seeded in a glass bottomed dish at a density of 500 000 cells per dish. After overnight incubation, the medium was replaced with 1 mL of fresh medium adjusted to pH 6.2, and cells were stained with LysoTracker Red DND-99 and Hoechst 33342. The dish was put in an environmental chamber, supplied with 5% CO₂ and mounted on Nikon A1R confocal microscope. The chamber, microscope stage and objective lens were heated to 37 °C. *PLGA-pD-LMWC NPs (0.1 mg) was added to the dish, and the cells were imaged over 4.5 h.

Macrophage uptake of *MPs was visualized with fluorescence microscopy. J774A.1 macrophages were seeded in a 24-well plate at a density of 100 000 cells per well and incubated overnight. The medium was replaced with fresh one containing 0.1 mg/mL *MPs. After 3 h, the medium was removed, and cells were washed with fresh medium twice. The cells were stained with Hoechst 33342 and imaged with a Cytation-3 imaging system (BioTek, Winooski, VT).

Paclitaxel delivery to cancer cells by NPs

Cellular uptake of PTX delivered by NPs was estimated at different pHs. SKOV-3 were seeded at a density of 200 000 cells per well in a 12-well plate. Next day, the medium was replaced with 0.8 mL of fresh medium of pH 6 or 7.4, which contained PTX-loaded PLGA-pD-LMWC- or PLGA-pD-PEG NPs equivalent to 4.8 mg of PTX. Free PTX dissolved in DMSO solution was added at the same concentration to a control group. The total amount of DMSO added to 0.8 mL of medium was 12 mL and non-toxic to the cells. After 2.5 h at 37 °C, the medium was removed, and cells were trypsinized, suspended in fresh medium of corresponding pH and centrifuged at 2000 rpm to separate cells from NPs. The cell pellet was lysed by three freeze-thaw cycles, suspended in 0.5 mL PBS and probe sonicated. The cell lysate was spiked with 35 mg of carbamazepine as an internal standard, extracted with 1.5 mL of ethyl acetate for 40 min, and centrifuged at 4000 rpm for 25 min to separate ethyl acetate layer. A 1.3 mL of ethyl acetate was dried under vacuum in a glass tube and reconstituted with 1:1 acetonitrile/water solution and analyzed with HPLC. A PTX calibration curve was drawn with different amounts of PTX added to cell suspension in PBS and treated in the same way.

Results

Particle preparation and characterization

LMWC was produced by H_2O_2 digestion. Three and a half hour digestion in 33% H_2O_2 reduced the chitosan molecular weight from 90 - 150 to 4.8 kDa, consistent with our previous study [9]. The MALDI spectrum of LMWC showed a peak at m/z 4800 (Figure S1). The AUC analysis confirmed the result with additional insight into the structure. The global analysis of fitted data identified two species with apparent MWs of 2.5 and 7.3 kDa, existing in a dynamic mixture in solution. The frictional coefficient ratio (f_{f_2}/f_{f_1}) was 1.2, which indicated that LMWC had a semi-flexible rod shape, in agreement with existing studies [24]. LMWC was soluble in water over a wide range of pH including 7 - 9, where the parent chitosan was not soluble (Figure S2).

LMWC-coated NPs were produced with a polymer pre-conjugated with LMWC (PLGA₄-LMWC NPs) or by LMWC conjugation via pD to the pre-formed PLGA NPs (PLGA-pD-LMWC NPs). PLGA₄-LMWC NPs or pre-formed core PLGA NPs showed similar sizes, 160 and 158 nm, respectively (Figure 2a). LMWC or PEG-NH₂ coating via pD increased the size to 209 nm (Figure 2a). The size increase is likely due to the aggregation by additional centrifugation rather than the thickness of the conjugated layer, given that the polydispersity increased with coating (Figure 2a) and individual NPs observed with TEM showed similar sizes irrespective of the coating (Figure 3 and Figure S4). TEM of negatively stained NPs revealed thin layer of pD coating on the NP surface. However, no other difference was observed in NPs further conjugated with LMWC or PEG-NH₂.

Although the presence of LMWC or PEG conjugated to pD were not visually identified in TEM images, their immobilization was confirmed by the altered surface properties. PLGA-pD-LMWC NPs showed a characteristic pH-dependent charge profile, negative at pH 7.4 and positive at pH 6.2, similar to PLGA₄-LMWC NPs. PLGA, PLGA-pD and PLGA-pD-PEG NPs remained negatively charged irrespective of the pH (Figure 2b and Figure S3b). PLGA NPs incubated with LMWC without pD prime coating (PLGA/LMWC NPs) did not show the pH-dependent charge profile, indicating that LMWC did not physically adsorb to PLGA and the LMWC

immobilization depended on the pD layer. The LMWC content in PLGA-pD-LMWC NPs was determined to be $4.7 \pm 3\%$ according to the ninhydrin assay, lower than the estimated value for PLGA₄-LMWC NPs ($8.7 \pm 1.5\%$) [9].

In vitro PTX release kinetics from NPs

PLGA₄-LMWC NPs and PLGA-pD-LMWC NPs were compared with respect to the DL of PTX and *in vitro* PTX release. PLGA₄-LMWC NPs showed a DL of $27.9 \pm 7.9\%$, higher than the theoretical DL (5.7%), which suggested partial loss of PLGA₄-LMWC polymer during NP preparation [9]. PLGA-pD-LMWC NPs made of PLGA₁₁₈ and PLGA₁₅₀ showed DLs of 12.8 ± 5.3 and $8.6 \pm 3.4\%$, corresponding to 77.0 and 51.7% of the theoretical DL (16.7%), respectively. *In vitro* PTX release kinetics study was performed in PBS containing 0.2% Tween 80 (pH 7.4). PLGA₄-LMWC showed initial burst release in this medium, releasing $90.4 \pm 8.5\%$ of the loaded dose in 7 h. On the other hand, PLGA₁₁₈-pD-LMWC and PLGA₁₅₀-pD-LMWC NPs released

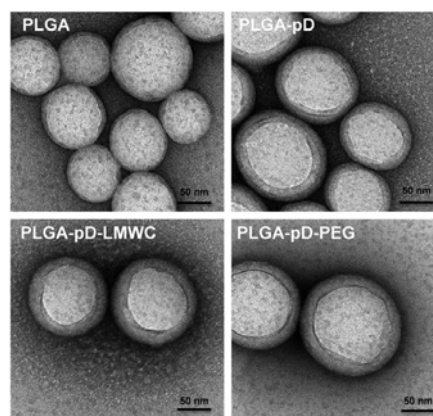
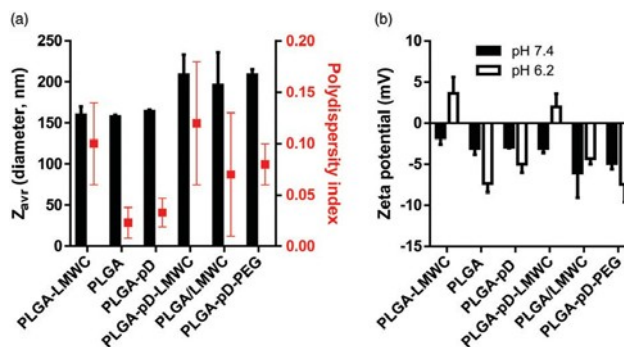


Figure 3. Transmission electron microscopy (TEM) images of NPs negatively stained with 2% uranyl acetate. Scale bar: 50 nm.

Figure 2. Particle size and surface charge of NPs: (a) average diameter (Z_{av} , black bars) and polydispersity index (red squares) and (b) zeta potential at pH 7.4 and 6.2.



PTX more slowly: 54.2 ± 5.5 and $39.9 \pm 9.0\%$ of the total dose in 7 h, reaching $\sim 80\%$ release in 48 h (Figure 4). Since PLGA₁₅₀-pD-LMWC NPs retained PTX most stably, they were used in the rest of the study, referred to as PLGA-pD-LMWC NPs without a subscript.

Protein adsorption to NP surface

To identify proteins binding to the NPs during incubation in serum-containing medium and correlate them with NP-cell interactions, the NPs were incubated in 50% FBS solution for 1 or 24 h and the proteins tightly bound to NPs (hard corona) were analyzed by gel electrophoresis. Proteins bound to NPs

were recovered with a detergent (SDS) and a reducing agent (5-mercaptoethanol), combined with heating [25,26] and analyzed with SDS-PAGE. The intensity of protein bands increased with time (Figure 5a and b), indicating the increase of protein binding to NPs, as previously observed [27]. Three major bands were identified at 66, 61 and 52 kDa, likely corresponding to bovine serum albumin, fetuin-A [28,29] and IgG [30], respectively. Albumin and fetuin-A made up dominant fractions, reflecting their abundance in FBS (Figure 5c) [31]. The relative intensity of IgG band increased with time in all NPs tested, irrespective of the coating polymers (LMWC versus PEG; Figure 5c). Consistent with the protein adsorption, the NPs with hard corona showed relatively more negative zeta potential than those in buffer (Figure S5).

NP-cell interactions

Given that PLGA-pD-LMWC NPs did not completely avoid protein binding in serum solution, we were curious if PLGA-pD-LMWC NPs would maintain the intended advantage of pH-sensitive surface in serum-containing medium. Fluorescently labeled NPs (*PLGA-pD-LMWC NPs and other control *NPs) had similar sizes and surface charges to those of unlabeled NPs (Figure S3a and S3b). The labeled *NPs were incubated with SKOV-3 cells in medium containing 10% FBS at pH 7.4 and 6.2. From flow cytometry analysis, only the cells incubated with *PLGA-pD-LMWC and *PLGA-LMWC NPs at pH 6.2 showed increased geometric mean, indicating NP-cell interaction (Figure 6a). Those incubated with *PLGA-pD-LMWC or *PLGA-LMWC NPs pH 7.4 did not show such increase, which means that

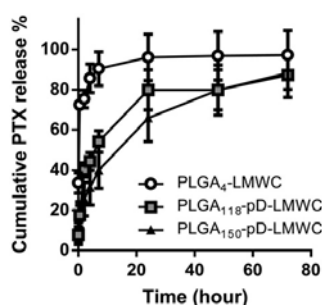


Figure 4. *In vitro* drug release of PTX from different NPs in PBS (0.2% Tween 80) at 37 °C. At 7th hour, there was significant difference in % cumulative release among three types of NPs ($p < 0.005$, one-way ANOVA, $n = 3$).

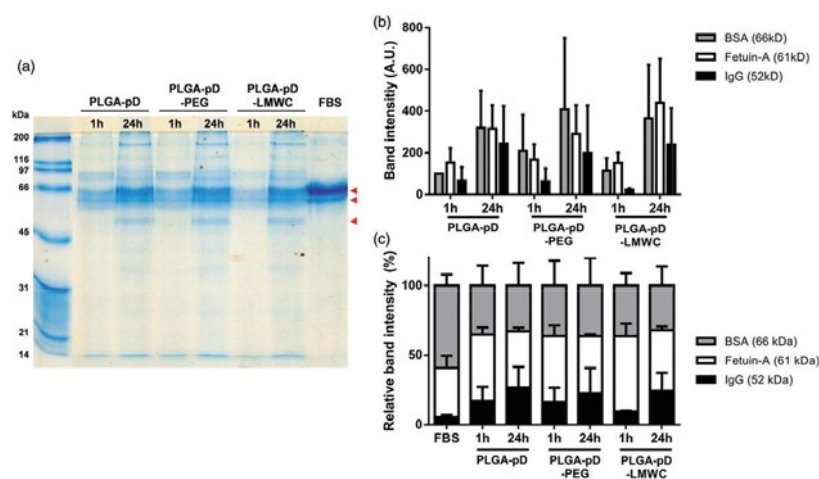
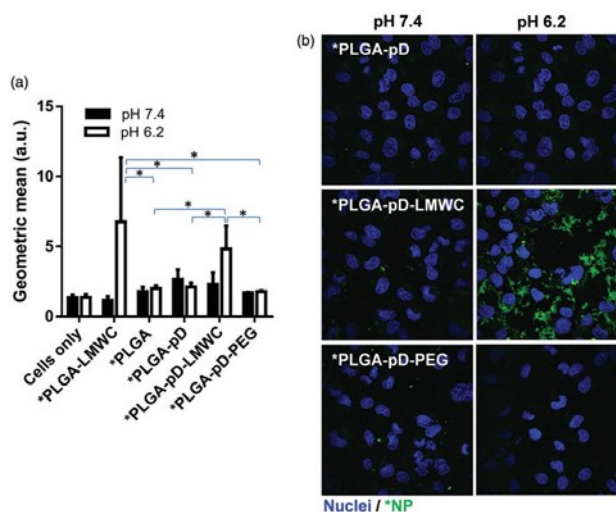


Figure 5. Analysis of the composition of protein hard corona formed on NP surface after incubation in 50% FBS for 1 or 24 h. Hard corona proteins were stripped off NPs and resolved via SDS-PAGE on a 12% gel along with size standards and 200-fold diluted FBS. Gels were stained with Coomassie blue G-250. (a) A representative gel of resolved hard corona proteins. Arrow heads indicate three prominent bands. (b) Band intensity of three proteins pointed with arrow heads in (a). (c) Relative band intensity (% of band intensity divided by the sum of three prominent band intensities). The gel image was analyzed via ImageJ 1.48v software. (b) and (c) show averages and standard deviations of four independently and identically run gels with four different batches.

DOI: 10.3109/1061186X.2015.1054829

Figure 6. pH-dependent interaction of *PLGA-pD, *PLGA-pD-LMWC and *PLGA-pD-PEG NPs with SKOV-3 cells, (a) quantified by flow-cytometry (Geometric means at pH 6.2 were significantly different for *PLGA-LMWC and *PLGA-pD-LMWC NPs from those of *PLGA, *PLGA-pD and *PLGA-pD-PEG NPs; *, $p < 0.05$ by two tailed *t*-test) and (b) visualized via confocal microscopy, after 3 h incubation (Green: *NPs; blue: nuclei). For color images, see online version.



LMWC-coated NPs can preferentially interact with cells in mildly acidic environment such as the extracellular matrix of solid tumors but not in normal tissues. *PLGA, *PLGA-pD and *PLGA-pD-PEG NPs had no cell interaction at either pH. Confocal microscopy confirmed this result (Figure 6b).

To locate *PLGA-pD-LMWC NPs with respect to cells, cell membrane or acidic intracellular organelles (late endosomes and lysosomes) were stained after removing uninternalized or loosely bound NPs. *PLGA-pD-LMWC NPs incubated with SKOV-3 cells at pH 6.2 for 3 h were observed on the membrane or within the membrane boundary (Figure 7a and b), indicating that they were partly internalized by the cells, but not at pH 7.4 (Figure 7a). *PLGA-pD-LMWC NPs were not co-localized with the acidic organelles at least in 3 h (Figure 8a). According to the time-lapse microscopy, cell binding of *PLGA-pD-LMWC NPs at pH 6.2 occurred in 60–75 min (Figure 8b). The NP signals increased over time (Figure 8b, Figure S6), both outside and inside the cells, but NPs were not intracellularly trafficked into the late endosomes and lysosomes at least up to 4.5 h (Figure 8b).

To test if the LMWC layer could reduce phagocytic uptake of particles despite the apparent protein binding, *PLGA-pD-LMWC MPs and control *MPs (2–3 μ m in diameter), with similar surface charge profiles to those of *NPs (Figure S3b and S3c), were incubated with J774A.1 macrophages in medium containing 10% FBS, and the extent of MP phagocytosis was determined by measuring the fluorescence of macrophages by flow cytometry and fluorescence microscopy. Here, MPs were used instead of NPs, as they could be more readily phagocytosed than NPs [32], hence serving as a more sensitive model for evaluating macrophage uptake of particles. *PLGA MPs were taken up most avidly (Figure 9). *PLGA-pD MPs were taken up less than the naked MPs due to the hydrophilicity imparted by amine-containing pD.

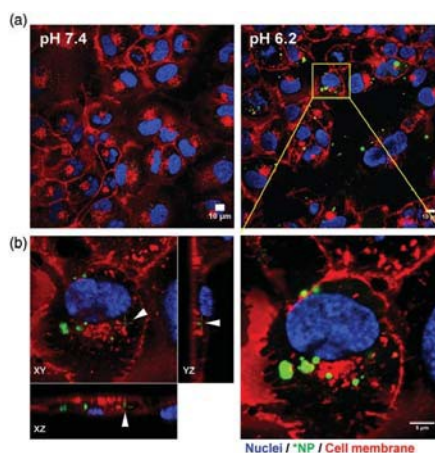


Figure 7. Cellular uptake of *PLGA-pD-LMWC NPs by SKOV-3 cells after 3 h of incubation at pH 7.4 or 6.2, imaged by confocal microscopy as (a) a cross-sectional image and (b) z-stack (left panel). XZ and YZ planes show NPs located in a cell. (Green: *NPs; red: cell membrane labeled by CellMask deep red; blue: nuclei). For color images, see online version.

*PLGA-pD-LMWC MPs showed significant reduction in macrophage uptake, to an even greater extent than *PLGA-pD-PEG MPs (Figure 9).

Paclitaxel delivery to cancer cells by NPs

We hypothesized that selective cell interaction of PLGA-pD-LMWC NPs at acidic pH would translate to superior

732 S. A. Abouelmagd et al.

J Drug Target, 2015; 23(7-8): 725-735

Figure 8. (a) Intracellular trafficking of *PLGA-pD-LMWC NPs in SKOV-3 cells, imaged by confocal microscopy after 3 h of incubation at pH 7.4 or 6.2. (b) Time-lapse confocal imaging of *PLGA-pD-LMWC NPs incubated with SKOV-3 cells at pH 6.2 for 270 min (Green: *NPs; red: LysoTracker Red DND-99; blue: nuclei). For color images, see online version.

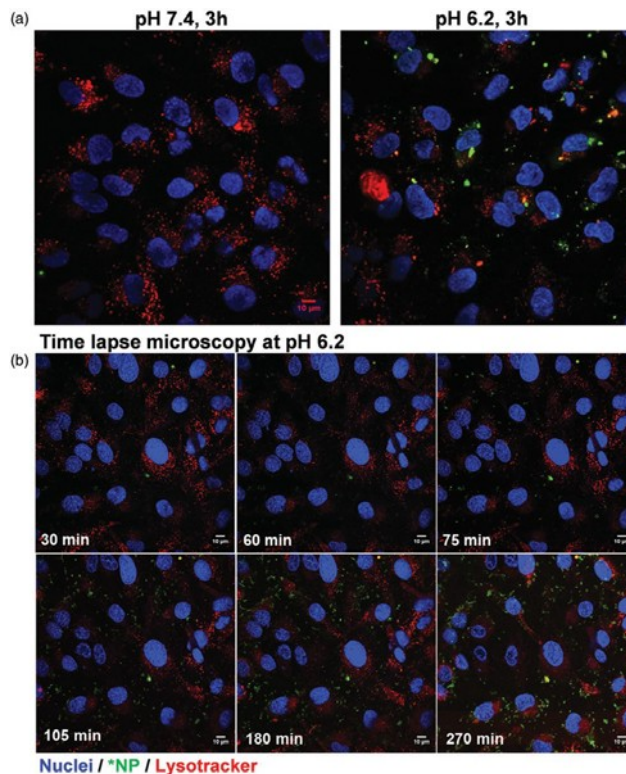
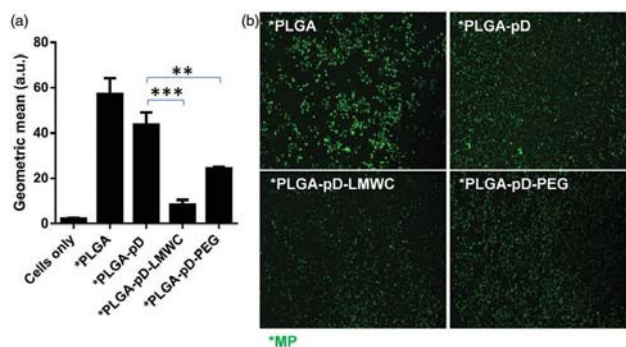


Figure 9. J774A.1 macrophage uptake of *PLGA, *PLGA-pD, *PLGA-pD-LMWC and *PLGA-pD-PEG MPs at pH 7.4 after 3 h incubation, (a) analyzed via flow cytometry and (b) visualized with Cytation 3 fluorescence imaging system (Green: *MPs). Flow cytometry data are expressed as averages and standard deviations of three independently and identically prepared NP samples. All geometric means were significantly different from each other ($p < 0.05$ by one-way ANOVA test). ** $p < 0.005$; *** $p < 0.0005$ by two-tailed t -test.



drug delivery. To test this, PTX-loaded PLGA-pD-LMWC NPs were incubated with SKOV-3 cells at pH 7.4 and 6 for 2.5 h, and the amount of PTX retained by the cells was quantified. Cells incubated at pH 6 had 44-fold

higher PTX content as compared to pH 7.4 (Figure 10). On the other hand, there was no such difference for the cells incubated with free PTX or PTX-loaded PLGA-pD-PEG NPs. This shows that the enhanced NP-cell

DOI: 10.3109/1061186X.2015.1054829

LMWC-coated polymeric NPs 733

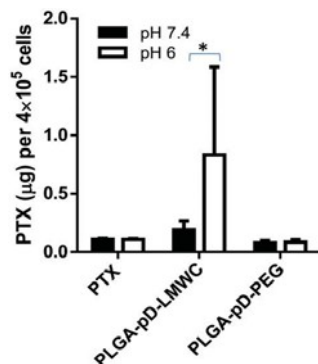


Figure 10. pH-dependent PTX retention after incubation of SKOV-3 cells with PTX-loaded NPs or free PTX at pH 7.4 or 6. Cells were incubated with the NPs for 2.5 h at either pH and separated from NPs, and analyzed for PTX content. Data are expressed as averages and standard deviations of 4–8 wells of cells treated with two independently and identically prepared batches of NPs. * $p < 0.05$, by two-tailed t -test.

interaction at acidic pH leads to similar enhancement in drug delivery to the cells.

Discussion

Polymeric NP systems have been pursued for decades as a way of achieving tumor-specific drug delivery [33]. One of the critical challenges in clinical translation of these systems is the increasing complexity of NP design and production methods. While the complexity is introduced to accommodate new knowledge of cancer biology, it also leads to increasing cost and regulatory scrutiny, making the development of a commercial product more challenging [33,34]. Moreover, the complicated design and synthesis can induce undesirable changes to the material properties of the NPs such as MW and hydrophobicity, which are essential for their primary roles: loading and retaining drugs. We experienced this problem in developing PLGA₄-LMWC NPs, where the LMWC conjugation not only allowed for specific drug delivery to acidic tissues but also increased the hydrophilicity of the polymer, compromising the NP's function as a carrier of PTX [9]. Here, we used a new surface modification method based on dopamine polymerization to decouple the NP formation from the surface modification, enabling independent control of NP cores and surface properties for drug loading/release and specific NP–cell interactions, respectively.

The LMWC-coated PLGA NPs via dopamine polymerization (PLGA-pD-LMWC NPs) showed a comparable average diameter and pH-dependent charge profile to those of PLGA₄-LMWC NPs (Figure 2). The LMWC content in PLGA-pD-LMWC NPs was lower than that of PLGA₄-LMWC NPs, but it does not necessarily indicate less efficient coating because in PLGA₄-LMWC NPs a fraction of the LMWC is supposed to be buried in the NPs and not exposed on the surface. Given the extent of charge change and NP–cell interaction profiles (Figure 6), the surface exposed LMWC of the two NPs is likely to be comparable.

The PTX DL of PLGA₄-LMWC NPs was apparently higher than that of PLGA-pD-LMWC NPs, but this is likely due to the hydrophilicity of PLGA₄-LMWC polymer, which was selectively washed out during the NP preparation [9]. PTX-loaded PLGA-pD-LMWC NPs produced with PLGA₁₁₈ and PLGA₁₅₀ showed more prolonged drug release than PTX-loaded PLGA₄-LMWC NPs, due to the greater hydrophobicity and MW of the polymers. PTX release in the first few hours from these NPs was much slower than that from PLGA₄-LMWC NPs and sustained over three days (Figure 4), suggesting that these NPs may reduce premature drug release in circulation during the critical period for NP biodistribution. The drug release from PLGA₄-LMWC NPs reported in this study appears faster than that in the previous study [9], but the two results are not directly comparable because the Tween 80 concentration in release medium was different (0.2 versus 0.1%). We chose 0.2% Tween 80 in PBS as release medium, as we determined that it was suitable to mimic the amphiphilic feature of physiological fluid and simulate a sink condition faced *in vivo* [35]. Even though the drug release attenuation appears to be modest as compared to the previous study, the actual extent of attenuation is deemed significant given the difference of the medium. The NP core can be further optimized, if additional release control is necessary, by simple replacement of the polymer with more hydrophobic and slowly degrading ones [36].

The LMWC layer introduced via pD layer to the pre-formed PLGA NPs provided pH-sensitive functionality necessary for desired NP–cell interactions (Figure 2b). Prior to testing cellular uptake of NPs, we investigated protein binding to PLGA-pD-LMWC NPs incubated in serum solution. As the NPs enter the blood stream, they instantaneously interact with plasma proteins to be covered with a protein corona on NPs surface. The protein corona is composed of a tightly bound stable 'hard' corona and a loosely bound 'soft' corona, which can be dynamically exchanged with other proteins [37]. Since NPs entering the bloodstream cannot completely avoid protein binding even with protective surface layer [38] and the identity of bound proteins has shown to be critical to the biological fate of NPs [39], we investigated the protein binding profile of the surface-modified NPs after incubation in 50% FBS, which mimicked the serum content in blood [40]. Protein binding occurred with all tested NPs (PLGA-pD, PLGA-pD-LMWC and PLGA-pD-PEG NPs) in a similar pattern (Figure 5). It is noteworthy that all NPs were increasingly enriched with IgG, antibodies responsible for opsonization and complement activation, over time. Figure 9 shows that pD, pD-LMWC and pD-PEG layers helped reduce phagocytic uptake of PLGA MPs by J774A.1 macrophages due to the hydrophilicity imparted by the surface polymers. However, the increasing IgG enrichment indicates that the function of LMWC or PEG in this NP system is still imperfect as a stealth layer and remains to be improved in future studies.

The surface charges of all NPs decreased after incubation in serum solution (Figure S5), reflecting protein binding. Nevertheless, the protein-bound PLGA-pD-LMWC NPs maintained the pH-sensitive charge profile, allowing for acid-specific NP–cell interactions in serum-containing

medium. Confocal microscopy showed that PLGA- pD-LMWC NPs established interactions with SKOV-3 cell membrane at pH 6.2 in 1 h and entered the cells in 3 h (Figure 8b), likely via adsorption-mediated endocytosis [41]. The internalized NPs did not co-localize with the late endosomes or lysosomes by 4.5 h (Figure 8b). This result is similar to an observation made with cationic NPs coated with quaternized chitosan, which were internalized by human proximal epithelial cells and showed little co-localization with lysosomes in 6 h [42]. Other types of NPs lacking LMWC (PLGA, PLGA-pD or PLGA-pD-PEG) did not show cellular uptake at pH 6.2. All tested NPs showed little uptake by SKOV-3 cells at pH 7.4 (Figure 6). This result indicates that while PLGA- pD-LMWC NPs did not interact with cells at normal physiological pH, they were able to establish interactions with cells at pH 5.65 as PLGA₄-LMWC NPs previously did [9] and get internalized into the cells without being trafficked into the acidic organelles. Given that hard corona compositions for all pD-coated NPs (PLGA-pD, PLGA-pD-PEG and PLGA-pD-LMWC NPs) were similar (Figure 5), yet PLGA- pD-LMWC NPs showed different behavior than the other NPs, the protein corona in this NP system did not play a role significant enough to interfere with the intended NP - cell interactions. This result is contrasted with transferrin-functionalized silica NPs that lost targeting capabilities in serum-containing medium due to the formation of protein corona [39].

The reliable drug encapsulation achieved by PLGA- pD-LMWC NPs allowed us to test the contribution of the LMWC surface to PTX delivery in acidic medium. SKOV-3 cells were exposed to PTX-loaded PLGA-pD-LMWC NPs at pH 7.4 and 6 for 2.5 h and analyzed with respect to the amount of PTX retained by the cells (through NP binding and/or uptake). The exposure time was limited to 2.5h since it would better represent dynamic *in vivo* situation, where NPs would continuously flow and get gradually diluted. PTX- loaded PLGA-pD-LMWC NPs delivered a significantly greater amount of PTX to SKOV-3 cells at pH 6 compared to pH 7.4 and those delivered as free PTX treatment or PTX- loaded PLGA-pD-PEG NPs, which showed similar cellular levels of PTX at both pHs (Figure 10). Since drug release from NPs was minimal (530%) in 2.5 h (Figure 4), the large amount of drug delivered by PLGA-pD-LMWC NPs would be readily attributable to the enhanced NP binding and uptake by the cells at acidic pH, previously observed by confocal microscopy and flow cytometry.

Conclusions

In summary, LMWC-coated PLGA NPs created by the dopamine polymerization method overcame the limitations of the earlier version based on a PLGA-LMWC covalent conjugate in loading and retaining PTX. The PLGA- pD-LMWC NPs provided pH-sensitive surface layer, which enabled acid-specific NP - cell interaction and enhanced drug delivery to cells in the weakly acidic environment. The LMWC layer did not completely prevent protein binding to the NPs incubated in serum solution but reduced phagocytic uptake. The surface layer remains to be further optimized to reduce IgG binding.

Acknowledgements

We thank Samyang Genex Corp (Seoul, Korea) for the kind donation of paclitaxel and Dr. Lake Paul at the Bindley Bioscience Center for technical assistance with MALDI and AUC analyses.

Declaration of interest

The authors report no declarations of interest. This work was supported by NIH R01 EB017791. We also acknowledge the fellowship support from the Egyptian Government Ministry of Higher Education Missions Sector to S.A.A.

References

- Bharali DJ, Khalil M, Gurbuz M, et al. Nanoparticles and cancer therapy: a concise review with emphasis on dendrimers. *Int J Nanomedicine* 2009;4:1 - 7.
- Torchilin V. Tumor delivery of macromolecular drugs based on the EPR effect. *Adv Drug Deliv Rev* 2011;63:131 - 5.
- Matsumura Y, Maeda H. A new concept for macromolecular therapeutics in cancer chemotherapy: mechanism of tumorotropic accumulation of proteins and the antitumor agent smancs. *Cancer Res* 1986;46:6387 - 92.
- Maeda H, Sawa T, Konno T. Mechanism of tumor-targeted delivery of macromolecular drugs, including the EPR effect in solid tumor and clinical overview of the prototype polymeric drug SMANCS. *J Control Release* 2001;74:47 - 61.
- Senior J, Delgado C, Fisher D, et al. Influence of surface hydrophilicity of liposomes on their interaction with plasma- protein and clearance from the circulation - studies with poly(ethylene glycol)-coated vesicles. *Biochim Biophys Acta* 1991;1062:77 - 82.
- Torchilin VP, Omelyanenko VG, Papisov MI, et al. Poly(ethylene glycol) on the liposome surface - on the mechanism of polymer-coated liposome longevity. *Biochim Biophys Acta Biomembr* 1994; 1195:11 - 20.
- Hatakeyama H, Akita H, Harashima H. A multifunctional envelope type nano device (MEND) for gene delivery to tumours based on the EPR effect: a strategy for overcoming the PEG dilemma. *Adv Drug Deliv Rev* 2011;63:152 - 60.
- Du H, Chandaroy P, Hui SW. Grafted poly-(ethylene glycol) on lipid surfaces inhibits protein adsorption and cell adhesion. *Biochim Biophys Acta* 1997;1326:236 - 48.
- Amoozgar Z, Park JY, Lin QN, Yeo Y. Low molecular-weight chitosan as a pH-sensitive stealth coating for tumor-specific drug delivery. *Mol Pharm* 2012;9:1262 - 70.
- Gerweck LE, Seetharaman K. Cellular pH gradient in tumor versus normal tissue: potential exploitation for the treatment of cancer. *Cancer Res* 1996;56:1194 - 8.
- Parveen S, Sahoo SK. Long circulating chitosan/PEG blended PLGA nanoparticle for tumor drug delivery. *Eur J Pharmacol* 2011; 670:372 - 83.
- Ishak RAH, Awad GAS, Zaki NM, et al. A comparative study of chitosan shielding effect on nano-carriers hydrophilicity and biodistribution. *Carbohydr Polym* 2013;94:669 - 76.
- Lee H, Dellatore SM, Miller WM, Messersmith PB. Mussel-inspired surface chemistry for multifunctional coatings. *Science* 2007;318:426 - 30.
- Ryu J, Ku SH, Lee M, Park CB. Bone-like peptide/hydroxyapatite nanocomposites assembled with multi-level hierarchical structures. *Soft Matter* 2011;7:7201 - 6.
- Wang GF, Huang H, Zhang XJ, Wang L. Electrically contacted enzyme based on dual hairpin DNA structure and its application for amplified detection of Hg²⁺. *Biosens Bioelectron* 2012;35:108 - 14.
- Lin MH, Liu YJ, Chen XF, et al. Poly(dopamine) coated gold nanocluster functionalized electrochemical immunosensor for brominated flame retardants using multienzyme-labeling carbon hollow nanochains as signal amplifiers. *Biosens Bioelectron* 2013; 45:82 - 8.

DOI: 10.3109/1061186X.2015.1054829

17. Black KCL, Yi J, Rivera JG, et al. Polydopamine-enabled surface functionalization of gold nanorods for cancer cell-targeted imaging and photothermal therapy. *Nanomedicine (UK)* 2013;8:17 – 28.
18. Park J, Brust TF, Lee HJ, et al. Polydopamine-based simple and versatile surface modification of polymeric nano drug carriers. *ACS Nano* 2014;8:3347 – 5.
19. Gullotti E, Park J, Yeo Y. Polydopamine-based surface modification for the development of peritumorally activatable nanoparticles. *Pharm Res* 2013;30:1956 – 67.
20. Du X, Li LX, Li JS, et al. UV-triggered dopamine polymerization: control of polymerization, surface coating, and photopatterning. *Adv Mater* 2014;26:8029 – 33.
21. Wei Q, Zhang FL, Li J, et al. Oxidant-induced dopamine polymerization for multifunctional coatings. *Polym Chem* 2010;1:1430 – 3.
22. Liu Y, Ai K, Liu J, et al. Dopamine-melanin colloidal nanospheres: an efficient near-infrared photothermal therapeutic agent for in vivo cancer therapy. *Adv Mater* 2013;25:1353 – 9.
23. Leane MM, Nankervis R, Smith A, Illum L. Use of the ninhydrin assay to measure the release of chitosan from oral solid dosage forms. *Int J Pharm* 2004;271:241 – 9.
24. Errington N, Harding SE, Varum KM, Illum L. Hydrodynamic characterization of chitosans varying in degree of acetylation. *Int J Biol Macromol* 1993;15:113 – 17.
25. Docter D, Distler U, Storck W, et al. Quantitative profiling of the protein coronas that form around nanoparticles. *Nat Protoc* 2014;9:2030 – 44.
26. Monopoli MP, Walczyk D, Campbell A, et al. Physical-chemical aspects of protein corona: relevance to in vitro and in vivo biological impacts of nanoparticles. *J Am Chem Soc* 2011;133: 2525 – 34.
27. Casals E, Pfäller T, Duschl A, et al. Time evolution of the nanoparticle protein Corona. *ACS Nano* 2010;4:3623 – 32.
28. Martel J, Wu CY, Young JD. Critical evaluation of gamma-irradiated serum used as feeder in the culture and demonstration of putative nanobacteria and calcifying nanoparticles. *PLoS One* 2010;5:e10343.
29. Young JD, Martel J, Young L, et al. Putative nanobacteria represent physiological remnants and culture by-products of normal calcium homeostasis. *PLoS One* 2009;4:e4417.
30. Ehrenberg MS, Friedman AE, Finkelstein JN, et al. The influence of protein adsorption on nanoparticle association with cultured endothelial cells. *Biomaterials* 2009;30:603 – 10.
31. Wu C-Y, Young L, Young D, et al. Bions: a family of biomimetic mineralo-organic complexes derived from biological fluids. *PLoS One* 2013;8:e75501.
32. Tabata Y, Ikada Y. Effect of the size and surface-charge of polymer microspheres on their phagocytosis by macrophage. *Biomaterials* 1988;9:356 – 62.
33. Cheng ZL, Al Zaki A, Hui JZ, et al. Multifunctional nanoparticles: cost versus benefit of adding targeting and imaging capabilities. *Science* 2012;338:903 – 10.
34. Goldberg MS, Hook SS, Wang AZ, et al. Biotargeted nanomedicines for cancer: six tenets before you begin. *Nanomedicine (UK)* 2013;8:299 – 308.
35. Abouelmagd SA, Sun B, Chang AC, et al. Release kinetics study of poorly water-soluble drugs from nanoparticles: are we doing it right? *Mol Pharm* 2015;12:997 – 1003.
36. Mittal G, Sahana DK, Bhardwaj V, Kumar MNVR. Estradiol loaded PLGA nanoparticles for oral administration: effect of polymer molecular weight and copolymer composition on release behavior in vitro and in vivo. *J Control Release* 2007;119:77 – 85.
37. Milani S, Bombelli FB, Pitek AS, et al. Reversible versus irreversible binding of transferrin to polystyrene nanoparticles: soft and hard corona. *ACS Nano* 2012;6:2532 – 41.
38. Walkey CD, Olsen JB, Guo H, et al. Nanoparticle size and surface chemistry determine serum protein adsorption and macrophage uptake. *J Am Chem Soc* 2012;134:2139 – 47.
39. Salvati A, Pitek AS, Monopoli MP, et al. Transferrin-functionalized nanoparticles lose their targeting capabilities when a biomolecule corona adsorbs on the surface. *Nat Nanotechnol* 2013;8:137 – 43.
40. Sherwood L. *Human physiology: from cells to systems*. 8th ed. Belmont: Cengage Learning; 2011.
41. Tahara K, Sakai T, Yamamoto H, et al. Improved cellular uptake of chitosan-modified PLGA nanospheres by A549 cells. *Int J Pharm* 2009;382:198 – 204.
42. Yue ZG, Wei W, Lv PP, et al. Surface charge affects cellular uptake and intracellular trafficking of chitosan-based nanoparticles. *Biomacromolecules* 2011;12:2440 – 6.

LMWC-coated polymeric NPs 735

Supplementary material available online.
Supplementary Figures S1 – S6.

Release Kinetics Study of Poorly Water-Soluble Drugs from Nanoparticles: Are We Doing It Right?

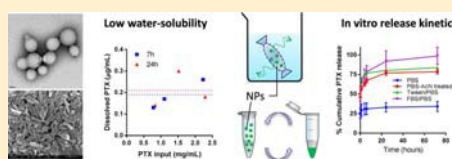
Sara A. Abouelmagd,^{†,§} Bo Sun,^{†,§} Alice C. Chang,[†] Youn Jin Ku,[†] and Yoon Yeo^{*,†,‡}

[†]Department of Industrial and Physical Pharmacy and [‡]Weldon School of Biomedical Engineering, Purdue University, West Lafayette, Indiana 47907, United States

^{*}Supporting Information

ABSTRACT: *In vitro* drug release kinetics studies are routinely performed to examine the ability of new drug formulations to modulate drug release. The underlying assumption is that the studies are performed in a sufficiently dilute solution, where the drug release is not limited by the solubility and the difference in release kinetics profile reflects the performance of a drug carrier *in vivo*. This condition is, however, difficult to meet with poorly water-soluble drug formulations, as it requires a very large volume of release medium relative to the formulation mass, which makes it challenging to measure the drug concentration accurately. These difficulties are aggravated with nanoparticle (NP) formulations, which are hard to separate from the release medium and thus require a dialysis bag or repeated high-speed centrifugation for sampling. Perhaps for these reasons, drug release kinetics studies of NPs of poorly water-soluble drugs are often performed in suboptimal conditions in which the NPs are not sufficiently diluted. However, such a practice can potentially underestimate drug release from NPs, leading to an inaccurate prediction that the NPs will attenuate the drug activity *in vivo*. Here we perform release kinetics studies of two different NP formulations of paclitaxel, a representative poorly water-soluble drug, according to common practices in the literature. We find that the drug release from NPs can be substantially underestimated depending on the choice of the release medium, NP/medium ratio, and handling of release samples. We discuss potential consequences of underestimating drug release, ending with suggestions for future studies with NP formulations of poorly water-soluble drugs.

KEYWORDS: poorly water-soluble drugs, paclitaxel, solubility, nanoparticles, *in vitro* release kinetics, sustained release



1. INTRODUCTION

Nanoparticles (NPs) are used in various drug delivery applications. NPs can be designed to attenuate drug release so that they have minimal side effects on nontarget tissues during circulation.¹ NPs are also used to solubilize poorly water-soluble drugs.² For example, polymeric micelles help disperse poorly water-soluble drugs in water by encapsulating the drugs in hydrophobic cores while facing water via hydrophilic shells.^{3,4} Alternatively, poorly water-soluble drugs can be processed into nanocrystals, pure drug particles of nanometric dimensions stabilized with surface active agents, to increase their dissolution rate in water.^{5–7} Irrespective of the purposes of NPs, *in vitro* drug release kinetics (cumulative drug release vs time profiles, also called dissolution kinetics) are almost always examined to demonstrate their ability to attenuate or enhance drug release.

Release kinetics studies or dissolution tests of NPs are performed by various methods.⁸ In the dialysis method, NP suspension is placed in a dialysis bag with a specified molecular

weight cutoff (MWCO), and drug molecules diffusing out of the bag are frequently sampled for quantitative analysis. Alternatively, NPs are suspended in a finite volume of release medium and incubated with agitation. The suspension is spun down at certain time points to separate a supernatant, which is

sampled and analyzed to determine the amount of drug released during the interval. A standardized United States Pharmacopoeia (USP) method is also available. In the USP apparatus 4 (flow-through cell apparatus) method, NPs are put in a small dialysis unit and placed in a small volume cell, through which the release medium is passed at a constant flow rate and analyzed at regular time points.

Irrespective of the test method, the assumption underlying the release kinetics studies is that the dose range of the NP products and the volume of release medium satisfy sink conditions (defined as the volume of medium at least three times that required to form a saturated solution of a drug¹⁰): i.e., the drug release is not limited by the solubility, and the difference in release kinetics profile reflects the performance of NPs as a drug carrier *in vivo*. To meet this requirement, it is important that one use a sufficient volume of release medium for the NPs. However, in the case of poorly water-soluble drugs, satisfying the sink condition can be quite challenging as it means a very low ratio of NP mass to the volume of release

Received: December 6, 2014

Revised: January 26, 2015

Accepted: February 6, 2015

Published: February 6, 2015

medium. A disadvantage of using a large volume of release medium is that drug analysis gets difficult due to the low concentration. In order to alleviate this difficulty, the sampled solution is concentrated prior to analysis or a dissolution aid such as surfactants or cosolvents is included in the release medium to increase the drug solubility (hence the ratio of NP mass to medium volume).^{10,11}

Given these requirements and constraints in fulfilling a sink condition, it is very important to know an accurate solubility value of a drug and set up appropriate experimental conditions in studying drug release kinetics from NPs. Nevertheless, we observe that solubility values of paclitaxel (PTX), a representative poorly water-soluble drug, reported in the literature vary over a range of orders of magnitude, and the release kinetics studies of PTX-loaded NPs are performed under different understandings of a sink condition. Here, we revisit the current practice of drug release kinetics studies on NP formulations of poorly water-soluble drugs and discuss potential pitfalls and consequences. We first determine the solubility and stability of PTX in potential release media (PBS, PBS with 0.2% Tween 80, and PBS with 50% fetal bovine serum (FBS)) and perform release kinetics studies of different PTX NP formulations in those media according to common practices in the literature. We discuss our results and other studies published in 2005–2014 based on our stability/solubility data, ending with suggestions for future studies with NP formulations of poorly water-soluble drugs.

2. EXPERIMENTAL SECTION

2.1. Determination of PTX Solubility in PBS, 0.2% Tween 80/PBS, and 50% FBS/PBS. PTX solubility in PBS (pH 7.4), PBS containing 0.2 v/v% Tween 80 (Tween/PBS), and PBS containing 50 v/v% FBS (FBS/PBS) were determined

by incubating excess PTX (0.6–2.4 mg) in 1 mL of each medium at 37 °C for 7 or 24 h with agitation. Samples were centrifuged at 10 000 rpm for 20 min to separate a supernatant. PTX dissolved in PBS and Tween/PBS was directly analyzed with high performance liquid chromatography (HPLC) as described in Section 2.7. PTX dissolved in FBS/PBS was filtered with 0.45 µm PVDF syringe filters, extracted with ethyl acetate as described in Section 2.7, and analyzed with HPLC.

PTX solubility was alternatively determined by diluting 10 mg/mL PTX stock solution dimethyl sulfoxide (DMSO) in each medium. To determine PTX solubility in PBS and Tween/PBS, PTX/DMSO solution (10 mg/mL) was first diluted with Tween/PBS to make 1 mg/mL of PTX solution, which was further diluted with PBS to final concentrations of 0.1–20 µg/mL ($n = 3$) or with Tween/PBS to 1–70 µg/mL ($n = 3$). Samples were incubated at 37 °C for 24 h with shaking. Finally, PTX solutions were separated by filtration with 0.45 µm PVDF syringe filters and analyzed with HPLC. To determine PTX solubility in FBS/PBS, PTX/DMSO solution (10 mg/mL) was sequentially diluted with FBS/PBS to yield final concentrations of 25–300 µg/mL ($n = 3$). Samples were incubated at 37 °C for 7 or 24 h with shaking. At the end of the incubation, the samples were centrifuged at 10 000 rpm for 20 min, and the supernatant was filtered with 0.45 µm PVDF syringe filters, extracted with ethyl acetate as described in Section 2.7, and analyzed with HPLC.

To determine how quickly PTX precipitated in PBS at 37 °C, PTX solution in PBS at a concentration of 20 µg/mL was prepared by diluting 10 mg/mL PTX/DMSO solution with PBS (final DMSO concentration: 0.2%), aliquoted by 1 mL,

and incubated at 37 °C with shaking. At predetermined time points, three aliquots were taken and centrifuged at 3000 rpm for 5 min. The supernatants were additionally centrifuged at 10 000 rpm for 20 min to remove precipitates and analyzed with HPLC.

2.2. Stability of PTX in 0.2% Tween 80/PBS. PTX solution (1.5 µg/mL) in Tween/PBS was prepared by diluting 10 mg/mL PTX/DMSO solution with Tween/PBS (final DMSO concentration: 0.015%). The solution was divided into several 1 mL aliquots, and the initial PTX concentration was determined with seven of them. The remaining aliquots were incubated at 37 °C, and three aliquots were taken at predetermined time points and kept at –80 °C until HPLC analysis. The frozen samples were thawed and analyzed with HPLC. The concentration of intact PTX at each time point was divided by the original PTX concentration (1.5 µg/mL) and expressed as the percentage of original PTX.

2.3. Preparation of PTX Nanoparticles (PTX/NPs). PLGA NPs loaded with PTX (PTX/NPs) were prepared by the single emulsion solvent evaporation method. Briefly, 20 mg of PLGA and 2.5 mg of PTX were dissolved in 1 mL of dichloromethane (DCM) and emulsified in 4 mL of 4% poly(vinyl alcohol) (PVA) solution by probe sonication. The o/w emulsion was dispersed in deionized (DI) water and stirred for 1 h, followed by rotary evaporation for another hour to ensure DCM evaporation. Finally, NPs were collected by centrifugation and washed three times with water. The NPs were lyophilized with trehalose as a lyoprotectant.

2.4. Preparation of PTX Nanocrystals (PNC) and Human Serum Albumin-Stabilized PNC (aPNC). PTX nanocrystals (PNC) were prepared according to the published method.¹² Briefly, 4 mg/mL PTX/ethanol solution was added to 20 mL of DI water and stirred for 10 min in a round-bottom flask immersed in a sonication bath filled with ice water. The formed PNC was filtered through a 100 nm polycarbonate membrane and resuspended in DI water. To further stabilize PNC, 1 mg/mL PNC suspension was mixed with 2 mg/mL of human serum albumin solution and incubated for 1.5 h at room temperature. The human serum albumin-stabilized PNC (aPNC) was collected by centrifugation (10 000 rpm, 15 min) and washed with DI water twice.

2.5. Release Kinetics of PTX/NPs in PBS, Tween/PBS, or FBS/PBS via Centrifugation Method. To determine the PTX content in NPs, the freeze-dried PTX/NPs was dissolved in a mixture of acetonitrile/water (50:50) for 2 h, and the supernatant was analyzed with HPLC. For release kinetics studies of PTX/NPs, the freeze-dried PTX/NPs equivalent to 4.4 or 27 µg of PTX were suspended in 1 mL of release medium (PBS, Tween/PBS, or FBS/PBS) and incubated at 37 °C with constant agitation. At predetermined time points, the suspension was centrifuged at 10 000 rpm for 10 min at room temperature to separate NP pellets and supernatants. Then 0.8 mL of supernatant was sampled and replaced with the same volume of fresh medium in which the NP pellet was resuspended and returned for further incubation. The sampled supernatant was analyzed immediately (PBS and Tween/PBS) or stored frozen (FBS/PBS) until HPLC analysis. At the end of the release experiment, the remaining NPs were dissolved in 1 mL of acetonitrile/water (50:50) for 2 h (PBS and Tween/PBS) or processed with the same extraction method as release samples (FBS/PBS) to determine the unreleased PTX.

2.6. Release Kinetics of PNC and aPNC in PBS via Dialysis Method. PNC or aPNC equivalent to 200 µg of PTX

Molecular Pharmaceutics

were suspended in 3 mL of PBS, put in a dialysis cassette (MWCO 3500), placed in 200 mL of PBS, and incubated at 37 °C under constant agitation. At timed intervals, 5 mL of release medium was sampled and replaced with 5 mL of fresh PBS.

2.7. HPLC Analysis of PTX. PTX in PBS or PTX in Tween/PBS solution was analyzed with HPLC after filtration with a 0.45 μm PVDF syringe filter with no other treatment. Optionally, PTX in PBS sample was mixed with acetonitrile in 1:1 volume ratio and then filtered for HPLC analysis. PTX in FBS/PBS was extracted with ethyl acetate prior to HPLC analysis. Briefly, 1 mL of PTX solution in FBS medium with 10 μg of carbamazepine as an internal standard was mixed with 3 mL of ethyl acetate and shaken on a rotating shaker for 40 min. The mixture was then centrifuged at 4000 rpm for 15 min to separate an organic layer, which was transferred to a new glass vial and dried under vacuum. The dried sample was resuspended in the HPLC mobile phase, filtered through a 0.45 μm syringe filter, and analyzed by HPLC. A calibration curve was drawn with PTX solutions in known concentrations, treated in the same manner as the sample solutions. PTX was analyzed with HPLC equipped with UV detector (1100 series, Agilent Technologies, Palo Alto, CA) and an Ascentis C18 column (25 cm \times 4.6 mm, particle size 5 μm) (Supelco, St. Louis, MO, USA). The mobile phase was a mixture of acetonitrile and water (50:50) run in the isocratic mode at a flow rate of 1 mL/min. PTX was detected at 227 nm.

3. RESULTS

3.1. PTX Solubility in PBS, Tween/PBS, and FBS/PBS. The reported values of PTX solubility in deionized water or phosphate-buffered saline (PBS, pH 7.4) range from 0.3 to 30 $\mu\text{g}/\text{mL}$ (Supporting Table 1). PTX solubility in a medium containing a surfactant such as Tween 80 is reported to be much higher: up to >100 $\mu\text{g}/\text{mL}$ (in 3% Tween 80).¹³ PTX solubility in calf serum is defined as 171 $\mu\text{g}/\text{mL}$.¹⁴ We evaluated PTX solubility in PBS, PBS containing 0.2% Tween 80 (Tween/PBS), and PBS containing 50% FBS (FBS/PBS) by suspending excess amounts of PTX in each medium and measuring the concentration of dissolved PTX. The results showed a similar trend as those in the literature, although our values fell in lower ends of the reported ranges. PTX solubility in PBS at 37 °C was measured at \sim 0.2 $\mu\text{g}/\text{mL}$ with no specific trend according to the incubation time, although the values were variable due to the limited sensitivity of HPLC (Figure 1a). PTX solubility in Tween/PBS was measured to be 3.3 $\mu\text{g}/\text{mL}$ irrespective of the incubation time (Figure 1b). PTX solubility in FBS/PBS was measured at 35 $\mu\text{g}/\text{mL}$ after 7 h incubation at 37 °C, much higher than those in PBS or Tween/PBS, which confirmed the solubilizing effect of serum proteins (Figure 1c). Notably, PTX concentration measured after 24 h incubation was 25 $\mu\text{g}/\text{mL}$, 28.6% lower than that after 7 h. This difference is attributable to the instability of PTX in serum, reported in our previous study¹⁵ as well as in others.^{16,17} This indicates that, if PTX release kinetics studies are performed in serum-containing medium and the medium is not sampled and analyzed frequently, one may not recover 100% of PTX from the formulation due to the degradation of released PTX. In contrast, PTX was relatively more stable in Tween/PBS, maintaining 94% of the initial concentration for 1 day (Figure 1d). This means that, as long as the medium is sampled at least once a day, PTX stability in Tween/PBS is less likely to be a problem.

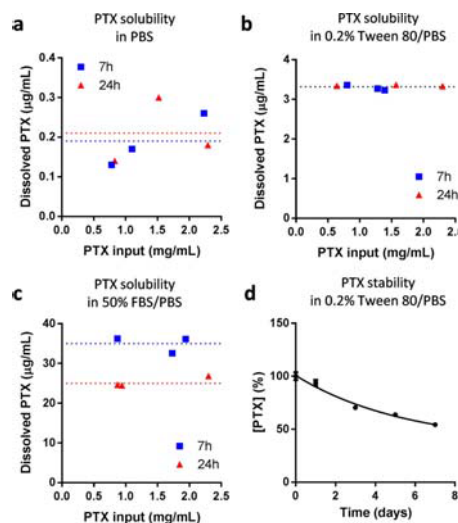


Figure 1. Paclitaxel (PTX) solubility in (a) PBS, (b) 0.2% Tween 80/PBS, and (c) 50% FBS/PBS. PTX solubility in each medium was determined by incubating excess PTX (0.6–2.4 mg) in 1 mL of medium at 37 °C for 7 or 24 h with agitation. Samples were centrifuged to remove precipitated PTX and analyzed with HPLC. (d) Stability of 1.5 $\mu\text{g}/\text{mL}$ PTX in 0.2% Tween 80/PBS at 37 °C.

PTX solubility was alternatively measured with solutions prepared by diluting a concentrated PTX/DMSO stock solution in each medium. This method helped handle small quantities of PTX with greater accuracy than the previous method. However, a small trace of DMSO in the solution (maximum 0.2% in PBS, 0.7% in Tween/PBS, and 3% in FBS/PBS) seemed to have affected PTX dissolution, resulting in slightly higher solubility values after 24 h incubation in 37 °C (\sim 0.4 $\mu\text{g}/\text{mL}$ in PBS and 3.9 $\mu\text{g}/\text{mL}$ in Tween/PBS, Supporting Figure 1a,b). In FBS/PBS, PTX concentration increased linearly with the PTX input and never reached a limit at least by 300 $\mu\text{g}/\text{mL}$ (Supporting Figure 1c). PTX concentrations measured after 24 h incubation at 37 °C were about 50% of those incubated for 7 h, confirming the instability of PTX in FBS/PBS. Of note, PTX solubility in Tween/PBS showed interesting variability across the measurements repeated four times. While the saturation solubility was measured to be 3.9 $\mu\text{g}/\text{mL}$ in the presence of far excess PTX (Supporting Figure 1b), PTX solutions prepared in the range of 4–18 $\mu\text{g}/\text{mL}$ in Tween/PBS showed concentrations greater than the saturation solubility to varying degrees in each experiment, indicating the formation of supersaturated solutions. This result indicates that one may observe variable solubility values in Tween/PBS, depending on the degree of supersaturation.

3.2. Release Kinetics of PTX NPs in PBS, Tween/PBS, or FBS/PBS via Centrifugation Method. We then prepared two types of PTX NPs (polymeric NPs and nanocrystals) and tested their release kinetics with conventional methods (centrifugation or dialysis methods). First of all, PTX was encapsulated in polymeric NPs (PTX/NPs) using the single

Molecular Pharmaceutics

emulsion method. PTX/NPs were spherical and had an average diameter of 161 nm (Supporting Figure 2). PTX release from PTX/NPs was tested using PBS, Tween/PBS, or FBS/PBS as release media. NPs equivalent to 4.4 μg of PTX was suspended in 1 mL of each release medium, creating a condition exceeding the solubility limit (in PBS), close to the solubility (in Tween/PBS), or satisfying the sink condition (in FBS/PBS). At regular intervals, 80% of the release medium (0.8 mL) was sampled after centrifugation and replaced with fresh buffers, and the sampled medium was analyzed by HPLC. In FBS/PBS, which satisfied a sink condition from the initial time point, NPs released $50.7 \pm 9.1\%$ of the loaded PTX upon the addition of the release medium and $98.7 \pm 11.0\%$ in 72 h (Figure 2a).

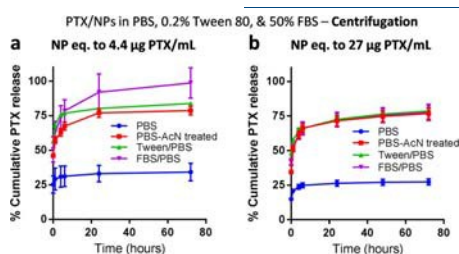


Figure 2. Release kinetics of PTX/NPs in media containing PBS, FBS, or Tween 80. PTX/NPs equivalent to (a) 4.4 μg or (b) 27 μg of PTX were suspended in 1 mL of release medium (PBS, Tween/PBS, or FBS/PBS) and incubated at 37 $^{\circ}\text{C}$ with constant agitation. At predetermined time points, the suspension was centrifuged to separate NP pellets and supernatants. Then 0.8 mL of supernatant was sampled and replaced with the same volume of fresh medium. The NP pellet was resuspended and returned for further incubation. The sampled supernatant was analyzed as sampled (PBS and Tween/PBS), with the addition of an equal volume of acetonitrile (PBS-AcN treated), or after extraction with ethyl acetate (FBS/PBS).

Similarly, in Tween/PBS, NPs released $56.6 \pm 1.2\%$ of the loaded PTX immediately and $83.9 \pm 1.3\%$ in 72 h (Figure 2a). It is worth mentioning that NPs in Tween/PBS did not satisfy the sink condition at the initial time point but resulted in a similar trend as in FBS/PBS. This may be attributable to the fact that Tween/PBS was capable of forming supersaturated PTX solution in the range of 4–18 $\mu\text{g}/\text{mL}$ (Supporting Figure 1b). On the other hand, PTX release in PBS was relatively small, reaching a cumulative release of $34.2 \pm 6.4\%$ in 72 h (Figure 2a). Since the total amount of PTX dispersed as NPs in PBS (4.4 $\mu\text{g}/\text{mL}$) was above the PTX solubility (0.2 $\mu\text{g}/\text{mL}$), we initially thought that PTX release was inhibited due to the low PTX solubility. However, the sum of total release (34.2%) and unreleased PTX (3.8%) fell far short of 100%, unlike those in Tween/PBS or FBS/PBS (Supporting Figure 3), suggesting a potential sample loss during the sampling or sample treatment. We thus added acetonitrile to the sampled PBS medium in 1:1 volume ratio and reanalyzed the samples. We found that a much greater amount of PTX was present in the sampled medium ($46.1 \pm 1.4\%$ as immediate release and $78.7 \pm 3.2\%$ as cumulative release by 72 h) than initially measured. This indicates that PTX was released in PBS to a similar level as in Tween/PBS and FBS/PBS but quickly precipitated out in the sampled medium due to the low solubility in PBS. When analyzed as sampled (without additional acetonitrile), the

precipitated PTX was removed during the HPLC sample preparation (i.e., filtration) and excluded from the analysis, which was avoided in the second analysis by the addition of acetonitrile. This result underscores the importance of keeping the ratio of total drug in NPs to medium volume below the drug solubility limit in the release kinetics studies. If this condition is not met (as in PBS in our case), one may observe low drug levels in the medium and incorrectly interpret them as sustained drug release, when in reality the drug has already been released and precipitated out in the sampled medium.

The release kinetics of PTX/NPs was also studied using a greater amount of NPs per release medium (NPs equivalent to 27 μg of PTX in 1 mL of release medium), which was

comparable to typical conditions described in the literature (Supporting Tables 2 and 3) (hence ending up violating sink conditions for all samples at the initial time point). A similar trend was observed (Figure 2b), with the cumulative release in PBS being the least when directly measured but similar to those in Tween/PBS and FBS/PBS when analyzed with additional acetonitrile. Interestingly, PTX concentrations in sampled media (4.0 $\mu\text{g}/\text{mL}$ in PBS and 13.1 $\mu\text{g}/\text{mL}$ in Tween/PBS at the first sampling time point) were much greater than its solubility limit in each medium (0.2 $\mu\text{g}/\text{mL}$ in PBS and 3.3 $\mu\text{g}/\text{mL}$ in Tween/PBS). This may be explained by the increase in dissolution rate due to the small particle size of PTX NPs, followed by temporary supersaturation of PTX in the release medium. However, since the extent of supersaturation can vary (Supporting Figure 1b), one may not be sure that the result will be reproducible.

3.3. Release Kinetics of PNC and aPNC in PBS via Dialysis Method. PTX was also formulated as nanocrystals (PNC) by nonsolvent and temperature-induced crystallization.⁷ PNC was optionally coated with human serum albumin to produce albumin-stabilized PNC (aPNC). Both PNC (Supporting Figure 2) and aPNC were rod-shaped particles with a length of ~ 400 nm and a width of ~ 100 nm. PTX release kinetics from PNC or aPNC was evaluated using the dialysis method and PBS as a release medium. Here, the NCs equivalent to 200 μg PTX was suspended in 3 mL of PBS, put in a dialysis cassette, and incubated in 200 mL of PBS with regular sampling and analysis, to make it comparable to typical conditions described in the literature (Supporting Tables 2). Figure 3a shows that PTX release (dissolution) from the NCs was very slow, reaching less than 10% cumulative release in 10 days. Given that the PTX concentration in the dialysis cassette was 66.7 $\mu\text{g}/\text{mL}$, far exceeding the solubility (0.2 $\mu\text{g}/\text{mL}$), and that the dialysis membrane could delay PTX diffusion into the release medium, we suspected that PTX might have precipitated in the dialysis cassette. Indeed a significant fraction of PTX remained in the dialysis cassette after 10 days. To estimate how quickly PTX precipitated in a dialysis cassette, we prepared a 20 $\mu\text{g}/\text{mL}$ PTX solution in PBS ($<1/3$ of the initial concentration in a dialysis cassette) and sampled the solution at different time points to quantify the dissolved PTX. PTX rapidly precipitated out in less than 30 min, leaving PTX in solution only to the solubility level (Supporting Figure 4). This result suggests that even though the small size of NCs had increased the dissolution rate of PTX, the dissolved PTX might have undergone reprecipitation in the dialysis cassette. In other words, PTX detected in the release medium did not necessarily reflect the dissolution of NCs but that of PTX precipitates entrapped in the cassette. Since only the dissolved PTX could pass the membrane and become diluted in the release medium,

Molecular Pharmaceutics

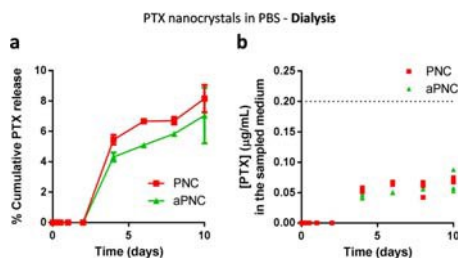


Figure 3. (a) Release kinetics of PNC and aPNC in PBS: PNC or aPNC equivalent to 200 μg of PTX were suspended in 3 mL of PBS, put in a dialysis cassette (MWCO 3500), placed in 200 mL of PBS, and incubated at 37 $^{\circ}\text{C}$ under constant agitation. At timed intervals, 5 mL of release medium was sampled and replaced with 5 mL of fresh PBS. (b) PTX concentration in the sampled medium at each time point. Symbols indicate each replicate. The dotted line indicates the saturation solubility of PTX in PBS.

the PTX concentration in the release medium was $<0.1 \mu\text{g/mL}$, below the solubility limit, at any time point (Figure 3b).

4. DISCUSSION

Our study demonstrates that release kinetics of a poorly water-soluble drug may be much underestimated when the ratio of the NP mass to release medium is not sufficiently low because the released drug reprecipitated in the sampled medium (Figure 2) or in the dialysis cassette (Figure 3). In light of this observation, we reviewed articles reporting *in vitro* release kinetics of PTX from NPs or other sustained delivery formulations, published in 2005–2014. In studies using the centrifugation method, PTX concentration in a test tube ranged from 25 to 1000 $\mu\text{g/mL}$ (Supporting Tables 2 and 3). In studies using the dialysis method, the concentration of PTX provided as NPs in total release medium (sum of the medium in dialysis bag and the bulk medium in which the bag was placed) was kept less than the saturation solubility, or the bulk medium was frequently replaced in most cases. However, the PTX concentration in a dialysis bag ranged from 40 to 1500 $\mu\text{g/mL}$ (Supporting Tables 2 and 3), exceeding the water solubility of PTX. These studies conclude that their NP formulations achieve sustained PTX release over various time periods. However, given that these concentration ranges are far above the solubility (0.2 $\mu\text{g/mL}$), we suspect that even if the drug release had been much faster in reality they would not have been able to detect it. As our release kinetics studies show, when PTX is present in excess of the solubility limit in the medium, the drug can precipitate out in the system shortly after it is released out of the formulation. This translates to a low drug level in the release medium, which can be incorrectly interpreted as sustained drug release. From this perspective, we revisit some of the previous studies with conflicting bioactivity results. For example, with slow *in vitro* drug release kinetics, one may expect that a NP formulation will be less effective than a free drug control.^{25–30} This may be interpreted as a consequence of enhanced cellular drug uptake or retention of NPs,^{25,26,29,30} but it could also be premature drug release, which

has been ignored in the release kinetics study. A potential hazard of underestimating *in vitro* drug release is that it can mislead to a prediction that a NP formulation will attenuate the drug activity during circulation and thus help reduce its side effects on nontarget tissues. However, unlike *in vitro*, NPs face an ultimate sink condition in the body, where the released drug is continuously diluted and undergoes protein binding, and can thus show very different drug release behaviors and biological performances than expected from the *in vitro* release studies. This may partly explain why many NPs expected to be effective *in vitro* do not readily translate to clinically effective products.

In order for *in vitro* release kinetics to provide some predictive potential, it is necessary that the release studies be performed with release media that simulate critical features of *in vivo* systems and sampling methods that maintainsimplicityand convenience of *in vitro* tests. PBS is the most simple and common medium for the release kinetics studies, but it requires a very low ratio of NPs to medium volume especially for poorly water-soluble drugs, which is met at the price of accuracy of the analysis. To avoid the analytical limitation, some have measured

drug remaining as NPs in the system at regular time points as an indirect estimate of drug release, where the difference between the initial and remaining dose is considered the released drug.³¹ This is a good alternative to measuring the released drug, as long as the released drug remains stable in the medium. Serum-containing buffers may be a reasonable choice of release medium for mimicking a physiological fluid with a complex composition that affects drug release. Because of the solubilizing effect of serum proteins, these media are also good for achieving a sink condition at a reasonably high concentration. However, PTX in serum-containing medium requires an additional extraction step to separate PTX from the proteins prior to analysis. Moreover, PTX is unstable in serum-containing solution; thus, the drug release may be underestimated unless the medium is exchanged frequently. We find that Tween/PBS is most recommendable among those tested in this study, as PTX in Tween/PBS is more stable than in FBS/PBS, does not require extra sample treatment for HPLC analysis, and generates a similar release profile as that in FBS/PBS, which satisfied a sink condition. However, Tween/PBS may not be compatible with the dialysis method. If Tween/PBS is used to disperse NPs in a dialysis bag, the released drug will be entrapped in the surfactant micelles and not freely pass the membrane. Conversely, if Tween/PBS is used as the bulk medium, NPs isolated in the bag cannot make a direct contact with the surfactants that aid in its dissolution in the medium, and the released drug can reprecipitate in the dialysis bag.

Centrifugation and dialysis are most widely used for sampling the release medium, but both have critical limitations. Centrifugation method requires centrifugation at a high speed for separating NPs from the free drug at each sampling. The pressure generated during the centrifugation can disturb the equilibrium between released drug and NPs and make it difficult to resuspend the NPs for further incubation. In addition, the separation is often incomplete, leading to cumulative errors in measurement of the released drug. Dialysis method eliminates the need for a separation step, but the fact that the dialysis membrane itself functions as a diffusion barrier creates a different problem, especially for the poorly water-soluble drugs. As observed in this study, a poorly water-soluble drug, accumulating in the bag due to the delay in diffusion across the membrane, can reprecipitate into larger aggregates, which then drive the apparent release kinetics. A similar

Molecular Pharmaceutics

concern has been raised by Anderson et al., who studied release kinetics of lipophilic drug-loaded liposomes with the dialysis method and observed reversible binding of the released drug to the liposomes within the dialysis bag.³¹ Given these disadvantages, it is worthwhile to consider various alternative methods proposed over the years. For example, Szoka et al. used agarose hydrogel to accommodate liposomes for non-invasive separation of the released drug from the carrier.³² Alternatively, a biphasic dissolution model is a conceivable option for studying the release kinetics of poorly water-soluble drugs.¹¹ Here, a water-immiscible organic solvent with a low density (e.g., octanol) is laid over an aqueous release medium that contains the formulation. A drug released into the medium partitions into the organic layer due to the lipophilicity, keeping the aqueous medium from saturation.¹¹ This method can, at least in theory, maintain the sink condition without excessive dilution and/or invasive sampling, although it is necessary to find a way to keep NPs from direct contact with the organic solvent.

In summary, our study illustrates how *in vitro* release kinetics studies of poorly water-soluble drugs designed without considering the solubility limitation can result in underestimation of drug release and a misleading conclusion of sustained drug release. To reasonably simulate *in vivo* conditions in which NPs are administered, the ratio of a drug in NP form to the initial volume of the release medium should be sufficiently lower than the saturation solubility of the drug. Inclusion of a dissolution aid in the release medium can help meet this requirement without compromising sample detection as long as it is in direct contact with NPs. In any combinations of release media and sampling methods, it is desirable to analyze the remaining NPs at the end of the study and check the mass balance, in order to exclude potential underestimation of drug release. Our discussion is limited to PTX NPs, but the same consideration can be extended to other formulations of drugs with similar stability and solubility limitations.

ASSOCIATED CONTENT

*Supporting Information

Supporting Figures and Tables. This material is available free of charge via the Internet at <http://pubs.acs.org>.

AUTHOR INFORMATION

Corresponding Author

*Phone: 765-496-9608. Fax: 765-494-6545. E-mail: [yyeo@purdue.edu](mailto:yyc@purdue.edu)

Author Contributions

[§]These authors contributed equally to this work.

Notes

The authors declare no competing financial interest.

ACKNOWLEDGMENTS

This work was supported by NIH R01 EB017791 and a Grant from the Lilly Endowment, Inc. to College of Pharmacy, Purdue University. We acknowledge the Fellowship support from the Egyptian Government Ministry of Higher Education Missions Sector to S.A.A. and the Ronald W. Dollens Scholarship support for B.S. We also thank Samyang Genex Corp (Seoul, Korea) for the kind donation of paclitaxel and the NAL Pharmaceuticals Ltd. (Monmouth Junction, NJ) for the gift support.

REFERENCES

- (1) Peer, D.; Karp, J. M.; Hong, S.; Farokhzad, O. C.; Margalit, R.; Langer, R. Nanocarriers as an Emerging Platform for Cancer Therapy. *Nat. Nanotechnol.* 2007, 2 (12), 751–760.
- (2) Merisko-Liversidge, E. M.; Liversidge, G. G. Drug Nanoparticles: Formulating Poorly Water-Soluble Compounds. *Toxicol. Pathol.* 2008, 36 (1), 43–48.
- (3) Batrakova, E. V.; Bronich, T. K.; Vetro, J. A.; Kabanov, A. V. Polymer Micelles as Drug Carriers. In *Nanoparticulates as Drug Carriers*; Torchilin, V. P., Ed.; Imperial College Press: London, 2006; pp 57–93.
- (4) Yu, B. G.; Okano, T.; Kataoka, K.; Kwon, G. Polymeric Micelles for Drug Delivery: Solubilization and Haemolytic Activity of Amphotericin B. *J. Controlled Release* 1998, 53 (1–3), 131–136.
- (5) Gao, L.; Liu, G.; Ma, J.; Wang, X.; Zhou, L.; Li, X.; Wang, F. Application of Drug Nanocrystal Technologies on Oral Drug Delivery of Poorly Soluble Drugs. *Pharm. Res.* 2013, 30 (2), 307–324.
- (6) Sun, B.; Yeo, Y. Nanocrystals for the Parenteral Delivery of Poorly Water-Soluble Drugs. *Curr. Opin. Solid State Mater. Sci.* 2012, 16 (6), 295–301.
- (7) Zhao, R.; Hollis, C. P.; Zhang, H.; Sun, L.; Gemeinhart, R. A.; Li, T. Hybrid Nanocrystals: Achieving Concurrent Therapeutic and Bioimaging Functionalities toward Solid Tumors. *Mol. Pharmaceutics* 2011, 8 (5), 1985–1991.
- (8) Cho, E. J.; Holback, H.; Liu, K. C.; Abouelmagd, S. A.; Park, J.; Yeo, Y. Nanoparticle Characterization: State of the Art, Challenges, and Emerging Technologies. *Mol. Pharmaceutics* 2013, 10 (6), 2093–2110.
- (9) Gao, Z. In Vitro Dissolution Testing with Flow-through Method: A Technical Note. *AAPS PharmSciTech* 2009, 10 (4), 1401–1405.
- (10) *The United States Pharmacopeia: The National Formulary (USP37/NF32)*; The United States Pharmacopeial Convention, Inc.: Rockville, MD, 2014.
- (11) Phillips, D. J.; Pygall, S. R.; Cooper, V. B.; Mann, J. C. Overcoming Sink Limitations in Dissolution Testing: A Review of Traditional Methods and the Potential Utility of Biphasic Systems. *J. Pharm. Pharmacol.* 2012, 64 (11), 1549–1559.
- (12) Zhao, R.; Hollis, C. P.; Zhang, H.; Sun, L.; Gemeinhart, R. A.; Li, T. Hybrid Nanocrystals: Achieving Concurrent Therapeutic and Bioimaging Functionalities toward Solid Tumors. *Mol. Pharmaceutics* 2011, 8 (5), 1985–1991.
- (13) Yang, T.; Cui, F. D.; Choi, M. K.; Cho, J. W.; Chung, S. J.; Shim, C. K.; Kim, D. D. Enhanced Solubility and Stability of Pegylated Liposomal Paclitaxel: In Vitro and in Vivo Evaluation. *Int. J. Pharm.* 2007, 338 (1–2), 317–326.
- (14) Lovich, M. A.; Creel, C.; Hong, K.; Hwang, C. W.; Edelman, E. R. Carrier Proteins Determine Local Pharmacokinetics and Arterial Distribution of Paclitaxel. *J. Pharm. Sci.* 2001, 90 (9), 1324–1335.
- (15) Bajaj, G.; Kim, M. R.; Mohammed, S. I.; Yeo, Y. Hyaluronic Acid-Based Hydrogel for Regional Delivery of Paclitaxel to Intraperitoneal Tumors. *J. Controlled Release* 2012, 158 (3), 386–392.
- (16) Willey, T. A.; Bekos, E. J.; Gaver, R. C.; Duncan, G. F.; Tay, L. K.; Beijnen, J. H.; Farmen, R. H. High-Performance Liquid Chromatographic Procedure for the Quantitative Determination of Paclitaxel (Taxol) in Human Plasma. *J. Chromatogr.* 1993, 621 (2), 231–238.
- (17) Ringel, I.; Horwitz, S. B. Taxol Is Converted to 7-Epitaol, a Biologically Active Isomer, in Cell Culture Medium. *J. Pharmacol. Exp. Ther.* 1987, 242 (2), 692–698.
- (18) Kim, J. H.; Kim, Y. S.; Kim, S.; Park, J. H.; Kim, K.; Choi, K.; Chung, H.; Jeong, S. Y.; Park, R. W.; Kim, I. S.; Kwon, I. C. Hydrophobically Modified Glycol Chitosan Nanoparticles as Carriers for Paclitaxel. *J. Controlled Release* 2006, 111 (1–2), 228–234.
- (19) Liang, H. F.; Chen, C. T.; Chen, S. C.; Kulkarni, A. R.; Chiu, Y. L.; Chen, M. C.; Sung, H. W. Paclitaxel-Loaded Poly(Gamma-Glutamic Acid)-Poly(Lactide) Nanoparticles as a Targeted Drug Delivery System for the Treatment of Liver Cancer. *Biomaterials* 2006, 27 (9), 2051–2059.

EXPERT OPINION

1. Introduction
2. Desired effects of extracellular activation of NPs
3. Stimuli
4. Extracellularly activatable nanocarriers
5. Conclusion
6. Expert opinion

informa
healthcare

Extracellularly activatable nanocarriers for drug delivery to tumors

Sara A Abouelmagd, Hyesun Hyun & Yoon Yeo[†]

[†]Purdue University, Department of Industrial and Physical Pharmacy, West Lafayette, IN, USA

Introduction: Nanoparticles (NPs) for drug delivery to tumors need to satisfy two seemingly conflicting requirements: they should maintain physical and chemical stability during circulation and be able to interact with target cells and release the drug at desired locations with no substantial delay. The unique microenvironment of tumors and externally applied stimuli provide a useful means to maintain a balance between the two requirements.

Areas covered: We discuss nanoparticulate drug carriers that maintain stable structures in normal conditions but respond to stimuli for the spatiotemporal control of drug delivery. We first define the desired effects of extracellular activation of NPs and frequently used stimuli and we review the examples of extracellularly activated NPs.

Expert opinion: Several challenges remain in developing extracellularly activatable NPs. First, some of the stimuli-responsive NPs undergo incremental changes in response to stimuli, losing circulation stability. Second, the applicability of stimuli in clinical settings is limited due to the occasional occurrence of the activating conditions in normal tissues. Third, the construction of stimuli-responsive NPs involves increasing complexity in NP structure and production methods. Future efforts are needed to identify new targeting conditions and increase the contrast between activated and nonactivated NPs, although keeping the production methods simple and scalable.

Keywords: drug delivery, extracellular activation, nanocarriers, nanoparticles, stimuli-responsive, tumor microenvironment

Expert Opin. Drug Deliv. (2014) *Early Online*: 1-18

1. Introduction

Nanoparticulate drug carriers can offer several features useful for the delivery of chemotherapeutic drugs. For example, nanoparticles (NPs) made of amphiphilic polymers can be used to solubilize hydrophobic drugs in aqueous media. NPs that securely encapsulate a drug can protect it from hydrolytic or enzymatic degradation and the loss of biological activity. NPs with an optimal size can modify the tissue distribution of a drug and reduce systemic toxicity [1,2]. NPs decorated with specific ligands can facilitate the cellular uptake of a drug and help bypass drug efflux pumps [3,4]. In order to realize these potentials, it is critical that an NP remain stable during circulation by not interacting with healthy cells, releasing the drug or entering off-target organs and tissues. On the other hand, once an NP manages to arrive at its intended targets, the NP should release the encapsulated drug in the vicinity of tumor cells or enters the cells to unload it inside. A balance between the circulation stability and the reactivity in tumors is, therefore, one of the most important properties of an ideal NP. For this purpose, many carriers are developed with materials that form stable, long-circulating NPs and maintain the chemical structures in normal physiological conditions but change their properties by chemical or mechanical stimuli to make the encapsulated drug available to target cells.

S. A. Abouelmagd *et al.*

Article highlights.
<ul style="list-style-type: none"> For successful drug delivery to tumors with nanoparticulate carriers, they should remain stable during circulation, without interacting with healthy cells, releasing drug, or entering off-target organs and tissues. Once nanoparticles (NPs) arrive at intended targets, they should release the encapsulated drug in the vicinity of tumor cells or enter the cells to unload it inside. Features of tumoral microenvironment and the externally applied physical stimuli provide a useful means to maintain the balance between circulation stability and reactivity in tumors. Unique features shared by many solid tumors such as hypoxia, acidity and overly expressed enzymes, are used as internal stimuli for the activation of nanocarriers. Noninvasive external stimuli such as light, ultrasound, magnetic field and temperature are also used for the spatiotemporal control of drug delivery. A single stimulus or combinations of multiple stimuli are employed for the extracellular activation of various types of nanoparticle systems such as inorganic or polymeric NPs, liposomes and dendrimers.
This box summarizes key points contained in the article.

Various types of stimuli-responsive NPs are extensively reviewed elsewhere [5-10]. In this review, we focus on nanocarriers that are activated in the extracellular matrix (ECM) of tumors to bring about drug release, cellular uptake or intratumoral transport (Figure 1). We briefly define the desired effects of extracellular NP activation and frequently used stimuli. We then review examples of extracellularly activated NPs or NP-related systems, ending with a discussion about

remaining challenges.

2. Desired effects of extracellular activation

of NPs

Systemic NP delivery to tumors is a three-step process: blood-borne delivery, extravasation and then passage through ECM to tumor cells [11]. The extravasation of NPs in tumors occur relatively selectively due to the difference between normal tissues and tumors in vascular permeability, a common feature shared by many solid tumors—part of the so-called enhanced permeability and retention (EPR) effect [12]. The contribution of the EPR effect to the delivery of NP to tumors has been well documented in preclinical animal studies, especially in xenograft models [13,14]. However, the universal utility of the EPR effect in human patients has recently been questioned due to significant heterogeneity within and between tumor types [15,16] and the lack of clinical evidence supporting the benefits [13,17]. Nevertheless, the EPR effect is arguably the most dominant mechanism by which NPs access solid tumors [17]. Once the NPs arrive at tumors, they are expected to distribute evenly in the tumor mass and release the payload either inside or

outside of the tumor cells. The extracellular activation of NPs is widely explored to facilitate the post-extravasation events.

2.1 Tumor-specific drug release

Once NPs are introduced to circulation, it typically takes 1–2 days for the NPs to achieve maximum tumor accumulation via the leaky vasculature [18]; therefore, it is critical to keep drug release from NPs in blood to the minimum during this period. On the other hand, the excessive attenuation of drug release also negatively influences the therapeutic effect. An ideal NP should keep the drug inside in a normal physiological condition but have a built-in mechanism to trigger drug release in a timely manner at intended targets such as tumor ECM and/or intracellular organelles.

2.2 Cellular uptake

NPs may release a drug outside the cells or enter the cells and unload the drug at the desired intracellular locations [19]. Either scenario will work if the drug can freely traverse the cell membrane. However, there are situations when NPs need to be internalized by the cells before they release the payload: when the drug is unable to cross the cell membrane efficiently (e.g., nucleic acids, peptides or proteins) or when the drug is readily removed from the cells due to drug efflux pumps in the cell membrane [20,21]. In these cases, it is often advantageous to encapsulate the drug in NPs, as they can help bypass the cellular barriers [22]. To facilitate the cellular uptake of NPs, their surfaces are decorated with cell-interactive ligands such as small molecules, peptides, antibodies or nucleic acids, which allow them to enter cells via specialized endocytosis pathways.

On the other hand, the ligand-modified NPs face a greater risk of removal by the mononuclear phagocyte system [23,24]. Therefore, NPs are designed to circulate as ‘stealth’ NPs (surface-protected with hydrophilic polymers to prevent opsonization) but expose the cell-interactive ligands or charges in

response to the applied stimuli after they arrive at tumors [25].

2.3 Extracellular particle transport

NPs arriving at tumors are expected to penetrate into the interior of the tumor mass and completely kill the tumor cells. In reality, NP distribution is limited to the periphery of the tumor mass close to the vasculature [26,27], whereas the central regions of the tumor remain unaffected [28,29] and become a potential source for tumor relapse or metastasis. Difficulties in NP penetration into tumors stem from at least two abnormal features: the increased stiffness of tumor ECM [30] and relatively high interstitial fluid pressure (IFP) [31–37]. Approaches to overcome these challenges involve pre- or co-treatment of tumors with enzymes to degrade the ECM [29,38–41], priming tumors with an apoptotic-inducer [42–45] or employing external stimuli to increase the mobility of NPs in tumors [46] or to disrupt the ECM [47–52]. In recent efforts, various stimuli were used to reduce the particle size, thereby enhancing intratumoral NP distribution.

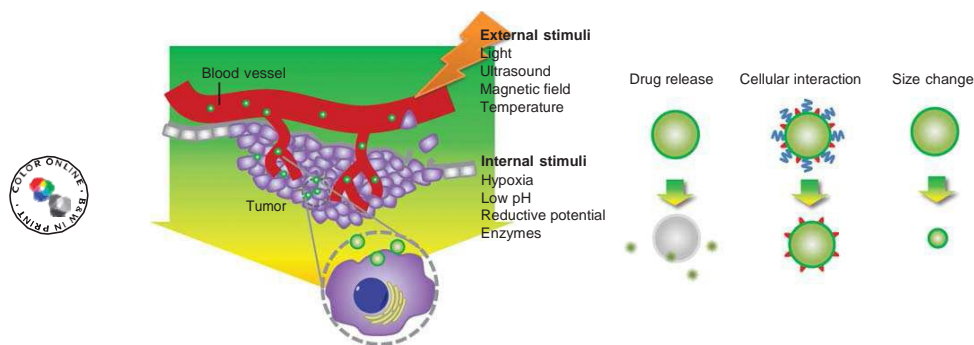


Figure 1. Schematic diagram of NPs activated in the tumoral extracellular matrix in response to internal or external stimuli. Specifically, the diagram illustrates that circulating NPs extravasate at tumors, undergo structural changes to release drug, interact with cells and/or change the particle size according to various stimuli such as light, ultrasound, magnetic field, temperature, hypoxia, low pH, reductive potential or increased enzyme levels.

NPs: Nanoparticles.

3. Stimuli

3.1 Internal stimuli

Tumor cells initiate several changes in the stroma to support their growth and progression, creating unique a microenvironment distinguished from normal tissues such as hypoxia, acidity, and overexpression of proteolytic enzymes [53,54]. Such differences have widely been used to induce the tumor-specific activation of NP drug carriers.

3.1.1 Oxygen level

Hypoxia, inadequate oxygen supplies to the interior of tumors, results from fast unorganized expansion of tumors and inadequate vascularization [54-56]. More than half of locally advanced solid tumors have regions of hypoxia, heterogeneously distributed throughout the tumor mass [54]. Hypoxia leads to several changes in cell metabolism and gene regulation responsible for increasing resistance to chemo- or radiation therapy [57]. Tumor hypoxia induces the upregulation of signaling pathways involved in the survival of hypoxic cells such as hypoxia-inducible factors, unfolded protein response and mammalian target of rapamycin [57]. Although these changes are exploited as direct targets for cancer therapy, tumor hypoxia also takes part in chemical changes serving as molecular cues to activate nanocarriers such as acidic pH and reductive environment.

3.1.2 pH

Mildly acidic pH of the tumor microenvironment is one of the most widely used features for the extracellular activation of nanocarriers [6]. The reported range of tumor extracellular pH varies with studies: some report a median value of

7.0 [58], 6.8–7.2 [56] or ~ 7.03 [59], as compared with 7.4–7.5 in normal tissues. A study on 67 tumor samples from 58 patients revealed that tumor extracellular pH ranged from 5.66 to 7.78 with an average of 7.01 [60]. The acidity of a solid tumor is attributable to metabolic abnormalities in tumor cells, including the high rate of aerobic and anaerobic glycolysis, which leads to accumulation of lactic acid [61,62], and the increased proton-pump activities in the plasma membrane, which promote the secretion of acidic metabolites into the extracellular milieu [61]. Moreover, the acidified tissues do not readily return to neutral pH due to the reduced blood flow in tumors [6]. In designing stimuli-sensitive drug carriers, the acidic pH is used to change the ionization status of the carrier molecules [63-66] or induce cleavage of acid-labile linkers [6,67]. A challenge in using the acidic pH of tumors is the small difference from the normal pH of 7.4, which require high sensitivity of the carrier molecules to the pH change [6].

3.1.3 Reductive potential

Difference in reductive potential is typically used for intracellular drug delivery [10]. The inside of the cells has glutathione (GSH) in millimolar range, which is kept reduced by NADPH and GSH reductase [68], whereas extracellular GSH concentration is around 10 μ M [69,70]. Such a difference in the reductive potential across the cell membrane is useful for intracellular activation of drug carriers, where the carriers with labile linkers like disulfide [71] or dithiobenzyl carbamate [72] are reduced in the cells to release the drug and/or undergo matrix degradation [71,73]. Normal ECM maintains a relatively more oxidized state than the intracellular environment as a function of redox-modulating proteins, extracellular thiol/disulfide couples and reactive oxygen/nitrogen species that travel across cell

S. A. Abouelmagd *et al.*

membranes [74,75]. This balance is perturbed in some tumors, resulting in elevation of the extracellular reductive potential. For example, an aggressive prostate cancer cell line (WPE1-NB26) showed twice as high extracellular GSH/GSSG ratio as that of nonmalignant prostate epithelial cells [74,75]. In addition, *in vivo* electron paramagnetic resonance spectroscopy revealed that the GSH level in radiation-induced fibrosarcoma tumors was four times higher than that in normal muscles [76]. In these tumors, the reductive potential may be used for extracellular activation of drug carriers as well.

3.1.4 Enzyme level

Enzymes overexpressed in tumors such as matrix metalloproteinases (MMPs), constitute another class of stimuli used for extracellular activation of carriers. The expression of these enzymes, which is tightly regulated in normal tissues, is upregulated in invasive tumors due to the increased need for ECM degradation [77,78]. Cathepsin B, a lysosomal cysteine proteinase, is also overexpressed in the ECM and cell surface of some tumors [79-81].

3.2 External stimuli

Although the internal stimuli are very useful for inducing disease-specific activation of drug carriers, not all the diseases have specific internal molecular triggers. In this case, noninvasive external stimuli such as light, ultrasound, magnetic field and temperature may be employed to attain the spatiotemporal control of drug delivery. Advantages of this approach include a high level of control over the duration and extent of stimuli and the possibility of combining multiple stimuli to increase the sensitivity of the system.

3.2.1 Light

Ultraviolet (UV), visible and near-infrared (NIR) lights are widely used as an external stimuli to trigger drug release and structural changes of nanocarriers. Light-stimulated systems are of particular interest because of the noninvasiveness and the ease of controlling the intensity and duration [82]. UV and short visible (< 410 nm) lights are used as an energy source to destabilize caged (deactivated) compounds, but their utility is limited to thin objects such as skin surface or external layers of organs due to the short penetration depth [83]. Longer visible and NIR (> 650 nm) lights, which can reach deeper tissues in the orders of hundreds of micrometers to centimeters, have thus gained increasing interest for *in vivo* applications [83-86]. On the other hand, lights with longer wavelengths cannot afford sufficient energy to initiate cleavage of chemical linkers directly. Therefore, long visible or NIR lights are combined with compounds such as gold NPs that absorb the lights and generate heat, which then trigger structural changes in drug carriers [83,84,87]. Alternatively, long visible or NIR lights are used with an agent that generate reactive oxygen species (ROS) upon radiation (photosensitizer) that help enhance drug release and/or intracellular trafficking of a drug [83].

3.2.2 Ultrasound

Ultrasound refers to acoustic sound with high frequencies (> 20 kHz) above those of audible sound, which penetrate deeper into inner organs than light [5,88]. Ultrasound generates various effects (heating, acoustic cavitation and acoustic radiation forces) useful for diagnosis and physical therapy of diseases [89]. These effects are lately being used as external stimuli for controlling drug delivery [90]. For example, acoustic cavitation, the growth and collapse of microbubbles in blood induce reversible changes in nanocarriers and trigger drug release [91,92]. Ultrasound applied at high amplitudes also produces mechanical actions called radiation forces, increasing extravasation and interstitial transport of drug and the carriers [89].

3.2.3 Magnetic field

External magnetic field is used in combination with magnetically responsive carriers as a way of positioning them in specific organs or tissues and triggering drug release [93,94]. A magnetic carrier should have superparamagnetism, the ability to strongly magnetize (align all magnetic moments of atoms parallel to the direction of a magnetic field) when exposed to a magnetic field and show no residual magnetization (remanence) upon the removal of the magnetic field [93,94]. Superparamagnetic iron oxide NPs (SPIONs) based on γ -Fe₂O₃, α -Fe₂O₃ and Fe₃O₄ are most commonly used as a magnetic carrier [87]. When used for external control of drug release, SPIONs are incorporated in polymer matrices or liposomes that can be deformed by heating or the movement of the magnetized particles [87].

3.2.4 Temperature

Most of the above-mentioned external stimuli generate mild heat, which provides a useful control over drug release when combined with thermosensitive materials [95]. For example, high-intensity focused ultrasound (HIFU) can produce local heating by focusing multiple ultrasound waves to deposit a high acoustic intensity in the focal volume [96]. Ideal temperature range for hyperthermia-triggered drug delivery is 41-42°C; above this range, vascular coagulation and tissue damage may occur [95,97]. For this reason, most thermosensitive liposomes are made of dipalmitoylphosphatidylcholine (DPPC), which undergoes phase transition at 41.5°C [95,98-101]. For polymeric NP systems, poly(*N*-isopropylacrylamide) (PNIPAM), which changes hydrophilicity according to the temperature, is typically used as a thermosensitive component. The transition temperature can be controlled by the polymer concentration [102], molecular weight of the polymer [103] and type and content of additional blocks [104,105]. Although thermal stimulus is mainly used to trigger drug release by causing structural changes in the carriers, it also contributes to drug delivery by increasing vascular permeability [97,106-108] and/or decreasing high interstitial tumor pressure [109], thereby enhancing extravasation and intratumoral transport of NPs.

4. Extracellularly activatable nanocarriers

295 Extracellular activation has been employed in various types of NP systems, including inorganic or polymeric NPs, liposomes and dendrimers. Such systems respond via drug release and cellular interactions through different mechanisms. The following section introduces recent examples of extracellularly activated NPs, classified by the consequences of the stimuli-triggered activations. Although drug carriers are the main focus of this review, imaging agents are also mentioned when relevant in principle. The readers are also advised to note that in many cases, NP activation was demonstrated in relatively extreme *in vitro* conditions (e.g., pH 5.5) than those faced *in vivo* to represent clear contrasts between the activated and nonactivated status.

4.1 Control over drug release

4.1.1 Internal stimuli

4.1.1.1 pH

310 For pH-triggered drug release, acid-labile linkers such as hydrazone, acetal or ester bonds are frequently used, although the triggering pHs for these linkers are somewhat low for extracellular drug release. Polyhistidine (pHis) is another chemical moiety widely used for pH-sensitive drug carriers. The pH sensitivity of pHis comes from the imidazole group, which protonates in acidic pH with a pKa value of ~6 [110]. Polymeric micelles prepared with a block-copolymer of pHis and PEG showed higher drug release at acidic pH as pHis block turned hydrophilic with protonation [110,111]. More recently, a pHis-based AB₂-miktoarm polymer (mPEG-*b*-pHis) was designed to form polymersomes, thin-walled polymer vesicles similar to liposomes [112]. Below pH 7.4, the polymersomes underwent conformation changes to cylindrical micelles, spherical micelles and finally to unimers, showing increasing drug release [112].

325 Alternatively, chitosan and its derivatives are used as a component of NPs for pH-triggered drug release. Magnetic nanocrystals and DOX were encapsulated in micelles made of amphiphilic chitosan derivative, *N*-naphthyl-*O*-dimethylmaleoyl chitosan with an average size of 158.8 nm at pH 7.4. Exposure to acidic medium induced hydrolysis of maleoyl group, which caused the loss of amphiphilicity and destabilization of micelle structure, as evidenced by a significant increase of particle size at pH 6.5 [113]. The pH-induced change caused an abrupt DOX release (90% release in 24 h) at pH 5.5 as compared with 20% at pH 7.4 [113]. In another study, chitosan NPs were used as a pH-sensitive carrier of methotrexate (MTX). MTX-loaded chitosan NPs (MTX-CS-NPs) were prepared by ionic gelation of chitosan via tripolyphosphate and an anionic surfactant (77KL), which has a membrane-lytic activity [114]. MTX release from the NPs increased with pH decrease due to the protonation of 77KL and MTX, leading to decreased electrostatic interactions with chitosan and destabilization of the NPs. Consequently, MTX-CS-NPs showed

enhanced cytotoxic effect on MCF-7 cells at pH 6.6 as compared with pH 7.4, whereas free MTX did not show such pH sensitivity [114].

4.1.1.2 Enzyme level

350 When the enzyme level in ECM is used to trigger drug release, the enzyme-cleavable peptide substrates are used as a structural component of a nanocarrier [67,115-117]. MMP-sensitive liposomes were developed using a lipopeptide with a cleavage site for MMP-9 [115]. The lipopeptide was mixed in the lipid bilayer of a liposome generating a triple helical structure that was destroyed by MMP-9 and caused the release of liposomal contents [115]. A model compound (carboxyfluorescein loaded in the liposomes) was released according to the concentration of MMP-9 in release medium (40% in 200 nM MMP-9 and 100% in 2.3 μ M MMP-9) [115]. Peptide cleavage was MMP-9-specific, with none of MMP-7, MMP-10 or trypsin able to trigger liposomal destabilization and payload release [115].

4.1.1.3 Reductive potential

365 Most nanocarriers using the redox potential difference as a trigger of drug release contain disulfide bond, which is cleaved in a relatively reductive environment. Although the increased reductive potential is a potentially useful cue for extracellular activation of NPs, most examples in the literature have been evaluated in the context of intracellular drug delivery. Collagen, a natural component of ECM, was conjugated on the MSN surface via disulfide bond to serve as a capping material [118]. The collagen-capped MSNs released only 7% of the encapsulated fluorescein isothiocyanate (FITC) in PBS (pH 7.4) in 3 h but released additional 80% of FITC after the addition of dithiothreitol (DTT) to 30 mM [118]. It is worthwhile to note that, despite the widespread use as a synthetic substitute for GSH, DTT may not result in similar drug release patterns as GSH, depending on the nature of drug-carrier interactions. Nanohydrogels composed of poly (methacrylic acid) cross-linked via *N,N*-bis(acryloyl)cystamine were prepared as a redox-sensitive carrier of DOX [119]. With the addition of 10 mM DTT to the medium, DOX release increased from 15 to 27% after 24 h, whereas with 10 mM GSH, drug release dramatically increased to 80% [119]. This difference is explained by the electrostatic interaction between the hydrogel and DOX that was effectively displaced by partially protonated GSH but not by DTT.

4.1.1.4 Hypoxia

390 For the synthesis of hypoxia-activated prodrugs for cancer therapy, 2-nitroimidazoles have been used, which undergo selective bioreduction in hypoxic conditions [57,120]. Using the same principle, a 2-nitroimidazole was conjugated to a hydrophilic carboxymethyl dextran backbone to produce a hypoxia-sensitive polymeric system [121]. This polymer conjugate formed an NP with a hydrophobic 2-nitroimidazole core,

S. A. Abouelmagd *et al.*

400 loaded with a base form of DOX. Under hypoxic conditions, 2-nitroimidazole underwent a series of bioreductions to form more hydrophilic 2-aminoimidazole, destabilizing the NP structure and releasing the loaded DOX [121]. *In vitro* release studies were performed in hypoxic (degassed PBS containing NADPH as electron donor) versus normoxic conditions (PBS containing NADPH with no degassing); after 12 h, complete DOX release was observed in hypoxic medium, but 49% in normoxic medium. The DOX-loaded NPs showed greater inhibition of SCC7 cancer xenograft growth than an equivalent dose of free DOX [121].

4.1.2 External stimuli

4.1.2.1 Temperature

410 Thermosensitive liposomes (TSLs) are frequently used for heat-induced drug release control. Several TSLs have been reported using DPPC as a main component. For example, TSLs prepared with DPPC, hydrogenated soy sn-glycero-3-phosphocholine, cholesterol and 1,2-distearoyl-sn-glycero-3-phosphoethanolamine-*N*-PEG 2000 (DSPE-PEG) released drug upon heating at 42–45°C for 30 min [122]. Various lipid compositions have been explored to control the thermosensitivity of TSLs. TSLs prepared with DPPC, MSPC (1-stearoyl-2-hydroxy-sn-glycero-3-phosphatidylcholine), DSPE-PEG released the drug completely at > 40°C in 10 min [123]. TSLs more quickly responding to temperature were prepared by replacing MSPC and DPSE-PEG with a nonionic surfactant (Brij78) [123]. TSLs responding to a relatively low temperature (39–40°C) for a short period of time (low TSL) were developed using a mixture of DPPC, 1-palmitoyl-2-hydroxy-sn-glycero-3-phosphocholine (MPPC) and DSPE-PEG [122] and used with HIFU-induced hyperthermia [124]. The low TSLs showed minimal drug release in 2 min at 37°C but 50% drug release 42°C during the same period. The low TSLs exposed to pulsed HIFU (1300 W/cm², 0.1 s on and 0.9 s off for 120 times) showed significantly faster and greater drug delivery to tumors as compared with non-TSLs [124]. The growth of tumors in animals treated with repeated IV injections of low TSLs and HIFU was significantly delayed as compared with no HIFU group [124].

4.1.2.2 Ultrasound

435 Acoustic cavitation is used to trigger drug release from nanocarriers. In a recent example, ultrasound was applied to localize drug release from liposomes on tumors [125]. Liposomes were prepared with DSPE, cholesterol, 1,2-distearoyl-sn-glycero-3-phosphocholine and DSPE-PEG, including luciferin as a model active ingredient. The liposomes circulated with no significant leakage of luciferin. When ultrasound was applied to tumors in the presence of SonoVue[®], phospholipid-stabilized microbubbles to enhance cavitation effects, the liposomes were destabilized and released luciferin, producing 16 times higher luminescence signal in tumors than nonstimulated ones [125]. An important feature of this approach is that with the aid of SonoVue the ultrasound

450 activation could be carried out under conditions used in diagnostic ultrasound scanners. This is a significant improvement over previous approaches as it alleviates the need to use a high-intensity ultrasound wave that may generate damages to nontarget tissues [125].

4.1.2.3 Light

455 To use NIR as an external stimulus to cause drug release, a reservoir-type drug carrier was developed using a nanocomposite ethylcellulose membrane containing gold nanoshells and PNIPAM-based thermosensitive nanogels as a drug diffusion barrier [126]. When triggered by a NIR laser (808 nm), gold nanoshells generated heat beyond a critical temperature of nanogels, causing them to shrink and leave pores in the membrane through which the encapsulated drug could be released [126]. This system allowed for NIR-triggered release of aspart, a fast-acting insulin analog, from the subcutaneously implanted device, effectively reducing blood glucose over 14 days. On the other hand, a critical challenge is to increase the response temperature substantially higher than 37°C and prevent accidental drug release due to fever or hot weather but to keep it low enough to avoid tissue damages (< 43°C) [127].

4.1.2.4 Magnetic field

460 The same principle was applied using an oscillating magnetic field as a release trigger [128,129]. For this purpose, the diffusion barrier was prepared with paramagnetic magnetite NPs as the triggering entity, which generated heat (+2°C) by an external oscillating magnetic field and induced nanogel shrinkage and drug diffusion from the device [128]. Depending on the phase-transition temperature and loading density of nanogels as well as the membrane thickness, this device showed 6–15 times increase in drug release rate by heating and maintained the zero-order release kinetics through the duration of on-state [129].

4.1.3 Multiple stimuli

485 Several stimuli may be used in combination to facilitate the formation of NPs, increase the flexibility in release control or increase the selective reactivity of a system to stimuli [5,130–132]. For example, pH- and temperature-sensitive micelle system was produced using a block copolymer consisting of poly(NIPAM-co-acrylic acid) and polycaprolactone [133]. The hydrophilic block of this polymer, poly(NIPAM-co-acrylic acid), imparted the sensitivity to temperature and pH based on the phase transition of PNIPAM in increasing temperature and protonation of acrylic acid in acidic pH [133]. Paclitaxel (PTX) encapsulated in this micelle system was released most quickly when both conditions were met [133].

495 A mesoporous silica material capped with boronic acid-modified gold NPs is another pH-/temperature-sensitive system [134]. A saccharide derivative was anchored on the external surface of mesoporous silica-based material 41, where multiple alcohol groups of the saccharide derivative had reversible interactions with boronic acid of gold NPs by forming boronate

Extracellularly activatable nanocarriers for drug delivery to tumors

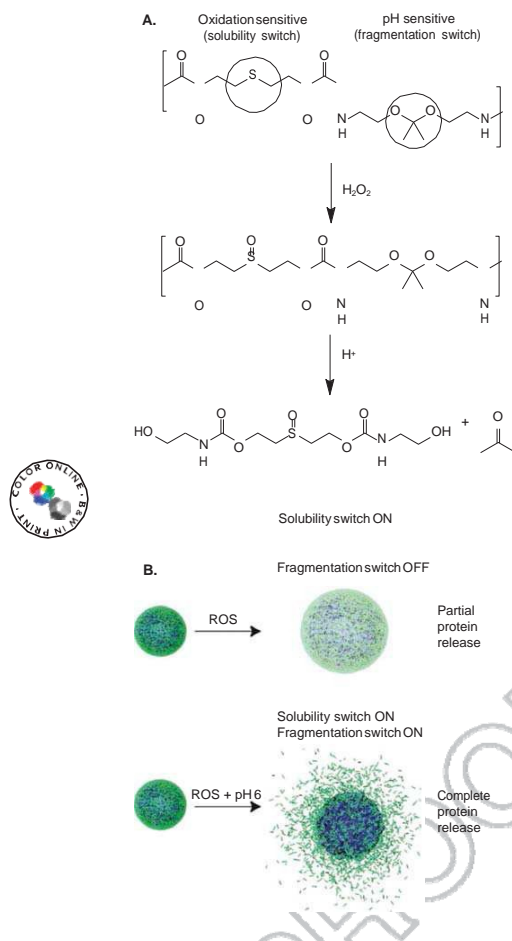


Figure 2. (A) Degradation mechanism of polythioether ketal. Hydrogen peroxide and acidic pH stimulate the degradation of the polymeric nanoparticles in tandem. (B) Schematic diagram of polythioether ketal-based NP system, which releases drug in response to acidic pH and ROS. Reprinted with permission from [135]. Copyright (2011) American Chemical Society. NP: Nanoparticle; ROS: Reactive oxygen species.

esters [134]. The boroster bonds were hydrolyzed at pH 3 or cleaved thermally by plasmonic heat emitted from NIR-irradiated gold NPs, removing the capping gold NPs and releasing molecules entrapped in the pores of the silica device [134]. Although this approach opens up a new possibility of designing stimuli-induced release systems, the present format has a limited utility for drug delivery purposes due to the low trigger pH (pH 3) and the heat generated by the long wavelength NIR laser itself.

A polythioether ketal-based NP system was produced to activate drug release in response to acidic pH and ROS, which changed hydrophilicity and degradation rate, respectively

(Figure 2) [135]. Upon the exposure to ROS, thioether groups in the polymer backbone underwent oxidation to sulfone, turning the polymer from hydrophobic to hydrophilic. On the other hand, ketal groups in the backbone underwent rapid acid-catalyzed hydrolysis in mildly acidic condition [135]. The polythioether ketal-based NPs showed complete degradation and drug release in 24 h when both conditions were

provided [135]. In contrast, the NPs in neutral pH with no oxidative reagents showed minimal release of model drugs over the same period of time [135].

An important advantage of multiple-stimuli-sensitive system is the potential to precisely regulate the drug release according to the combination of stimuli. To enhance the precision of control, a polymeric micelle system responding to triple stimuli (temperature, pH and redox potential) was developed using a block-copolymer comprising of an acid-sensitive hydrophobic core (poly(hydroxyethyl methacry-

late), temperature-sensitive hydrophilic shell (PNIPAM) and redox-sensitive interface (disulfide linker) [136]. The decrease of pH converted acid-sensitive hydrophobic block to hydrophilic one, temperature increase made PNIPAM hydrophobic and a reducing environment induced cleavage of block-copolymer to individual homopolymers, all contributing to disassembly of the micelle system. Notably, individual stimulus caused slow or incomplete release of the encapsulated dye, but combined stimuli led to a significantly faster and greater release [136].

4.2 Control over cellular uptake

Promoting selective interaction of nanocarrier systems with tumor cells is achieved by removing protective surface layers from the carriers or transforming the surface properties in a tumor-specific manner. Most nanocarriers are protected by

nonionic hydrophilic polymers to avoid nonspecific interac-

tions with immune cells and normal tissues during circulation. Removal or transformation of such a protective surface results in exposure of cationic charges or cell-interactive ligands, thereby allowing for electrostatic or ligand-mediated interactions with the cell membrane. This effect can be achieved by employing a stimulus-sensitive linker as a component of the carrier polymer or using a stimulus-sensitive polymer for a protective surface.

4.2.1 Internal stimuli

4.2.1.1 pH

To increase cellular uptake at acidic tumoral pH, a polymeric micelle system was developed using a blend of pHis-based amphiphilic polymers [137]. The micelle was made of a blend of pHis_{2kD}-*b*-PEG and PLA-*b*-PEG-*b*-pHis_{2kD}-TAT, where pHis_{2kD} and PLA blocks from each polymer formed a hydrophobic core and PEG formed a shell. At pH 7.4, PEG from the latter polymer formed a loop as pHis_{2kD} block remained

S. A. Abouelmagd *et al.*

unionized and associated with the hydrophobic core, keeping the cell-interactive TAT away from the surface. Below pH 7.2, pHis_{20D} started to ionize, exposing the TAT on the surface to facilitate cellular uptake of the polymeric micelles [137]. Due to the enhanced cellular uptake, the micelles carrying showed a greater cytotoxic effect on drug-resistant lower, where PAMAM dendrimer was no longer protected and allowed to A consistent result was observed in a mouse model of a drug-resistant ovarian cancer xenograft [137].

The PAMAM dendrimer was electrostatically coated with ZWC, which was anionic in neutral pH, reducing toxicity associated with the cationic charge of the dendrimer and preventing cellular uptake of PAMAM dendrimers (Figure 3). On the other hand, in mildly acidic pH such as pH 6.5 or DOX showed a greater cytotoxic effect on drug-resistant lower, where ZWC acquired more positive charges, the NCI/ADR-RES cells interact with the cell membrane and enter the cells (Figure 3) [66].

In another study, a layer-by-layer approach was used to multilayered ~ 80 nm NPs with a fluorescent core and be used to promote pH-sensitive cell interactions [142]. A pH PEG-coated surface [138]. The core particle was a carboxyl- low insertion peptide (pHLIP) is a pH-sensitive peptide functionalized quantum dot (QD). The negatively charged made of 38 amino acids with moderate water solubility [142]. core particle was first coated with poly-L-lysine (PLL)-imino- As pH drops from 7.4 to 6.5, it becomes more hydrophobic biotin conjugate and neutravidin, which was then coated with with protonation of Asp and Glu residues and inserts its tail mPEG-biotin conjugate. Under acidic pH, the iminobio- into the cell membrane lipid bilayer, helping NPs modified tin- neutravidin linker was decomposed due to the reduced with the peptide to enter cells [142,143]. pHLIP was conjugated affinity of the protonated iminobiotin for neutravidin. The with MSN, an inorganic drug carrier, via a disulfide decomposition of iminobiotin--neutravidin bonds were dem- bond [143]. When placed in mildly acidic pH, the pHLIP- onstrated over a range of pH 4--7.4, where the decomposition conjugated MSNs were readily taken up by cells in which rate increased linearly with the decrease of pH. This caused the disulfide linker was reduced and the loaded DOX the external PEG layer to be shed and a cationic PLL layer released. Due to the pH-induced cellular uptake, this system exposed, thereby facilitating cellular uptake of QD cores in showed greater cytotoxic effects in both drug sensitive acidic environment. After incubation in a pH 5.5 medium, (MCF-7) and resistant (MCF-7/ADR) cell lines at pH 6.5 NPs showed significantly higher cellular uptake in five differ- relative to those at pH 7.4 [143]. A similar approach was used ent cancer cell lines as compared with those in pH 7.4 [138]. As to enhance tumor uptake of gold NPs [142].

4.2.1.2 Enzyme level

The removal of a protective layer can be induced by enzymes abundant in tumor ECM. PLGA NPs were dual-coated with layer that becomes more cell interactive in tumoral pH. For a cell penetrating peptide (TAT peptide) and PEG for example, low- molecular-weight chitosan (LMWC) was used promoting cellular uptake and preventing nonspecific exposure of the TAT peptide, respectively [67]. The surface 595 as a pH-sensitive surface coating. Chitosan is a polysaccharide with primary amines, which impart a unique pKa of 5.5--6.5 PEG was conjugated to the NP surface via a MMP-2 cleavable 650 [139], matching the weakly acidic pH of tumor tissues [63]. Due to the reduced molecular weight (< 6500 Da), LMWC remains neutral yet hydrophilic at pH 7.4, thus qualifying for a stealth peptide linker, so that it could be removed in a MMP-2-rich to environment such as tumoral ECM, allowing the TAT peptide to promote cellular uptake of NPs. The dual-modified PLGA 655 NPs showed minimal uptake by SKOV-3 cells in MMP-2-free medium but significantly enhanced cellular uptake after treat- ment with MMP-2. In contrast, NPs with noncleavable PEG slightly showed minimal cellular uptake, irrespective of the presence in acidic 660 pH. Consequently, PLGA-LMWC NPs showed of MMP-2. Consistent with the MMP-2-dependent cellular uptake, the dual-modified NPs loaded with PTX resulted in greater interactions with SKOV-3 cells at pH 6.2 than at pH uptake, the dual-modified NPs showed a greater cytotoxic effect after MMP-2 treatment than non- 665 7.4, whereas the unmodified PLGA NPs showed limited cellular uptake irrespective of the pH [63]. treated ones, although the difference was not as clear as the cellular uptake due to the high initial burst release of the drug [67].

Another example involves a cationic polyamidoamine (PAMAM) dendrimer coated with a zwitterionic chitosan derivative (ZWC) [66]. Amine-terminated PAMAM dendrimer is an attractive carrier of drug and gene therapeutics due to the well-defined structure and functionalization potential; how- ever, the utility is limited because of undesirable cytotoxic itate cellular uptake and then to lower lysosomal pH (5--5.5) effects [140]. Created by partial amidation of chitosan, ZWC to enhance intracellular drug release [144]. A DOX--polymer 670 showed a negative charge in a relatively basic condition and conjugate (PPC-Hyd-DOX-DA) was synthesized by conju- gating 3-dimethylmaleic anhydride (DA) and DOX to a positive charge in an acidic condition, where the transition block-copolymer of mPEG and cysteamine-modified poly

Extracellularly activatable nanocarriers for drug delivery to tumors

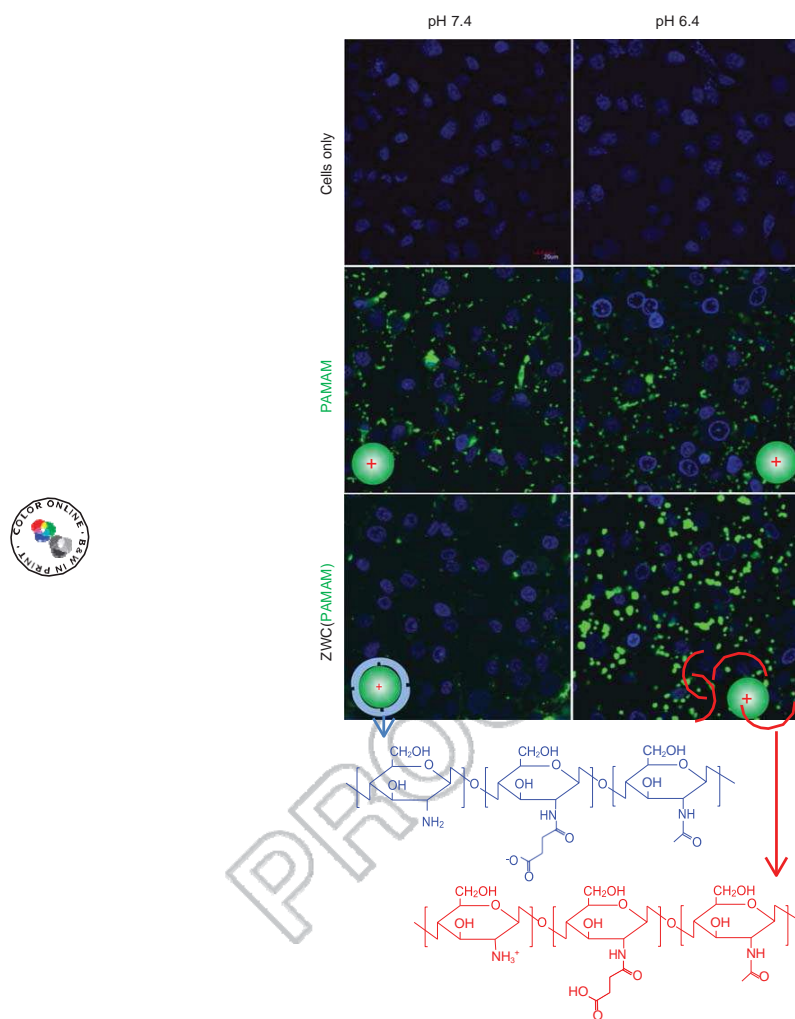


Figure 3. Cellular uptake of PAMAM or ZWC(PAMAM) at pH 7.4 (left) and pH 6.4 (right). Green: PAMAM dendrimers; blue: nuclei. Fluorescently labeled PAMAM dendrimers (green) appeared in or on the cells irrespective of the pH. In contrast, PAMAM dendrimers coated with ZWC showed minimal cellular interactions at pH 7.4, whereas strong green signals were observed in or on the cells at pH 6.4, where the dendrimers were no longer protected by ZWC.



Adapted with permission from [66]. Copyright (2013) American Chemical Society.

PAMAM: Polyamidoamine; ZWC: Zwitterionic chitosan derivative.

S. A. Abouelmagd *et al.*

(allyl ethylene phosphate) (mPEG-*b*-PAEP-Cya, PPC), via amide and hydrazone bond, respectively. Here, the amide bond with *b*-carboxylic acid of DA and amino group of cysteamine is cleavable at slightly acidic conditions like pH 6.8 [145], whereas hydrazone bond is cleaved at lower pHs. The polymer conjugate formed self-assembled NPs with an average diameter of ~ 27 nm that underwent two levels of changes according to the pH [144]. First, the *b*-carboxylic amide bond between DA and polymer cleaved at pH 6.8,

680 increasing the cationic charge density, thus enhancing cellular uptake of NPs. After the uptake and endosomal localization, the hydrazone link between DOX and polymer was cleaved off and the drug was released [144]. Due to the pH-sensitive enhancement of cellular uptake and intracellular drug release, 685 the NPs achieved greater cytotoxicity in drug-resistant cancer stem cells than free DOX at pH 6.8 [144].

Similarly, NPs responding to multiple levels of pH were developed to induce NP-cell interaction and drug release according to the environment. Dual-pH-sensitive polymeric 690 micelles were prepared using two block copolymers, poly(L-histidine)-*b*-short branched polyethyleneimine (pHis-*b*-sbPEI) and mPEG-*b*-polysulfadimethoxine (mPEG-*b*-PSDM) [64]. pHis-*b*-sbPEI self-assembled to yield core polymeric micelles, where pHis formed a pH-sensitive hydrophobic core and sbPEI

695 formed a cationic shell. The core micelles were coated with mPEG-*b*-PSDM via pH-sensitive electrostatic interactions between sbPEI and PSDM. The pH-sensitivity of the shielded micelles came from PSDM, negatively charged at neutral pH but uncharged in slightly acidic conditions. At mildly acidic 700 pH, the micelles lost an mPEG-*b*-PSDM layer due to the weakening electrostatic interactions with the PEI shell and the exposed cationic surface then interacted with the surface of tumor cells. Once taken up by cells, the core pHis-*b*-sbPEI micelles were destabilized and released the loaded PTX in the 705 endo/lysosomal pH as the pHis block started to protonate. The shielded micelles were stable in serum due to the protective effect of PEG and showed minimal cellular uptake at pH 7.4 but significantly enhanced uptake at < pH 6.6. When injected IV in MCF-7 tumor-bearing mice, the shielded micelles 710 showed superior tumor growth inhibition as compared with free PTX or the unshielded core micelles [64].

In a recent example, pH and ultrasound were used in combination for the delivery of oncolytic adenovirus to tumors [146]. Adenovirus was coated with a new stealth polymer, *N*-(2-hydroxypropyl) methacrylamide copolymer containing pH-sensitive hydrazone bonds that degraded at acidic intratumoral pH to restore the ability of virus to bind and infect specific cancer cells. Focused ultrasound was used along with SonoVue to produce an intense cavitation effect

720 that enhanced the penetration of viral particles into the acidic interior of tumors. The combination of ultrasound-mediated tumor penetration and pH-sensitive deshielding of virus led to significant improvement in tumor growth inhibition and survival of tumor-bearing mice as compared with non-ultrasound-stimulated ones [146].

4.3 Control over extracellular particle transport

Although the approved NP products have particle sizes ranging from 100 nm or higher (e.g., Doxil), recent animal studies find that sub-100 nm sizes are required for effective tumor penetration. Kataoka *et al.* report that only 30 nm polymeric micelles can penetrate poorly permeable pancreatic tumors to achieve an antitumor effect [147]. Similarly, Allen *et al.* found that 25 nm, but not 60 nm, polymeric micelles penetrate into breast tumor xenografts [2]. Chan *et al.* also showed using PEGylated gold NPs that smaller particles (20 nm) penetrated better into tumor matrix than larger NPs (40–100 nm) [148]. On the other hand, such a small NP is not necessarily beneficial for the accumulation and retention in tumors [148] and the drug loading capacity [149]. To address these conflicting needs, NPs are engineered to circulate as relatively large particles and be reduced to smaller NPs by internal and external stimuli. Alternatively, stimuli are also used to *increase* the particle size after arrival at tumors [150]. In this case, NPs are delivered as relatively small particles to take advantage of the EPR effect but swell in the tumoral ECM so that their retention in the intended locations may be improved.

4.3.1 Internal stimuli

4.3.1.1 Enzyme level

Wong *et al.* reported an NP system changing the size in tumor ECM according to high MMP levels [11]. The NPs consist of cross-linked gelatin core with an average diameter of 100 nm, on which 10 nm QD NPs were covalently bound on the surface. The 100 nm size allowed the NPs to circulate and reach the tumor via the EPR effect; once in the tumor with an elevated level of MMP-2, the gelatin core degraded to release 10 nm QD NPs that could better penetrate into tumors. When injected intratumorally in mice bearing HT-1080 tumors with high MMP-2 activity, the gelatin-QD NPs showed greater penetration into tumor tissues than silica-QD NPs that did not change the size [11].

4.3.2 External stimuli

4.3.2.1 Light

To improve tissue penetration and drug release in target tissues, Tong *et al.* developed a lipid-based NP system composed of DSPE-PEG, lecithin and a spiropyran-alkyl conjugate (SP-C9), which reduced the average size from 150 to 40 nm upon the exposure to UV light (365 nm) (Figure 4) [151]. The photo-triggered shrinkage resulted from the isomerization of hydrophobic SP to zwitterionic merocyanine (MC) and subsequent movement of MC to hydrophilic PEG layer, which let alkyl chains of DSPE and lecithin form tighter assembly in the hydrophobic core [151]. The shrunken NPs swelled back with the removal of UV as MC reverted to SP and translocated to the core. After photo-triggering, NPs encapsulating fluorescent dyes showed greater penetration into a dense collagen gel and the cornea than free dyes and NPs with no UV trigger [151]. Although the use of UV light may limit the utility of this system in drug delivery to tumors,

Extracellularly activatable nanocarriers for drug delivery to tumors

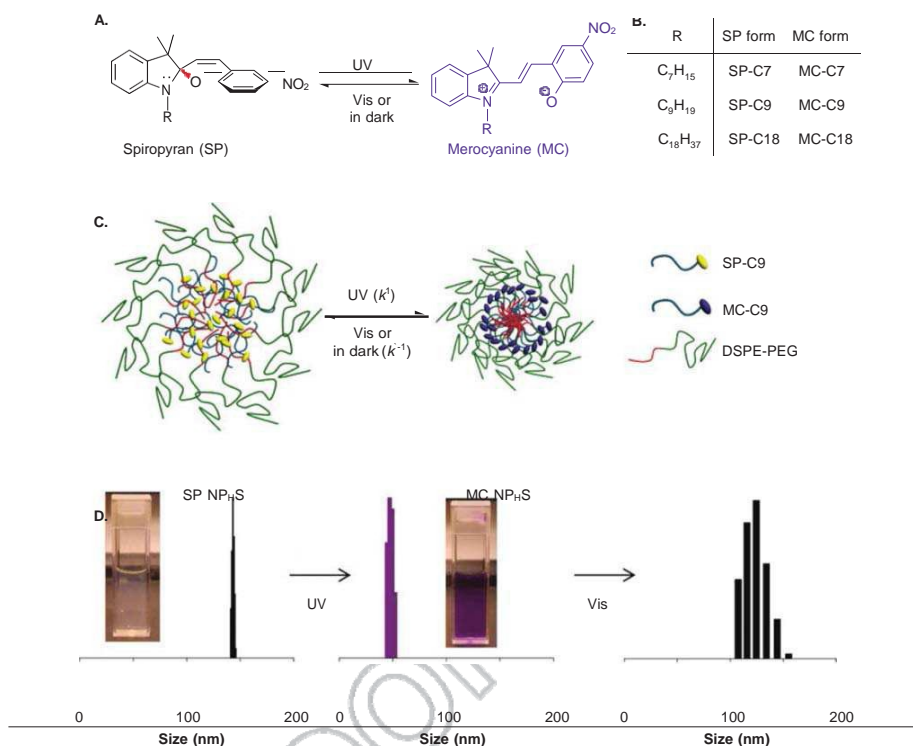


Figure 4. (A) Structure and photoisomerization reaction between SP and MC. (B) Abbreviations for SP and MC derivatives. (C) Scheme of photoswitching SP NP composed of SP-C9 and DSPE-PEG. Yellow oval, SP molecule; blue line, alkyl chain (R) in SP; red, lipid part; green line, PEG. SP NP are converted to MC NP (purple oval, MC molecule) by UV light irradiation; the reversible photoisomerization from MC NP to SP NP happens in dark but is accelerated by visible light (500–600 nm). (D) Dynamic light scattering measurement of size changes of SP NP composed of SP-C9, DSPE-PEG and lecithin. Inset: the solution of NPs before and after UV irradiation.

Reprinted with permission from [151]. Copyright (2012) American Chemical Society.

DSPE-PEG: 1,2-distearoyl-sn-glycero-3-phosphoethanolamine-PEG; MC: Merocyanine; NP: Nanoparticle; SP: Spiropyran; UV: Ultraviolet.

780 it is conceivable to introduce similar features in other types of
NPs to enhance drug delivery into the tumor interior, which
can be hard to reach due to the dense interstitial matrix.

4.3.2.2 Temperature

785 Thermosensitive composite microparticles were developed to
control the surface adhesion of circulating particles by thermal
stimulus [152]. The microparticle consisted of a PNIPAM core
particle containing SPIONs and a surface stabilized with SiO₂
particles. Heating SPIONs with the magnetic field resulted in a
790 reduction of the particle size, which in turn reduced the drag
force on the particles in the flow and helped them remain bet-
ter adherent to a surface [152]. This principle may be useful for
controlling distribution and retention of the circulating
nanocarriers.

4.3.3 Multiple stimuli

795 A dual temperature- and pH-responsive polymeric micelle
system based on mPEG-*b*-P(HPMA-Lac-co-His) was devel-
oped to facilitate drug encapsulation and micelle retention in
tumors [150]. The hydrophobic segment of this polymer
consisted of poly(*N*-(2-hydroxypropyl) methacrylate dilactate
(HPMA-Lac) and pHis, which provided thermosensitivity and
pH-sensitivity, respectively [150]. P(HPMA-Lac-co-His) had a
low cloud temperature (< 10°C), allowing for efficient micelle
formation and drug encapsulation by quick heating [150]. At
physiological temperature, the particle size gradually increased
and drug release occurred due to the accelerated hydrolysis of
lactic acid side chains and further accelerated at relatively
805 acidic pH of tumor ECM [150]. The authors propose that the
micelles initially maintain a desirable size (< 60 nm)

S. A. Abouelmagd *et al.*

for circulation and tumor accumulation but are better retained in tumors due to the increasing size (> 80 nm) in a condition
810 best met by tumor ECM (physiological temperature and acidic pH).

5. Conclusion

The success of NP-based drug delivery depends on the circulation stability of NPs and their ability to deliver the drug at the
815 right location and time. Unique microenvironment of tumors and externally applied physical stimuli provide useful means to maintain a fine balance between the two properties. Recent studies show examples of NP systems that respond to a wide variety of internal and external cues in the tumor ECM. The
820 majority of these systems are studied at preclinical levels and a lot remains to be done to translate the technical potential to clinical benefits. Future efforts are required to increase the choices of stimuli-sensitive biomaterials. Equally important is the advancement in imaging technology to locate tumor
825 lesions and technologies to apply external stimuli in a focused and noninvasive manner.

6. Expert opinion

Extracellularly activatable nanocarriers have shown a great potential to achieve drug delivery to tumors in a target-specific
830 manner, but several challenges remain.

First, some of the stimuli-responsive NPs undergo incremental changes in response to stimuli, which often translates to low circulation stability. For example, DOX conjugated to MSNs via a pH-sensitive hydrazone linker showed a linear increase in
835 drug release with the decrease of the solution pH [153] and MMP-sensitive liposomes showed gradual increase in the release of a model compound with the increase of the MMP-9 concentration [115]. When the responses are linearly proportional to the intensity of stimuli, there is a good chance that
840 the NPs undergo inadvertent changes upon small fluctuations in environmental conditions. If the changes are irreversible, their circulation stability will be significantly compromised. The instability issues tend to be underestimated during development because of the overly simplified test conditions (e.g.,
845 buffered saline in lieu of blood) or the lack of analytical tools to predict the stability of NPs in complex fluids. Many NP systems with promising *in vitro* effects fail at later stages of development due to the insufficient improvement from free drugs, resulting from their instability during circulation [154]. On the
850 other hand, an effort to improve the NP stability can lead to poor responsiveness to the stimuli. In this regard, it is worthwhile to note recent approaches that combine multiple stimuli to increase the contrast between responses to normal and tumoral conditions [135, 136].

855 Second, although many internal stimuli inherent to tumors have been identified in the literature, their applicability in

clinical settings is often questioned as such conditions occasionally occur in normal tissues. For example, acidic environment can develop in conditions like ischemia or inflammation [155, 156] and small fluctuations in body temperature can occur due to fever or hot weather. It is also suggested that MMP activation occurs in circulation rather than in tumor tissues [157]. Moreover, conditions to activate NPs may not be readily met if they are located far away (e.g., acidic and hypoxic regions) from the perivascular regions where NPs typically accumulate [158] or parts of the NP construct interfere with the access of the activating conditions (e.g., interference of PEG with an enzyme access to the cleavage site). In order to further advance the field of stimuli-responsive nanocarriers, it is necessary to make interdisciplinary efforts to identify new targeting stimuli and understand their physiological backgrounds.

Third, the need to address the intricate nature of tumor biology often leads to increasing complexity in NP structure and production methods. Technical complexity is seldom considered an issue in academia but rather encouraged for the advancement of materials science. However, if the complexity is not justified by the substantial improvement in therapeutic benefits, it is difficult to gain significant attention from the consumers. In particular, the growing complexity leads to increasing difficulties in quality control of the production, toxicological studies of the product and regulatory approval processes, which pose significant obstacles in the late stage of new product development. Whereas multiple chemical functionalities may be an integral part of a versatile carrier, a conscious effort towards a simple and scalable method should
885 be made in tandem in the early phase of development.

Acknowledgment

SA Abouelmagd and H Hyun contributed equally to this work.

Declaration of interest

The authors were supported by a Lilly endowment to the College of Pharmacy at the authors University. This work was supported by the National Institute of Biomedical Imaging and Bioengineering of the National Institutes of Health under Award Number R01EB017791, a grant from the Lilly Endowment, Inc., to College of Pharmacy, and a Doctoral Fellowship from the Egyptian Government Ministry of Higher Education Missions Sector to S.A.A. The authors have no other relevant affiliations or financial involvement with any organization or entity with a financial interest in or financial conflict with the subject matter or materials discussed in the manuscript apart from those disclosed.

Extracellularly activatable nanocarriers for drug delivery to tumors

Bibliography

Papers of special note have been highlighted as either of interest (.) or of considerable interest (•) to readers.

1. Chu KS, Hasan W, Rawal S, et al. Plasma, tumor and tissue pharmacokinetics of docetaxel delivered via nanoparticles of different sizes and shapes in mice bearing SKOV-3 human ovarian carcinoma xenograft. *Nanomedicine* 2013;9(5):686-93
2. Lee H, Fonge H, Hoang B, et al. The effects of particle size and molecular targeting on the intratumoral and subcellular distribution of polymeric nanoparticles. *Mol Pharm* 2010;7(4):1195-208
3. Brotschie A, Grieser F, Ashokkumar M. Characterization of acoustic cavitation bubbles in different sound fields. *J Phys Chem B* 2010;114:11010-16
4. Wu J, Nyborg WL. Ultrasound, cavitation bubbles and their interaction with cells. *Adv Drug Deliv Rev* 2008;60(10):1103-16
5. Cheng R, Meng FH, Deng C, et al. Dual and multi-stimuli responsive polymeric nanoparticles for programmed site-specific drug delivery. *Biomaterials* 2013;34(14):3647-57
6. Tian L, Bae YH. Cancer nanomedicines targeting tumor extracellular pH. *Colloids Surf B Biointerfaces* 2012;99:116-26
7. Liu J, Huang Y, Kumar A, et al. pH-sensitive nano-systems for drug delivery in cancer therapy. *Biotechnol Adv* 2013. [Epub ahead of print]
8. Du JZ, Mao CQ, Yuan YY, et al. Tumor extracellular acidity-activated nanoparticles as drug delivery systems for enhanced cancer therapy. *Biotechnol Adv* 2013. [Epub ahead of print]
9. Lehner R, Wang X, Wolf M, Hunziker P. Designingswitchable nanosystems for medical application. *J Control Release* 2012;161(2):307-16
10. Fleige E, Quadir MA, Haag R. Stimuli-responsive polymeric nanocarriers for the controlled transport of active compounds: concepts and applications. *Adv Drug Deliv Rev* 2012;64(9):866-84
11. Wong C, Stylianopoulos T, Cui J, et al. Multistage nanoparticle delivery system for deep penetration into tumor tissue. *Proc Natl Acad Sci USA* 2011;108(6):2426-31
12. Matsumura Y, Maeda H. A new concept for macromolecular therapeutics in cancer chemotherapy: Mechanism of tumorotropic accumulation of proteins and the antitumor agent smanes. *Cancer Res* 1986;46(12 Part 1):6387-92
13. Stiffland DL, Nichols JW, Miura S, Bae YH. Mind the gap: a survey of how cancer drug carriers are susceptible to the gap between research and practice. *J Control Release* 2013;172(3):1045-64
14. Koo H, Min KH, Lee SC, et al. Enhanced drug-loading and therapeutic efficacy of hydrotropic oligomer-conjugated glycolchitosan nanoparticles for tumor-targeted paclitaxel delivery. *J Control Release* 2013;172(3):823-31
15. Prabhakar U, Maeda H, Jain RK, et al. Challenges and key considerations of the enhanced permeability and retention effect for nanomedicine drug delivery in oncology. *Cancer Res* 2013;73(8):2412-17
16. Bertrand N, Wu J, Xu X, et al. Cancer nanotechnology: the impact of passive and active targeting in the era of modern cancer biology. *Adv Drug Deliv Rev* 2014;66:662-25
17. Nichols JW, Bae YH. Epr: evidence and fallacy. *J Control Release* 2014; [Epub ahead of print]
18. Matsumura Y. Poly (amino acid) micelle nanocarriers in preclinical and clinical studies. *Adv Drug Deliv Rev* 2008;60(8):899-914
19. Romberg B, Hennink W, Storm G. Sheddable coatings for long-circulating nanoparticles. *Pharm Res* 2008;25(1):55-71
20. Krishna R, Mayer LD. Multidrug resistance (MDR) in cancer - mechanisms, reversal using modulators of mdr and the role of mdr modulators in influencing the pharmacokinetics of anticancer drugs. *Eur J Pharm Sci* 2000;11(4):265-83
21. Borst P, Evers R, Kool M, Wijnholds J. A family of drug transporters: the multidrug resistance-associated proteins. *J Natl Cancer Inst* 2000;92(16):1295-302
22. Sahoo SK, Labhasetwar V. Enhanced antiproliferative activity of transferrin-conjugated paclitaxel-loaded nanoparticles is mediated via sustained intracellular drug retention. *Mol Pharm* 2005;2(5):373-83
23. Gu F, Zhang L, Teply BA, et al. Precise engineering of targeted nanoparticles by using self-assembled biointegrated block copolymers. *Proc Natl Acad Sci USA* 2008;105(7):2586-91
24. Cheng J, Teply BA, Sherifi I, et al. Formulation of functionalized PLGA-PEG nanoparticles for in vivo targeted drug delivery. *Biomaterials* 2007;28(5):869-76
25. Gullotti E, Yeo Y. Extracellularly activated nanocarriers: a new paradigm of tumor targeted drug delivery. *Mol Pharm* 2009;6(4):1041-51
26. Minchinton AI, Tannock IF. Drug penetration in solid tumours. *Nat Rev Cancer* 2006;6(8):583-92
27. Kuh HJ, Jang SH, Wientjes MG, et al. Determinants of paclitaxel penetration

AQ8

AQ9

AQ10

S. A. Abouelmagd *et al.*

- and accumulation in human solid tumor. *J Pharmacol Exp Ther* 1999;290(2):871-80
28. Lankelma J, Dekker H, Luque RF, et al. Doxorubicin gradients in human breast cancer. *Clin Cancer Res* 1999;5(7):1703-7
 29. McKee TD, Grandi P, Mok W, et al. Degradation of fibrillar collagen in a human melanoma xenograft improves the efficacy of an oncolytic herpes simplex virus vector. *Cancer Res* 2006;66(5):2509-13
 30. Paszek MJ, Zahir N, Johnson KR, et al. Tensional homeostasis and the malignant phenotype. *Cancer Cell* 2005;8(3):241-54
 31. Young JS, Lumsden CE, Stalker AL. The significance of the tissue pressure of normal testicular and of neoplastic (Brown-Pearce carcinoma) tissue in the rabbit. *J Pathol Bacteriol* 1950;62(3):313-33
 32. Jain RK. Delivery of molecular and cellular medicine to solid tumors. *Adv Drug Deliv Rev* 2001;46(1-3):149-68
 33. Baxter LT, Jain RK. Transport of fluid and macromolecules in tumors. 1. Role of interstitial pressure and convection. *Microvasc Res* 1989;37(1):77-104
 34. Jain RK, Baxter LT. Mechanisms of heterogeneous distribution of monoclonal-antibodies and other macromolecules in tumors - significance of elevated interstitial pressure. *Cancer Res* 1988;48(24):7022-32
 35. Willett CG, Boucher Y, di Tomaso E, et al. Direct evidence that the vegf-specific antibody bevacizumab has antivascular effects in human rectal cancer. *Nat Med* 2004;10(2):145-7
 36. Boucher Y, Baxter LT, Jain RK. Interstitial pressure-gradients in tissue-isolated and subcutaneous tumors - implications for therapy. *Cancer Res* 1990;50(15):4478-84
 37. Heldin CH, Rubin K, Pietras K, Ostman A. High interstitial fluid pressure - an obstacle in cancer therapy. *Nat Rev Cancer* 2004;4(10):806-13
 38. Eikenes L, Tari M, Tufto I, et al. Hyaluronidase induces a transcapillary pressure gradient and improves the distribution and uptake of liposomal doxorubicin (caelyx (tm)) in human osteosarcoma xenografts. *Br J Cancer* 2005;93(1):81-8
 39. Goodman TT, Chen JY, Matveev K, Pun SH. Spatio-temporal modeling of nanoparticle delivery to multicellular tumor spheroids. *Biotechnol Bioeng* 2008;101(2):388-99
 40. Kuhn SJ, Finch SK, Hallahan DE, Giorgio TD. Proteolytic surface functionalization enhances in vitro magnetic nanoparticle mobility through extracellular matrix. *Nano Lett* 2006;6(2):306-12
 41. Goodman TT, Olive PL, Pun SH. Increased nanoparticle penetration in collagenase-treated multicellular spheroids. *Int J Nanomedicine* 2007;2(2):265-74
 42. Jang SH, Wientjes MG, Au JL. Determinants of paclitaxel uptake, accumulation and retention in solid tumors. *Invest New Drugs* 2001;19(2):113-23
 43. Zheng JH, Chen CT, Au JLS, Wientjes MG. Time- and concentration-dependent penetration of doxorubicin in prostate tumors. *AAPS PharmSci* 2001;3(2):E15
 44. Jang SH, Wientjes MG, Au JL. Enhancement of paclitaxel delivery to solid tumors by apoptosis-inducing pretreatment: effect of treatment schedule. *J Pharmacol Exp Ther* 2001;296(3):1035-42
 45. Lu Z, Tsai M, Lu D, et al. Tumor-penetrating microparticles for intraperitoneal therapy of ovarian cancer. *J Pharmacol Exp Ther* 2008;327(3):673-82
 46. Kuhn SJ, Hallahan DE, Giorgio TD. Characterization of superparamagnetic nanoparticle interactions with extracellular matrix in an in vitro system. *Ann Biomed Eng* 2006;34(1):51-8
 47. Goldberg SN, Girnan GD, Lukyanov AN, et al. Percutaneous tumor ablation: increased necrosis with combined radio-frequency ablation and intravenous liposomal doxorubicin in a rat breast tumor model. *Radiology* 2002;222(3):797-804
 48. Ahmed M, Goldberg SN. Combination radiofrequency thermal ablation and adjuvant iv liposomal doxorubicin increases tissue coagulation and intratumoral drug accumulation. *Int J Hyperthermia* 2004;20(7):781-802
 49. Monsky WL, Kruskal JB, Lukyanov AN, et al. Radio-frequency ablation increases intratumoral liposomal doxorubicin accumulation in a rat breast tumor model. *Radiology* 2002;224(3):823-9
 50. Chen PY, Liu HL, Hua MY, et al. Novel magnetic/ultrasound focusing system enhances nanoparticle drug delivery for glioma treatment. *Neuro-oncol* 2010;12(10):1050-60
 51. Grainger SJ, Serna JV, Sunny S, et al. Pulsed ultrasound enhances nanoparticle penetration into breast cancerspheroids. *Mol Pharm* 2010;7(6):2006-19
 52. Manzoor AA, Lindner LH, Landon CD, et al. Overcoming limitations in nanoparticle drug delivery: triggered, intravascular release to improve drug penetration into tumors. *Cancer Res* 2012;72(21):5566-75
 53. Junttila MR, de Sauvage FJ. Influence of tumour micro-environment heterogeneity on therapeutic response. *Nature* 2013;501(7467):346-54
 54. Vaupel P, Mayer A. Hypoxia in cancer: significance and impact on clinical outcome. *Cancer Metastasis Rev* 2007;26(2):225-39
 55. Denison TA, Bae YH. Tumor heterogeneity and its implication for drug delivery. *J Control Release* 2012;164(2):187-91
 56. Gerweck LE, Seetharaman K. Cellular pH gradient in tumor versus normal tissue: potential exploitation for the treatment of cancer. *Cancer Res* 1996;56(6):1194-8
 - Highlights mildly acidic pH of tumor microenvironment.
 57. Wilson WR, Hay MP. Targeting hypoxia in cancer therapy. *Nat Rev Cancer* 2011;11(6):393-410
 - Introduces hypoxia as a unique feature of tumor.
 58. Tannock IF, Rotin D. Acid pH in tumors and its potential for therapeutic exploitation. *Cancer Res* 1989;49(16):4373-84
 59. Yamagata M, Hasuda K, Stamato T, Tannock IF. The contribution of lactic acid to acidification of tumours: studies of variant cells lacking lactate dehydrogenase. *Br J Cancer* 1998;77(11):1726-31
 60. Engin K, Leeper DB, Cater JR, et al. Extracellular pH distribution in human

Extracellularly activatable nanocarriers for drug delivery to tumors

- tumors. *Int J Hyperthermia* 1995;11(2):211-16
61. Kato Y, Ozawa S, Miyamoto C, et al. Acidic extracellular microenvironment and cancer. *Cancer Cell Int* 2013;13(1):89
62. Cairns R, Papandreou I, Denko N. Overcoming physiologic barriers to cancer treatment by molecularly targeting the tumor microenvironment. *Mol Cancer Res* 2006;4(2):61-70
63. Amoozgar Z, Park JY, Lin QN, Yeo Y. Low molecular-weight chitosan as a pH-sensitive stealth coating for tumor-specific drug delivery. *Mol Pharm* 2012;9(5):1262-70
- A review of pH-sensitive stealth coating.
64. Hu J, Miura S, Na K, Bae YH. pH-responsive and charge shielded cationic micelle of poly(l-histidine)-block-short branched PEI for acidic cancer treatment. *J Control Release* 2013;172(1):69-76
- A dual pH-responsive system.
65. Guan XW, Li YH, Jiao ZX, et al. A pH-sensitive charge-conversion system for doxorubicin delivery. *Acta Biomater* 2013;9(8):7672-8
66. Liu KC, Yeo Y. Zwitterionic chitosan-polyamidoamine dendrimer complex nanoparticles as a pH-sensitive drug carrier. *Mol Pharm* 2013;10(5):1695-704
67. Gullotti E, Park J, Yeo Y. Polydopamine-based surface modification for the development of peritumorally activatable nanoparticles. *Pharm Res* 2013;30(8):1956-67
68. Gilbert HF. Molecular and cellular aspects of thiol-disulfide exchange. *Advances in enzymology and related areas of molecular biology*. John Wiley & Sons, Inc; 2006. p. 69-172
69. Arner ES, Holmgren A. Physiological functions of thioredoxin and thioredoxin reductase. *Eur J Biochem* 2000;267(20):6102-9
70. Saito G, Swanson JA, Lee KD. Drug delivery strategy utilizing conjugation via reversible disulfide linkages: role and site of cellular reducing activities. *Adv Drug Deliv Rev* 2003;55(2):199-215
71. Sun HL, Guo BN, Cheng R, et al. Biodegradable micelles with sheddable poly(ethylene glycol) shells for triggered intracellular release of doxorubicin. *Biomaterials* 2009;30(31):6358-66
72. Zalipsky S, Qazen M, Walker JA, et al. New detachable poly(ethylene glycol) conjugates: cysteine-cleavable lipopolymers regenerating natural phospholipid, diacyl phosphatidylethanolamine. *Bioconj Chem* 1999;10(5):703-7
73. Koo AN, Min KH, Lee HJ, et al. Tumor accumulation and antitumor efficacy of docetaxel-loaded core-shell-corona micelles with shell-specific redox-responsive cross-links. *Biomaterials* 2012;33(5):1489-99
74. Chaiswing L, Zhong W, Cullen JJ, et al. Extracellular redox state regulates features associated with prostate cancer cell invasion. *Cancer Res* 2008;68(14):5820-6
75. Chaiswing L, Oberley TD. Extracellular/microenvironmental redox state. *Antioxid Redox Signal* 2010;13(4):449-65
76. Kuppasamy P, Li HQ, Ilangoan G, et al. Noninvasive imaging of tumor redox status and its modification by tissue glutathione levels. *Cancer Res* 2002;62(1):307-12
77. Egeblad M, Werb Z. New functions for the matrix metalloproteinases in cancer progression. *Nat Rev Cancer* 2002;2(3):161-74
78. Vihinen P, Ala-aho R, Kahari VM. Matrix metalloproteinases as therapeutic targets in cancer. *Curr Cancer Drug Targets* 2005;5(3):203-20
79. Sloane BF. Cathepsin b and cystatins: Evidence for a role in cancer progression. *Semin Cancer Biol* 1990;1(2):137-52
80. Campo E, Munoz J, Miquel R, et al. Cathepsin B expression in colorectal carcinomas correlates with tumor progression and shortened patient survival. *Am J Pathol* 1994;145(2):301-9
81. Heidtmann HH, Salge U, Abrahamson M, et al. Cathepsin B and cysteine proteinase inhibitors in human lung cancer cell lines. *Clin Exp Metastasis* 1997;15(4):368-81
82. Volodkin DV, Skirtach AG, Mohwald H. Near-ir remote release from assemblies of liposomes and nanoparticles. *Angew Chem Int Ed Engl* 2009;48(10):1807-9
83. Bio M, You Y. Emerging strategies for controlling drug release by using visible/near IR light. *Med Chem* 2013;3192-8
84. Alvarez-Lorenzo C, Bromberg L, Concheiro A. Light-sensitive intelligent drug delivery systems. *Photochem Photobiol* 2009;85(4):848-60
85. Juzenas P, Juzeniene A, Kallhus O, et al. Noninvasive fluorescence excitation spectroscopy during application of 5-aminolevulinic acid in vivo. *Photochem Photobiol Sci* 2002;1(10):745-8
86. O' Neal DP, Hirsch LR, Halas NJ, et al. Photo-thermal tumor ablation in mice using near infrared-absorbing nanoparticles. *Cancer Lett* 2004;209(2):171-6
87. Timko BP, Dvir T, Kohane DS. Remotely triggerable drug delivery systems. *Adv Mater* 2010;22(44):4925-43
- An overview of external stimuli-triggerable drug delivery systems.
88. Bains VK, Mohan R, Bains R. Application of ultrasound in periodontics: part I. *J Indian Soc Periodontol* 2008;12(2):29-33
89. Frenkel V. Ultrasound mediated delivery of drugs and genes to solid tumors. *Adv Drug Deliv Rev* 2008;60(10):1193-208
90. O' Neill BE, Rapoport N. Phase-shift, stimuli-responsive drug carriers for targeted delivery. *Ther Deliv* 2011;2(9):1165-87
91. Schroeder A, Avnir Y, Weisman S, et al. Controlling liposomal drug release with low frequency ultrasound: mechanism and feasibility. *Langmuir* 2007;23(7):4019-25
92. Husseini GA, Diaz de la Rosa MA, Gabuji T, et al. Release of doxorubicin from unstabilized and stabilized micelles under the action of ultrasound. *J Nanosci Nanotechnol* 2007;7(3):1028-33
93. Sensenig R, Sapir Y, MacDonald C, et al. Magnetic nanoparticle-based approaches to locally target therapy and enhance tissue regeneration in vivo. *Nanomedicine (Lond)* 2012;7(9):1425-42
94. Wahajuddin Arora S. Superparamagnetic iron oxide nanoparticles: magnetic nanopatforms as drug carriers. *Int J Nanomedicine* 2012;7:3445-71
95. Grull H, Langereis S. Hyperthermia-triggered drug delivery from temperature-sensitive liposomes using mri-guided high intensity focused

A11

S. A. Abouelmagd *et al.*

- ultrasound. *J Control Release* 2012;161(2):317-27
96. Kennedy JE. High-intensity focused ultrasound in the treatment of solid tumours. *Nat Rev Cancer* 2005;5(4):321-7
97. Kong G, Braun RD, Dewhirst MW. Hyperthermia enables tumor-specific nanoparticle delivery: effect of particle size. *Cancer Res* 2000;60(16):4440-5
98. Magin RL, Niesman MR. Temperature-dependent permeability of large unilamellar liposomes. *Chem Phys Lipids* 1984;34(3):245-56
99. Gaber MH, Hong K, Huang SK, Papahadjopoulos D. Thermosensitive sterically stabilized liposomes: formulation and in vitro studies on mechanism of doxorubicin release by bovine serum and human plasma. *Pharm Res* 1995;12(10):1407-16
100. Gopal R, Anyarambhatla DN. Enhancement of the phase transition permeability of DPPC liposomes by incorporation of mppc: a new temperature-sensitive liposome for use with mild hyperthermia. *J Liposome Res* 1999;9(4):491-506
101. Needham D, Anyarambhatla G, Kong G, Dewhirst MW. A new temperature-sensitive liposome for use with mild hyperthermia: characterization and testing in a human tumor xenograft model. *Cancer Res* 2000;60(5):1197-201
102. Boutris C, Chatzi EG, Kiparisides C. Characterization of the LCST behaviour of aqueous poly(n-isopropylacrylamide) solutions by thermal and cloud point techniques. *Polymer (Guildf)* 1997;38(10):2567-70
103. Kawaguchi T, Kojima Y, Osa M, Yoshizaki T. Cloud points in aqueous poly(n-isopropylacrylamide) solutions. *Polym J* 2008;40(5):455-9
104. Iizawa T, Terao A, Ohuchida M, et al. Synthesis and swelling/de-swelling behavior of core-shell type gel consisting of two different poly(n-alkylacrylamide) gel layers. *Polym J* 2007;39(11):1177-84
105. Piskin E. Molecularly designed water soluble, intelligent, nanosize polymeric carriers. *Int J Pharm* 2004;277(1-2):105-18
106. Koning GA, Eggermont AM, Lindner LH, ten Hagen TL. Hyperthermia and thermosensitive liposomes for improved delivery of chemotherapeutic drugs to solid tumors. *Pharm Res* 2010;27(8):1750-4
107. Chu KF, Dupuy DE. Thermal ablation of tumours: biological mechanisms and advances in therapy. *Nat Rev Cancer* 2014;14(3):199-208
108. Kong G, Braun RD, Dewhirst MW. Characterization of the effect of hyperthermia on nanoparticle extravasation from tumor vasculature. *Cancer Res* 2001;61(7):3027-32
109. Giustini AJ, Petryk AA, Hoopes PJ. Ionizing radiation increases systemic nanoparticle tumor accumulation. *Nanomedicine* 2012;8(6):818-21
110. Lee ES, Shin HJ, Na K, Bae YH. Poly(-histidine)-PEG block copolymer micelles and pH-induced destabilization. *J Control Release* 2003;90(3):363-74
111. Lee ES, Na K, Bae YH. Polymeric micelle for tumor pH and folate-mediated targeting. *J Control Release* 2003;91(1-2):103-13
112. Yin H, Kang HC, Huh KM, Bae YH. Biocompatible, pH-sensitive ab(2) mikoarm polymer-based polymersomes: preparation, characterization, and acidic pH-activated nanostructural transformation. *J Mater Chem* 2012;22(36):91968-19178
113. Lim EK, Sajomsang W, Choi Y, et al. Chitosan-based intelligent theragnosis nanocomposites enable pH-sensitive drug release with MR-guided imaging for cancer therapy. *Nanoscale Res Lett* 2013;8(1):467
114. Nogueira DR, Tavano L, Mitjans M, et al. In vitro antitumor activity of methotrexate via pH-sensitive chitosan nanoparticles. *Biomaterials* 2013;34(11):2758-72
115. Elegbede AI, Banerjee J, Hanson AJ, et al. Mechanistic studies of the triggered release of liposomal contents by matrix metalloproteinase-9. *J Am Chem Soc* 2008;130(32):10633-42
116. Niidome T, Ohga A, Akiyama Y, et al. Controlled release of PEG chain from gold nanorods: targeted delivery to tumor. *Bioorg Med Chem* 2010;18(12):4453-8
117. Glangchai LC, Calderera-Moore M, Shi L, Roy K. Nanoimprint lithography based fabrication of shape-specific, enzymatically-triggered smart nanoparticles. *J Control Release* 2008;125(3):263-72
118. Luo Z, Cai K, Hu Y, et al. Mesoporous silica nanoparticles end-capped with collagen: redox-responsive nanoreservoirs for targeted drug delivery. *Angew Chem Int Ed Engl* 2011;50(3):640-3
119. Pan YJ, Chen YY, Wang DR, et al. Redox/pH dual stimuli-responsive biodegradable nanohydrogels with varying responses to dithiothreitol and glutathione for controlled drug release. *Biomaterials* 2012;33(27):6570-9
120. Hodgkiss RJ, Jones G, Long A, et al. Flow cytometric evaluation of hypoxic cells in solid experimental-tumors using fluorescence immunodetection. *Br J Cancer* 1991;63(1):119-25
121. Thambi T, Deepagan VG, Yoon HY, et al. Hypoxia-responsive polymeric nanoparticles for tumor-targeted drug delivery. *Biomaterials* 2014;35(5):1735-43
122. Kong G, Anyarambhatla G, Petros WP, et al. Efficacy of liposomes and hyperthermia in a human tumor xenograft model: importance of triggered drug release. *Cancer Res* 2000;60(24):6950-7
123. Tagami T, Ernsting MJ, Li SD. Efficient tumor regression by a single and low dose treatment with a novel and enhanced formulation of thermosensitive liposomal doxorubicin. *J Control Release* 2011;152(2):303-9
124. Dromi S, Frenkel V, Luk A, et al. Pulsed-high intensity focused ultrasound and low temperature-sensitive liposomes for enhanced targeted drug delivery and antitumor effect. *Clin Cancer Res* 2007;13(9):2722-7
- A good example of temperature-sensitive liposomes with high-intensity focused ultrasound -induced hyperthermia.
125. Graham SM, Carlisle R, Choi JJ, et al. Inertial cavitation to non-invasively trigger and monitor intratumoral release of drug from intravenously delivered liposomes. *J Control Release* 2014;178:101-7
126. Timko BP, Arruebo M, Shankarappa SA, et al. Near-infrared-actuated devices for remotely controlled drug delivery. *Proc Natl Acad Sci USA* 2014;111(4):1349-54
127. Hildebrandt B, Wust P, Ahlers O, et al. The cellular and molecular basis of hyperthermia. *Crit Rev Oncol Hematol* 2002;43(1):33-56

Extracellularly activatable nanocarriers for drug delivery to tumors

128. Hoare T, Santamaria J, Goya GF, et al. A magnetically triggered composite membrane for on-demand drug delivery. *Nano Lett* 2009;9(10):3651-7
129. Hoare T, Timko BP, Santamaria J, et al. Magnetically triggered nanocomposite membranes: a versatile platform for triggered drug release. *Nano Lett* 2011;11(3):1395-400
130. Qiao ZY, Zhang R, Du FS, et al. Multi-responsive nanogels containing motifs of ortho ester, oligo(ethylene glycol) and disulfide linkage as carriers of hydrophobic anti-cancer drugs. *J Control Release* 2011;152(1):57-66
131. Soppimath KS, Tan DCW, Yang Y. pH-triggered thermally responsive polymer core-shell nanoparticles for drug delivery. *Adv Mater* 2005;17(3):318-23
132. Soppimath KS, Liu LH, Seow WY, et al. Multifunctional core/shell nanoparticles self-assembled from pH-induced thermosensitive polymers for targeted intracellular anticancer drug delivery. *Adv Funct Mater* 2007;17(3):355-62
133. Zhang L, Guo R, Yang M, et al. Thermo and pH dual-responsive nanoparticles for anti-cancer drug delivery. *Adv Mater* 2007;19(19):2988-92
134. Aznar E, Marcos MD, Martínez-Manez R, et al. pH- and photo-switched release of guest molecules from mesoporous silica supports. *J Am Chem Soc* 2009;131(19):6833-43
- An example of a dual (pH- and laser light-) responsive system.
135. Mahmoud EA, Sankaranarayanan J, Morachis JM, et al. Inflammation responsive logic gate nanoparticles for the delivery of proteins. *Bioconjug Chem* 2011;22(7):1416-21
- An example of a dual (internal and external) stimuli-sensitive nanoparticle system.
136. Klaiherd A, Nagamani C, Thayumanavan S. Multi-stimuli sensitive amphiphilic block copolymer assemblies. *J Am Chem Soc* 2009;131(13):4830-8
137. Lee ES, Gao Z, Kim D, et al. Super pH-sensitive multifunctional polymeric micelle for tumor pH(e) specific targeting and multidrug resistance. *J Control Release* 2008;129(3):228-36
138. Poon Z, Chang D, Zhao X, Hammond PT. Layer-by-layer nanoparticles with a pH-sheddable layer for in vivo targeting of tumor hypoxia. *ACS Nano* 2011;5(6):4284-92
139. Xiaolin T, Dafeng T, Zhongyan W, Fengkui M. Synthesis and evaluation of chitosan-vitamin C complexes. *J Appl Polym Sci* 2009;114(5):2986-91
140. Domanski DM, Klajnert B, Bryszewska M. Influence of PAMAM dendrimers on human red blood cells. *Bioelectrochemistry* 2004;63(1-2):189-91
141. Xu P, Bajaj G, Shugg T, et al. Zwitterionic chitosan derivatives for pH-sensitive stealth coating. *Biomacromolecules* 2010;11(9):2352-8
142. Yao L, Daniels J, Moshnikova A, et al. Philp peptide targets nanogold particles to tumors. *Proc Natl Acad Sci USA* 2013;110(2):465-70
- An introduction of pH sensitive insertion peptides.
143. Zhao Z, Meng H, Wang N, et al. A controlled-release nanocarrier with extracellular pH value driven tumor targeting and translocation for drug delivery. *Angew Chem Int Ed Engl* 2013;52(29):7487-91
144. Du JZ, Du XJ, Mao CQ, Wang J. Tailor-made dual pH-sensitive polymer-doxorubicin nanoparticles for efficient anticancer drug delivery. *J Am Chem Soc* 2011;133(44):17560-3
145. Zhou ZX, Shen YQ, Tang JB, et al. Charge-reversal drug conjugate for targeted cancer cell nuclear drug delivery. *Adv Funct Mater* 2009;19(22):3580-9
146. Carlisle R, Choi J, Bazan-Peregrino M, et al. Enhanced tumor uptake and penetration of virotherapy using polymer stealth and focused ultrasound. *J Natl Cancer Inst* 2013;105(22):1701-10
147. Cabral H, Matsumoto Y, Mizuno K, et al. Accumulation of sub-100 nm polymeric micelles in poorly permeable tumours depends on size. *Nat Nanotechnol* 2011;6(12):815-23
148. Perrault SD, Walkey C, Jennings T, et al. Mediating tumor targeting efficiency of nanoparticles through design. *Nano Lett* 2009;9(5):1909-15
149. Feczko T, Toth J, Dosa G, Gyenis J. Optimization of protein encapsulation in PLGA nanoparticles. *Chem Eng Process* 2011;50(8):757-65
150. Chen YC, Liao LC, Lu PL, et al. The accumulation of dual pH and temperature responsive micelles in tumors. *Biomaterials* 2012;33(18):4576-88
151. Tong R, Hemmati HD, Langer R, Kohane DS. Photoswitchable nanoparticles for triggered tissue penetration and drug delivery. *J Am Chem Soc* 2012;134(21):8848-55
- Demonstrates nanoparticle size reduction by ultraviolet light.
152. Tokarova V, Pittermannova A, Cech J, et al. Thermo-responsive adhesion properties of composite hydrogel microcapsules. *Soft Matter* 2012;8(4):1087-95
153. Lee JE, Lee DJ, Lee N, et al. Multifunctional mesoporous silica nanocomposite nanoparticles for pH controlled drug release and dual modal imaging. *J Mater Chem* 2011;21(42):16869-72
154. Liu KC, Yeo Y. Extracellular stability of nanoparticulate drug carriers. *Arch Pharm Res* 2014;37(1):16-23
- Discusses the circulation stability of NP drug carriers with examples.
155. Hunjan S, Mason RP, Mehta VD, et al. Simultaneous intracellular and extracellular pH measurement in the heart by *f*-19 NMR of 6-fluoropyridoxol. *Magn Reson Med* 1998;39(4):551-6
156. Punnia-Moorthy A. Evaluation of pH changes in inflammation of the subcutaneous air pouch lining in the rat, induced by carrageenan, dextran and *Staphylococcus aureus*. *J Oral Pathol* 1987;16(1):36-44
157. van Duijnhoven SM, Robillard MS, Nicolay K, Grull H. Tumor targeting of MMP-2/9 activatable cell-penetrating imaging probes is caused by tumor-independent activation. *J Nucl Med* 2011;52(2):279-86
158. Helmlinger G, Yuan F, Dellian M, Jain RK. Interstitial pH and pO₂ gradients in solid tumors in vivo: High-resolution measurements reveal a lack of correlation. *Nat Med* 1997;3(2):177-82

S. A. Abouelmagd *et al.*

Affiliation

Sara A Abouelmagd¹, Hyesun Hyun¹ &
Yoon Yeo^{1,2}

¹Author for correspondence

¹Purdue University, Department of Industrial
and Physical Pharmacy, 575 Stadium Mall Drive,
West Lafayette, IN 47907, USA

Tel: +1 765 496 9608;

Fax: +1765 494 6545;

E-mail: yyeo@purdue.edu

²Purdue University, Weldon School of
Biomedical Engineering, 206 South Martin
Jischke Drive, West Lafayette, IN 47907, USA

PROOF ONLY

Nanoparticle Characterization: State of the Art, Challenges, and Emerging Technologies

Eun Jung Cho,[†] Hillary Holback,[†] Karen C. Liu,[‡] Sara A. Abouelmagd,^{†,§} Joonyoung Park,[†] and Yoon Yeon^{*,†,‡}

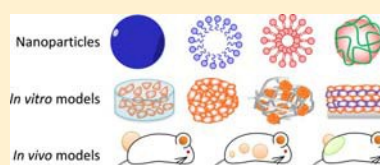
[†]Department of Industrial and Physical Pharmacy, Purdue University, 575 Stadium Mall Drive, West Lafayette, Indiana 47907, United States

[‡]Weldon School of Biomedical Engineering, Purdue University, West Lafayette, Indiana 47907, United States

[§]Department of Pharmaceutics, Faculty of Pharmacy, Assiut University, Assiut 71526, Egypt

ABSTRACT: Nanoparticles have received enormous attention as a promising tool to enhance target-specific drug delivery and diagnosis. Various *in vitro* and *in vivo* techniques are used to characterize a new system and predict its clinical efficacy. These techniques enable efficient comparison across nanoparticles and facilitate a product optimization process. On the other hand, we recognize their limitations as a prediction tool, due to inadequate applications and overly simplified test conditions. We provide a critical review of *in vitro* and *in vivo* techniques currently used for evaluation of nanoparticles and introduce emerging techniques and models that may be used complementarily.

KEYWORDS: nanomedicine, nanoparticles, particle characterization, *in vitro*, animal models



1. INTRODUCTION

The field of nanomedicine has seen significant progress in the past decades, both in design and in the scope of applications. Various techniques are used to characterize nanoparticles (NPs) and predict their ultimate fates in the human body. However, current technology is challenged in a sense that the characterization is often performed in a condition that does not reflect the complexity of the physiological environment. Moreover, *in vivo* studies based on animal models largely remain a black box approach, where pharmacokinetics and biodistribution of NPs are driven by a series of biological events that are not readily predicted *in vitro*. In order to expedite the transition of a benchtop effort to a clinically effective product, it is imperative that investigators employ adequate methodologies to characterize nanomedicine, correlate their effects and biological consequences, and predict the therapeutic outcomes in clinical subjects in the early stage of product development. The purpose of this review is to highlight current techniques used in NP evaluation from a critical perspective, discuss potential pitfalls and cautions, and introduce emerging technologies that deserve keen attention from the field of nanomedicine.

2. *IN VITRO* CHARACTERIZATION OF NPS

2.1. Physical Properties. 2.1.1. Particle Size. Particle size is the most basic information of NPs, one of the main determinants of biodistribution and retention of the NPs in target tissues. Dynamic light scattering (DLS) is commonly used for particle size determination. DLS measures Brownian motion of NPs in suspension and relates its velocity, known as

translational diffusion coefficient, to the size of NPs according to the Stokes–Einstein equation.¹ The particle size is defined as the size of a hypothetical hard sphere that diffuses in the same fashion as that of the NPs being measured. The result is reported as a mean particle size and homogeneity of size distribution. The latter is expressed as polydispersity index (PDI), a dimensionless parameter calculated from a cumulant analysis of the DLS-measured intensity autocorrelation function.² A PDI value from 0.1 to 0.25 indicates a narrow size distribution, and a PDI value greater than 0.5 indicates a broad distribution.³ While DLS provides a simple and speedy estimate of the particle size, several studies suggest inherent limitations of DLS. For example, DLS is relatively poor at analyzing multimodal particle size distribution.^{3,4} For example, when a mixture of 20 and 100 nm NPs is measured, the signal of smaller particles is lost because the signal intensity of a spherical particle with a radius r is proportional to r^6 ; thus, the scattering intensity of small particles tends to be masked by that of larger particles.

Microscopy provides an accurate assessment of the size and shape of an NP; however, it often requires complicated sample preparation steps specific to microscope techniques,⁴ which can change samples and create artifacts (e.g., NP agglomeration during the drying process for electron microscopy⁵). Moreover,

Special Issue: Emerging Technology in Evaluation of Nanomedicine

Received: December 8, 2012

Revised: February 23, 2013

Accepted: March 5, 2013

Published: March 5, 2013

due to the limited throughput, it is difficult to obtain particle size distribution.⁶ Another imaging-based method is the NP tracking analysis (NTA), a single particle tracking technique based on dark field or fluorescence microscopy and automatic imaging analysis.⁷ In this method, NP size is derived from the average displacement of NPs undergoing Brownian motion within a fixed time frame.^{7,8} An advantage of this method is that it tracks individual NPs and thus provides a high resolution for multimodal samples and aggregation.⁷ On the other hand, it requires a sample to be sufficiently diluted so that the observation fields may not be overly crowded.⁵ Alternatively, NP size may be estimated by disk centrifugation, which depends on sedimentation speed of NPs. Since NPs with a few percent size differences settle at significantly different rates, the disk centrifugation method can resolve a very small size difference (as little as 2%).⁹ Moreover, this method can analyze a broad range of particle sizes, ranging from 5 nm to 75 μm . On the other hand, it takes longer than other methods, lasting 15 to 30 min, and requires that NPs be denser than the suspended fluid.⁹

Since these techniques rely on different physical principles and sample preparation, the results vary according to the employed methods.⁵ For example, electron microscopy, DLS, NTA, and disk centrifugation gave rise to highly variable results even for the well-defined, homogeneous NPs. Depending on the methods and the type of averages reported (intensity, number, or volume), silver NPs (70 nm) and gold NPs (15 nm) were measured as 40–124 nm and 11–52 nm, respectively.⁷ In addition to the underlying principles, it should be considered that sample status in each method is not the same. For example, the size of NPs measured in solution is generally much larger than the size of dried NPs because of the hydration layer.

The measured particle size can also be different depending on how the samples are prepared even in the same method. For example, in DLS measurement, it is critical to ensure that the NPs are well dispersed. NPs are typically dispersed via probe/bath sonication or vortex mixing. A high energy dispersion method can temporarily reduce agglomeration, but the NPs do not remain dispersed for a long time and agglomerate again.¹⁰ Therefore, it is often observed that the increased duration of sonication and/or higher energy sonication method ultimately promotes agglomeration after initial dispersion due to the enhanced interaction of NPs with high surface energy.^{10–12} Ionic strength of the NP suspension is another important factor.¹¹ When TiO₂ NPs or quantum dots were analyzed, an increase in ionic strength from 0.001 to 0.1 M resulted in a 50-fold increase in the hydrodynamic diameter.¹¹ This is because the increasing ions shield the electrical layer on NPs that has kept the NPs apart at a lower ionic strength. The pH of the NP suspension also plays a role in particle size measurement.¹¹ When pH is distant from the isoelectric point of NPs, the electrostatic repulsive force is dominant over the van der Waals force, and NPs are well dispersed. On the other hand, the repulsive force decreases and the hydrodynamic size increases, when the pH is close to the isoelectric point and, thus, the NP surface is less charged. Due to the dependence on pH and ionic strength, the size distribution in a condition where the bioactivity of NPs is tested is quite different from that measured in water. Murdock et al. measured sizes of various inorganic and organic NPs in water or cell culture medium (with or without serum) with DLS.¹⁰ In many cases, NPs aggregated to a greater extent in serum-free medium than in

water.¹⁰ The presence of serum proteins attenuated the size increase, likely due to surface stabilization by the adsorbed proteins. Given the variability, it is necessary to record the conditions in which NP size is measured when DLS is used for size measurement.

Additional cautions are needed in measuring sizes of NPs with nonspherical shape. DLS assumes spherical shape for NPs; therefore, it is important to validate this assumption via microscopic examination. When the shape significantly deviates from a sphere, the DLS measurement may be less accurate; thus, DLS must be accompanied by image analysis.¹³ It is also noteworthy that the particle size can differ by a factor of 2 to 4 depending on the type of particle size distribution used in DLS (i.e., intensity, volume, and number-based); therefore, one should report the type of size distribution in addition to the average size.⁵

2.1.2. Surface Charge. Surface charge, expressed as zeta potential, critically influences the interaction of an NP with the environment.³ There are two liquid layers surrounding an NP: strongly bound inner part (Stern layer) and weakly bound outer layer. Zeta potential is commonly measured by laser Doppler electrophoresis, which evaluates electrophoretic mobility of suspended NPs in the medium, thus measuring the potential at the boundary of the outer layer. Generally, particles with zeta potential more positive than +30 mV or

more negative than –30 mV have colloidal stability maintained by electrostatic repulsion. One limitation is that in bimodal samples the zeta potential value of larger particles dominates the scattering signal of smaller particles, similar to DLS size measurements.¹⁰

The zeta potential measurement depends on the strength and valency of ions contained in the NP suspension. High ionic strength and high valency ions compress the electric double layer, resulting in reduction of the zeta potential.^{14,15} The pH, the concentration of hydrogen ions in the medium, greatly influences the zeta potential as well. When the suspension is acidic, the NPs acquire more positive charge, and vice versa. Therefore, a zeta potential value without indication of solution pH is a virtually meaningless number.¹ It is recommended that information of the NP suspension be precisely described in reporting the zeta potential, including the ionic strength, composition of the medium, and the pH.^{16,17} For comparison of results across different studies, it is conceivable to normalize the zeta potential by pC (negative logarithm of concentration of counterion species).¹⁷

2.1.3. Drug Release Kinetics. When an NP is used for delivery of a drug, the ability of the NP to release the drug is evaluated over a period of time, since it ultimately determines the availability of a drug at target tissues, thereby the therapeutic outcomes.³ There are three possible mechanisms of drug release: desorption of the surface bound/adsorbed drug, diffusion from the polymer matrix, and release subsequent to polymer erosion. In the case of a matrix-type polymer NP, in which the drug is uniformly distributed in the matrix, the release occurs by diffusion and/or erosion of the matrix. If the diffusion occurs more rapidly than matrix degradation, diffusion is likely to be a main mechanism of drug release. Rapid initial burst release is attributed to the fraction of the drug adsorbed or weakly bound to the surface of the NPs.¹⁸

Drug release from NPs is studied in at least three ways: sampling and separation, dialysis membrane diffusion, and *in situ* analytical technique.¹⁹ In the sampling and separation technique, the released drug is separated from NPs by filtration,

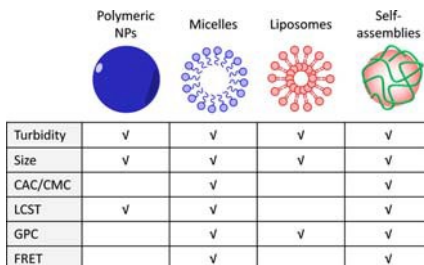
Molecular Pharmaceutics

centrifugation, or centrifugal filtration, and quantified by various analytical methods. The NPs are supplemented with fresh release medium, resuspended, and incubated further for the next sampling. While this method can be performed with a small amount of samples and simple analytical equipment, several shortcomings exist. Irrespective of the separation methods, the process is slow and inefficient, which makes them less suitable for studying NPs that rapidly release a drug. Moreover, centrifugal force or shear stress during filtration required for NP separation, which becomes increasingly strong when NPs are relatively small, can alter the NPs and the release kinetics. Dialysis membrane diffusion depends on continuous diffusion across the dialysis membrane. Advantages of this method are that the NPs are not subject to invasive separation processes and sampling is quick and simple. On the other hand, the dialysis membrane can attenuate the drug release as a

diffusion barrier and adsorptive surface; therefore, this method should be accompanied by a control experiment with a free drug to account for the membrane effect. The dialysis membrane diffusion method typically employs a large volume of release medium. While the large volume helps maintain a sink condition for drug release, drug analysis may become difficult due to the low concentration. *In situ* analytical technique is useful for studying nanocrystals, which is made almost exclusively of a drug. This technique analyzes the properties of NPs *in situ* to determine the quantity of the released (dissolved) drug indirectly. Various analytical techniques, including electrochemical analysis, solution calorimetry, or turbidimetric method, and light scattering technique, are employed for this purpose.¹⁹ This technique does not need NP separation and enables real-time assessment of the release kinetics. However, it is limited in determining the integrity of the released drug.

2.2. Prediction of Physical and Chemical Stability of NPs. Maintaining NP stability in the bloodstream is a crucial requirement for successful drug delivery to target tissues. The fate of NPs *in vivo* is in large part determined by its ability to maintain the size, to retain drug payload external to the target tissues, and to properly release drug to the cells. Ideally, an NP must remain stable (i.e., resist aggregation or degradation and retain drug) in the blood until it reaches the target sites. Instability of NPs results in altered biodistribution and premature drug release, thereby compromising the efficacy of the delivery system. Hence, evaluation of NP stability is an important aspect of NP characterization and an essential component to the success of the system. This section reviews commonly used techniques to investigate NP stability in various biologically relevant media *in vitro* (Figure 1). Well-established studies of micelles or similar self-assembled NP systems are mainly used as examples. Although NP stability needs to be ultimately measured *in vivo*, these techniques provide reasonable prediction of NP stability in a physiological environment.

2.2.1. Determination of Critical Aggregation/Micelle Concentration. The critical association or aggregation concentration (CAC) or critical micelle concentration (CMC) can be used to evaluate the stability of self-assembled NP systems including polymeric or surfactant micelle systems. The CAC, or CMC, is defined as the concentration at which a self-assembled particle or micelle associates/dissociates. This value provides a quantitative measure of the physical stability of NPs. A relatively low CAC/CMC indicates a more stable micelle system than one with a high CAC/CMC. In other



	Polymeric NPs	Micelles	Liposomes	Self-assemblies
Turbidity	✓	✓	✓	✓
Size	✓	✓	✓	✓
CAC/CMC		✓		✓
LCST	✓	✓		✓
GPC		✓	✓	✓
FRET		✓		✓

Figure 1. Techniques used for prediction of physical and chemical stability of various NPs. Techniques are listed in the order of required time and resources (top to bottom: least to most).

words, NPs with a low CAC/CMC are more likely to resist dissociation upon dilution in the blood.

CMC can be measured using a variety of different detection methods, such as conductivity, chromatography, surface tension, fluorescent probes, and light scattering. When measuring CMC using surface tension, the CMC is defined as the concentration of a surfactant (i.e., an amphiphilic polymer) above which the surface tension becomes constant. At concentrations below CMC, a surfactant has not yet saturated the surface and lends itself to reduce surface tension of the solution. On the other hand, at concentrations above CMC, this saturation has occurred, and the excess surfactants form micelles and do not contribute to the surface tension change. Many studies have utilized this method to determine the CMC of micelles.^{20–23} Another commonly used method to measure CAC/CMC is to utilize fluorescence probes, such as pyrene, as an indicator of micelle dissociation. Pyrene is a hydrophobic aromatic hydrocarbon, which partitions in the hydrophobic domain of self-assembled NPs during assembly.²⁴ When an NP dissociates, pyrene is exposed to water, where it shows a different fluorescence profile than when in the hydrophobic domain of the NP. Therefore, the CAC/CMC can be determined by monitoring the change in fluorescence profile of pyrene, defined as the concentration at which a drastic band shift is observed. The pyrene technique has widely been used as an indicator of relative micelle stability.^{25–29} In addition, light scattering is used to determine CAC/CMC. This technique measures the count rate (the intensity of scattered light in DLS), which is proportional to the number of NPs in solution when NP size is constant.³⁰ The count rate is plotted with respect to NP concentration, and the CAC/CMC is defined as a concentration above which the count rate shows a linear increase with concentration of the components of NPs.³⁰ The CAC/CMC measurement is a relatively simple and sensitive method of evaluating NP stability, but a disadvantage is that the application is limited to micelles and self-assembled NPs, whose formation is influenced by concentrations of the components.

2.2.2. Determination of Low Critical Solution Temperature. Temperature-sensitive micelle systems composed of a copolymer of hydrophobic block and thermosensitive block can utilize lower critical solution temperature (LCST) as a measure of their stability. The LCST is defined as the temperature at which phase transition of a thermosensitive polymer occurs (from hydrophilic to hydrophobic with increase in temperature).³¹ This phase change provides the system with the ability

to release a drug in response to an external thermal stimulus at a specific temperature via local and controlled hyperthermia in a specific region of the body.³² At temperatures below LCST, the polymer is amphiphilic and the drug remains encapsulated in micelles; however, at temperatures above LCST, the thermosensitive block becomes hydrophobic, destabilizing the micelle structure and releasing the drug.³³ As an inherent property of a thermosensitive polymer, LCST can be utilized in comparing the stability of NPs based on such polymers. For example, LCST of poly(*N*-isopropylacrylamide-*co*-maleic anhydride) copolymer increased from 31.1 to 45 °C as the content of maleic anhydride and molecular weight increased.³⁴ Conversely, LCST of Pluronic and poly(*N*-isopropylacrylamide) decreased when mixed with saccharides.³⁵ One may expect that NPs based on a polymer with a relatively high LCST will be more resistant to thermal dissociation.

2.2.3. Monitoring NP Size or Turbidity of an NP Suspension. Changes in NP size can be used to predict the stability of most NPs. Assuming that the assembled NPs form within a constant size range, deviations from the average NP size range can be interpreted as an indication of NP dissociation or instability in that particular environment or concentration. In one study, the stability of different NPs in 10% bovine serum albumin (BSA) and 10% human plasma solution was studied by monitoring their size change.³⁶ Here, an increase in NP size provides evidence of protein adsorption and, therefore, potential instability *in vivo*. A similar study evaluated micellar NP stability by incubating the NPs with 5% BSA and measuring the size using DLS.³⁷ Changes in turbidity of NP suspension may also be used as an indication of instability. For example, one study monitored the change in absorbance at 550 nm of NPs in a suspension and utilized the kinetics of absorbance decay (decomposition of NPs) as an indicator of NP stability.³⁸ In another example, turbidity of a sulfonamide-containing hydrogel NP suspension was measured at different pH values to study the pH-sensitive aggregation behavior of the NPs.³⁹ The NPs showed constant particle size and turbidity at pH 7 or higher but increased turbidity and size at pH below 7, indicative of NP aggregation due to hydrophobic interactions of the deionized polymer.³⁹ These methods may be used for virtually any type of NP systems and performed with basic analytical equipment. However, they take into account any materials present in the medium; thus, it is difficult to monitor the stability of NPs in a complex fluid that contains additional components such as serum proteins.

2.2.4. Gel Permeation Chromatography. Gel permeation chromatography (GPC) can be used to determine the physical stability of self-assembled NPs. This technique separates self-assembled NPs from degraded NPs or their components. NP stability can be estimated based on the elution times, given that degrading NPs or their components are eluted later than intact NPs. Yokoyama et al. used GPC to study the formation of different polymeric micelles and their stability in aqueous media.⁴⁰ In subsequent studies, GPC was used to study the stability of drug-loaded micellar structures of different compositions in the presence of serum^{41,42} or purified serum albumins.⁴² This technique was also used to assess the formation and dissociation of insulin-hydrophobized pullulan NP assemblies.⁴³ The assemblies showed high colloidal stability in water and buffer, but insulin was released rapidly from the assemblies upon the addition of bovine serum albumin.⁴³ Many other studies have also used GPC as a means to evaluate stability of self-assembled NPs in the presence of serum

proteins.^{44–48} While this technique is straightforward, interactions between the column beads and NPs may affect the outcome of the analysis.

2.2.5. Forster Resonance Energy Transfer Technique. Recently, Forster resonance energy transfer (FRET) has been employed to study the stability of NPs at the molecular level. Cheng et al. encapsulated a FRET pair, consisting of hydrophobic fluorescent probes DiO (donor) and DiI (acceptor), in a polymeric micelle to study the stability of micelles.⁴⁹ The FRET pair retained in the hydrophobic core of the micelles shows a FRET signal due to their proximity to each other, whereas the FRET signal disappears as the micelles dissociate and release the dyes. Using this phenomenon, micelle stability during cellular uptake has been studied.⁴⁹ When FRET dye-loaded micelles were incubated with KB cells for 2 h, a strong DiO signal was observed on the plasma membrane, indicating that the dyes were already released from the micelle core while passing the cell membrane.⁴⁹ Following internalization, a FRET signal was partially restored, suggesting the two dyes were trafficked to and concentrated in the same endosomal vesicles.⁴⁹ The FRET technique was used to study the stability of NPs *in vivo* as combined with intravital microscopy.⁵⁰ Many other studies have utilized FRET in evaluating the stability of the NP systems *in vitro* or *in vivo*.^{25,48,50,51} One challenge in FRET analysis is the need for technical adjustment to avoid optical artifacts that may interfere with FRET detection. For example, an acceptor dye can be excited directly with light that is supposed to excite the donor.⁵² Alternatively, fluorescence from the donor can leak into the detection channel of the acceptor fluorescence (bleed-through).⁵² For accurate assessment of FRET signals, several optical corrections need to be made to account for these issues. Furthermore, for NP systems that require covalent labeling of NP-dye, this conjugation may affect the formation or chemical conformation of the NPs, thus potentially changing its properties.

2.3. In Vitro Prediction of in Vivo Fates of NPs. Once NPs are introduced into the circulation, plasma proteins almost instantaneously adsorb to their surfaces. The protein corona changes the nature of the NPs and induces sequential immune responses, leading to uptake by phagocytes of the reticuloendothelial system (RES) and rapid clearance from the circulation.^{53,54} Therefore, it is important that NPs resist the adsorption of plasma proteins and premature clearance by the immune system.⁵⁵ Protein adsorption to the NP surface is mainly influenced by its hydrophobicity and charge among other properties.⁵⁶ Typically, hydrophilic and electrically neutral NPs are less likely to engage with serum proteins; therefore, polyethylene glycol (PEG) is widely used to decorate the NP surface (“PEGylate”) and prevent binding of plasma proteins to the NPs. The PEGylated stealth NPs thus acquire a longer half-life in circulation,^{55,57,58} which translates to greater accumulation in solid tumors via the enhanced permeability and retention (EPR) effect.^{59,60} On the other hand, an accelerated blood clearance of PEGylated liposomes has been reported following the injection of the first dose in animals,⁶¹ mediated by the production of anti-PEG IgM.⁶² Clinical studies show an occurrence of anti-PEG antibodies in human subjects following the treatment with PEGylated agents.⁶³ Therefore, alternative stealth coatings are investigated to circumvent the immunogenicity of PEG, such as polysaccharides including dextran, heparin, and low molecular weight chitosan, or synthetic polymers.^{55,64–66}

2.3.1. Protein Adsorption. Given the immunogenicity of an NP has only been detected in costly *in vivo* studies, there has been increasing interest in predicting the immunological responses to NPs in earlier phases of NP development, preferably *in vitro*. One of the basic techniques to study the stealth properties of NPs is to examine the extent of protein adsorption on the NP surface, the first step of phagocytic removal of NPs.^{67–69} To assess the extent of protein adsorption, NPs with constant surface area are incubated in serum for a period of time and washed with water to remove proteins loosely adsorbed to the surface. The proteins bound to NPs are desorbed with a surfactant like sodium dodecyl sulfate and subjected to gel electrophoresis and/or quantitative protein assay. Attempts have been made to correlate protein adsorption to the NP surface and the *in vivo* fate of the NPs.⁵⁵ For example, polystyrene NPs coated with a series of amphiphilic polyethylene oxide-polypropylene oxide block copolymers showed much reduced protein adsorption *in vitro* and a prolonged circulation in rats.⁵⁵ However, protein adsorption alone provides only a rough prediction of the potential immunogenicity, as it does not reflect the complex nature of subsequent immune reactions leading to elimination of NPs.

2.3.2. Phagocytic Uptake. Another technique to predict the fate of NPs in blood is to measure the degree of phagocytic uptake of NPs by incubating fluorescently labeled NPs with macrophages for a certain period of time and quantifying the amount of NPs taken up by the phagocytes.^{70–72} The size and surface properties are important determinants of phagocytosis.⁷³ According to a study with microparticles, their shape at the initial contact with a phagocyte is shown to be critical in the phagocytosis process.⁷⁴ The shape has similar importance in NPs.^{75,76} For example, linear polymer micelles (filomicelles) had a longer circulation time than their spherical counterparts with similar chemistry due to their resistance to phagocytic uptake in flow.⁷⁷ Similarly, PEGylated gold nanorods, as compared to spherical NPs, were taken up by macrophages to a lesser extent and showed a longer circulation time upon injection in mice.⁷⁵ One limitation of the phagocytosis assay is that it is carried out in cell culture medium, which does not completely resemble the concentration and composition of proteins in blood; thus, the extent of protein adsorption and phagocytosis can be underestimated.

2.3.3. Complement Activation. Adsorption of a group of soluble plasma proteins, also called the complement system, on the NP surface initiates a biochemical cascade leading to NP clearance from the circulation via complement receptor-mediated phagocytosis.⁵⁴ The degree of complement system activation can be measured to predict the ability of NPs to evade or elicit the phagocytic clearance. As foreign particles trigger the system activation, one of the soluble protein components, C3, is cleaved into C3b and C3a. Therefore, the ratio of C3b to C3 is determined as a measure of the extent of complement activation by NPs, via crossed immunoelectrophoresis of serum solution incubated with NPs.^{78–81} The complement system activation assay has been used to analyze the effect of chain length, conformation, charge, and composition of a surface-decorating polymer on its stealth functions.^{73,82–84} When chitosans with different chain lengths (8.8 to 80 kDa) were compared, complement activation increased with chain length and number of NH₂ groups.⁸⁵ Difference in the conformation of polymer chains on the NP surface can dramatically influence the ability to bind to plasma proteins and activate the complement system. For example,

polyalkylcyanoacrylate (PACA) NPs with dextran coating prepared by two different methods had two types of dextran conformation and density, which had opposite complement activation effects.⁸² Dextran chains bound forming flexible “loops” on the NP surface had a strong complement activation effect, but dense “brush” like conformation showed resistance to protein adsorption.⁸² Similar observations were reported with poly(isobutylcyanoacrylate) (PIBCA) NPs coated with dextran or chitosan.⁷⁸ Vauthier et al. reported that the complement activation effects of PIBCA NPs with different dextran coatings did not necessarily correlate with their albumin binding, indicating that each protein interacts with surface coatings uniquely according to its size, conformation, and flexibility.⁸³

2.3.4. NCL Protocols. The Nanotechnology Characterization Laboratory (NCL) has published a series of *in vitro* protocols specifically designed for the evaluation of nanomaterials' compatibility with various biological environments and the immune system, which include tests of blood coagulation, complement activation, protein binding, platelet aggregation, and phagocytosis due to nanomaterials.⁸⁶ Although no *in vitro* test may exactly mimic real physiological conditions *in vivo*, combinations of these approaches can help predict *in vivo* behaviors of NPs.

3. CELL-BASED EVALUATION OF NPS

Once NPs are characterized with respect to their physical and chemical properties, their biological effects are tested in cell culture models prior to *in vivo* applications. This section describes widely used cell models and their advantages and weaknesses.

3.1. Two-Dimensional (2D) Monolayer Cell Culture. In frequently used 2D cell culture, cells are grown as a monolayer on a plate or flask surface, which is treated via physical methods or adhesive biological materials to encourage cell attachment. The cells are bathed in culture medium supplemented with nutrients and grown at 37 °C in a humidified environment that provides uniform exposure to oxygen (and carbon dioxide). These conditions provide minimum requirements for maintaining cell viability. As a consequence of convenience, the monolayer cell culture model is extremely beneficial for quick determination of cellular uptake and intracellular trafficking of NPs, bioactivity of drugs delivered as NPs, and toxicity of the vehicles. These studies are usually done with multiple established cell lines.

3.1.1. Cellular Uptake. Confocal microscopy and flow cytometry are widely used to study the cellular uptake of NPs. These methods require that NPs be labeled with a fluorescent marker, which is done by physical entrapment or covalent conjugation. While the former has the advantage of simplicity, one should be aware that a lipophilic dye may leach out of NPs upon contact with amphiphilic or lipophilic components and misrepresent NPs.⁸⁷ When the intention is to track a vehicle, it is desirable to label the component by covalent conjugation of a dye and confirm the stability of the conjugation in a solution similar to physiological fluid. Ideally, a drug and a vehicle should be separately labeled so that drug delivery attributable to the vehicle may be accurately evaluated.

Ekkapongpisit et al. studied the potential of silica (10 nm, no surface modification) and polystyrene NPs (30 nm, carboxyl surface modification) as theranostic agents in the treatment of ovarian cancer.⁸⁸ Cellular uptake of the fluorescently labeled NPs were studied with OVCAR-3 and SKOV-3 ovarian cancer

cell lines using fluorescence microscopy.⁸⁸ Initially mesoporous silica NPs were associated along nuclei, with subsequent diffusion into the cytoplasm.⁸⁸ Polystyrene NPs were observed as punctate signals restricted to cell peripheries, which disappeared in 120 min.⁸⁸ At subtoxic levels of the NPs, mesoporous silica NPs showed faster cellular uptake and longer intracellular retention than polystyrene NPs.⁸⁸

While confocal microscopy helps locate NPs within cells, quantitative analysis of NP uptake relies on flow cytometry. In flow cytometry, cells in suspension are passed through an interrogation point, where the cells are individually examined by a laser with respect to their optical or fluorescent properties.⁸⁹ Quantitative information is acquired based on the number of fluorescent cells or an average fluorescence intensity of the cell population and used to determine the fraction of cells killed by therapeutic treatments or the amount of a fluorescent drug internalized by the cells. In one example, magnetic NPs (MNPs) were used as a drug carrier to tumor cells.⁹⁰ Iron oxide (Fe₃O₄) was covered with carboxymethyl chitosan (CMCS),⁹⁰ in which montmorillonite (MMT) was intercalated to enhance cellular uptake of the NPs.^{90,91} A lipophilic fluorescent dye, coumarin-6, was covalently intercalated to MMT to label the CMCS/MMT-covered MNPs for a cellular uptake study.^{90,92} Flow cytometry was used in quantifying the uptake of the coumarin-6 labeled CMCS/MMT-MNPs by HeLa cells.⁹⁰ The researchers observed that cellular uptake of their delivery system increased with increasing MMT content.⁹⁰ On the other hand, the amount of NPs associated with the cells did not increase in proportion to the NP concentration, indicating that the cellular uptake was a saturable process.⁹⁰ Gratton et al. used flow cytometry to evaluate cellular uptake kinetics of PEG hydrogel particles with different sizes and shapes in HeLa cells, prepared with a lithographic fabrication (particle replication in nonwetting templates, PRINT) technique.⁹³ This study found that submicrometer particles were taken up by HeLa cells to a greater extent than microparticles and the high aspect ratio (height:diameter = 3:1) particles showed a greater rate and extent of cellular uptake than the low aspect ratio (1:1) particles with a comparable volume.⁹³

Alternatively, cellular uptake can be quantified by direct measurement of intracellular drug or dye contents. Here, cells are destroyed at the end of a treatment to release the internalized drug. For example, in the evaluation of doxorubicin (DOX)-loaded polymeric micelles, SiHa human cervical tumor cells were incubated with the micelles or a free drug for various time periods, washed, and the drug extracted with dimethyl sulfoxide (DMSO).⁹⁴ DOX content in the extract was determined according to the fluorescence intensity.⁹⁴ This study found no difference between free DOX and DOX-loaded micelles in cellular uptake at each time point but significant difference in cytotoxicity (concentration for 50% cell death (IC₅₀): DOX < micellar DOX), which was interpreted as delay in DOX release from the micelles.⁹⁴

3.1.2. Mechanisms of Cellular Uptake. The mechanism by which NPs enter cells is as much important as the quantity of the internalized NPs because the subsequent intracellular events are dependent on the uptake pathway. Depending on their physicochemical properties, NPs can enter cells via various pathways.^{95–98} For example, particles with a size ranging from a fraction of a micrometer to ~10 μm depend on phagocytosis, performed by specialized phagocytic cells.^{96,99} Smaller NPs may be taken up by macropinocytosis^{96,99,100} or clathrin- or

caveolae-mediated endocytosis.^{95,96,101–103} Cells can internalize NPs up to 300 nm in diameter by macropinocytosis, where the cell membrane protrudes and fuses back with another part of the membrane to produce large vesicles around the NPs.^{5,9} Clathrin-mediated endocytosis occurs as clathrin proteins in the cell membrane polymerize and form a vesicle (~100 nm) around an NP, which is then transported to an early endosome.⁹⁶ Some NPs may utilize a caveolar route,¹⁰⁵ where the cell membrane is coated with caveolin along with cholesterol and lipids and forms a flask-shaped invagination called caveolae.⁹⁶ In particular, clathrin- or caveolae-mediated endocytosis involves cellular receptors for specific ligands,¹⁰⁰ such as folic acid,¹⁰⁴ transferrin,¹⁰⁵ or albumin,¹⁰⁶ which facilitate endo- or transcytosis of these molecules. For this reason, NPs incorporating these ligands have been widely explored as a way of achieving cell-specific NP delivery.

For studying the NP uptake pathway, cells are treated with specific inhibitors of specific internalization pathways^{107–109} prior to incubation with fluorescently labeled NPs. Chlorpromazine is an inhibitor of clathrin-mediated endocytosis, and filipin and methyl-β-cyclodextrin (MβCD) are inhibitors of caveolae-mediated endocytosis.¹⁰⁷ Macropinocytosis and phagocytosis can be inhibited by pretreatment with amiloride (inhibitor of Na–K exchange) or cytochalasin D (F-actin-depolymerizing drug).¹⁰⁷ Following the pretreatment, cells are cultured with NPs and analyzed with flow cytometry or confocal microscopy combined with quantitative imaging analysis software to determine the sensitivity of the NP uptake to each inhibitor. For instance, the uptake pathways of mesoporous silica and carboxyl-terminated polystyrene NPs were compared by investigating their responses to pretreatment of MβCD.⁸⁸ MβCD has high affinity for cholesterol and forms inclusion complexes with cholesterol when added to cells at 5–10 mM.¹⁰⁷ This way, MβCD removes cholesterol from the plasma membrane, interfering with cholesterol-dependent uptake pathways such as caveolae-mediated endocytosis.¹⁰⁷ The two NPs showed opposite responses to the MβCD treatment. The uptake of mesoporous silica NPs was hindered by the MβCD treatment, whereas that of polystyrene NPs did not change, indicating that mesoporous silica NPs, but not polystyrene NPs, were taken up via caveolae-mediated endocytosis.⁸⁸

The cellular entry of NPs incorporating specific ligands, the so-called targeted NPs, mirrors the interaction between the ligands and corresponding receptors.¹¹⁰ Moreover, NPs act as a scaffold on which multiple ligands are concentrated, thus enabling simultaneous interactions with multiple receptors on the cells (i.e., multivalent effect).¹¹⁰ As a result, the binding strength of ligand-modified NPs to cell receptors is often orders of magnitude higher than that of free ligands.^{111,112} Several studies demonstrate that the NPs modified with receptor-specific ligands achieve a greater cytotoxicity than nonmodified ones due to the enhancement of cellular binding and uptake. For example, Liu et al. produced folate-receptor targeted polymeric micelles, where folic acid was conjugated to the hydrophilic block.¹¹³ Cellular uptake of the targeted micelles by mouse breast cancer (4T1) and human epidermal carcinoma (KB) cells was significantly enhanced by the presence of folic acid on the micelles compared to the untargeted micelles.¹¹³ Consequently, the folate-targeted micelles carrying DOX were more cytotoxic than untargeted NPs due to folate-receptor mediated endocytosis.¹¹³ A similar result was reported with another folate-receptor targeted micelle based on a different

polymer.¹¹⁴ In addition to naturally overexpressed targets, cells may be pretreated to induce overexpression of specific receptors, such as p32 receptors that are upregulated by thermal treatment. Park et al. reported that magnetic nanoworms and DOX-loaded liposomes, decorated with a peptide ligand targeted to p32 receptors, showed increased binding and internalization by MDA-MB-435 human carcinoma cells, which were preheated with gold nanorods to induce expression of p32 receptors.¹¹⁵

Once NPs targeted to specific cellular receptors are developed, it is important to confirm whether the cellular uptake is indeed mediated by the intended receptor–ligand interactions. One common way is to compare cellular uptake of the targeted NPs in cells that express the specific receptors to different degrees. For example, Kim et al. produced PLGA NPs targeted to folate receptors and compared their uptake in KB cells (folate receptor overexpressing cell line) and A549 lung cancer cells (folate receptor-deficient cell line) to find that the NP uptake was much higher for KB cells than for A549 cells.¹¹⁶ Additionally, cells are pretreated or coincubated with free ligands in addition to the targeted NPs to investigate whether the NP uptake is competitively inhibited. If the NP uptake is receptor-mediated, cellular uptake and/or bioactivity of a drug delivered by the NPs is diminished by the presence of excess free ligands in a concentration-dependent manner.^{113,117,118}

In addition to the presence of ligands, several other factors affect the endocytic pathway that NPs take to enter a cell.^{95,119,120} Particle size has a direct influence on NP uptake pathway. It is assumed that NPs carried via the receptor-mediated endocytic pathways have average hydrodynamic diameters close to the sizes of vesicles formed during clathrin- or caveolae-mediated endocytosis, which are 100 or 60 nm, respectively.^{96,101} Macropinocytosis has a greater flexibility in the upper limit of particle size.⁹⁶ Particle size has an additional role in targeted NPs as a main determinant of ligand density on the NP surface.^{110,112,119} A small particle has a high surface curvature that limits relative orientation between ligands, leaving large background area without ligand coverage.¹¹² Relatively large NPs can have a higher ligand density on the surface, but if the membrane cannot catch up with the high demand for receptors within the area of binding, NP uptake is also limited.¹¹² Therefore, Jiang et al. concludes that 40–50 nm is an optimal size for receptor-mediated endocytosis.¹¹² According to Gratton et al., the cellular uptake pathway is also influenced by the particle shape.⁹³ They used the PRINT technique to produce particles with different aspect ratios and observed that the particles had different sensitivity to inhibitors of various endocytosis pathways.⁹³ Another factor to influence endocytic pathway is the surface charge of NPs. Typically cationic NPs are internalized more readily than anionic ones, due to the ability to interact with negatively charged cell membrane and clathrin-coated pits in the membrane.^{95,96,110,119,121}

3.1.3. Intracellular Trafficking. Once an NP is internalized by cells, its intracellular fate critically influences its therapeutic effect, especially when the drug target is localized in a particular

organelle and/or the drug is unstable in a specific intracellular environment (e.g., acidic pH or lysozyme in late endo/lysosomes). To track the intracellular trafficking of the NPs, markers of intracellular organelles are colocalized with NPs and observed over a period of time. Alternatively, the organelles are located using fluorescently labeled antibodies after fixation and permeabilization of cells. One pitfall of the latter technique is

potential artifacts resulting from the fixation/permeabilization process, such as protein extraction or relocalization.^{122,123}

In the study of mesoporous silica and polystyrene NPs discussed earlier, the NPs were incubated with cells which were prelabeled with LysoTracker, a fluorescent probe that accumulates in acidic organelles.⁸⁸ The mesoporous silica NPs and the LysoTracker signals colocalized in 5 min, indicating the residence of silica NPs in lysosomal vesicles. With time the fluorescence of the silica NPs and LysoTracker signals separated, which suggested the escape of NPs from the acidic vesicles.⁸⁸ On the other hand, carboxyl-terminated polystyrene NPs did not show colocalization with LysoTracker signals at any time, indicating their residence in recycling vesicles.⁸⁸ This result is consistent with the limited intracellular accumulation of the polystyrene NPs.⁸⁸

3.1.4. Bioactivity of NPs. When an NP is developed for drug delivery, it is of utmost interest whether the potency and efficacy of a drug are changed and/or target specificity of the drug is enhanced due to the delivery system. When an anticancer drug is delivered via NPs, various methods measuring the metabolic activity or cell membrane integrity are used to estimate the viability of the treated cells. For example, colorimetric assays such as MTT, MTS, and XTT assays measure mitochondrial function of live cells, according to the ability to reduce these tetrazolium salts to intensely colored formazan dyes.¹²⁴ Bioluminescence assays measure ATP produced by live cells using luciferase. Since luciferase metabolizes luciferin in an energy-dependent manner, the luciferase activity (luminescence intensity) is proportional to the amount of ATP (i.e., cell viability).¹²⁴ Dye/stain exclusion assays utilize chemicals such as trypan blue, propidium iodide, and calcein-AM, which are selectively excluded from or trapped in live cells according to membrane integrity or esterase activity. Lactate dehydrogenase (LDH) assays also reflect the integrity of the cell membrane. LDH is a constitutive cytoplasmic enzyme, which is released when the cell membrane is compromised. Therefore, the LDH activity in cell medium indicates the proportion of nonviable cells.¹²⁵

In the CMCS/MMT-covered MNPs introduced earlier, doxorubicin (DOX) was electrostatically complexed to the NP at pH 6, forming DOX/CMCS/MMT-MNPs.⁹⁰ DOX release from the NP was faster at pH 5 versus pH 7.4 due to the protonation of CMCS at pH 5, where DOX was no longer retained via electrostatic interactions.⁹⁰ The cytotoxic effect of the NPs was observed in MCF-7 cells via MTT assay in comparison with free DOX and the vehicle.⁹⁰ Cytotoxicity in MCF-7 cells increased in the order of CMCS-MNPs (vehicle), CMCS/MMT-MNPs (vehicle), free DOX, and DOX/CMCS/MMT-MNPs.⁹⁰ Interestingly, the toxicity of DOX/CMCS/MMT-MNPs in H9c2 cardiomyocytes was less than that of free DOX, due to the antioxidant effects of CMCS.⁹⁰

Lei et al. studied the cytotoxicity and cellular uptake of DOX-loaded poly(lactic-co-glycolic acid) (PLGA) NPs in drug-sensitive and resistant cell lines: SKOV-3 ovarian carcinoma cells (drug resistant, p53 mutation, HER2+), MES-SA uterine sarcoma cells (drug sensitive), and its drug resistant variant

MES-SA/Dx5 cells (P-glycoprotein (P-gp)-overexpressing). DOX-PLGA NPs (DNPs) and antibody-conjugated DOX-PLGA NPs (ADNPs) were comparable in particle size (163 and 213 nm) and drug loading (2.7% and 2.3%), except that ADNPs had 9.3 µg of anti-HER2 antibody per mg of NPs.¹²⁶ Due to the HER2-mediated endocytosis, ADNPs were taken up better than DNPs by SKOV-3 cells. In contrast, no difference in

Molecular Pharmaceutics

cellular uptake was observed between the two NPs in MES-SA and MES-SA/Dx5 cells, which did not express HER-2. Notably, both NPs showed higher uptake than free DOX in MES-SA/Dx5 cells, indicating that the NPs were not subject to P-gp efflux. In this study, cytotoxicity of the NPs reflected the cellular uptake profile: ADNPs were more cytotoxic than DNPs or free DOX in SKOV-3 cells, although the difference did not reach statistical significance. Both ADNPs and DNPs showed higher toxicity than free DOX in MES-SA/Dx5 cells.¹²⁶

On the other hand, there are examples where bioactivity of NPs does not necessarily match their cellular uptake.¹²⁷ In our recent study, PLGA NPs conjugated to a cell-penetrating peptide, TAT, were used to increase intracellular delivery of paclitaxel (PTX) to multidrug resistant (MDR) cells. As expected, the PLGA-TAT NPs were more efficiently taken up by MDR cells than PLGA NPs, but they did not increase PTX

delivery to the MDR cells (hence their killing). This discrepancy can be interpreted as indirect evidence of extracellular drug release from the NPs, which may not be observed in typical *in vitro* release kinetics studies using a buffered saline.¹²⁷

3.2. Three-Dimensional (3D) Approaches. In *in vitro* 2D cell culture, target cells are directly and uniformly exposed to NPs for a desired period of time with no limitation in the higher end of a concentration range. However, this condition may not be an accurate reflection of *in vivo* events occurring at 3-dimensional (3D) masses such as solid tumors, where NPs face various access barriers to target cells.¹²⁸ Moreover, due to the highly unnatural geometric and mechanical properties, there is a good possibility that the 2D-cultured cells have limited potential to represent the phenotype and genetic functions of living tissues, which can drastically affect their responses to chemical stimuli.^{129–131} The fact that *in vivo* efficacy often betrays the drug screening results obtained in 2D cell culture is not irrelevant to the artificial nature of 2D culture models.¹³² Therefore, several efforts have been made to develop 3D cell models, which can better mimic cell–cell and cell–extracellular matrix (ECM) interactions seen in a living organism, as a test bed of NP systems. This section introduces various 3D models and examples in which 3D models were used for evaluation of the efficacy of a drug or drug-loaded NPs.

Commonly used models include (i) cells encapsulated in scaffolds, (ii) multicellular spheroids,¹³³ (iii) a combination of

spheroids and scaffolds,¹³⁴ and (iv) multilayer cell models¹³² (Figure 2). Other 3D models include excised tissues or tissue components¹³⁵ and a microfluidic device based on polydimethylsiloxane template.^{136–138}

In the *cells-in-scaffold* model, which has been widely studied in the context of tissue engineering, cancer cells are grown in either synthetic or natural scaffolds such as hydrogels of ECM components,^{139–141} PEG hydrogels,¹⁴² peptide nanofiber scaffolds,¹⁴³ multilayered paper scaffolds,¹⁴⁴ or polymers.¹³⁰ An advantage of this model is that cells are exposed to a microenvironment similar to their native ECM and reflect its influence on the cell growth. In one example, 3D tumor models were created by seeding MDA-MB-231 human breast cancer cells in collagen I hydrogels.¹⁴⁰ The 3D tumor models expressed a phenotype reflecting *in vivo* tumor progression, such as hypoxia, necrosis, and angiogenic gene upregulation, in a manner dependent on the thickness of the collagen gels.¹⁴⁰ In another study, C4-2B bone metastatic prostate cancer cells were cultured in *in situ* cross-linkable hyaluronic acid (HA)

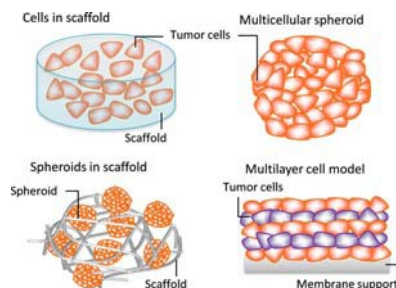


Figure 2. Commonly used 3D tumor models to determine NP efficacy.

hydrogels, where cancer cells grew forming clustered structures similar to real tumors.¹⁴¹ This model was used in testing the efficacy of anticancer drugs to show that cells in the HA gels were more sensitive to camptothecin than those in 2D culture.¹⁴¹ The increased drug sensitivity of cells in the HA hydrogel is attributed to the biological activities of HA on cancer cells, which may be reflective of the ECM–cell interactions *in vivo*.¹⁴¹ Conversely, epithelial ovarian cancer cells grown in PEG hydrogels showed a reduced sensitivity to PTX treatment than those in 2D culture.¹⁴² These results suggest that a scaffold is not simply a space-filler but plays an active role in expression of phenotypes relevant to drug sensitivity.

Mitra et al. developed a cells-in-scaffold model of Y79 retinoblastoma for the study of NP efficacy. Here, large and porous PLGA microparticles (~150 μm) were produced as a scaffold, in which dispersed cells were seeded and allowed to grow.¹³⁰ The porous microparticles were produced by the double emulsion method using sucrose as a porogen. Gelatin, polyvinyl alcohol, and chitosan were incorporated to promote cell attachment to the microparticle scaffold.¹³⁰ Cells in the 3D model not only attached to the microparticle surface but infiltrated the particles over time.¹³⁰ Compared to the cells grown in 2D, those grown in the 3D model exhibited higher ECM production and altered gene regulation.¹³⁰ When dosed with carboplatin-, etoposide-, or DOX-loaded NPs or their free

drug counterparts, 4.5–21.8-fold higher IC_{50} values were observed in the 3D model as compared with 2D.¹³⁰ These results indicate that 3D culture conditions can greatly change the chemical and biological environment of the cells and, thereby, the therapeutic outcomes of the tested drug.¹³⁰

Multicellular spheroids refers to spherical aggregates of cancer cells that can reflect tight junctions between cells and ECM synthesis.¹⁴⁵ A multicellular spheroid model was used in the evaluation of DOX-loaded micelles based on a poly(ethylene oxide)-poly[(R)-3-hydroxybutyrate]-poly(ethylene oxide) (PEO-PHB-PEO/DOX) with respect to their ability to penetrate the spheroids.⁹⁴ Here, the 37 nm micelles or free DOX were incubated with SiHa cell spheroids with a diameter of 400 μm .⁹⁴ In 30 min, DOX-loaded micelles penetrated spheroid cores to a greater extent than free DOX, although this difference disappeared in 2 h.⁹⁴ This difference was explained by the ability of the PEGylated micelles to avoid nonspecific binding to ECM and immediate cellular uptake.⁹⁴ In another example, Kim et al. used a multicellular cylindroid model to

Molecular Pharmaceutics

investigate how surface charges control the penetration and cellular uptake of gold NPs in tumor matrix.¹⁴⁶ Gold NPs (6 nm) were modified with trimethyl ammonium- or carboxylate-terminated tetra(ethylene glycol) to produce cationic or anionic surfaces, respectively. The NPs were additionally conjugated with fluorescein and incubated with a cylindroid, and the fluorescence in the cylindroid was quantified according to time and radial position. The results showed that gold NPs with a cationic surface were readily consumed by actively proliferating cells at the periphery, whereas negative NPs penetrated into the apoptotic/necrotic interior of the cylindroid at a higher rate than cationic ones.¹⁴⁶

Hoetal. used a *spheroid/scaffold combination model* of U251 human glioma cells to study the effect of the geometry of a cell model on DOX and irinotecan drug resistance.¹³⁴ Spheroids were first formed by growing cells in a plate coated with poly(2-hydroxyethyl methacrylate), which prevented cell attachment to the well bottom. Subsequently, the spheroids were seeded into a porous PLGA scaffold coated with collagen.¹³⁴ The spheroids maintained their structure for 2 days, allowing for a time window in which the drug effect could be tested. Drug resistance was highest for the spheroids seeded in the scaffold, followed by those seeded as dispersed cells in a comparable scaffold, with cells grown in 2D having the least drug resistance.¹³⁴ Lactate production was highest in the spheroid-seeded scaffold model, while the 2D cell culture model produced the lowest lactate per cell.¹³⁴ The authors attributed the increased drug resistance in the 3D model to the tendency to form hypoxic regions, supported by the high lactate production, rather than the limitation in drug transport.

In the *multilayer cell models*, cancer cells are grown on a permeable membrane support to reach 200–250 μm thick cell layers.¹⁴⁵ Hosoya et al. created multilayer cell models simulating pancreatic cancer with fibrotic tissue to study intratumoral transport of different macromolecules.¹³² These models consisted of alternating layers of fibroblasts and fibronectin-gelatin films on Transwell inserts.¹³² The thickness of the models with 5 layers of cultured cells was 30–50 μm . Transport of FITC-dextran across the cell model was quantified by measuring the fluorescence of the medium below the Transwell.¹³² As readily expected, the dextran transport decreased as the number of cell layers increased or the molecular size of dextran increased. Approximately 29% of the 250 kDa FITC-dextran conjugate (12 nm) permeated the K643f monolayer over 24 h.¹³² During the same time, the 12 nm dextran had approximately 21% and 19% permeability through 2 and 5 layer models, respectively.¹³²

4. IN VIVO STUDIES

Once NPs demonstrate a proof of concept *in vitro*, their safety and therapeutic effectiveness are tested in animal models. The results of animal studies play a pivotal role in decision making toward clinical trials. An animal model that can reflect pathophysiology of a human disease is an invaluable tool for predicting therapeutic outcomes in human. This section discusses the currently available experimental animal models, their strengths and weakness, and emerging trends in the animal model development. Given that the majority of *in vivo* NP studies have been performed in the context of cancer therapy, the discussion focuses on animal models of tumors unless specified otherwise.

4.1. Evaluation of NPs in Animal Models of Tumors: State of the Art.

Mouse models with allograft or human

xenograft tumors are widely used in *in vivo* evaluation of NPs due to the relatively low cost and well-established protocols. In these models, cancer cells are inoculated or tumor tissues are implanted (typically subcutaneously) in immunodeficient mice (athymic nude or severe combined immunodeficient mice), allowed to grow to visible tumors (Figure 3), and treated with experimental therapeutics to examine the pharmacokinetics, biodistribution, and the pharmacological effects.

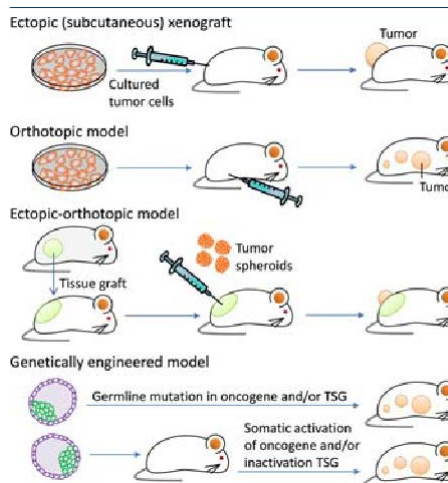


Figure 3. Animal models of tumors used in the evaluation of *in vivo* efficacy of NPs. TSG: Tumor suppressor genes.

For example, therapeutic efficacy of PEGylated liposomal DOX (PLD) was tested in a mouse model of cancer.¹⁴⁷ C-26 mouse colon carcinoma cells were inoculated subcutaneously in the left flank of a BALB/c mouse, and the response to a treatment was monitored by measuring the size of tumors.¹⁴⁷ Here, free DOX at a dose of 6 mg/kg only slightly delayed tumor growth compared with the saline control, whereas with PLD at a dose of 6 or 9 mg/kg tumors regressed to nonmeasurable sizes.¹⁴⁷ Consequently, all animals receiving PLD groups survived 120 days (duration of the experiment), whereas those receiving saline and free DOX groups survived a mean of 50 and 49 days, respectively.¹⁴⁷ The therapeutic benefit of PLD is attributable to its high bioavailability and preferential accumulation in tumors.¹⁴⁷ Similarly, Vaage et al. used human prostate carcinoma PC-3 implanted subcutaneously into mice and reported that the therapeutic efficacy of DOX was increased and its toxic side effects were reduced when delivered as PEGylated liposomes.¹⁴⁸ The superior efficacy of PLD over free DOX was further demonstrated in mouse models of murine mammary carcinomas,¹⁴⁹ xenografted human ovarian carcinomas,¹⁵⁰ and pancreatic carcinomas.¹⁵¹

However, the performance of NPs in these animal models is not always predictive of clinical outcomes. The PLD that demonstrated 100% survival of tumor-bearing mice¹⁴⁷ was at best equivalent to free DOX in clinical efficacy (progression-free survival (PFS) and overall survival) in a randomized phase III trial with metastatic breast cancer patients.¹⁵² Here, women

Molecular Pharmaceutics

with metastatic breast cancer ($n = 509$) were randomly assigned to either PLD 50 mg/m² (every 4 weeks) or DOX 60 mg/m² (every 3 weeks). PLD and DOX were comparable with respect to PFS (6.9 versus 7.8 months) and overall survival (21 versus 22 months).¹⁵² In a phase II study with metastatic breast cancer patients, the overall response rate of the PLD-treated group (45 to 60 mg/m² every 3 to 4 weeks for a maximum of six cycles) was 31% (95% confidence interval, 20% to 43%),¹⁵³ comparable to the response rates (25 to 40%) for free DOX at conventional doses (50 to 75 mg/m² every 3 weeks) in advanced breast cancer patients with similar characteristics.^{154–157}

The discrepancy between preclinical *in vivo* results and clinical outcomes is found in another example. PK1, a covalent conjugate of DOX and *N*-(2-hydroxypropyl) methacrylamide (HPMA) copolymer via biodegradable (Gly-Phe-Leu-Gly) oligopeptide, was evaluated in various animal models.^{158,159} The models were created by intraperitoneal (ip) injection of L1210 leukemia cells, subcutaneous (sc) injections of B16F10 melanoma cells, Walker sarcoma cells, P388 leukemia cells, and M5076 cells, or subcutaneous implantation of LS174T human colon xenograft.¹⁵⁸ When administered ip to mice bearing L1210 ascitic tumor, PK1 showed relatively good antitumor activity as compared to free DOX.¹⁵⁸ The highest *T/C*, a ratio of median survival of the test group (*T*) to that of untreated control (*C*), seen in the PK1-treated group was >762%, as opposed to 214%, that of the free DOX-treated group.¹⁵⁸ In the case of solid tumor models (B16F10, Walker, P388, M5076, and LS174T xenograft), ip administration of PK1 resulted in an increase in survival rate as compared to free DOX. In particular, P388 and Walker sarcoma showed remarkable regression after the treatment.¹⁵⁸ On the other hand, the phase II studies of PK1 in patients with non-small-cell lung (NSCLC, $n = 29$), colorectal ($n = 16$), and breast ($n = 17$) cancer showed less exciting outcomes.¹⁶⁰ Of 26 evaluable patients with NSCLC, 3 chemotherapy-naïve patients had partial responses, and none of the 16 evaluable patients with colorectal cancer showed responses.¹⁶⁰ Of 14 evaluable patients with breast cancer, only 3 anthracycline-naïve patients had partial responses.¹⁶⁰

Another example is a macromolecular conjugate of PTX and poly(L-glutamic acid) (PTX poliglumex). PTX poliglumex demonstrated a prolonged circulation half-life and greater tumor uptake as compared to Taxol (PTX solubilized with Cremophor EL) in a mouse model.¹⁶¹ Consequently, PTX poliglumex exhibited significant tumor growth delay after a single intravenous (iv) injection at 80 mg/kg (as PTX equivalent) compared with Taxol at the same dose in mice bearing syngeneic ovarian OCA-1 carcinoma.¹⁶¹ A similar antitumor effect was shown in a rat model with 13762F rat mammary adenocarcinoma.¹⁶¹ Clinical outcomes in phase II trials were modest. In women with recurrent epithelial ovarian, primary peritoneal, or fallopian tube carcinoma, the response rate and median time to disease progression of PTX poliglumex (175 mg/m², every 21 days) were 10% and 2.1 months, respectively,¹⁶² and the median PFS was 2.8 months.¹⁶³ Even considering variability due to prior treatment history, these responses were not favorable as compared with those of the standard regimen based on PTX (135 mg/m²) and platinum (75 mg/m²) based chemotherapy,¹⁶⁴ which showed >70% of response rate and 18 months of median PFS.¹⁶⁵ The lack of advantages over existing regimens, combined with unexplained toxicity, led the developer to officially withdraw the application for a marketing authorization of PTX poliglumex in 2009.¹⁶⁶

4.2. Limitations of Current Tumor Models in Predicting Clinical Efficacy.

In explaining the gap between the results of rodent models and clinical outcomes, several limitations of current animal models may be considered. First, the frequently used sc tumor implants do not represent the primary human cancers (e.g., lung, colon, breast) nor the preferred sites of metastasis (e.g., liver for colon cancer metastasis).¹⁶⁷ Instead, allograft or xenograft tumors are artificially implanted sc (mostly for the sake of convenience), where the tumors grow in an environment different from the primary organs, with much reduced potential for metastasis.^{168,169} Second, immortalized cancer cell lines used in many models as the source of xenografts have been maintained over many passages in culture and may have lost architectural and cellular properties unique to the original tumors.^{170,171} Even though grafted tumors can represent important attributes of the original tumors, it is uncertain whether it captures the genetic and epigenetic variability of tumors in its entirety.¹⁷⁰ Third, when human xenografts are inoculated in mouse models, the tumors build stroma and vasculature out of murine sources.^{168,170,171} The potential impact of this artificial

arrangement on the architecture of stroma, cell–stroma interactions, and tumor propagation is barely considered in the establishment of models and interpretation of preclinical studies. Fourth, due to the foreign origin of tumors, it is inevitable to use mice with compromised immune systems, such as athymic or severe combined immunodeficient (SCID) mice.¹⁷² Consequently, potential immune responses to NPs, which directly influence their bioavailability,^{61,173–175} are not properly evaluated in these models. Fifth, the size and growth rate of tumors in mice are not comparable to those of human patients. While human tumors typically develop over a number of years, tumors in murine models are designed to grow in days or weeks for high throughput evaluation.¹⁷⁰ In addition, typical sc tumors can be as large as ~1 cm³ for a 25 g mouse (4% of the body weight). Human patients with tumors that can be visibly identified would be candidates for surgical debulking rather than chemotherapy. One of the likely reasons to favor rapidly growing tumor models in the evaluation of NPs is the positive correlation between tumor growth rate and the EPR effect,¹⁷⁶ the main driving force for tumor-selective NP accumulation.^{177,178} Nonetheless, one should be aware that the clinical significance of vascular permeability effect in drug delivery is much debated,^{60,179} and little is known about the effectiveness of the EPR effect in metastatic or microscopic residual tumors, where targeted chemotherapy is most desired.

4.3. Alternative Animal Models of Tumor. To make a reliable and clinically relevant evaluation tool, an animal model of tumor must fulfill several requirements. It should faithfully recapitulate the pathophysiology of human cancer, reproduce the problems associated with a specific type and location of primary and metastatic cancer, and allow for evaluation of biological events associated with tumor progression.¹⁸⁰ In addition, the model should be reproducible and affordable and provide a quantitative end point of therapeutic responses.¹⁸⁰ It may not be possible to develop a single model that meets all the requirements and works for all, but several efforts are currently made to develop models that better address each requirement. Based on an understanding of these models, one may choose an experimental model that is most appropriate for the specific questions asked in each study.

4.3.1. Orthotopic Tumor Models. In an orthotopic model, a tumor allo- or xenograft is grown in proximity to the tissues or

organs that the tumor cells were derived from (Figure 3).¹⁷⁰ The orthotopic model is advantageous over ectopic sc models in that it provides a host environment closer to a normal milieu of the tumor, where the cells can grow in the same manner as in human cancer. The histological, biochemical, and immunological properties of primary tumors determine their metastatic potential.¹⁸⁰ In many cases, orthotopically implanted tumor cells have a greater potential for metastasis compared to the same cells implanted sc;¹⁸¹ therefore, when the desired effect of a new drug product is against metastasis, it is desirable to use an orthotopic model. The microenvironment also influences responses of tumors to a therapeutic agent.^{181–183} Fidler et al. reported that a sc human colon cancer xenograft was relatively noninvasive and sensitive to DOX, whereas the same tumor implanted in the cecal wall was less responsive.¹⁸² The difference in therapeutic responses was attributed to differential expression of P-gp in the tissues.¹⁸² In another example, human small-cell lung cancer (SCLC) cells were grown orthotopically (in the lung) or ectopically (sc) in SCID mice and administered with cisplatin and mitomycin C (MMC). The two models displayed opposite response profiles: while an orthotopic SCLC model was responsive to cisplatin but not to MMC, similar to the clinical situation, a sc model showed sensitivity to MMC but not to cisplatin.¹⁸³ According to this model, an orthotopic model better reflects the clinical effects of drugs on human SCLC than the tumors growing sc.¹⁸³

On the other hand, one challenge of an orthotopic model is that tumor burden is not readily detectable as in sc models.^{167,181} Except for breast tumor models, which develop superficial tumors, most orthotopic tumors are located in internal organs such as prostate, kidney, brain, lungs, and liver and are not conducive to caliper measurement.¹⁸¹ One way to monitor therapeutic responses is to assess tumor burden terminally after serial sacrifice of animals. In this case, group size needs to be determined considering potential “non-takers” (animals that have not developed tumors at the time of treatment).¹⁸¹ The main disadvantage of this approach is that it is labor-intensive and necessitates a large number of animals. Alternatively, noninvasive imaging techniques may be used together with cancer cells producing fluorescent or luminescent signals.^{181,184} Genes encoding fluorescent proteins and/or luciferase are introduced to human or murine cell lines *in vitro* to stably express the proteins in living animals.^{185–188} Optical imaging tools, such as fluorescence or bioluminescence, are used to monitor the growth of orthotopic tumors and metastasis in host organs externally in real time.^{188–191} The two techniques are often used in combination: fluorescence imaging for high throughput *in vitro* tests or superficial tumor imaging and bioluminescence imaging for detection of relatively deep tissues.¹⁸⁸ Orthotopic models of pancreatic cancer¹⁹² and bladder cancer¹⁹³ expressing luciferase have been used for evaluating therapeutic efficacy of the targeted gold NPs and hyperbranched polyglycerol NPs, respectively.

4.3.2. Ectopic–Orthotopic Tumor Models. The ectopic–orthotopic model is a hybrid of sc and orthotopic model.^{194–196} In this system, an exogenous tissue sample is first implanted ectopically (in the skin), and a tumor sample is then implanted within the tissue graft (Figure 3).^{195,196} For example, mammary fat pad from a lactating female mouse, prostate tissue from a male mouse, lung, or liver is prepared as minced tissue fragments and implanted in the skin of a host animal. Tumor tissues grown as spheroids are then placed upon the engrafted tissue stroma, which provides the orthotopic environment

essential for tumor–mesenchymal interactions.¹⁹⁵ To visualize the extent of vascularization and tumor progression, the tissues may be grown in a window chamber implanted into a dorsal skinfold in the host animal.

The presence of orthotopic tissue environment is shown to play a critical role in the growth and vascularization of tumors. For example, Transgenic Adenocarcinoma Mouse Prostate-C2 prostate tumors were poorly angiogenic and showed no significant growth in the absence of prostate tissue, whereas tumors grown with prostate stroma were highly angiogenic and proliferative.¹⁹⁶ On the other hand, tumor spheroids implanted on the orthotopic tissue stroma showed less vascular permeability than those directly implanted on the skinfold.¹⁹⁵ Consequently, a single iv administration of DOX was much less effective on the ectopic–orthotopic tumors than the sc tumors, consistent with clinical outcomes.¹⁹⁵ This result suggests that many preclinical results obtained in the subcutaneous animal models may have been exaggerated due to the pervasive vascular leakiness less natural to human tumors.¹⁹⁵

4.3.3. Humanized mice. When narrowly defined, the term humanized mice refers to animal models in which human immune cells or hematopoietic stem cells are adoptively transferred to mice so that human immune systems are established in the mice at least partly.^{197–199} Zhou et al. used a BALB/c-Rag2^{-/-}/Vc^{-/-} humanized mouse (RAG-hu) model in the evaluation of cationic PAMAM dendrimers carrying a small interfering RNA (siRNA) for the therapy of HIV-1 infection.²⁰⁰ The RAG-hu model was prepared by injecting human fetal liver-derived CD34⁺ hematopoietic progenitor cells into the liver of a neonatal mouse, preconditioned by irradiation. When the animals no longer produced antibodies to a human antigen, they were infected with HIV-1 and then treated with dendrimer-siRNA NPs. Upon systemic application, the NPs decreased viral loads in animals by several orders of magnitude and protected CD4⁺ T-cells from virus-induced depletion.²⁰⁰ In the context of cancer research, the humanized mice are used in studying human immune responses to tumors and their roles in tumor progression and metastasis.¹⁷² Although the human histocompatibility alleles that can be expressed in a mouse are currently limited,¹⁹⁹ humanized mice are a useful tool for evaluating drugs that provide protection against cancer by controlling the immune system.

4.3.4. Genetically Engineered Mouse Models. In genetically engineered mouse (GEM) models, tumor formation is driven by genetic manipulation of animals. GEMs are created by activating clinically relevant oncogenes or inactivating tumor suppressor genes (TSG) via germline or somatic mutations, which predispose animals to certain types of tumors (Figure 3).^{172,201–203} The main advantage of GEM models is that they reflect genetic changes responsible for specific tumors and syngeneic tumor–host interactions;¹⁸¹ therefore, they are very useful for studying the roles of oncogenes of interest and interactions between tumor cells and microenvironment.¹⁷² GEMs have not been used as widely as other models in routine evaluation of NPs due to the high cost, time, and intellectual property issues. The challenges in tumor monitoring discussed in the orthotopic models also apply to the GEM models.²⁰⁴

Recently, Sengupta et al. used a GEM with somatic PTEN and K-Ras mutations (K-ras^{1SL/+}/Pten^{B/B}), which predispose the animals to ovarian cancer,²⁰⁵ to demonstrate the antitumor efficacy of cholesterol-tethered platinum II-based supramolecular NPs.²⁰⁶ Ovarian tumors were induced by intrabursal injection of adenovirus carrying Cre recombinase (Adeno-Cre)

and luciferase.²⁰⁶ Tumor growth in animals receiving treatments was quantified by monitoring bioluminescence resulting from tumor luciferase expression.²⁰⁶ In another example, Dibirdik et al. studied the anticancer activity of a PEGylated liposomal NP carrying a multifunctional tyrosine kinase inhibitor in a MMTV/Neu transgenic mouse model of metastatic ErbB2/HER-2⁺ chemotherapy-resistant breast cancer.²⁰⁷ In MMTV/Neu transgenic mice, the wild-type neu gene is overexpressed in the mammary gland under the control of the MMTV long terminal repeat,²⁰⁸ which induces progressive and metastatic breast cancer.²⁰⁹ The PEGylated liposomal formulation of the multifunctional tyrosine kinase inhibitor was more effective than standard chemotherapy against the chemotherapy-resistant breast cancer in the MMTV/Neu transgenic mice.²⁰⁷

There is also an increasing appreciation of GEM as a valuable model for identifying biomarkers related to human diseases and developing therapeutics targeted to the biomarkers. For example, Kelly et al. used pancreatic ductal adenocarcinoma (PDAC) cell lines isolated from GEM to screen peptides specifically binding to cell surface antigens on the cells.²¹⁰ A magnetofluorescent NP was modified with the identified peptide and used as an imaging agent to locate incipient PDAC in GEM.²¹⁰

5. FUTURE PERSPECTIVES

The field of nanomedicine has grown enormously in the past few decades. Nanoparticulate drug carriers are now created in various forms based on organic and inorganic material platforms with an unprecedented control over the size, shape, surface properties, drug loading, and release. On the other hand, their clinical translation is relatively slow, with only a handful of commercial products from the early time, such as liposomes or micelles. One of the main reasons is that the knowledge obtained from *in vitro* and preclinical studies has little value in predicting clinical outcomes of new NP products. It may not be an exaggeration to say that it is not the talent to create NPs but the technology to evaluate them that currently limits further advancement of nanomedicine. For example, new NPs are routinely characterized with respect to surface charge and ligand density, which are then correlated with their behaviors in cell models. On the other hand, in blood or other physiological fluids, NPs are easily covered with protein corona, which ultimately dictates *in vivo* fates and therapeutic outcomes of the NPs.^{110,119} In recognition of the disparity between *in vitro* properties and *in vivo* outcomes, many groups now migrate to research models that involve early *in vivo* proof of concept studies. However, the majority of investigators in academia may not be able to afford this approach, nor is it necessarily acceptable in an ethical perspective. Moreover, clinical predictive values of some animal models are recently revisited, with respect to their relevance to human diseases and the ability to recapitulate disease progression. Therefore, it is important for the investigators to initiate an open discussion of the limitations and challenges of current methodologies and explore a new avenue of nanomedicine characterization, which can predict the clinical outcomes in the early stage of product development with a greater reliability. These methods may include new cell models, labeling and detection methods, analytical technologies, mathematical modeling, and animal models that portray critical attributes of human diseases. The need for a new NP evaluation method is another reason to pay attention to recent advances in microfluidic technologies, which

have emerged as a promising tool to create *in vitro* microenvironments that mimic *in vivo* conditions.²¹¹

AUTHOR INFORMATION

Corresponding Author

*Phone: 765.496.9608. Fax: 765.494.6545. E-mail: yyeo@purdue.edu.

Notes

The authors declare no competing financial interest.

ACKNOWLEDGMENTS

This work was supported by NSF DMR-1056997, NIH R21 CA135130, and a grant from the Lilly Endowment, Inc., to College of Pharmacy. This study was also partly supported by the NIH/NCRR-Indiana Clinical and Translational Sciences Institute Predoctoral Fellowship (TL1 RR025759, PI: A. Shekhar) to K.C.L. and the Egyptian Government Ministry of Higher Education Missions Sector to S.A.A.

REFERENCES

- (1) Dynamic Light Scattering: An introduction in 30 minutes. Malvern Instruments. <http://www.malvern.com/malvern/kbase.nsf/allbyno/KB000734?opendocument> (accessed on 11/1/12).
- (2) Dynamic Light Scattering: Common Terms Defined (MRK 1764-01). Malvern Instruments. <http://www.malvern.com/common/downloads/campaign/MRK1764-01.pdf> (accessed on 11/1/12).
- (3) Lu, X. Y.; Wu, D. C.; Li, Z. J.; Chen, G. Q. Polymer nanoparticles. *Prog. Mol. Biol. Transl. Sci.* 2011, **104**, 299–323.
- (4) Hoo, C. M.; Starostin, N.; West, P.; Mecartney, M. L. A comparison of atomic force microscopy (AFM) and dynamic light scattering (DLS) methods to characterize nanoparticle size distributions. *J. Nanopart. Res.* 2008, **10**, 89–96.
- (5) Mahl, D.; Diendorf, J.; Meyer-Zaika, W.; Eppler, M. Possibilities and limitations of different analytical methods for the size determination of a bimodal dispersion of metallic nanoparticles. *Colloids Surf., A* 2011, **377**, 386–392.
- (6) Boyd, R. D.; Pichaimuthu, S. K.; Cuenat, A. New approach to inter-technique comparisons for nanoparticle size measurements; using atomic force microscopy, nanoparticle tracking analysis and dynamic light scattering. *Colloids Surf., A* 2011, **387**, 35–42.
- (7) Saveyn, H.; De Baets, B.; Thas, O.; Hole, P.; Smith, J.; Van der Meer, P. Accurate particle size distribution determination by nanoparticle tracking analysis based on 2-D Brownian dynamics simulation. *J. Colloid Interface Sci.* 2010, **352**, 593–600.
- (8) Finder, C.; Wohlgenuth, M.; Mayer, C. Analysis of particle size distribution by particle tracking. *Part. Part. Syst. Charact.* 2004, **21**, 372–378.
- (9) Disk centrifuge. <http://www.cpsinstruments.eu/centrifuge.html> (accessed on 10/30/12).
- (10) Murdock, R. C.; Braydich-Stolle, L.; Schrand, A. M.; Schlager, J. J.; Hussain, S. M. Characterization of nanomaterial dispersion in solution prior to *in vitro* exposure using dynamic light scattering technique. *Toxicol. Sci.* 2008, **101**, 239–253.
- (11) Jiang, J.; Oberdörster, G.; Biswas, P. Characterization of size, surface charge, and agglomeration state of nanoparticle dispersions for toxicological studies. *J. Nanopart. Res.* 2009, **11**, 77–89.
- (12) Vasylyk, O.; Sakka, Y. Synthesis and colloidal processing of zirconia nanopowder. *J. Am. Ceram. Soc.* 2001, **84**, 2489–2494.
- (13) Bowen, P. Particle size distribution measurement from millimeters to nanometers and from rods to platelets. *J. Dispersion Sci. Technol.* 2002, **23**, 631–662.
- (14) Brant, J.; Lecoanet, H.; Wiesner, M. R. Aggregation and deposition characteristics of fullerene nanoparticles in aqueous systems. *J. Nanopart. Res.* 2005, **7**, 545–553.
- (15) Widegren, J.; Bergström, L. Electrostatic stabilization of ultrafine titania in ethanol. *J. Am. Ceram. Soc.* 2002, **85**, 523–528.

Molecular Pharmaceutics

- (16) Kirby, B. J.; Hasselbrink, E. F., Jr. Zeta potential of microfluidic substrates: 1. Theory, experimental techniques, and effects on separations. *Electrophoresis* 2004, 25, 187–202.
- (17) Kirby, B. J.; Hasselbrink, E. F., Jr. Zeta potential of microfluidic substrates: 2. Data for polymers. *Electrophoresis* 2004, 25, 203–13.
- (18) Hoffman, A. S. The origins and evolution of “controlled” drug delivery systems. *J. Controlled Release* 2008, 132, 153–163.
- (19) Anhalt, K.; Geissler, S.; Harms, M.; Weigandt, M.; Fricker, G. Development of a new method to assess nanocrystal dissolution based on light scattering. *Pharm. Res.* 2012, 29, 2887–2901.
- (20) Accardo, A.; Tesaro, D.; Roscigno, P.; Gianolio, E.; Paduano, L.; D’Errico, G.; Pedone, C.; Morelli, G. Physicochemical properties of mixed micellar aggregates containing CCK peptides and Gd complexes designed as tumor specific contrast agents in MRI. *J. Am. Chem. Soc.* 2004, 126, 3097–3107.
- (21) Cheng, C.; Wei, H.; Zhang, X.-Z.; Cheng, S.-X.; Zhuo, R.-X. Thermo-triggered and biotinylated biotin-P(NIPAAm-co-HMAAm)-b-PMMA micelles for controlled drug release. *J. Biomed. Mater. Res., Part A* 2009, 88A, 814–822.
- (22) Toncheva, V.; Schacht, E.; Ng, S. Y.; Barr, J.; Heller, J. Use of block copolymers of poly(ortho esters) and poly(ethylene glycol) micellar carriers as potential tumour targeting systems. *J. Drug Targeting* 2003, 11 (6), 345–353.
- (23) Yang, X.; Li, L.; Wang, Y.; Tan, Y. Preparation, pharmacokinetics and tissue distribution of micelles made of reverse thermo-responsive polymers. *Int. J. Pharm.* 2009, 370, 210–215.
- (24) Kalyanasundaram, K.; Thomas, J. K. Environmental effects on vibronic band intensities in pyrene monomer fluorescence and their application in studies of micellar systems. *J. Am. Chem. Soc.* 1977, 99, 2039–2044.
- (25) Chen, W.; Cheng, Y.; Wang, B. Dual-responsive boronate crosslinked micelles for targeted drug delivery. *Angew. Chem., Int. Ed.* 2012, 51, 5293–5295.
- (26) Lin, W.-J.; Juang, L.-W.; Lin, C.-C. Stability and release performance of a series of pegylated copolymeric micelles. *Pharm. Res.* 2003, 20, 668–673.
- (27) Xu, P.; Tang, H.; Li, S.; Ren, J.; Van Kirk, E.; Murdoch, W. J.; Radosz, M.; Shen, Y. Enhanced stability of core-surface cross-linked micelles fabricated from amphiphilic brush copolymers. *Biomacromolecules* 2004, 5, 1736–1744.
- (28) Yang, C.; Ebrahim Attia, A. B.; Tan, J. P. K.; Ke, X.; Gao, S.; Hedrick, J. L.; Yang, Y.-Y. The role of non-covalent interactions in anticancer drug loading and kinetic stability of polymeric micelles. *Biomaterials* 2012, 33, 2971–2979.
- (29) Zhao, X.; Poon, Z.; Engler, A. C.; Bonner, D. K.; Hammond, P. T. Enhanced stability of polymeric micelles based on postfunctionalized poly(ethylene glycol)-b-poly(γ -propargyl L-glutamate): the substituent effect. *Biomacromolecules* 2012, 13, 1315–1322.
- (30) Surfactant micelle characterization using dynamic light scattering (MRK809-01). Malvern Instruments. [http://www.malvern.com/malvern/kbase.nsf/allbyno/KB001097/\\$file/MRK809-01.pdf](http://www.malvern.com/malvern/kbase.nsf/allbyno/KB001097/$file/MRK809-01.pdf) (accessed on 11/15/12).
- (31) Zhang, X.-Z.; Wu, D.-Q.; Chu, C.-C. Synthesis, characterization and controlled drug release of thermosensitive IPN–PNIPAAm hydrogels. *Biomaterials* 2004, 25, 3793–3805.
- (32) Needham, D.; Anyarambhatla, G.; Kong, G.; Dewhurst, M. W. A new temperature-sensitive liposome for use with mild hyperthermia: characterization and testing in a human tumor xenograft model. *Cancer Res.* 2000, 60, 1197–1201.
- (33) Nakayama, M.; Okano, T.; Miyazaki, T.; Kohori, F.; Sakai, K.; Yokoyama, M. Molecular design of biodegradable polymeric micelles for temperature-responsive drug release. *J. Controlled Release* 2006, 115, 46–56.
- (34) Piskin, E. Molecularly designed water soluble, intelligent, nanosize polymeric carriers. *Int. J. Pharm.* 2004, 277, 105–118.
- (35) Kim, Y.-H.; Kwon, I. C.; Bae, Y. H.; Kim, S. W. Saccharide effect on the lower critical solution temperature of thermosensitive polymers. *Macromolecules* 1995, 28, 939–944.
- (36) Zhang, L.; Chan, J. M.; Gu, F. X.; Rhee, J.-W.; Wang, A. Z.; Radovic-Moreno, A. F.; Alexis, F.; Langer, R.; Farokhzad, O. C. Self-assembled lipid-polymer hybrid nanoparticles: a robust drug delivery platform. *ACS Nano* 2008, 2, 1696–1702.
- (37) Sun, T.-M.; Du, J.-Z.; Yan, L.-F.; Mao, H.-Q.; Wang, J. Self-assembled biodegradable micellar nanoparticles of amphiphilic and cationic block copolymer for siRNA delivery. *Biomaterials* 2008, 29, 4348–4355.
- (38) Isaacs, S. R.; Choo, H.; Ko, W.-B.; Shon, Y.-S. Chemical, thermal, and ultrasonic stability of hybrid nanoparticles and nanoparticle multilayer films. *Chem. Mater.* 2005, 18, 107–114.
- (39) Na, K.; Bae, Y. H. Self-assembled hydrogel nanoparticles responsive to tumor extracellular pH from pullulan derivative/sulfonamide conjugate: characterization, aggregation, and adriamycin release in vitro. *Pharm. Res.* 2002, 19, 681–688.
- (40) Yokoyama, M.; Sugiyama, T.; Okano, T.; Sakurai, Y.; Naito, M.; Kataoka, K. Analysis of micelle formation of an adriamycin-conjugated poly(ethylene glycol)-poly(aspartic acid) block copolymer by gel permeation chromatography. *Pharm. Res.* 1993, 10, 895–899.
- (41) Masayuki, Y.; Kwon, G. S.; Teruo, O.; Yasuhisa, S.; Mayumi, N.; Kazunori, K. Influencing factors on in vitro micelle stability of adriamycin-block copolymer conjugates. *J. Controlled Release* 1994, 28, 59–65.
- (42) Opanasopit, P.; Yokoyama, M.; Watanabe, M.; Kawano, K.; Maitani, Y.; Okano, T. Influence of serum and albumins from different species on stability of camptothecin-loaded micelles. *J. Controlled Release* 2005, 104, 313–321.
- (43) Akiyoshi, K.; Kobayashi, S.; Shichibe, S.; Mix, D.; Baudys, M.; Wan Kim, S.; Sunamoto, J. Self-assembled hydrogel nanoparticle of cholesterol-bearing pullulan as a carrier of protein drugs: Complexation and stabilization of insulin. *J. Controlled Release* 1998, 54, 313–320.
- (44) Iijima, M.; Nagasaki, Y.; Okada, T.; Kato, M.; Kataoka, K. Core-Polymerized Reactive micelles from heterotelechelic amphiphilic block copolymers. *Macromolecules* 1999, 32, 1140–1146.
- (45) Jones, M.-C.; Leroux, J.-C. Polymeric micelles: A new generation of colloidal drug carriers. *Eur. J. Pharm. Biopharm.* 1999, 48, 101–111.
- (46) Opanasopit, P.; Yokoyama, M.; Watanabe, M.; Kawano, K.; Maitani, Y.; Okano, T. Block copolymer design for camptothecin incorporation into polymeric micelles for passive tumor targeting. *Pharm. Res.* 2004, 21, 2001–2008.
- (47) Watanabe, M.; Kawano, K.; Yokoyama, M.; Opanasopit, P.; Okano, T.; Maitani, Y. Preparation of camptothecin-loaded polymeric micelles and evaluation of their incorporation and circulation stability. *Int. J. Pharm.* 2006, 308, 183–189.
- (48) Lu, J.; Owen, S. C.; Shochet, M. S. Stability of self-assembled polymeric micelles in serum. *Macromolecules* 2011, 44, 6002–6008.
- (49) Chen, H.; Kim, S.; Li, L.; Wang, S.; Park, K.; Cheng, J.-X. Release of hydrophobic molecules from polymer micelles into cell membranes revealed by Förster resonance energy transfer imaging. *Proc. Natl. Acad. Sci. U.S.A.* 2008, 105, 6596–6601.
- (50) Chen, H.; Kim, S.; He, W.; Wang, H.; Low, P. S.; Park, K.; Cheng, J.-X. Fast release of lipophilic agents from circulating PEG-PDLLA micelles revealed by in vivo Förster resonance energy transfer imaging. *Langmuir* 2008, 24, 5213–5217.
- (51) Miller, T.; Rachel, R.; Beshceer, A.; Uezguen, S.; Weigandt, M.; Goepferich, A. Comparative investigations on in vitro serum stability of polymeric micelle formulations. *Pharm. Res.* 2012, 29, 448–459.
- (52) Piston, D. W.; Kremers, G.-J. Fluorescent protein FRET: the good, the bad and the ugly. *Trends Biochem. Sci.* 2007, 32, 407–414.
- (53) Walkey, C. D.; Chan, W. C. Understanding and controlling the interaction of nanomaterials with proteins in a physiological environment. *Chem. Soc. Rev.* 2012, 41, 2780–2799.
- (54) Dobrovolskaia, M.; Aggarwal, P.; Hall, J.; McNeil, S. Preclinical studies to understand nanoparticle interaction with the immune system and its potential effects on nanoparticle biodistribution. *Mol. Pharmaceutics* 2008, 5, 487–495.

- (55) Tan, J.; Butterfield, D.; Voycheck, C.; Caldwell, K.; Li, J. Surface modification of nanoparticles by PEO/PPO block copolymers to minimize interactions with blood components and prolong blood circulation in rats. *Biomaterials* 1993, **14**, 823–833.
- (56) Vonarbourg, A.; Passirani, C.; Saulnier, P.; Simard, P.; Leroux, J.; Benoit, J. Evaluation of pegylated lipid nanocapsules versus complement system activation and macrophage uptake. *J. Biomed. Mater. Res., Part A* 2006, **78**, 620–628.
- (57) Senior, J.; Delgado, C.; Fisher, D.; Tilcock, C.; Gregoriadis, G. Influence of surface hydrophilicity of liposomes on their interaction with plasma protein and clearance from the circulation: studies with poly(ethylene glycol)-coated vesicles. *Biochim. Biophys. Acta* 1991, **1062**, 77–82.
- (58) Torchilin, V.; Omelyanenko, V.; Papisov, M.; Bogdanov, A.; Trubetskoy, V.; Herron, J.; Gentry, C. Poly(ethylene glycol) on the liposome surface: on the mechanism of polymer-coated liposome longevity. *Biochim. Biophys. Acta* 1994, **1195**, 11–20.
- (59) Matsumura, Y.; Maeda, H. A new concept for macromolecular therapeutics in cancer chemotherapy: mechanism of tumorotropic accumulation of proteins and the antitumor agent smancs. *Cancer Res.* 1986, **46**, 6387–6392.
- (60) Bae, Y. H.; Park, K. Targeted drug delivery to tumors: myths, reality and possibility. *J. Controlled Release* 2011, **153**, 198–205.
- (61) Dams, E.; Laverman, P.; Oyen, W.; Storm, G.; Scherphof, G.; van Der Meer, J.; Corstens, F.; Boerman, O. Accelerated blood clearance and altered biodistribution of repeated injections of sterically stabilized liposomes. *J. Pharmacol. Exp. Ther.* 2000, **292**, 1071–1079.
- (62) Wang, X.; Ishida, T.; Kiwada, H. Anti-PEG IgM elicited by injection of liposomes is involved in the enhanced blood clearance of a subsequent dose of PEGylated liposomes. *J. Controlled Release* 2007, **119**, 236–244.
- (63) Garay, R.; El-Gewily, R.; Armstrong, J.; Garratty, G.; Richette, P. Antibodies against polyethylene glycol in healthy subjects and in patients treated with PEG-conjugated agents. *Expert Opin. Drug Delivery* 2012, **9**, 1319–1323.
- (64) Amoozgar, Z.; Park, J.; Lin, Q.; Yeo, Y. Low molecular-weight chitosan as a pH-sensitive stealth coating for tumor-specific drug delivery. *Mol. Pharmaceutics* 2012, **9**, 1262–1270.
- (65) Passirani, C.; Barratt, G.; Devissaguet, J.; Labarre, D. Long-circulating nanoparticles bearing heparin or dextran covalently bound to poly(methyl methacrylate). *Pharm. Res.* 1998, **15**, 1046–1050.
- (66) Doh, K.-O.; Yeo, Y. Application of polysaccharides for surface modification of nanomedicines. *Ther. Delivery* 2012, **3**, 1447–1456.
- (67) Fang, C.; Shi, B.; Pei, Y.-Y.; Hong, M.-H.; Wu, J.; Chen, H.-Z. In vivo tumor targeting of tumor necrosis factor- α -loaded stealth nanoparticles: effect of MePEG molecular weight and particle size. *Eur. J. Pharm. Sci.* 2006, **27**, 27–36.
- (68) Goppert, T. M.; Muller, R. H. Protein adsorption patterns on poloxamer- and poloxamine-stabilized solid lipid nanoparticles (SLN). *Eur. J. Pharm. Biopharm.* 2005, **60**, 361–372.
- (69) Gessner, A.; Waicz, R.; Lieske, A.; Paulke, B.; Mader, K.; Muller, R. H. Nanoparticles with decreasing surface hydrophobicities: influence on plasma protein adsorption. *Int. J. Pharm.* 2000, **196**, 245–249.
- (70) Zhang, W.; Liu, J.; Li, S.; Chen, M.; Liu, H. Preparation and evaluation of stealth Tashinone II A-loaded solid lipid nanoparticles: Influence of Poloxamer 188 coating on phagocytic uptake. *J. Microencapsulation* 2008, **25**, 203–209.
- (71) Bocca, C.; Caputo, O.; Cavalli, R. B.; Gabriel, L.; Miglietta, A.; Gasco, M. R. Phagocytic uptake of fluorescent stealth and non-stealth solid lipid nanoparticles. *Int. J. Pharm.* 1998, **175**, 185–193.
- (72) Rolland, A.; Merdignac, G.; Gouranton, J.; Bourel, D.; Le Verge, R.; Genetet, B. Flow cytometric quantitative evaluation of phagocytosis by human mononuclear and polymorphonuclear cells using fluorescent nanoparticles. *J. Immunol. Methods* 1987, **96**, 185–193.
- (73) Vonarbourg, A.; Passirani, C.; Saulnier, P.; Benoit, J.-P. Parameters influencing the stealthiness of colloidal drug delivery systems. *Biomaterials* 2006, **27**, 4356–4373.
- (74) Champion, J.; Mitragotri, S. Role of target geometry in phagocytosis. *Proc. Natl. Acad. Sci. U.S.A.* 2006, **103**, 4930–4934.
- (75) Arnida; Janat-Amsbury, M. M.; Ray, A.; Peterson, C. M.; Ghandehari, H. Geometry and surface characteristics of gold nanoparticles influence their biodistribution and uptake by macrophages. *Eur. J. Pharm. Biopharm.* 2011, **77**, 417–423.
- (76) Longmire, M. R.; Ogawa, M.; Choyke, P. L.; Kobayashi, H. Biologically optimized nanosized molecules and particles: more than just size. *Bioconjugate Chem.* 2011, **22**, 993–1000.
- (77) Geng, Y.; Dalhaimer, P.; Cai, S.; Tsai, R.; Tewari, M.; Minko, T.; Discher, D. E. Shape effects of filaments versus spherical particles in flow and drug delivery. *Nat. Nano* 2007, **2**, 249–255.
- (78) Bertholon, I.; Vauthier, C.; Labarre, D. Complement activation by core-shell poly(isobutylcyanoacrylate)-polysaccharide nanoparticles: influences of surface morphology, length, and type of polysaccharide. *Pharm. Res.* 2006, **23**, 1313–1323.
- (79) Sahu, A.; Lambris, J. Structure and biology of complement protein C3, a connecting link between innate and acquired immunity. *Immunol. Rev.* 2001, **180**, 35–48.
- (80) Laurell, C. Quantitative estimation of proteins by electrophoresis in agarose gel containing antibodies. *Anal. Biochem.* 1966, **15**, 45–52.
- (81) Boackle, R.; Caughman, G.; Vesely, J.; Medgyesi, G.; Fudenberg, H. Potentiation of factor H by heparin: a rate-limiting mechanism for inhibition of the alternative complement pathway. *Mol. Immunol.* 1983, **20**, 1157–1164.
- (82) Alhareth, K.; Vauthier, C.; Bourasset, F.; Gueutin, C.; Ponchel, G.; Moussa, F. Conformation of surface-decorating dextran chains affects the pharmacokinetics and biodistribution of doxorubicin-loaded nanoparticles. *Eur. J. Pharm. Biopharm.* 2012, **81**, 453–457.
- (83) Vauthier, C.; Persson, B.; Lindner, P.; Cabane, B. Protein adsorption and complement activation for di-block copolymer nanoparticles. *Biomaterials* 2011, **32**, 1646–1656.
- (84) Labarre, D.; Vauthier, C.; Chauvierre, C.; Petri, B.; Muller, R.; Chehimi, M. M. Interactions of blood proteins with poly(isobutylcyanoacrylate) nanoparticles decorated with a polysaccharidic brush. *Biomaterials* 2005, **26**, 5075–5084.
- (85) Suzuki, Y.; Miyatake, K.; Okamoto, Y.; Muraki, E.; Minami, S. Influence of the chain length of chitosan on complement activation. *Carbohydr. Polym.* 2003, **54**, 465–469.
- (86) http://ncl.cancer.gov/assay_cascade.asp (accessed on 10/5/12).
- (87) Xu, P.; Gullotti, E.; Tong, L.; Highley, C. B.; Errabelli, D. R.; Hasan, T.; Cheng, J.-X.; Kohane, D. S.; Yeo, Y. Intracellular drug delivery by poly(lactic-co-glycolic acid) nanoparticles, revisited. *Mol. Pharmaceutics* 2009, **6**, 190–201.
- (88) Ekkapongpisit, M.; Giovia, A.; Follo, C.; Caputo, G.; Isidoro, C. Biocompatibility, endocytosis, and intracellular trafficking of mesoporous silica and polystyrene nanoparticles in ovarian cancer cells: effects of size and surface charge groups. *Int. J. Nanomed.* 2012, **7**, 4147–4158.
- (89) Brown, M.; Wittwer, C. Flow cytometry: Principles and clinical applications in hematology. *Clin. Chem.* 2000, **46**, 1221–1229.
- (90) Anirudhan, T. S.; Sandeep, S. Synthesis, characterization, cellular uptake and cytotoxicity of a multifunctional magnetic nanocomposite for the targeted delivery and controlled release of doxorubicin to cancer cells. *J. Mater. Chem.* 2012, **22**, 12888–12899.
- (91) Anirudhan, T. S.; Sandeep, S. Synthesis and characterization of a novel pH-controllable composite hydrogel for anticancer drug delivery. *New J. Chem.* 2011, **35**, 2869–2876.
- (92) Fujii, K.; Kuroda, T.; Sakoda, K.; Iyi, N. Fluorescence resonance energy transfer and arrangements of fluorophores in integrated coumarin/cyanine systems within solid-state two-dimensional nanospace. *J. Photochem. Photobiol., A* 2011, **225**, 125–134.
- (93) Gratton, S. E. A.; Ropp, P. A.; Pohlhaus, P. D.; Luft, J. C.; Madden, V. J.; Napier, M. E.; DeSimone, J. M. The effect of particle design on cellular internalization pathways. *Proc. Natl. Acad. Sci. U.S.A.* 2008, **105**, 11613–11618.

- (94) Kim, T. H.; Mount, C. W.; Gombotz, W. R.; Pun, S. H. The delivery of doxorubicin to 3-D multicellular spheroids and tumors in a murine xenograft model using tumor-penetrating triblock polymeric micelles. *Biomaterials* 2010, *31*, 7386–7397.
- (95) Huang, R. B.; Mocherla, S.; Heslinga, M. J.; Charoenphol, P.; Eniola-Adefeso, O. Dynamic and cellular interactions of nanoparticles in vascular-targeted drug delivery. *Mol. Membr. Biol.* 2010, *27*, 312–327.
- (96) Harush-Frenkel, O.; Altschuler, Y.; Benita, S. Nanoparticle-cell interactions: drug delivery implications. *Crit. Rev. Ther. Drug Carrier Syst.* 2008, *25*, 485–544.
- (97) Soldati, T.; Schliwa, M. Powering membrane traffic in endocytosis and recycling. *Nat. Rev. Mol. Cell Biol.* 2006, *7*, 897–908.
- (98) Vandeurs, B.; Petersen, O. W.; Olsnes, S.; Sandvig, K. The ways of endocytosis. *Int. Rev. Cytol.* 1989, *117*, 131–177.
- (99) Garnett, M. C.; Kallinteri, P. Nanomedicines and nanotoxicology: some physiological principles. *Occup. Med.* 2006, *56*, 307–311.
- (100) Polo, S.; Di Fiore, P. P. Endocytosis conducts the cell signaling orchestra. *Cell* 2006, *124*, 897–900.
- (101) Conner, S. D.; Schmid, S. L. Regulated portals of entry into the cell. *Nature* 2003, *422*, 37–44.
- (102) Roth, M. G. Clathrin-mediated endocytosis before fluorescent proteins. *Nat. Rev. Mol. Cell Biol.* 2006, *7*, 63–68.
- (103) Rejman, J.; Oberle, V.; Zuborn, I. S.; Hoekstra, D. Size-dependent internalization of particles via the pathways of clathrin- and caveolae-mediated endocytosis. *Biochem. J.* 2004, *377*, 159–169.
- (104) Sabharanjak, S.; Mayor, S. Folate receptor endocytosis and trafficking. *Adv. Drug Delivery Rev.* 2004, *56*, 1099–1109.
- (105) Grant, B. D.; Donaldson, J. G. Pathways and mechanisms of endocytic recycling. *Nat. Rev. Mol. Cell Biol.* 2009, *10*, 597–608.
- (106) Carver, L. A.; Schnitzer, J. E. Caveolae: Mining little caves for new cancer targets. *Nat. Rev. Cancer* 2003, *3*, 571–581.
- (107) Ivanov, A. I. Pharmacological inhibition of endocytic pathways: is it specific enough to be useful? *Methods Mol. Biol.* 2008, *440*, 15–33.
- (108) Perumal, O. P.; Inapagolla, R.; Kannan, S.; Kannan, R. M. The effect of surface functionality on cellular trafficking of dendrimers. *Biomaterials* 2008, *29*, 3469–3476.
- (109) Ranjan, A.; Pothayee, N.; Selem, M. N.; Sriranganathan, N.; Kasimanicam, R.; Makris, M.; Riffle, J. S. In vitro trafficking and efficacy of core-shell nanostructures for treating intracellular *Salmonella* infections. *Antimicrob. Agents Chemother.* 2009, *53*, 3985–3988.
- (110) Albanese, A.; Tang, P. S.; Chan, W. C. W. The effect of nanoparticle size, shape, and surface chemistry on biological systems. *Annu. Rev. Biomed. Eng.* 2012, *14*, 1–16.
- (111) Myung, J. H.; Gajjar, K. A.; Saric, J.; Eddington, D. T.; Hong, S. Dendrimer-mediated multivalent binding for the enhanced capture of tumor cells. *Angew. Chem., Int. Ed.* 2011, *50*, 11769–11772.
- (112) Jiang, W.; KimBetty, Y. S.; Rutka, J. T.; ChanWarren, C. W. Nanoparticle-mediated cellular response is size-dependent. *Nat. Nano* 2008, *3*, 145–150.
- (113) Liu, S. Q.; Wiradharma, N.; Gao, S. J.; Tong, Y. W.; Yang, Y. Y. Bio-functional micelles self-assembled from a folate-conjugated block copolymer for targeted intracellular delivery of anticancer drugs. *Biomaterials* 2007, *28*, 1423–1433.
- (114) Bae, Y.; Nishiyama, N.; Kataoka, K. In vivo antitumor activity of the folate-conjugated pH-Sensitive polymeric micelle selectively releasing adriamycin in the intracellular acidic compartments. *Bioconjugate Chem.* 2007, *18*, 1131–1139.
- (115) Park, J. H.; von Maltzahn, G.; Xu, M. J.; Fogal, V.; Kotamraju, V. R.; Ruoslahti, E.; Bhatia, S. N.; Sailor, M. J. Cooperative nanomaterial system to sensitize, target, and treat tumors. *Proc. Natl. Acad. Sci. U.S.A.* 2010, *107*, 981–986.
- (116) Kim, S. H.; Jeong, J. H.; Chun, K. W.; Park, T. G. Target-specific cellular uptake of PLGA nanoparticles coated with poly(L-lysine)-poly(ethylene glycol)-folate conjugate. *Langmuir* 2005, *21*, 8852–8857.
- (117) Jiang, G.; Park, K.; Kim, J.; Kim, K. S.; Hahn, S. K. Target specific intracellular delivery of siRNA/PEI-HA complex by receptor mediated endocytosis. *Mol. Pharmaceutics* 2009, *6*, 727–737.
- (118) Han, S. E.; Kang, H.; Shim, G. Y.; Kim, S. J.; Choi, H. G.; Kim, J.; Hahn, S. K.; Oh, Y. K. Cationic derivatives of biocompatible hyaluronic acids for delivery of siRNA and antisense oligonucleotides. *J. Drug Targeting* 2009, *17*, 123–132.
- (119) Zhao, F.; Zhao, Y.; Liu, Y.; Chang, X. L.; Chen, C. Y.; Zhao, Y. L. Cellular uptake, intracellular trafficking, and cytotoxicity of nanomaterials. *Small* 2011, *7*, 1322–1337.
- (120) Huang, J. G.; Leshuk, T.; Gu, F. X. Emerging nanomaterials for targeting subcellular organelles. *Nano Today* 2011, *6*, 478–492.
- (121) Harush-Frenkel, O.; Debotton, N.; Benita, S.; Altschuler, Y. Targeting of nanoparticles to the clathrin-mediated endocytic pathway. *Biochem. Biophys. Res. Commun.* 2007, *353*, 26–32.
- (122) Schnell, U.; Dijk, F.; Sjollem, K. A.; Giepmans, B. N. G. Immunolabeling artifacts and the need for live-cell imaging. *Nat. Methods* 2012, *9*, 152–158.
- (123) Melan, M. A.; Sluder, G. Redistribution and differential extraction of soluble proteins in permeabilized cultured cells. Implications for immunofluorescence microscopy. *J. Cell. Sci.* 1992, *101*, 731–743.
- (124) Slater, K. Cytotoxicity tests for high-throughput drug discovery. *Curr. Opin. Biotechnol.* 2001, *12*, 70–74.
- (125) Decker, T.; Lohmann-Matthes, M.-L. A quick and simple method for the quantitation of lactate dehydrogenase release in measurements of cellular cytotoxicity and tumor necrosis factor (TNF) activity. *J. Immunol. Methods* 1988, *115*, 61–69.
- (126) Lei, T. J.; Srinivasan, S.; Tang, Y.; Manchanda, R.; Nagesetti, A.; Fernandez-Fernandez, A.; McGoron, A. J. Comparing cellular uptake and cytotoxicity of targeted drug carriers in cancer cell lines with different drug resistance mechanisms. *Nanomedicine* 2011, *7*, 324–332.
- (127) Gullotti, E.; Yeo, Y. Beyond the imaging: Limitations of cellular uptake study in the evaluation of nanoparticles. *J. Controlled Release* 2012, *164*, 170–176.
- (128) Holback, H.; Yeo, Y. Intratumoral drug delivery with nanoparticulate carriers. *Pharm. Res.* 2011, *28*, 1819–1830.
- (129) Lee, G. Y.; Kenny, P. A.; Lee, E. H.; Bissell, M. J. Three-dimensional culture models of normal and malignant breast epithelial cells. *Nat. Methods* 2007, *4*, 359–365.
- (130) Mitra, M.; Mohanty, C.; Harilal, A.; Maheswari, U. K.; Sahoo, S. K.; Krishnakumar, S. A novel in vitro three-dimensional retinoblastoma model for evaluating chemotherapeutic drugs. *Mol. Vision* 2012, *18*, 1361–1378.
- (131) Sun, T.; Jackson, S.; Haycock, J. W.; MacNeil, S. Culture of skin cells in 3D rather than 2D improves their ability to survive exposure to cytotoxic agents. *J. Biotechnol.* 2006, *122*, 372–381.
- (132) Hosoya, H.; Kadowaki, K.; Matsusaki, M.; Cabral, H.; Nishihara, H.; Ijichi, H.; Koike, K.; Kataoka, K.; Miyazono, K.; Akashi, M.; Kano, M. R. Engineering fibrotic tissue in pancreatic cancer: A novel three-dimensional model to investigate nanoparticle delivery. *Biochem. Biophys. Res. Commun.* 2012, *419*, 32–37.
- (133) Khademhosseini, A.; Eng, G.; Yeh, J.; Fukuda, J.; Blumling, J., III; Langer, R.; Burdick, J. A. Micromolding of photocrosslinkable hyaluronic acid for cell encapsulation and entrapment. *J. Biomed. Mater. Res., Part A* 2006, *79*, 522–532.
- (134) Ho, W. J.; Pham, E. A.; Kim, J. W.; Ng, C. W.; Kim, J. H.; Kamei, D. T.; Wu, B. M. Incorporation of multicellular spheroids into 3-D polymeric scaffolds provides an improved tumor model for screening anticancer drugs. *Cancer Sci.* 2010, *101*, 2637–2643.
- (135) Astashkina, A. I.; Mann, B. K.; Prestwich, G. D.; Grainger, D. W. A 3-D organoid kidney culture model engineered for high-throughput nephrotoxicity assays. *Biomaterials* 2012, *33*, 4700–4711.
- (136) Ng, C. P.; Pun, S. H. A perfusable 3D cell-matrix tissue culture chamber for in situ evaluation of nanoparticle vehicle penetration and transport. *Biotechnol. Bioeng.* 2008, *99*, 1490–1501.

Molecular Pharmaceutics

- (137) Blake, A. J.; Pearce, T. M.; Rao, N. S.; Johnson, S. M.; Williams, J. C. Multilayer PDMS microfluidic chamber for controlling brain slice microenvironment. *Lab Chip* 2007, 7, 842–849.
- (138) Chang, R.; Emami, K.; Wu, H.; Sun, W. Biofabrication of a three-dimensional liver micro-organ as an in vitro drug metabolism model. *Biofabrication* 2010, 2, 045004.
- (139) Zhang, H.; Lee, M.-Y.; Hogg, M. G.; Dordick, J. S.; Sharfstein, S. T. Gene delivery in three-dimensional cell cultures by superparamagnetic nanoparticles. *ACS Nano* 2010, 4, 4733–4743.
- (140) Szot, C. S.; Buchanan, C. F.; Freeman, J. W.; Rylander, M. N. 3D in vitro bioengineered tumors based on collagen I hydrogels. *Biomaterials* 2011, 32, 7905–7912.
- (141) Gurski, L. A.; Jha, A. K.; Zhang, C.; Jia, X. Q.; Farach-Carson, M. C. Hyaluronic acid-based hydrogels as 3D matrices for in vitro evaluation of chemotherapeutic drugs using poorly adherent prostate cancer cells. *Biomaterials* 2009, 30, 6076–6085.
- (142) Loessner, D.; Stok, K. S.; Lutolf, M. P.; Huttmacher, D. W.; Clements, J. A.; Rizzi, S. C. Bioengineered 3D platform to explore cell-ECM interactions and drug resistance of epithelial ovarian cancer cells. *Biomaterials* 2010, 31, 8494–8506.
- (143) Zhang, S. G.; Gelain, F.; Zhao, X. J. Designer self-assembling peptide nanofiber scaffolds for 3D tissue cell cultures. *Semin. Cancer Biol.* 2005, 15, 413–420.
- (144) Derrda, R.; Laromaine, A.; Mammoto, A.; Tang, S. K. Y.; Mammoto, T.; Ingber, D. E.; Whitesides, G. M. Paper-supported 3D cell culture for tissue-based bioassays. *Proc. Natl. Acad. Sci. U.S.A.* 2009, 106, 18457–18462.
- (145) Minchinton, A. I.; Tannock, I. F. Drug penetration in solid tumours. *Nat. Rev. Cancer* 2006, 6, 583–592.
- (146) Kim, B.; Han, G.; Toley, B. J.; Kim, C.-k.; Rotello, V. M.; Forbes, N. S. Tuning payload delivery in tumour cylindroids using gold nanoparticles. *Nat. Nano* 2010, 5, 465–472.
- (147) Huang, S. K.; Mayhew, E.; Gilani, S.; Lasic, D. D.; Martin, F. J.; Papahadjopoulos, D. Pharmacokinetics and therapeutics of sterically stabilized liposomes in mice bearing C-26 colon carcinoma. *Cancer Res.* 1992, 52, 6774–6781.
- (148) Vaage, J.; Barberaguillem, E.; Abra, R.; Huang, A.; Working, P. Tissue distribution and therapeutic effect of intravenous free or encapsulated liposomal doxorubicin on human prostate carcinoma xenografts. *Cancer* 1994, 73, 1478–1484.
- (149) Vaage, J.; Mayhew, E.; Lasic, D.; Martin, F. Therapy of primary and metastatic mouse mammary carcinomas with doxorubicin encapsulated in long circulating liposomes. *Int. J. Cancer* 1992, 51, 942–948.
- (150) Vaage, J.; Donovan, D.; Mayhew, E.; Abra, R.; Huang, A. Therapy of human ovarian carcinoma xenografts using doxorubicin encapsulated in sterically stabilized liposomes. *Cancer* 1993, 72, 3671–3675.
- (151) Vaage, J.; Donovan, D.; Uster, P.; Working, P. Tumour uptake of doxorubicin in polyethylene glycol-coated liposomes and therapeutic effect against a xenografted human pancreatic carcinoma. *Br. J. Cancer* 1997, 75, 482–486.
- (152) O'Brien, M. E.; Wiegler, N.; Inbar, M.; Rosso, R.; Grischke, E.; Santoro, A.; Catane, R.; Kieback, D. G.; Tomeczak, P.; Ackland, S. P.; Orlandi, F.; Mellars, L.; Alland, L.; Tendler, C. Reduced cardiotoxicity and comparable efficacy in a phase III trial of pegylated liposomal doxorubicin HCl (CAELYX/Doxil) versus conventional doxorubicin for first-line treatment of metastatic breast cancer. *Ann. Oncol.* 2004, 15, 440–449.
- (153) Ranson, M. R.; Carmichael, J.; Obyrne, K.; Stewart, S.; Smith, D.; Howell, A. Treatment of advanced breast cancer with sterically stabilized liposomal doxorubicin: Results of a multicenter phase II trial. *J. Clin. Oncol.* 1997, 15, 3185–3191.
- (154) Van Oosterom, A. T.; Mouridsen, H. T.; Wildiers, J.; Paridaens, R.; Cocconi, G.; Rotmensz, N.; Sylvester, R. Carminomycin versus doxorubicin in advanced breast cancer, a randomized phase II study of the E.O.R.T.C. Breast Cancer Cooperative Group. *Eur. J. Cancer Clin. Oncol.* 1986, 22, 601–605.
- (155) Lawton, P. A.; Spittle, M. F.; Ostrowski, M. J.; Young, T.; Madden, F.; Folkes, A.; Hill, B. T.; MacRae, K. A comparison of doxorubicin, epirubicin and mitoxantrone as single agents in advanced breast carcinoma. *Clin. Oncol. (R. Coll. Radiol.)* 1993, 5, 80–84.
- (156) Cowan, J. D.; Osborne, C. K.; Neidhart, J. A.; Von Hoff, D. D.; Constanzi, J. J.; Vaughn, C. B. A randomized trial of doxorubicin, mitoxantrone and bisantrene in advanced breast cancer (a South West Oncology Group Study). *Invest. New Drugs* 1985, 3, 149–152.
- (157) Pfeiffer, P.; Cold, S.; Rose, C. Cytotoxic treatment of metastatic breast cancer. Which drugs and drug combinations to use? *Acta Oncol.* 1992, 31, 219–224.
- (158) Duncan, R.; Seymour, L. W.; O'Hare, K. B.; Flanagan, P. A.; Wedge, S.; Hume, I. C.; Ulbrich, K.; Strohalm, J.; Subr, V.; Spreafico, F.; Grandi, M.; Ripamonti, M.; Faraò, M.; Suarato, A. Preclinical evaluation of polymer-bound doxorubicin. *J. Controlled Release* 1992, 19, 331–346.
- (159) Duncan, R. Drug-polymer conjugates: potential for improved chemotherapy. *Anticancer Drugs* 1992, 3, 175–210.
- (160) Seymour, L. W.; Ferry, D. R.; Kerr, D. J.; Rea, D.; Whitlock, M.; Poyner, R.; Boivin, C.; Hessewood, S.; Twelves, C.; Blackie, R.; Schatzlein, A.; Jodrell, D.; Bissett, D.; Calvert, H.; Lind, M.; Robbins, A.; Burtles, S.; Duncan, R.; Cassidy, J. Phase II studies of polymer-doxorubicin (PK1, FCE28068) in the treatment of breast, lung and colorectal cancer. *Int. J. Oncol.* 2009, 34, 1629–1636.
- (161) Li, C.; Yu, D. F.; Newman, R. A.; Cabral, F.; Stephens, L. C.; Hunter, N.; Milas, L.; Wallace, S. Complete regression of well-established tumors using a novel water-soluble poly(L-glutamic acid)-paclitaxel conjugate. *Cancer Res.* 1998, 58, 2404–2409.
- (162) Sabbatini, P.; Aghajanian, C.; Dixon, D.; Anderson, S.; Dupont, J.; Brown, J. V.; Peters, W. A.; Jacobs, A.; Mehdi, A.; Rivkin, S.; Eisenfeld, A. J.; Spriggs, D. Phase II study of CT-2103 in patients with recurrent epithelial ovarian, fallopian tube, or primary peritoneal carcinoma. *J. Clin. Oncol.* 2004, 22, 4523–4531.
- (163) Sabbatini, P.; Sill, M. W.; O'Malley, D.; Adler, L.; Secord, A. A. A phase II trial of paclitaxel poliglumex in recurrent or persistent ovarian or primary peritoneal cancer (EOC): A gynecologic oncology group study. *Gynecol. Oncol.* 2008, 111, 455–460.
- (164) Yang, D.; Yu, L.; Van, S. Clinically relevant anticancer polymer paclitaxel therapeutics. *Cancers* 2010, 3, 17–42.
- (165) McGuire, W. P.; Hoskins, W. J.; Brady, M. F.; Kucera, P. R.; Partridge, E. E.; Look, K. Y.; Clarke-Pearson, D. L.; Davidson, M. Cyclophosphamide and cisplatin compared with paclitaxel and cisplatin in patients with stage III and stage IV ovarian cancer. *N. Engl. J. Med.* 1996, 334, 1–6.
- (166) European Medicines Agency Questions and answers on the withdrawal of the marketing authorisation application for Opaxio (Paclitaxel poliglumex). http://www.ema.europa.eu/docs/en_GB/document_library/Medicine_QA/2010/01/WC500060347.pdf (accessed on 10/15/12).
- (167) Bibby, M. C. Orthotopic models of cancer for preclinical drug evaluation: advantages and disadvantages. *Eur. J. Cancer* 2004, 40, 852–857.
- (168) Kelland, L. R. "Of mice and men": values and liabilities of the athymic nude mouse model in anticancer drug development. *Eur. J. Cancer* 2004, 40, 827–836.
- (169) Damia, G.; D'Incalci, M. Contemporary pre-clinical development of anticancer agents: What are the optimal preclinical models? *Eur. J. Cancer* 2009, 45, 2768–2781.
- (170) Kamb, A. What's wrong with our cancer models? *Nat. Rev. Drug Discovery* 2005, 4, 161–165.
- (171) Sausville, E. A.; Burger, A. M. Contributions of human tumor xenografts to anticancer drug development. *Cancer Res.* 2006, 66, 3351–3354.
- (172) Talmadge, J. E.; Singh, R. K.; Fidler, I. J.; Raz, A. Murine models to evaluate novel and conventional therapeutic strategies for cancer. *Am. J. Pathol.* 2007, 170, 793–804.
- (173) Ishida, T.; Masuda, K.; Ichikawa, T.; Ichihara, M.; Irimura, K.; Kiwada, H. Accelerated clearance of a second injection of PEGylated liposomes in mice. *Int. J. Pharm.* 2003, 255, 167–174.

Molecular Pharmaceutics

phosphate] (Compound 003), a novel nucleoside analog. *Arzneim. Forsch.* 2004, 54, 715–31.

(210) Kelly, K. A.; Bardeesy, N.; Anbazhagan, R.; Gurumurthy, S.; Berger, J.; Alencar, H.; Depinho, R. A.; Mahmood, U.; Weissleder, R. Targeted nanoparticles for imaging incipient pancreatic ductal adenocarcinoma. *PLoS Med.* 2008, 5, e85.

(211) Valencia, P. M.; Farokhzad, O. C.; Karnik, R.; Langer, R. Microfluidic technologies for accelerating the clinical translation of nanoparticles. *Nat. Nanotechnol.* 2012, 7, 623–629.